THE UNIVERSITY
of EDINBURGH

THE ORIGIN AND FUNCTION OF THE STROMA IN CHOLANGIOCARCINOMA

Andrew John Robson

A thesis presented for the degree of Doctor of Philosophy at the University of Edinburgh

2014

ABSTRACT

Background: Intrahepatic cholangiocarcinoma (CCA) is a highly treatment-resistant malignancy of biliary epithelium with increasing global mortality. Histologically, CCA is characterised by a pronounced inflammatory stroma of tumour-associated myofibroblasts, macrophages, immune cells and a modified extracellular matrix (ECM). In other solid cancers, the stroma plays a tumour promoting role. The functional role of the stroma in CCA remains unclear. The origin and the proportional contribution to the stroma by haematopoietic and mesenchymal bone marrow (BM) -derived cells is not known in CCA. Intriguingly, reports suggest that mesenchymal stem cells (MSCs) may contribute to the epithelial compartment of malignant tumours. Furthermore, the Notch signalling pathway is known to play oncogenic and tumour suppressive roles in diverse neoplasms but its role in CCA remains unclear.

Aims and Methods: The functional role of myofibroblasts and macrophages in the tumour stroma of CCA was investigated together with an analysis of the origin and contribution of BM-derived cells to the stromal and epithelial compartments of CCA. The Notch signalling pathway was studied as a potential signalling mechanism through which the stroma and malignant epithelial compartments of CCA may interact.

Results: The thioacetamide rat model of CCA was optimised and found to display excellent histological congruence with human lesions. The tumour cellular microenvironment comprised of myofibroblasts, migratory macrophages and immune cells. During cholangiocarcinogenesis, progressive intrahepatic accumulation of inflammatory cells and proliferation of bipotential progenitor cells preceded the development of invasive CCA. In vitro, CCA lines were identified to contain a side population of stem cells. Adoptive transfer of BM from Enhanced Green Fluorescent Protein (EGFP) transgenic rats to wild type rats to establish chimeras was undertaken. In transplanted rats, persistent EGFP+ chimerism of both haematopoietic and mesenchymal stem cell compartments was established. In

tumours, macrophages and neutrophils were overwhelmingly EGFP+ve, whereas myofibroblasts, fibroblasts and benign and malignant bile ducts were EGFP-ve. There was no evidence of cell fusion or EGFP silencing. These findings were confirmed in spontaneous breast, skin and colon tumours in EGFP+ chimeric rats not treated with TAA. In vitro studies to recapitulate the cellular and extracellular elements of the tumour niche identified that ECM components induce characteristic cell proliferation patterns dependent on the matrix component but do not appear to affect chemosensitivity. Bidirectional interaction between CCA cells and hepatic stellate cells (mediated by soluble factors) was identified. Furthermore, in direct co-culture, M2 polarised macrophages appear to enhance CCA cell proliferation compared to M1 macrophages. In considering the Notch pathway, Notch signalling components (particularly Notch3) and target genes were upregulated in human CCA specimens. Immunohistochemical analysis identified apparent distribution of Notch ligand on tumour stroma and Notch receptor subtypes on malignant epithelia. Although direct co-culture of CCA cells with myofibroblasts and M1/M2 polarised macrophages did not clearly demonstrate stromal:epithelial Notch pathway activation, this may have been a function of in vitro experimental limitations. Gamma-secretase inhibition downregulated the Notch pathway, reduced proliferation and appeared to enhance chemosensitivity of CCA cells in vitro.

Conclusions: A stereotypical niche forms around CCA in developing and malignant lesions. There was no evidence of a BM-derived stem cell contribution to the epithelial component of CCA, breast, colon or skin malignancies. Haematopoietic but not mesenchymal components of the tumour stroma were of BM origin. Notch signalling is upregulated in CCA and appears to play a tumour promoting role in CCA; pathway inhibition represents a potential therapeutic target.

DECLARATION

This thesis has been written by me and represents research that I have undertaken. Where work has been undertaken in collaboration, this has been specifically indicated in the text. This thesis has not been submitted elsewhere in application for a university degree and all sources of information have been acknowledged.

The Medical Research Council funded these studies through a Clinical Research Training Fellowship (G0700562).

Andrew Robson

ACKNOWLEDGEMENTS

I am immensely grateful to my supervisors, Professor Stuart Forbes and Professor John Iredale for their considerable input and advice during this thesis. Their scientific vision is breath-taking. I am very grateful to Professor O James Garden for his guidance and support. I also thank Professor Steve Wigmore for his surgical perspective on matters and for tissue provision.

To those in the Forbes/Iredale laboratory and the wider University community who helped me enormously with my work – a very sincere thank you. I am indebted to Kay Samuel, Antonella Pellicoro and Davina Wojtacha for their invaluable scientific advice and help. Thank you to all members of the Forbes/Iredale laboratory, specifically Tim Gordon-Walker, Prakash Ramachandran, Tom Bird, Luke Boulter, James Thomas, Joerg Schraeder, Rebecca Aucott, Rachel Guest and Caroline Pope.

Many thanks indeed to Dr Martin Waterfall, Institute of Infection and Immunity Research, University of Edinburgh, for his assistance with flow cytometry. Professor David Harrison and Dr David Brownstein, Department of Pathology, University of Edinburgh, provided invaluable advice with pathological tissue analysis. Dr Maurits Jansen and Dr Carmel Moran of the Preclinical Imaging Facility, University/BHF Centre for Cardiovascular Science and Dr Alan Serrels, Edinburgh Cancer Research Centre, were essential for the MRI, ultrasound and fluorescent imaging studies respectively. I am grateful to Mr Ewen Harrison, Department of Surgery, for his statistical advice.

I acknowledge with grateful thanks others who gave generous advice, equipment and assistance: In particular, Dr Sally Lowell, Scottish Centre for Regenerative Medicine, together with Dr Sabrina Gordon-Keylock, Dr Tiina Kipari, Professor Sarah Howie, Dr Marieke Hoeve, Dr Stephen McNally, Shonna Johnstone, Fiona Rossi, and Dr Melany Jackson, all of the MRC Cente for Inflammation Research.

Finally and most importantly, to my wife Jenny, Thank You.

HYPOTHESIS AND AIMS

Hypothesis: The tumour stroma in cholangiocarcinoma is bone marrow derived and contributes to both epithelial and mesenchymal components of lesions. Notch signalling promotes tumour survival through stromal-epithelial cell signalling.

Aim 1: Establish a model of cholangiocarcinoma

Aim 2: Characterise the stromal component in cholangiocarcinoma lesions

Aim 3: Define the origin of the stroma surrounding cholangiocarcinoma by characterising the role of the bone marrow in stroma formation

Aim 4: Define the functional role of stromal cell - cholangiocyte interaction in tumour survival

Aim 5: Investigate whether Notch signalling is implicated in the stromal-epithelial relationship

CONTENTS

Monocyte Maturation and Polarisation

Cholangiocarcinoma (CCA) cell lines and cell culture

Generation of Conditioned Media

Co-culture of Cells

Staining of Cells for Co-culture

Fixation of Co-cultured Cells

Staining of transplanted BM cells with DiD

Side Population (SP) Analysis

Clone Formation

qPCR for Genomic Rat Y-Chromosome

Reconstitution of Haematopoeitic and Mesenchymal compartments

Cell tracking in Cholangiocarcinoma experimental design

Immunohistochemistry and Immunoflourescence

Antibody Types

Immunohistochemistry

Immunoflourescence

Dual Immunoflourescence – Two Step

Dual Immunoflourescence – Tyramide Signal Amplification (TSA)

Fluorescent In Situ Hybridization (FISH) analysis of transplanted tissue

Antigen Retrieval

Cytospins

Immunocytochemistry

Picrosirius Red Staining for Quantification of Liver Fibrosis

Microscopy and Image Capture

RNA extraction from cultured cells and tissue samples

Reverse Transcription

qPCR for Notch pathway components and Macrophage markers

Cytotoxicity assays and inhibition of Notch signalling

Luciferase Reporter Assays

Human tissue samples

MTS and MTT Cell Proliferation Assays

Lactate Dehydrogenase (LDH) Assay

LIST OF FIGURES

ABBREVIATIONS

AAF	Acetyl amino fluorine
AAH	Aspartyl asparginyl beta hydroxylase
ABC	Adenosine triphosphate binding cassette
AFP	Alpha fetoprotein
AJCC	American Joint Cancer Committee
ASIR	Age-Standardised Incidence Rate
BM	Bone marrow
BMT	Bone marrow transplantation
BSA	Bovine serum albumin
CA	Carbohydrate antigen
CAF	Cancer-associated fibroblast
CCA	Cholangiocarcinoma
CCL	Chemokine (C-C motif) ligand
CD	Cluster of differentiation
CEA	Carcinoembryonic antigen
CK19	Cytokeratin 19
Co-A	Co-activator
COX-2	Cyclooxygenase-2
CSC	Cancer stem cell
CT	Computed tomography
CXCL	Chemokine (C-X-C motif) ligand
CYFRA	Cytokeratin-19 fragment
CYP1A2	Cytochrome P450 1A2
DMEM	Dulbecco's modified Eagle medium
DNA	Deoxyribonucleic acid
DEN	Diethylnitrosamine
DMSO	Dimethyl sulphoxide
DNER	Delta/Notch-like EGF-related receptor
DSL	Delta/Serrate/LAG-2
EAPC	Estimated annual percentage change

ECM	Extracellular matrix
EDTA	Ethylenediaminetetraacetic acid
EGF	Epidermal growth factor
EGFP	Enhanced green fluorescent protein
EGFR	Epidermal growth factor receptor
EMT	Epithelial-mesenchymal transition
ERCP	Endoscopic retrograde cholangiopancreatography
FAP	Fibroblast activation protein–α
FCS	Foetal calf serum
FGF	Fibroblast growth factor
FISH	Fluorescent *in situ* hybridisation
FSP-1	Fibroblast-specific protein-1
GM-CSF	Granulocyte-macrophage colony stimulating factor
GPCR	G-protein coupled receptor
HBSS	Hank's buffered saline solution
HCC	Hepatocellular carcinoma
HES	Hairy and enhancer of split
HGF	Hepatocyte growth factor
HIF	Hypoxia-inducible factor
HIV	Human Immunodeficiency Virus
HSC	Haematopoietic stem cells
IBD	Inflammatory Bowel Disease
ICD-O	International Classification of Diseases for Oncology
ICD-10	International Classification of Diseases -10
IFNγ	Interferon-γ
IGF-1	Insulin-like growth factor-1
IL	Interleukin
IMDM	Iscove's modified Dulbecco's medium
iNOS	Inducible nitric oxide synthetase
IRF-3	Interferon regulatory factor
JAK	Janus kinase
JNK	c-Jun N-terminal kinase

LAIR-1	Leucocyte-associated immunoglobulin-like receptor-1
LCSGJ	Liver Cancer Study Group of Japan
LDH	Lactate dehydrogenase
LOX	Lysyl oxidase
LPS	Lipopolysaccharide
M1	Classically activated macrophage
M2	Alternatively activated macrophage
MACS	Magnetic-activated cell sorting
MAPK	Mitogen-activated protein kinases
M-CSF	Macrophage colony stimulating factor
MHC	Major histocompatibility complex
miRNA	Micro ribonucleic acid
MMP	Matrix metalloproteinase
MR	Magnetic resonance
MRA	Magnetic resonance angiography
MRCP	Magnetic resonance cholangiopancreatography
MSC	Mesenchymal stem cells
MUC1	Mucin 1
NAT2	N-acetyltransferase 2
NICD	Notch intracellular domain
NO	Nitric oxide
NK	Natural killer
OR	Odds Ratio
PAR1	Proteinase-activated receptor 1
PBMC	Peripheral blood mononuclear cells
PBS	Phosphate buffered saline
PDT	Photodynamic therapy
PET-CT	Positron emission tomography-computed tomography
PGE2	Prostaglandin E2
PDGF	Platelet-derived growth factor
PMS	Phenazine methosulphate
PRP	Platelet-rich plasma

PSC	Primary Sclerosing Cholangitis
PSR	Picrosirius red
PTC	Percutaneous transhepatic cholangiography
qPCR	Quantitative polymerase chain reaction
RAM	RBP-Jkappa-associated module
RBPJκ	Recombination signal binding protein for immunoglobulin Jkappa region
RCF	Relative centrifugal force
RFA	Radiofrequency ablation
RNOS	Reactive nitric oxide species
RPM	Revolutions per minute
RPMI	Roswell Park Memorial Institute medium
SCC	Squamous cell carcinoma
SDF	Stromal-derived factor 1
siRNA	Small interfering ribonucleic acid
αSMA	α-smooth muscle actin
SEER	Surveillance, Epidemiology and End Results
SP	Side population cells
SPARC	Secreted protein, acidic rich in cysteine
SR-A	Scavenger receptor A
STAT	Signal transducer and activator of transcription
TAA	Thioacetamide
TACE	Tumour necrosis factor-α converting enzyme
TAM	Tumour-associated macrophages
TGFβ	Transforming growth factor β
TERT	Telomerase Reverse Transcriptase
Th1/Th2	T helper cell type 1 or 2
TIMP	Tissue inhibitor of metalloproteinases
TNFα	Tumour necrosis factor α
TLR	Toll-like receptor
TR	Repetition time
TSA	Tyramide signal amplification

TNM	Tumour Nodes Metastasis Classification of Malignant Tumours
UICC	Union International Contre le Cancer
VEGF	Vascular endothelial growth factor
WHO	World Health Organisation
WISP	Wnt-inducible signalling pathway 1v

CHAPTER ONE

INTRODUCTION

1. Cholangiocarcinoma (CCA)

Globally, malignancies of the liver and bile ducts account for 10.6% of annual tumour deaths and represent a significant cancer burden. Cholangiocarcinoma (CCA) - neoplasia of the bile ducts - is the second commonest hepatic malignancy, comprising 10-20% of primary liver neoplasms [1, 2]. The World Health Organisation's (WHO) International Classification of Diseases (ICD-10) identifies that primary lesions in the liver and intrahepatic bile ducts (code C22) comprise 9.2% of deaths, whilst gallbladder (C23) and extra-hepatic bile duct (C24) tumours account for 1.4% of all cancer deaths [3].

Classification of CCA

Anatomically, CCAs are described as being intrahepatic, hilar or distal extra-hepatic. Lesions may have both intra- and extrahepatic components. Intrahepatic CCA arises from biliary epithelia at any portion of the intrahepatic biliary system, from the ductules to the segmental bile ducts. Hilar lesions (Klatskin tumours [4]) are located at the level that the biliary tree exits the liver and arise from the right and left hepatic bile ducts at or near their confluence. Proximally they are separated from intrahepatic CCA by the second-order bile ducts, and are separated from distal extrahepatic CCA at the level of the insertion of the cystic duct of the gallbladder into the extrahepatic biliary tree. Distal extrahepatic CCAs are located along the common bile duct between the cystic duct and the ampulla of Vater (the hepatopancreatic ampulla) which is formed by the union of the common bile duct and pancreatic duct. Ampullary carcinomas are classified separately [5-7].

Figure 1.1 – Anatomical Distribution of CCA

Figure 1.1: Anatomical distribution of Cholangiocarcinoma (CCA)

Intra and extrahepatic CCA are separated from each other at the level of the second-order bile ducts. Extrahepatic CCA is further divided into hilar and distal extrahepatic CCA at the level of the cystic duct insertion into the common bile duct.

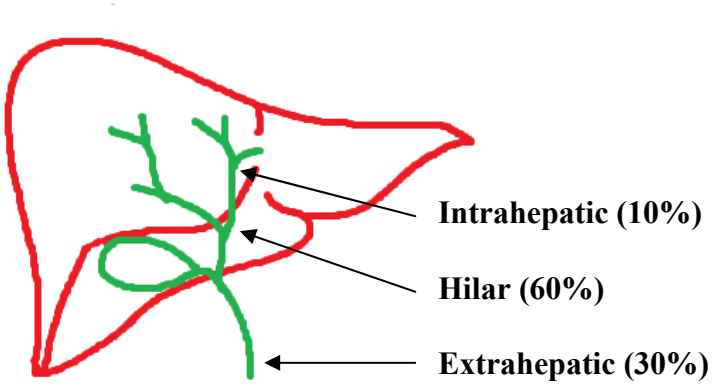

Adapted from Patel T, Nat Clin Pract Gastroenterol Hepatol. 2006 Jan;3(1):33-42

Hilar and distal extrahepatic tumours are grouped together as extrahepatic CCA for classification of tumour types by the WHO ICD-10 [5]. In contrast, they are considered as separate entities in the American Joint Cancer Committee / Union International Contre le Cancer (AJCC/UICC) Tumour Node Metastasis (TNM) Classification of Malignant Tumours 7th Edition for staging purposes[6]. Furthermore, the exact anatomical boundaries that qualify a tumour to be considered as a hilar cholangiocarcinoma differs slightly between the two systems, with the ICD-10 classification not including the second-order bile ducts or insertion of the cystic duct as anatomical boundaries for tumour location, but rather using only the right and left hepatic bile ducts as the location descriptor.

Bismuth [8] further subdivided the anatomical location of hilar lesions, primarily with an interest in determining surgical resectability and operative strategy.

Figure 1.2 – Bismuth Classification of CCA

Figure 1.2: Bismuth classification of hilar lesions and surgical treatment options for CCA

A

Bismuth classification of hilar CCA lesions:

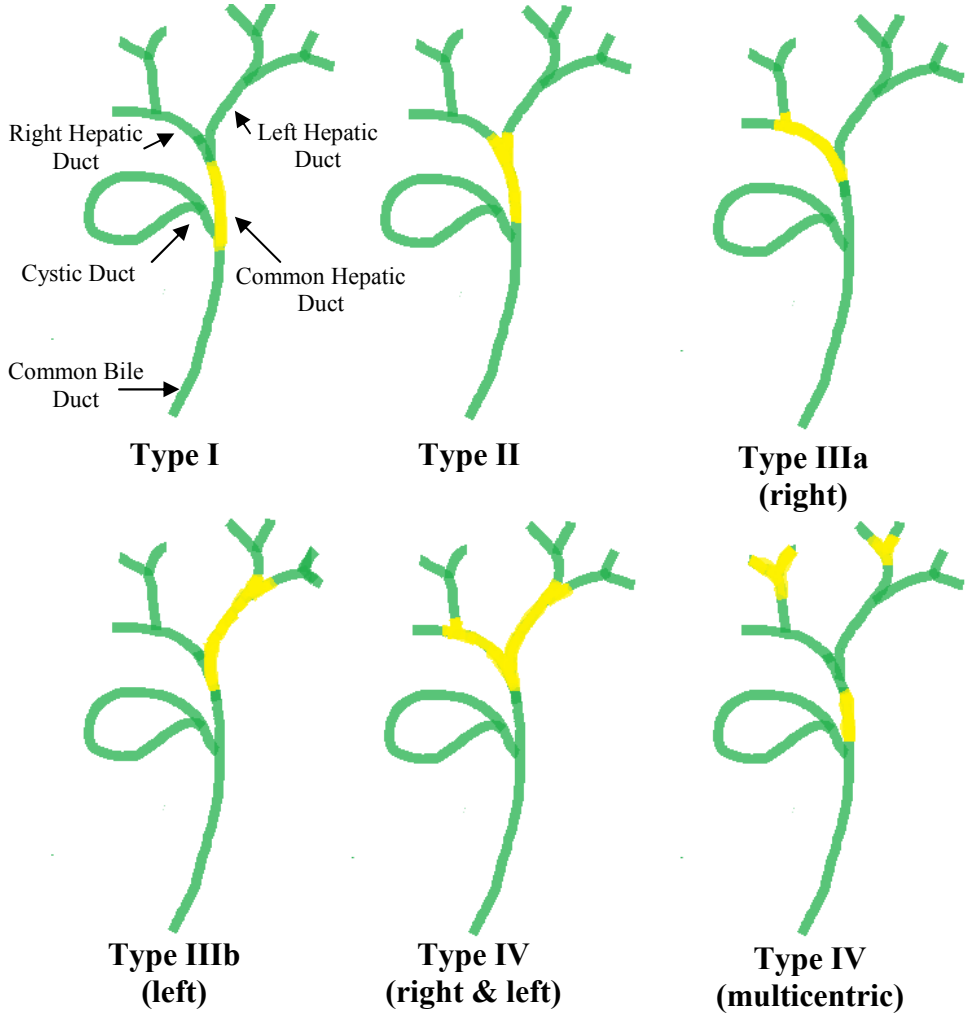

Type I: Below the confluence of the left and right hepatic ducts

Type II: Reaches the confluence but not involving the left or right hepatic duct

Type III: Occludes common hepatic duct and right (IIIa) or left (IIIb) hepatic duct

Type IV: Involves the confluence, right and left hepatic ducts or is multicentric

Adapted from Patel T, Nat Clin Pract Gastroenterol Hepatol. 2006 Jan;3(1):33-42

B

Surgical treatment options for hilar CCA lesions:

Intrahepatic CCA: resection of the involved segments or lobe of the liver.

Hilar tumours:

Types I and II: *en bloc* resection of the extrahepatic bile ducts and gall bladder, regional lymphadenectomy, and Roux-en-Y hepaticojejunostomy;

Type III: as above plus right or left hepatectomy;

Type IV: as above plus extended right or left hepatectomy.
(Consider removal of segment 1 of the liver stages II–IV as this segment may preferentially harbour metastatic disease)

Distal Extrahepatic CCA: Pancreatoduodenectomy

Depending on their growth pattern, tumours are described either as mass-forming, periductal-infiltrating or intraductal, using a classification system devised by the Liver Cancer Study Group of Japan (LCSGJ) [9, 10]. Most intrahepatic CCAs form mass lesions that invade the hepatic parenchyma via the portal venous system and invade lymphatic vessels at advanced stages. Hilar and extrahepatic tumours are usually periductal infiltrating types that predominantly extend longitudinally along and within the bile duct, often resulting in dilatation of the intrahepatic bile ducts. The periductal-infiltrating type tends to spread along Glisson's sheath (a fascial envelope encompassing the bile ducts) via the lymphatic vessels. The intraductal-growth type proliferates towards the lumen of the bile duct; this form of CCA often has papillary growth characteristics. Tumours not following any of these criteria are categorised as 'undefined' [7]. The AJCC/UICC TNM 7th edition concurs with this classification but does not include intraductal as a separate entity [11].

Figure 1.3 – Liver Cancer Study Group of Japan Classification of CCA

Figure 1.3: Liver Cancer Study Group of Japan classification of CCA

CCA lesions are either intrahepatic or extrahepatic, with the same three broad types of tumours arising: mass-forming, periductal infiltrating and intraductal lesions.

Mass-forming:

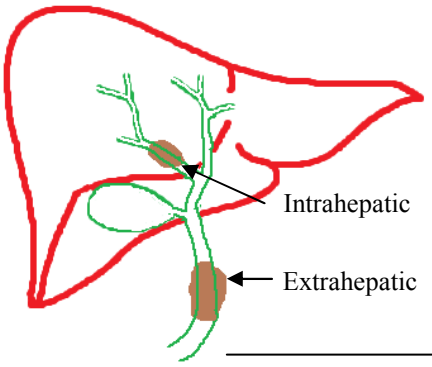

Commonest form of Intrahepatic CCA, only occasionally causing jaundice

Intrahepatic lesions: Up to 15cm
Extrahepatic lesions: 1-2cm

Invade the hepatic parenchyma via the portal venous system and invade lymphatic vessels at advanced stages.

Periductal Infiltrating:

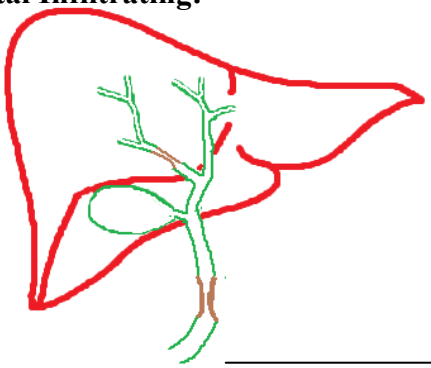

Commonest form of Hilar and extrahepatic tumours

Intrahepatic: 0.5-6cm
Extrahepatic: Up to 1cm

Extend along and within the bile duct, resulting in concentric thickening of the wall along bile ducts and obstructing the upstream intrahepatic bile ducts, resulting in jaundice.

Invade along Glisson's sheath via lymphatics

Intraductal/Papillary:

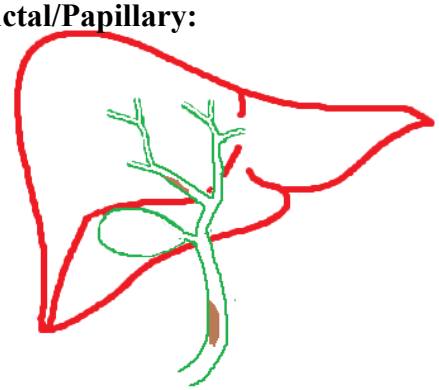

Intraluminal growth in the bile duct

Usually small and flat, but can form a polyp or cast to fill bile duct lumen

Spread along mucosa of bile ducts, tumour cells can slough and spread distally.

These lesions characteristically do not penetrate the duct wall but (but have potential to invade)

Adapted from Sripa PLoS Medicine 2007, 4: 7, (e201 06-PLME-ND-0923 [pii] 10.1371/journal.pmed.0040201) and Lim *et al,* Abdom Imaging 2004;29:540-7

Macroscopically, mass lesions appear white or grey in colour, and are firm to touch. Intrahepatic lesions may be very large (up to 15 cm in diameter), whilst extrahepatic tumours tend to be no larger than 2 cm at clinical presentation. Periductal tumours result in concentric thickening of the wall along bile ducts to form an elongated, spiculated, or branch-like structure. These lesions are difficult to identify macroscopically and, when seen, they appear as ill-defined strictures. In contrast, intraductal-growing papillary tumours of the bile ducts are low-grade malignancies that form sessile or polypoid masses that block bile ducts by either forming a polyp or growing as a cast that fills the shape of the bile ducts. These lesions characteristically do not penetrate the duct wall [10].

Regardless of tumour location and morphology, the overwhelming majority arise as adenocarcinomas (90%) and are associated to a varying degree with a desmoplastic reaction [10, 12]. The tumour-associated desmoplasia comprises modified extracellular matrix (ECM) proteins, myofibroblasts, and immune cells together with expression of a multitude of cytokines, growth factors, and ECM metabolizing enzymes. The WHO International Classification of Diseases for Oncology (ICD-O), that differs from ICD by including a morphology code (based on histology) in addition to the topographical codes shared between the two systems, lists several subtypes of bile duct cancer [13]. The categories described in the 3rd edition (ICD-O-3) are very rare, and information from adenocarcinoma of the bile ducts may have limited applicability in these tumours.

Table 1.1 – WHO Classification of Subtypes of CCA

Carcinomas of the extrahepatic bile ducts	Carcinomas of the liver
Carcinoma *in situ*	Hepatocellular carcinoma
Adenocarcinoma	Intrahepatic CCA
Papillary adenocarcinoma	Combined hepatocellular CCA
Adenocarcinoma, intestinal-type	Bile duct cystadenocarcinoma
Mucinous adenocarcinoma	Hepatoblastoma
Clear cell adenocarcinoma	Undifferentiated carcinoma
Signet ring cell carcinoma	
Adenosquamous carcinoma	
Squamous cell carcinoma	
Biliary cystadenocarcinoma	
Undifferentiated carcinoma	
Endocrine carcinomas (commoner in gallbladder): small cell (oat cell), large cell neuroendocrine, carcinoid tumour, goblet cell carcinoid, tubular carcinoid, mixed carcinoid-adenocarcinoma	Ref: WHO Classification of Tumours, Pathology and Genetics of Tumours of the Digestive System Ed: Hamilton, Aaltonnen 2000, IARC Press. Lyon.

Aetiology of CCA

Many cases of CCA arise spontaneously. However, established risk factors for CCA unite around the common theme of prolonged inflammation of the biliary tract. Biliary epithelial inflammation may be either direct (such as primary sclerosing cholangitis) or may occur secondarily as part of the spectrum of hepatic parenchymal inflammation (such as diabetes). The majority of aetiological factors are associated with both intra- and extrahepatic CCA, however a proportion appear to be related to one form of the tumour only.

Biliary Factors

The prevalence of CCA amongst patients with primary sclerosing cholangitis (PSC) ranges from 5 to 15%, with a cumulative annual risk of 1.5% per year [14-16] although the risk of developing CCA does not appear to be related to the duration of PSC [17, 18].

Both the intra- and extra-hepatic forms of CCA may occur. Furthermore, a population-based case control series has recently suggested that primary biliary cirrhosis may be a possible risk factor in intrahepatic CCA [19], although the authors recommend that this be further assessed since database misclassification of secondary biliary cirrhosis is a potential confounding factor.

In certain areas of South East Asia (Thailand, Laos, Malaysia), liver fluke infestation of the biliary tree with *Opisthorchis viverini* (and, less commonly, *Clonorchis sinensis*) from eating raw fish is endemic (northern Thailand 90% infection prevalence). The parasite persists and progressively accumulates in the biliary system leading to a chronic inflammatory response and increased risk of CCA [16, 20]. Conditions that cause biliary stasis such as choledochal cysts (cystic dilation of the biliary tract that require surgical excision) and biliary-pancreatic malformations (extrahepatic CCA) [21] are other aetiological factors in the development of CCA [22]. Hepatolithiasis, common in the Far East, is a well recognised risk factor with up to 10% of patients developing intrahepatic CCA [23 24]. A recent Danish case-control study suggests that choledocholithiasis (odds ratio, OR, 24) and cholecystolithiasis (OR 4.0) are associated with an increased risk of intrahepatic CCA [25, 26].

Other Factors

Hepatic parenchymal inflammation of any type that leads to cirrhosis is associated with intrahepatic CCA [27]. A large United States population-based case control series of 535 intrahepatic CCA patients and 549 extra-hepatic CCA patients compared to 102,792 cancer-free controls identified (in addition to biliary-specific factors above) an increased incidence of both the intra- and extrahepatic forms of CCA in patients with alcoholic liver disease, nonspecific cirrhosis, diabetes, thyrotoxicosis and chronic pancreatitis. Conditions only associated with intrahepatic CCA were obesity, chronic non-alcoholic fatty liver disease, hepatitis C virus infection and smoking [19]. The rate of inflammatory bowel disease (IBD) was significantly higher among both intrahepatic CCA and extrahepatic CCA cases than controls ($p = 0.04$ and $p<0.0001$, respectively). However, when IBD was categorized into its components, Crohn's disease was significantly more common only among the extrahepatic CCA cases

(p=0.02), while ulcerative colitis was significantly more common only among the intrahepatic CCA cases (p<0.0001). Duodenal ulcer and chronic pancreatitis were both significantly more common in extrahepatic CCA and intrahepatic CCA cases compared to controls. In a similar case-control series by the same authors, Human Immunodeficency Virus (HIV) infection was noted to be associated with intrahepatic CCA (OR: 5.9, 1.8–18.8) [28]. A recent meta-analysis of case-control studies of intrahepatic CCA subsequently confirmed hepatitis B but not smoking as a risk factor for CCA and estimated the overall odds ratios (with 95% confidence intervals) for defined risk factors (hepatitis B OR: 5.10, 2.91–8.95, hepatitis C OR: 4.84, 2.41–9.71, obesity OR: 1.56, 1.26–1.94, diabetes mellitus type II OR: 1.89, 1.74–2.07, alcohol use OR: 2.81, 1.52–5.21, and smoking OR: 1.31, 0.95–1.82,) [29].

Thorotrast was used as a radiographic contrast medium from 1930 to 1955 and comprised a colloidal suspension of thorium dioxide with Th-232, a highly carcinogenic alpha-emitter with a physical half-life of 14 billion years. Thorotrast is absorbed by the bone, liver, spleen and lymph nodes and the tissues in which it was deposited are irradiated by alpha-radiation for the entire lifetime of the subject, with biological clearance half-life times ranging from 700 days for the liver to as long as 22 years in bone [30]. Thorotrast associated malignancies include CCA (commonest lesion), hepatocellular carcinoma, angiosarcoma, erythroleukemia and myelodysplastic syndromes. Mutation analyses suggest that genetic changes of thorotrast-induced cancers are mainly delayed mutations, and not the result of the direct effects of radiation [31]. Other chemical carcinogens such as dioxins and vinyl chloride [32] and nitrosamines [33] have also been epidemiologically linked to CCA. Geographical distribution of CCA cases in the UK between 1981-2004 suggest a preponderance of cases in rural areas, leading some to suggest that agricultural toxins may be in part responsible [34].

Table 1.2 – Risk factors for CCA

Current risk factors for CCA; confident factors are in bold text whereas probable or possible factors are included in normal text. Risk factors do not have an exclusive intra/extrahepatic preponderence and may be associated with converse locations to those listed below.

INTRAHEPATIC CCA:	BOTH INTRA AND EXTRA:
Hepatitis B virus infection	***Opisthorchis viverini* infection**
Hepatitis C virus infection	***Clonorchis sinensis* infection**
Hepatolithiasis	**Primary sclerosing cholangitis**
Smoking	**Liver cirrhosis**
Obesity	**Thorotrast exposure**
Non-Alcoholic Fatty Liver Disease (NAFLD)	Primary Biliary Cirrhosis
	Choledocholithiasis
	Cholecystolithiasis
	HIV infection
EXTRAHEPATIC CCA:	Alcoholic liver disease
Anomalous biliary–pancreatic malformation	Type II Diabetes
Biliary tract-enteric drainage procedures	Thyrotoxicosis
	Choledochal cysts
	Toxin exposure—dioxin, polyvinyl chloride, nitrosamines
	Inflammatory Bowel Disease

Epidemiology of CCA

The median age at diagnosis of CCA is 65 years, except for lesions associated with PSC, where the median age is 55 years. The disease is rare before 40 years old. Men are affected 1.5 times more commonly than women, and Asians are affected almost twice as commonly as white and black people [24]. The incidence of tumours is highest in the Far East (e.g. 96 per 100,000 men in Thailand) and lower in countries such as Australia (0.2 per 100,000 men)[24], which is likely to represent the distribution of risk factors such as liver flukes. In the United Kingdom, where both incidence and mortality rates have increased over the past three decades[35], CCA has overtaken hepatocellular carcinoma as the leading cause of death from primary liver cancer[36]. Globally, the incidence of intrahepatic CCA has increased whereas extrahepatic incidence has remained broadly stable or decreased [24, 36-39]. In the United States, age-adjusted mortality rates for intrahepatic cholangiocarcinoma progressively increased from 0.07 per 100,000 in 1973 to 0.69 per 100,000 in 1997 with an estimated annual percent change (EAPC) of 9.44% [40]. This change is mirrored in an observed increase in reported cases of intrahepatic CCA in Scotland [41].

Figure 1.4 – Changing incidence of CCA

Figure 1.4: **Changing global incidence of intrahepatic and extrahepatic CCA**

A

Age-standardised incidence rates (ASIR) per 100,000 population/year, for intra-hepatic and extrahepatic tumours, between 1990 and 2008 in England and Wales. (Khan, J Hepatol 2012, 56: 848-54)

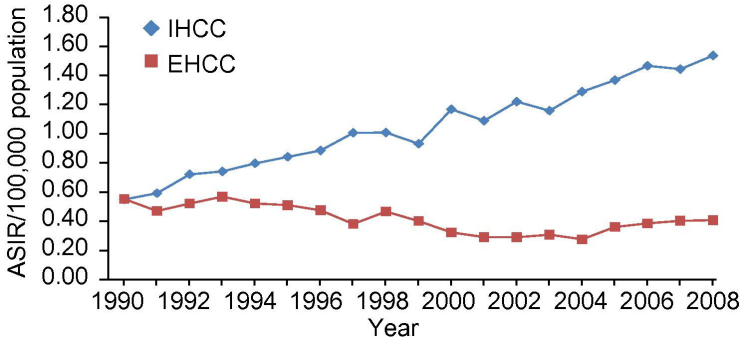

B

Age-standardised mortality rates (ASMR) for (**1**) gall bladder and extrahepatic CCA and (**2**) intrahepatic CCA in selected countries. (Khan Lancet 2005, 366: 1303-14)

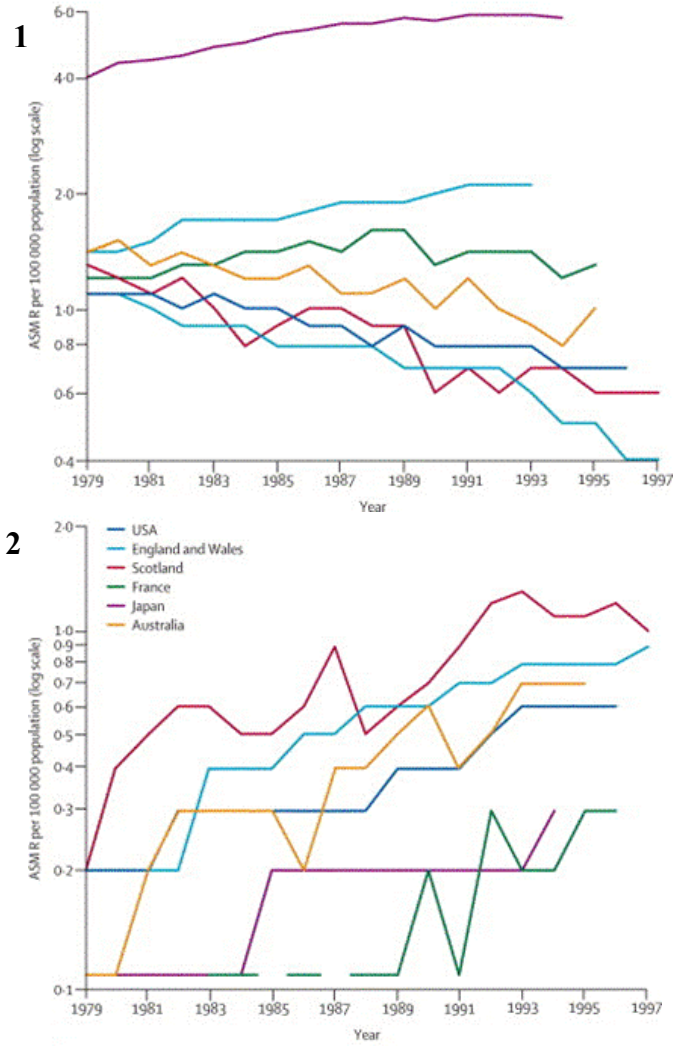

Generating accurate epidemiological data for CCA is challenging due to the complexity of CCA classification systems and the several revisions of the WHO ICD and AJCC/UICC TNM coding systems for liver and biliary tract tumours over the past three decades, with each revision being adopted by various countries at different times [42]. The effect of coding systems and misclassification has been specifically investigated and the observed incidence pattern appears to be genuine rather than merely an improvement in detection or in more accurate categorization of tumours previously misclassified by systems such as the USA Surveillance, Epidemiology and End Results (SEER) database [38].

ICD-O-2 (used between 1992 and 2000) misclassified hilar/Klatskin CCA as being intrahepatic. Consequently, for example in the USA, 91% (246 of 269) of hilar CCA during this time were incorrectly coded as being intrahepatic, resulting in an overestimation of intrahepatic CCA incidence by 13% and underestimation of extrahepatic CCA incidence by 15%[43]. Only 8% of all CCA were described as hilar, which likely reflects coding practice. However, following correction, annual intrahepatic CCA incidence in the USA still increased during this period (EAPC = 4%, 95% CI = 2-6, P <.001).

The effect of misclassification has been studied in England and Wales with similar results. Following correction for hilar CCA misclassification, the age-standardised incidence rate (ASIR) of intrahepatic CCA (code C22.1) in England and Wales rose from 0.87 to 1.62 per 100,000 population, between 1995 (when ICD-O-2 was introduced) and 2008 (when ICD-O-3 was adopted in the UK). Concurrently, despite including misclassified hilar tumours in the extrahepatic CCA (C24.0) data, a marked decrease in ASIR of extrahepatic CCA was identified from 0.55 in 1995 to 0.47 in 2008 [42].

The reason for the rise in incidence of intrahepatic CCA remains unclear but may represent the cumulative effect of the aetiological risk factors for intrahepatic CCA, which appear increasingly similar to hepatocellular carcinoma [44].

Molecular Pathogenesis of CCA

The relatively low incidence of CCA is an obstacle to elucidating the mechanistic processes in the development of lesions. In a similar fashion to other solid organ tumours, CCA is likely to develop in a multistep process of malignant transformation of cholangiocytes, with the accumulation of genetic, epigenetic and chromosomal aberrations resulting in alterations in regulatory genes in cholangiocytes that lead to the activation of oncogenes and the dysregulation of tumor suppressor genes[45]. Of note, a subset of intrahepatic CCA display combined hepatocellular carcinoma/CCA features which suggests that they may arise from progenitors or stem-cell type precursors [46, 47].

The promotion of CCA development is thought to arise following chronic biliary epithelial inflammation and cholestasis. Biliary inflammation results in release of inflammatory cytokines including inducible nitric oxide synthetase (iNOS), impaired deoxyribose nucleic acic (DNA) repair and cyclooxygenase-2 (COX-2) upregulation (which confers resistance to apoptosis[45]). Additionally, iNOS is upregulated in cholangiopathies and CCA [48]. Inducible nitric oxide synthetase produces nitric oxide and reactive nitric oxide species (RNOS), that interact with cellular DNA and proteins to induce mutations and DNA strand breaks [1]. Cholestasis causes cholangiocyte proliferation as a result of bile acid signalling driving activation of growth factors [49]. Once epithelial clonal proliferation is established, genetic and epigenetic mutations drive unlimited replication (through activation of telomerase reverse transcriptase [TERT]), evasion of apoptosis (COX-2 and Bcl-2 mutations), angiogenesis (vascular endothelial growth factor [VEGF]) and invasion and metastasis (overexpression of subtypes of matrix metalloproteases [MMP], downregulation of E-cadherin and upregulation of N-cadherin) [1, 35, 49-52].

Genetic mutational analysis is hindered by small sample size and the heterogeneous nature of tumours studied. There is associative evidence that polymorphisms in key pathway genes may be implicated including biliary transporter proteins such as

ATP8B1 [53], and hepatocyte metabolic enzymes including CYP1A2 and NAT2 [54]. Activating mutations of KRAS (22% overall incidence in studies, range 5-57% - unlike pancreatic cancer where mutations are present in >90% [55]), BRAF (7% overall, 1-22%), Epidermal Growth Factor Receptor (EGFR) (2% overall, range 0-20%) and IDH1/2 (14% overall) have been identified. Additionally, loss-of-function mutations of p53 (15% overall, range 0.7-37%) have been reported for intrahepatic CCA (Studies summarised in [49]). The contributory significance of these different mutations is not yet clear. However, mutation of p53 is known to play a role in cholangiocarcinogenesis in experimental models [56, 57].

Chromosomal aberrations in CCA have been infrequently studied, with reports relying on small data sets and different ethnicities. The largest study to date analysed 149 intrahepatic CCA lesions in the United States and Europe, identifying gains at 1q and 7p, with losses for 3p, 4q, 6q, 13q, 14q, 17p and 21q chromosomes [58].

Aberrant epigenetic regulation of CCA through promotor hypermethylation and micro ribonucleic acic (miRNA) dysregulation has been identified, in a similar fashion to other solid organ tumours. Aberrant methylation of genes include SOCS-3 (implicated in IL-6/STAT3 activation, 27% of CCA tumours), $p14^{ARF}$ (prevents p53 degradation and therefore cell cycle arrest, 18% CCA), and RUNX3 (42% CCA). Specific tumour suppressor genes that appear to be hypermethylated include $p16^{INK4a}$/CDKN2 (47% CCA), RASSFA1A (56%) and APC (29%) (summarised in [49]). A panel of 38 miRNAs has been identified in a small number of intrahepatic CCAs with interactions with key signalling pathways including HGF/MET and IL-6/STAT3[59]. Specific miRNAs such as mir-214[60], mir-21[61] and miR-200c[62] have also been shown to correlate with poor prognosis in intrahepatic CCA. However, these data remain small scale and preliminary and, as such, should be interpreted with caution[49].

Selected dysregulated signalling pathways in cholangiocarcinogenesis

Multiple pathways are known to be dysregulated during carcinogenesis. Some of the pathways have been identified as playing a role in development of CCA.

Hedgehog signalling: These pathways are important in embryogenesis, wound healing and stem cell homeostasis [63]. Subtypes include sonic hedgehog, Indian hedgehog and desert hedgehog. Dysregulation of hedgehog pathways has been associated with a broad range of malignancies [64]. Hedgehog receptors comprise Patched and Smoothened which, when canonical or non-canonical ligands bind, result in nuclear localisation of the transcription factor Glioma-associated oncogene homologue and subsequent downstream pathway activation. Hedgehog signalling components have been found to be associated with poor outcomes and metastases in human intrahepatic CCA specimens [65]. In co-culture *in vitro* models, hepatic stellate cells appear to drive CCA cell line growth, migration and invasion through hedgehog-mediated pathways [66]. As such, this pathway represents a potential therapeutic target in CCA.

Interleukin-6 /signal transducer and activation of transcription (Il-6/STAT) signalling: IL-6 is a known mitogen that is secreted in inflammatory conditions, is upregulated in biliary inflammatory disorders and CCA [67, 68] and is known to be a critical signaling molecule in other human cancers [69]. Interleukin-6 drives growth of malignant cholangiocytes [70] and interacts with multiple cell cycle pathways. Interleukin-6 binds to gp130 receptor which activates the Janus kinase (JAK)/STAT3 pathway and so drives expression of multiple genes essential for cell growth, differentiation, proliferation, and resistance to apoptosis [71]. Interleukin-6 activates p44/p42 and p38 mitogen-activated protein kinases (MAPKs)[67] which are critical for cholangiocyte proliferation. In addition to a direct effect of inflammation on IL-6 expression, it is possible that IL-6 is upregulated in CCA as a result of SOCS-3 epigenetic silencing[70].

Epidermal growth factor receptor: Members of the EGFR family (particularly EGFR and ERBB2 [HER-2/neu]) are associated with CCA. Over-expression has been reported in 10-32% of CCA [49, 72] and is thought to be due to a loss of internalisation of the ligand-receptor complex (and thus loss of homeostatic receptor inactivation). Experimental inhibition of EGFR signalling downregulates CCA growth *in vitro* [73]. EGFR and ERBB2 drive COX-2 expression in CCA through activation of p44/p42 and p38 MAPKs. COX-2 expression inhibits apoptosis and promotes cell growth in CCA [1].

Hepatocyte growth factor/c-Met signalling: Hepatocyte growth factor expression by CCA cells and overexpression of the c-Met receptor has been noted in intrahepatic CCA[74]. Experimental studies have identified autocrine stimulation of CCA growth [75] and invasion [76] as a result of HGF-c-Met signalling. Furthermore, HGF/c-Met activation triggers MAPK, PI3K/AKT and STAT signalling cascades (similar targets of IL-6 and EGFR signalling) [49, 77].

A complex network of signalling pathways has emerged, many of which interact with each other and have similar effective outputs. IL-6, EGFR and HGF pathways all interact with COX-2, MAPK, PI3K/AKT and STAT signalling systems. These pathways have all been found to promote different aspects of CCA cell survival and proliferation. Furthermore, there are complex relationships between the main signalling pathways as illustrated by activating mutations of EGFR that drive IL-6 signaling in lung cancer[78], promoting lung cancer growth. IL-6 is thus both up- and downstream of other key oncogenes [1].

A potential additional signalling mechanism that may interact with these systems is the Notch pathway. Inducible Nitric Oxide Synthetase is associated with Notch1 signaling in CCA where Notch1 appears to confer resistance to apoptosis. Notch1 upregulation by iNOS appears to be mediated through the JAK/STAT pathway (via c-Jun N-terminal kinase; JNK), but not MAPK or COX-2 pathways[79]. For example, IL-6 is known to drive expression of Notch-3 (a potent stem cell regulator) in breast cancer [80]. Epidermal growth factor receptor pathways are closely related to Notch

signalling as Notch receptors have multiple EGFR repeats in their extracellular components [81], both pathways exert activity through gamma-secretase [82] and Notch-1 signalling mediates control over EGFR signalling via p53 [83].

Clinical Presentation and Diagnosis

CCA typically presents at a late stage when treatment options are limited and the prognosis for patients is dismal. Patients with extrahepatic or hilar lesions manifest clinically with features of obstructive jaundice, including icterus, pruritis, steatorhoea and dark urine (conjugated bilirubin) whereas weight loss and pain are late features. Conversely, patients with intrahepatic CCA (or hilar lesions with only one duct occluded) more commonly display abdominal pain or systemic features of malignancy such as malaise and weight loss. Furthermore, a sizeable proportion of lesions are detected incidentally whilst investigating other symptoms.

There are no diagnostic blood investigations for CCA. Liver function tests may be deranged with an obstructive pattern (raised alkaline phosphatase, bilirubin and gamma glutamyl transpeptidase). Aminotransferases may also be raised in acute obstruction or cholangitis. Furthermore, derangements of clotting profiles (prolonged prothrombin time) or reduction in fat-soluble vitamins (A, D, E, and K) may arise from chronic obstruction. Systemic malignancy-related abnormalities include reduced albumin, lactate dehydrogenase and anaemia [84]. There are no serum tumour markers specific for CCA. Markers such as carbohydrate antigen 19-9 (CA19-9; 85% of patients), carcinoembryonic antigen (CEA; 40-50%) and carbohydrate antigen 125 (CA 125; 30%) may be elevated in CCA [85]. Although CA19-9 is raised in the majority of patients with CCA and is currently the most useful tumour marker, it does not distinguish between CCA, pancreatic, or gastric malignancy and may also be elevated in severe hepatic injury from any cause (including obstructive jaundice) [35]. CA19-9 may be useful in identifying patients with PSC who proceed to develop CCA as when measured at 100 U/mL it has a sensitivity of 75% and specificity of 80% for CCA in PSC [86]. However, the sensitivity falls to 53% in patients without

PSC, with a specificity of 76% and 92% when compared against non-malignant liver disease and benign bile duct strictures respectively [87]. Currently, it is recommended that a panel of serum markers be assessed but that diagnosis should not be based on the results [85]. Other serum markers, such as serum cytokeratin-19 fragment (CYFRA 21-1) and CA242, have been reported to have higher specificities than CA 19-9 for intrahepatic CCA in a limited number of studies, but are not in routine use [7, 88-90].

As an initial diagnostic tool, the majority of patients undergo upper abdominal ultrasound scanning to identify the presence of biliary tree dilatation, cholelithiasis and mass lesions. Computed tomography (CT) scanning identifies lesions with more accuracy and is useful for tumour staging [91]. However, magnetic resonance (MR) imaging is the modality of choice for suspected CCA [92], delineating hepatobiliary anatomy and the local extent of the tumour, hepatic parenchymal abnormalities and the presence of liver metastases. The extent of bile duct involvement is identified by MR cholangiopancreatography (MRCP) and hilar vascular invasion is studied using MR angiography. Combined positron emission tomography and computed tomography (PET-CT) with [^{18}F]-fluorodeoxyglucose provides both metabolic and anatomic information and has high sensitivity and specificity for intrahepatic CCA and distant metastases but lower accuracy for extrahepatic lesions and locoregional lymph nodes [93]. Sensitivity and specificity of integrated PET-CT in identifying primary lesions is reported as 93% and 80% for intrahepatic CCA but as low as 55% and 33% for extrahepatic CCA [94]. Currently, this modality is only used in a clinical trial setting or in specific clinical cases, for example when attempting to elucidate whether a bile duct stricture is benign or malignant.

Tissue diagnosis is important both for diagnostic certainty and for planning of chemotherapeutic trials. However, it is not essential before surgery and UK guidelines recommend avoidance of open or percutaneous biopsy techniques in potentially curable patients due to the risk of tumour seeding [85, 86]. The Mayo Clinic, Rochester does not perform transperitoneal biopsies where curative strategies may be employed in order to avoid tumour cell seeding along the needle track [95]. Staging laparoscopy may be employed to determine the presence of peritoneal or superficial

liver metastases in those considered resectable on imaging, as additional criteria of unresectability are identified in one third of cancers [96]. Where appropriate, endoscopic retrograde cholangiopancreatography (ERCP) or percutaneous transhepatic cholangiography (PTC) may be used for tissue acquisition, and epithelial brushings or bile samples may be obtained for cytology and fluorescent in situ hybridisation (FISH) studies. Confident diagnosis of malignancy is difficult and a negative result does not exclude CCA. Indeed, brush cytology is positive in only 15-70% of CCA [97, 98], with FISH appearing to improve diagnostic sensitivity in lower yield diagnostic series [98]. Endoscopic ultrasound is useful in the assessment of distal extrahepatic lesions, can identify local lymphadenopathy, and with fine needle biopsy may be more sensitive and less likely to contaminate the biliary tree than ERCP with brushings [99]. Diagnostic cholangioscopy (e.g. Spyglass^{TM}) appears to have significantly higher sensitivity and overall accuracy than conventional ERCP-guided cytology brushings and standard forceps biopsies in the assessment of indeterminate biliary lesions [100, 101]. Novel imaging modalities such as confocal laser endomicroscopy [102] and light scattering low-coherence enhanced backscattering spectroscopy (LEBS)[103] remain experimental but have potential for *in situ* diagnosis of CCA

Staging of CCA

Staging of the anatomical extent and spread of CCA lesions is necessary to determine therapeutic options and estimate disease prognosis. Inaccurate staging may result in inappropriate selection of treatment that either deprives patients of a potentially curative procedure or exposes them to undue morbidity and mortality. Additionally, staging assists in evaluation of intervention, facilitates the exchange of information between treatment centres and contributes to the study of cancer.

Several distinct classification systems exist for subtypes of CCA. There are three main staging systems for intrahepatic CCA – the AJCC/UICC TNM system [6], the LCSGJ system [104] and the National Cancer Centre of Japan (NCCJ) staging system

[105]. The main difference between the systems is the weighting placed on the T stage of the tumour, in terms of the significance of size, number of lesions and vascular invasion[7]. The performance of these systems has been studied by analysing the outcomes of 598 surgically treated, microscopically confirmed cases of intrahepatic CCA from the Surveillance, Epidemiology and End Results (SEER) database [106]. Although the LCSGJ system was found to identify no difference in survival between different T states, when all three systems and a modified version of the AJCC/UICC TNM system (6th edition) – where the significance of tumour size and multiple tumours was removed – were analysed, they performed comparably to each other in overall predictive value.

With regard to hilar CCA, systems that have failed to demonstrate accurate predictive value include the Memorial Sloan-Kettering Cancer Center system [107]. Two newer staging systems have been proposed – from the Mayo Clinic [108], and from an international working group co-ordinated from Zurich [109] – but these have yet to be externally validated. There are no isolated staging systems for distal extrahepatic CCA.

The most commonly used staging system for CCA is the AJCC/UICC TNM classification system that considers the extent of the tumour (T), lymph node involvement (N) and the presence of metastasis (M)[6]. Prior to treatment, a clinical classification (TNM or cTNM) is used to select the most appropriate treatment strategy based on imaging and biopsies. Pathological classification is only possible following tissue diagnosis from a resection specimen (pTNM). The TNM score is then converted to a Stage (0-IV).

Importantly, the new 7th edition of the AJCC/UICC TNM Manual [6] considers intrahepatic CCA and extrahepatic CCA separately, with a further subdivision of extrahepatic CCA into hilar and distal lesions. Of note, 5% of extrahepatic cholangiocarcinomas are multifocal. Assessment of the 7th edition suggests it accurately predicts survival in resectable intrahepatic lesions, provided lymphadenectomy has been performed [11]. Inevitably, groups have proposed further

modifications [110], which will likely be assessed in future iterations of the Manual. However, the 7th edition represents the most widely accepted staging system internationally. In view of the practical necessity for oncologists and surgeons to co-operate within the broader remit of trials and studies of gastroenterological cancers in general, it is the system which is most likely to benefit from further refinement, with an emphasis on improving pre-operative staging accuracy in order to optimise stratification of therapy.

With respect to CCA in broad terms, stage 0, I and II are potentially curative whereas III and IV are considered surgically irresectable [111].

Figure 1.5 – TNM 7th edition staging of CCA.

Surgical Treatment of CCA

Complete surgical resection of the tumour (an R0 resection is defined as a 5mm tumour free resection margin) is the only broadly available curative strategy but this is suitable for only 6.3% of patients [112]. The Bismuth classification is most commonly used to determine the surgical approach undertaken dependent upon the anatomical features of the lesions (Fig 1.2B.) Even for "resectable lesions", post-surgical five year survival rates range from 11-44% depending on anatomic location of the tumours and the treatment series [1]. Five-year survival rates following resection of intrahepatic CCA, distal extrahepatic CCA and hilar tumours are 22-44%, 27-37% and 11-41% respectively [85, 113, 114]. Recent multi-centre data identified that median survival for intrahepatic CCA after surgical resection was 27.3 months. One-, 3-, and 5-year overall survival was 77.5%, 44.3%, and 30.7%, respectively[115].

There is no role for liver transplantation to treat intrahepatic lesions due to rapid recurrence [116], neither is transplantation suitable for distal extrahepatic lesions where resection remains the most appropriate strategy with curative intent. However,

Figure 1.5: AJCC 7th Edition TNM Classification of CCA

TNM Classification for Intrahepatic CCA

Primary Tumour (T)

Tx	Primary tumour cannot be assessed
T0	No evidence of primary tumour
Tis	Carcinoma *in situ* (intraductal)
T1	Solitary tumour, no vascular invasion
T2a	Solitary tumour, vascular invasion
T2b	Multiple tumours (+/- vascular invasion)
T3	Tumour perforating visceral peritoneum or directly invading local extra-hepatic structures
T4	Tumour with periductal invasion

Regional Lymph Nodes (N)

Nx	Regional lymph nodes cannot be assessed
N0	No regional lymph node metastasis
N1	Regional lymph node metastasis identified

Distant Metastasis (M)

M0	No distant metastasis
M1	Distant metastasis identified

Stage Grouping

Stage 0	Tis	N0	M0
Stage I	T1	N0	M0
Stage II	T2	N0	M0
Stage III	T3	N0	M0
Stage IVA	T4	N0	M0
	AnyT	N1	M0
Stage IVb	AnyT	AnyN	M1

TNM Classification for Distal Extrahepatic CCA

Primary Tumour (T)

Tx	Primary tumour cannot be assessed
T0	No evidence of primary tumour
Tis	Carcinoma *in situ* (limited to mucosa)
T1	Tumour histologically confined to bile duct
T2	Tumour invades beyond wall of bile duct but no further
T3	Tumour invades gallbladder, pancreas, duodenum, or other adjacent organs but no involvement of coeliac axis or superior mesenteric artery
T4	Tumour involves coeliac axis or superior mesenteric artery

Regional Lymph Nodes (N)

Nx	Regional lymph nodes cannot be assessed
N0	No regional lymph node metastasis
N1	Regional lymph node metastasis identified

Distant Metastasis (M)

M0	No distant metastasis
M1	Distant metastasis identified

Stage Grouping

Stage 0	Tis	N0	M0
Stage IA	T1	N0	M0
Stage IB	T2	N0	M0
Stage IIA	T3	N0	M0
Stage IIB	T1	N1	M0
	T2	N1	M0
	T3	N1	M0
Stage III	T4	AnyN	M0
Stage IV	AnyT	AnyN	M1

Edge SB, Byrd DR, Compton CC, Fritz AG, Greene FL, Trotti A. American Joint Committee on Cancer. *AJCC Cancer Staging Manual*. 7th ed. New York, NY: Springer; 2010: 201-205; 219-230.

TNM Classification for Extrahepatic Hilar CCA

Primary Tumour (T)

Tx	Primary tumour cannot be assessed
T0	No evidence of primary tumour
Tis	Carcinoma *in situ*
T1	Tumour histologically confined to bile duct to muscularis or fibrous layer
T2A	Tumour invades beyond wall of bile duct into surrounding adipose tissue
T2B	Tumour invades adjacent hepatic parenchyma
T3	Tumour invades unilateral branches of hepatic artery or portal vein
T4	Tumour invades main portal vein or branches bilaterally; or common hepatic artery; or second-order biliary radical bilaterally; or unilateral second-order biliary radicals with contralateral portal vein or hepatic artery involvement

Stage Grouping

Stage 0	Tis	N0	M0
Stage I	T1	N0	M0
Stage II	T2A/B	N0	M0
Stage IIIa	T3	N0	M0
Stage IIIb	T1	N1	M0
	T2	N1	M0
	T3	N1	M0
Stage IVa	T4	N0/1	M0
Stage IVb	AnyT	N2	M0
	AnyT	AnyN	M1

Regional Lymph Nodes (N)

Nx	Regional lymph nodes cannot be assessed
N0	No regional lymph node metastasis
N1	Regional lymph node metastasis identified (including nodes along the cystic duct, common bile duct, hepatic artery, and portal vein)
N2	Metastases to periaortic, pericaval, superior mesenteric artery, and/or celiac artery lymph nodes

Distant Metastasis (M)

M0	No distant metastasis
M1	Distant metastasis identified

Edge SB, Byrd DR, Compton CC, Fritz AG, Greene FL, Trotti A. American Joint Committee on Cancer. *AJCC Cancer Staging Manual*. 7th ed. New York, NY: Springer; 2010: 201-205; 219-230.

liver transplantation with neo-adjuvant chemoradiotherapy for localised, irresectable hilar CCA is a controversial option that shows promise in experienced hands [117]. The technique has been pioneered at the Mayo Clinic, Rochester. The authors report a 54% 5 year survival for patients selected to enter into the transplant programme and a 73% 5 year survival following liver transplantation. Early attempts by a small number of institutions failed to replicate the apparently excellent results from the Mayo Clinic. Explanations may include local deviations from the Mayo protocol, such as pre-operative biopsying and a lower completion rate of neo-adjuvant brachytherapy[118]. A recent analysis of data from 12 transplant centres in the United States reviewed the outcomes of 287 patients treated for CCA (216 patients transplanted, 71 dropped out). 193 patients were from the Mayo Clinic, although survival rates were reported as similar across all centres. The overall 5 year survival was 53% whereas the post-transplant five year recurrence free survival was 65% [119].

Figure 1.6 – Mayo Clinic Transplant Protocol for Hilar CCA

Patients who require extended hepatectomy with a predicted future liver remnant of less than 25% benefit from ipsilateral portal vein embolisation to induce compensatory hypertrophy in the presumptive remnant. This has reduced the incidence of liver failure in extended hepatectomy from 20% to 6% [120]. Pre-operative jaundice is associated with poor post-operative outcomes from major hepatectomy for CCA, however pre-operative biliary drainage does not improve survival [121] and reduced survival from pre-operative percutaneous transhepatic biliary drainage have been noted by some groups [122]. Adjuncts such as pre-operative biliary drainage to mitigate the effects of distal obstructions causing cholestasis and liver failure should be avoided as there is no evidence of survival benefit, [123, 124] but instead a significantly increased risk of septic complications of the biliary tree due to instrumentation (74% in patients undergoing biliary drainage compared with 39% in those proceeding straight to surgery) [124]. However, biliary drainage should still be considered for those who are severely malnourished or have acute suppurative cholangitis but remain candidates for surgical resection [85, 125, 126].

Figure 1.6: Mayo Clinic protocol for liver transplant treatment of hilar CCA

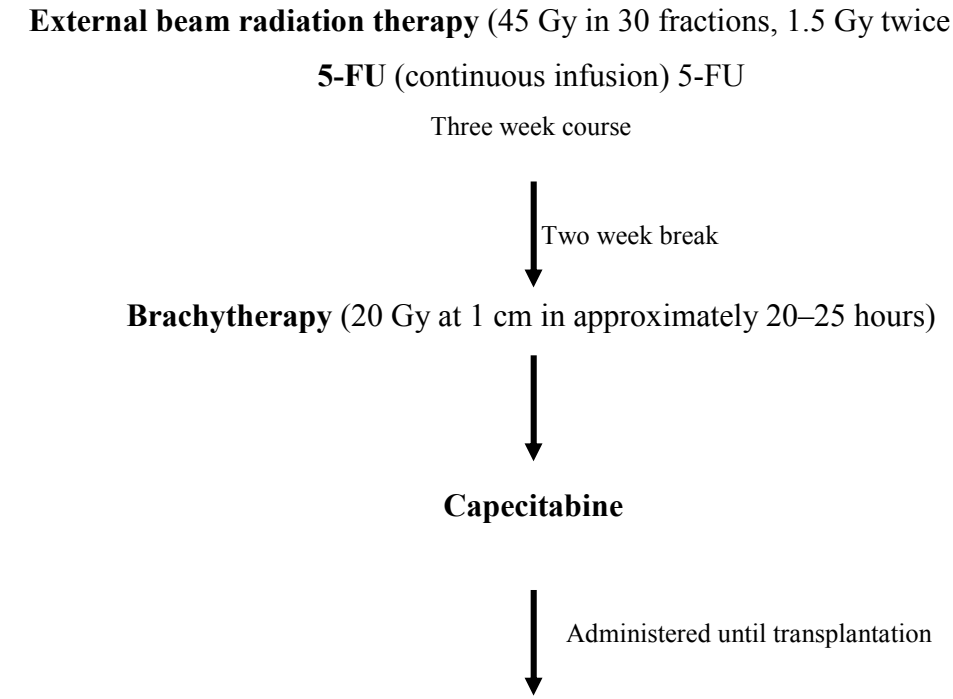

Analysis of 12 USA transplant programmes identified that for patients treated as above, the overall 5 year survival was 53% whereas the post-transplant five year recurrence free survival was 65% (Darwish Murad Gastroenterology 2012;143:88-98)

Palliative Strategies in the management of CCA

For the overwhelming majority of patients for whom treatment with curative intent is not available, given the short life expectancy, the goal of care should be focused first on quality of life and relief of symptoms (pain, pruritis, jaundice) and second on extending survival. When a patient is deemed irresectable, the diagnosis should ideally be confirmed by biopsy in order to assist in palliative chemotherapy and/or radiation therapy [125]. Relief of jaundice is undertaken by operative biliary-enteric bypass or biliary stenting. Biliary stents may be placed via either ERCP or PTC. Metal stents have more favourable cost outcomes if the patient is expected to survive longer than six months [127]. Semicovered stents appear to have superior patency rates to uncovered metal stents [128].

Photodynamic Therapy

Photodynamic therapy (PDT) for irresectable biliary tract cancers involves photosensitisation with intravenous haematoporphyrin followed by endoscopically delivered local photoirradiation with a laser. Early, small studies suggested that PDT for irresectable extrahepatic lesions improved survival compared to biliary stenting alone [129, 130]. Survival was shown to be 16.4 months v 3.3 months [129] and 21 months v 7 months [130]. Post-procedural cholangitis is a common complication [102]. However, the United Kingdom Photostent-02 trial, which aimed to recruit 240 patients, closed early at 92 participants. This study identified poorer survival outcomes for PDT plus stenting (5.6 months) versus stenting alone (8.5 months) with a Hazard Ratio of 1.6 (corrected for chemotherapy)[131]. Reasons for the excess risk from PDT are not currently clear but PDT cannot currently be recommended for routine use.

Chemoradiotherapy

There is no current evidence to support the use of adjuvant chemotherapy or radiotherapy in resectable tumours [85]. There are a number of actively recruiting

registered therapeutic studies: chemotherapy (26 trials), radiotherapy (9), RFA (6), PDT (2), chemotherapy and liver transplantation (2), and biological therapy (2). (A search of clinicaltrials.gov on 11 July 2013 with search terms cholangiocarcinoma OR bile duct cancer, followed by a manual search, excluding closed or unknown trial status). There is no evidence to support adjuvant (post-operative) chemotherapy or radiotherapy outwith the clinical research trial setting, given the poor outcomes currently obtained [22]. The BILCAP trial is currently recruiting in the United Kingdom - a randomised clinical trial evaluating adjuvant capecitabine chemotherapy (oral 5-fluorouracil) compared to expectant treatment alone following surgery for biliary tract cancer. The trial is expected to report in 2015. There are currently no robust data addressing the effect of neoadjuvant (pre-operative) chemotherapy.

Until recently, for patients with inoperable CCA, chemotherapy was not routinely employed due to poor results and small studies. In 2010, the Advanced Biliary Cancer -02 (ABC-02) trial of cisplatin with gemcitabine was shown to provide a survival advantage of 3.6 months over gemcitabine alone for patients with locally advanced or metastatic biliary tract cancer (11.7 v 8.1 months) [132] without the addition of significant toxicity. This regime shows an equivalent cost-effectiveness compared to gemcitabine alone [133] and has now been recommended for patients with locally advanced or metastatic irresectable CCA in the United Kingdom [85] .

Radiotherapy may be delivered as external beam, intraluminal brachytherapy (via drains) or radioactive spheres [134]. Although some studies have demonstrated the utility of adjuvant external beam radiotherapy in CCA, large prospective randomised studies are limited and convincing evidence for radiation therapy as a standard adjuvant treatment for CCA is lacking. There is also currently no evidence to support adjuvant external beam radiotherapy in patients with negative resection margins [135] [136]. Similarly, in patients with irresectable disease, although retrospective USA SEER database studies have suggested prolonged survival for intrahepatic CCA[137] and extrahepatic CCA[138] when external beam radiotherapy is combined with biliary tract stenting compared to stenting alone, robust clinical trial data are not available.

Radiotherapy is not recommended outwith a clinical trial setting. Radiotherapy may however have palliative value, for example in treating localised metastases or uncontrolled bleeding [85].

Other Therapeutic Strategies

Other strategies currently employed in hepatocellular carcinoma and colorectal hepatic metastases have been assessed in irresectable CCA. These techniques remain essentially experimental for CCA and include transcatheter arterial chemoembolisation [139, 140], radiofrequency ablation (RFA)[141] and microwave ablation of tumours, and radioembolisation using (90)Y microspheres[142]. Early data show potential promise but no formal trial data yet exist.

There is increasing interest in the applicability of targeted biological agents such as inhibitors of the IL-6, VEGF, EGFR, ERBB2 and HGF/c-Met signalling pathways that are upregulated in CCA. Examples include the Advanced Biliary Cancer-03 (ABC-03) trial, which is a randomized, phase II/III study of cediranib (AZD2171 – VEGF receptor tyrosine kinase inhibitor) or placebo in combination with cisplatin/gemcitabine for patients with advanced biliary tract cancers[143].

Figure 1.7 - Signaling pathways and molecular therapies in intrahepatic CCA, together with a summary of current trials.

Given the current dismal clinical outcomes, further research to clarify the biology of CCA is urgently required to develop targeted therapies. Solid organ tumour biology is being gradually understood; multiple therapeutic targets exist, not only in terms of cellular pathways of malignant cells, but also focused targeting of cancer stem cells and non-malignant cells within the tumour mass that serve to promote tumour growth and worsen outcomes.

Figure 1.7: Signalling Pathways and Molecular Therapies in Intrahepatic CCA
Summary of ongoing Phase II/III trials using targeted therapy.
(Adapted from Sia Jan 2013 Oncogene, onc2012617 [pii] 10.1038/onc.2012.617)

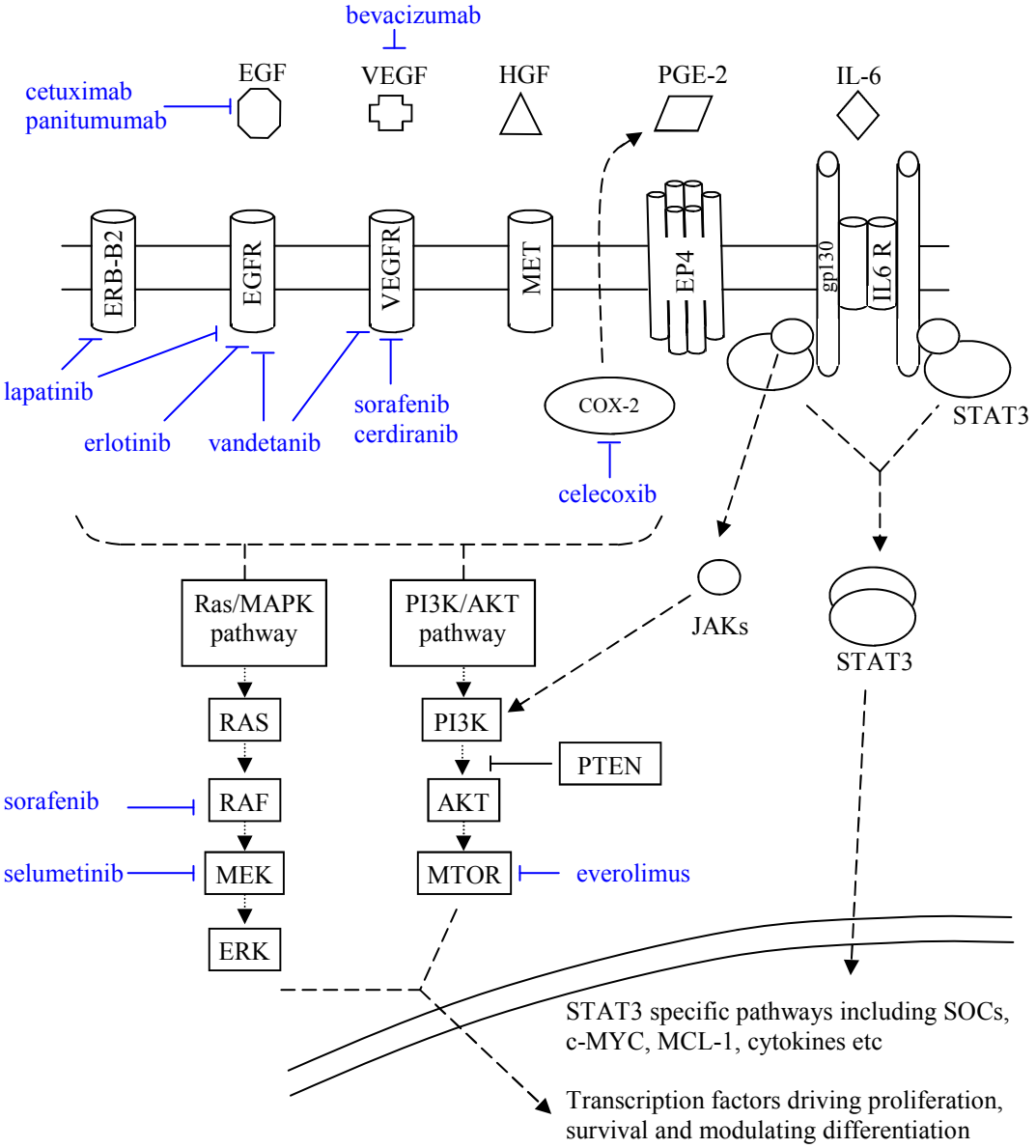

Treatment	Targets	Clinical Phase	No of Trials	Trial Type
everolimus	mTOR	II	2	NRCT
chemo+/- cetuximab	EGFR	II	2	NRCT/RCT
chemo +/- panitumab	EGFR	II	5	NRCT/RCT
chemo +/- bevacizumab	VEGF-A	II	2	NRCT
chemo+/- cediranib	VEGFR	II , II/III	2	NRCT/RCT
chemo +/- vandetanib	VEGFR, EGFR	I , II	2	NRCT/RCT
chemo + sorafenib	BRAF, VEGFR, PDGR	I , II	1	NRCT
chemo + selumetinib	MEK 1/2	I , II	1	NRCT

Chemotherapy regimes include gemcitabine, cisplatin and mFOLFOX

2. The Tumour Microenvironment in Solid Organ Malignancies:

Chronic inflammation in the microenvironment around cancer cells promotes proliferation, drug resistance and angiogenesis.

Solid organ tumours are heterogeneous three-dimensional structures consisting of malignant cancer cells couched in a tissue stroma. This specialised microenvironment bears striking similarities to an on-going wound reaction [144]. The cellular elements of the tumour stroma include fibroblasts, myofibroblasts, immune cells (tumour-associated macrophages, lymphocytes, mast cells), vascular cells (endothelial cells, pericytes, smooth muscle cells), and adipocytes. These are embedded within a modified ECM. Furthermore, the tumour niche is rich in inflammatory profibrotic and angiogenic cytokines [145]. Indeed, the cytoarchitectural features and mechanisms of tumour development comprise a disordered form of organogenesis, prompting some commentators to argue that solid tumours should be viewed as neo-organs [146]. Histologically, CCAs are characterised by the presence of an extensive tumour stroma[147], but relatively little is known about the specific roles played by the stromal elements in CCA lesions.

The tumour stroma plays an important role in cancer progression and metastasis with complex bidirectional interplay between tumour cells and their niche elements. Tumour stroma is rich in two predominant cell types - myofibroblasts and tumour associated macrophages. The overall mechanism by which the tumour stroma promotes cancer growth is due to an unintended consequence of the homeostatic role played by stromal elements (both cellular and ECM) in attempting to re-establish tissue healing. Although this is a desired process in damaged, inflamed tissue (whether the induced injury is infective, traumatic or hypoxic), in tumours this is a maladaptive process due to the persistence of malignant cells that take advantage of the restorative mileau with the result that tumour growth is promoted by the “healing stroma”.

Figure 1.8: Macroscopic and microscopic features of human intrahepatic CCA

Figure 1.8: Macroscopic and microscopic features of human intrahepatic CCA

A and B: Intrahepatic mass forming CCA; **C and D**: Hilar periductal infiltrating CCA;
E and F: Intrahepatic Intraductal/Papillary CCA

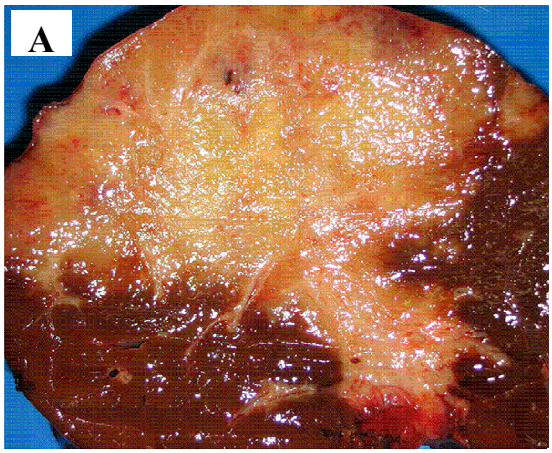

Peripherally located, mass forming lesion with dense stromal contribution

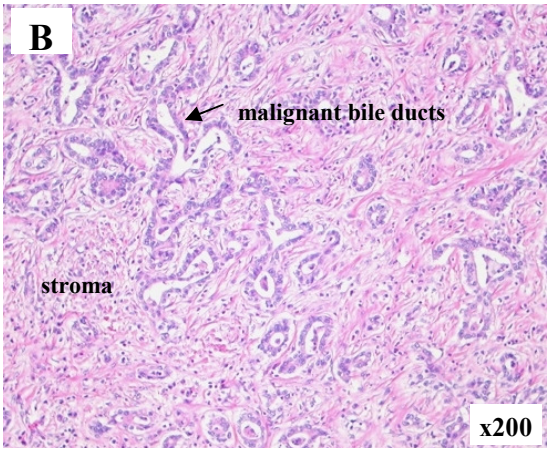

Well differentiated adenocarcinoma with infiltrating stromal cells and extracellular matrix

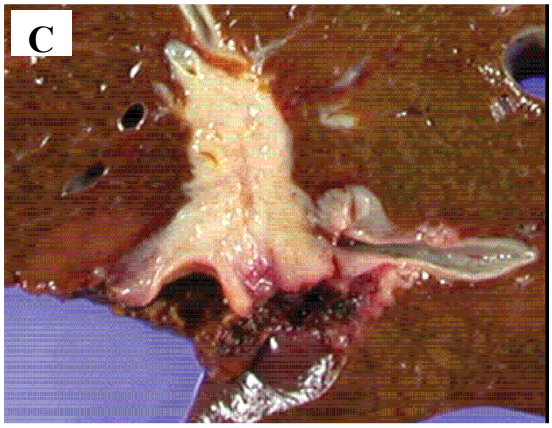

Elongated and branchlike tumour along the bile duct

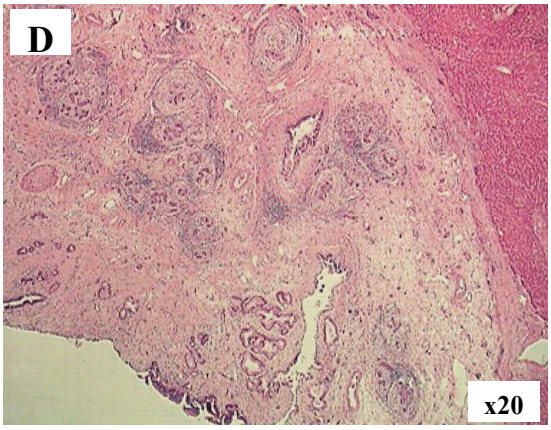

Well-differentiated adenocarcinoma confined to periductal connective tissue

Dilated bile duct, multiple impacted small polypoid lesions representing tubular carcinomas

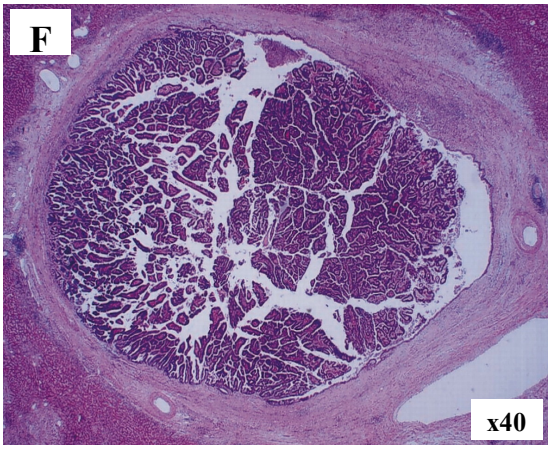

Dilated duct filled with a papillary tumour. Tumour predominantly confined within the ducts. Some focal areas of stromal invasion

Image Sources:

A: Sripa B. PLoS Neglected Tropical Dis 2008.

B: Enjoji M, Aishima S. Liver: Intrahepatic cholangiocarcino. Atlas Genet Cytogenet Oncol Haematol. January 2008 . URL : http://AtlasGeneticsOncology.org/Tumors/IntraCholangioCarID5330.html.

C, E: Used with permission from
Figures 10b, 12b, 14c
Chung Y E, Kim M-J, Park Y N, et al. Varying appearances of cholangiocarcinoma: radiologic-pathologic correlation. *Radiographics* 2009;29:683-700.

D, F: Used with permission from
Figures 4d, 5d
Han J K, Choi B I, Kim A Y, et al. Cholangiocarcinoma: pictorial essay of CT and cholangiographic findings. *Radiographics* 2002;22:173-187.

Extracellular Matrix in health and malignancy

The extracellular matrix in normal tissues comprises of basement membrane and interstitial matrix. The basement membrane is produced jointly by epithelial/endothelial and stromal cells to separate epithelium/endothelium from stroma, whereas the interstitial matrix is primarily made by stromal cells and contributes to the tensile strength of tissues. Basement membrane (collagen IV, laminins, fibronectin, and linker proteins such as nidogen and entactin, which connect collagens with other protein components) is more compact and less porous than the highly charged and hydrated interstitial matrix (fibrillar collagens I [the main constituent], III, V and XI, proteoglycans, and glycoproteins such as tenascin C and fibronectin) [148]. In addition to determining tissue stiffness, the ECM acts to provide cellular anchorage within tissues and control cell migration (either by inhibiting it or by permissively enabling migration routes). The ECM also acts as an extracellular reservoir of signalling molecules, creating signalling concentration gradients (e.g. sonic hedgehog in limb bud development [149]) and acting as a pool of cytokines that may be released upon remodelling of the ECM (e.g. VEGF-A) [150]. The ECM can present matrix-bound signalling molecules to cells (e.g. matrix-bound transforming growth factor β, TGFβ [151]) and also act as a co-signaller in concert with matrix-bound ligands (e.g. fibroblast growth factor, FGF) signalling requiring heparin sulphate as a cofactor [152]). This relationship is bidirectional, as growth factors such as TGFβ also regulate the ECM itself by increasing target cell production of ECM components or enhancing synthesis of matrix degrading enzymes [153]. These matrix breakdown products themselves (derived from the remodelling action of MMPs) act as behavioural signals to tissue cells [154]. Cells bind to the ECM through focal adhesion complexes (integrins and an aggregation of adaptors and signaling proteins) that may be viewed as mechanosensors linking the cellular cytoskeleton with the ECM [148] and reacting dynamically to changes in ECM tension, such as changes in stiffness/tension that control cell polarity and phenotype [155].

In the inflammatory microenvironment of cancer, the normal composition of the ECM is radically altered due to the behaviour of stromal cells (predominantly

fibroblasts but also macrophages) that act within the initially inflammatory response followed by the "healing" phenotype of the microenvironment. ECM is thus generated that abnormally persists. The tumour-associated ECM differs from the basement membrane and interstitial matrix of healthy organs both anatomically [156] and in terms of relative contribution of different components [157, 158]. The desmoplastic (or reactive) stroma of many advanced tumours demonstrate increased scar-associated fibrillar collagens (I and III predominantly) at the expense of basement membrane collagen (IV) [159]. These collagens are often linearised and crosslinked, which progressively stiffens the ECM [160] and induces diverse effects on cellular differentiation, gene expression, proliferation, survival and migration [155]. For example, linearized collagens appear to upregulate migratory capacities in cancer cells [160] that are able to rapidly transit along the neo-fibrils in a mechanism that is likely to be, at least in part, integrin-mediated [161]. Conversely, collagens act as an anatomical barrier to cell migration in health and disease, and therefore proteolytic degradation of ECM collagens are essential for tissue invasion in many solid cancers [162 163].

Several studies of different tumour types have demonstrated the role of ECM components in enhancing cancer cell tumourigenicity [164] and conferring resistance to chemotherapeutic agents [165, 166], mediated principally through integrin signalling. The ECM is an essential player in the physiological maintenance of stem cell niches, as evidenced by depletion of cell receptors such as integrins [167] or by modification of the components [168] or stiffness [169] of the ECM itself. This concept has been postulated to persist in cancer, which is in essence a disordered stem cell niche. It is possible that deregulated ECM dynamics within stem cell niches may lead to cancer stem cell overexpansion and loss of differentiation. This remains to be tested rigorously [148].

Physiological and tumour angiogenesis is in part directed and facilitated by the ECM. VEGF-A, a key regulator of angiogenesis, is ECM-bound [170] and released by macrophages degrading the matrix. Multiple proteolytic components of the ECM regulate angiogenesis [148] and indeed even stiffness (induced by tissue hypoxia that

upregulates cross-linking of the ECM via lysyl oxidase (LOX)-like protein-2 [171]). This upregulates neo-vascularisation. In acute inflammation, the proteolytic fragments of the "damaged" ECM act as chemoattractants for immune cells [172]. In established tumours, the ECM plays unclear roles in tumour immunity as the ECM upregulates T cells [173], but it is notable that collagen I (a key over-expressed component of tumour stroma), appears to inhibit the activation and cytotoxic tumour cell killing capacity of macrophages [148, 174], possibly through the leucocyte-associated immunoglobulin-like receptor-1 (LAIR-1) [175].

Fibroblasts in health and disease

Fibroblasts comprise the mesenchymal, non-vascular, non-epithelial and non-inflammatory cells of the connective tissue and are the major cellular contributor to this compartment [176]. Fibroblasts display remarkable heterogeneity across different organs [177] with differentially expressed genes (that control ECM synthesis, lipid metabolism, and cell signalling pathways) depending on anatomic location of the cells.

In health, fibroblasts play an important role in tissue homeostasis by controlling the phenotype of the ECM, in which they are embedded, bound to the ECM by receptors from the integrin, heparin sulphate and proteoglycan families [178]. The ECM is to a large extent synthesised by fibroblasts that produce components of both the basement membrane (Type IV collagen, laminin) and the fibrillar ECM (Type I, III & V collagens, fibronectin, proteoglycans) [177, 179-181]. In addition, fibroblasts remodel the ECM by producing MMPs and their inhibitors, tissue inhibitors of metalloproteinase (TIMPs) [177, 181]. Fibroblasts appear to play the major role in maintenance of interstitial pressure in normal tissues by actively regulating the tension applied to the ECM through collagen-binding β1 integrins that exert tension on the collagen microfibrillar network which in turn restrains the intrinsic swelling pressure of hyaluronin and proteoglycans in the ECM[182, 183]. Fibroblasts also play an important role in controlling epithelial morphogenesis as identified from skin models [184]. This

has been confirmed by the mouse "cleared mammary fat pad" model, where co-injection of human fibroblasts together with mammary breast epithelial cells is necessary to enable the transplanted epithelial cells to develop into breast epithelial structures [185].

In the context of inflammation and wounds, fibroblasts undergo a change from their normal relatively quiescent state, to a proliferative and contractile phenotype termed myofibroblasts, characterised by activated intracellular contractile element synthetic pathways such as α-smooth muscle actin (α-SMA) filaments[186]. Myofibroblasts play a prominent role in wound repair by migrating into damaged tissues in response to multiple growth factors including TGFβ1[187] platelet derived growth factor (PDGF), and FGF [188]. TGFβ signalling appears to play a cytodifferentiating rather than a proliferative role [189]. Although it is inhibitory to epithelial cell growth, TGFβ in the context of cancers has been found to be abundantly expressed as cancer cells "acquire resistance" to the inhibitory effects of TGFβ signalling and instead utilise the cytokine to promote their tumour stroma phenotype [190]. This is in contrast to PDGF, which appears to act as a mobiliser rather than a transformer of fibroblasts[189]. In wound healing, fibroblasts upregulate production of ECM components (especially collagens) that form a scaffold for other tissue healing cells [191], actively facilitate wound contraction [192] and promote other cellular contributors to the healing wound, such as keratinocytes in injured skin [193]. Following resolution of tissue injury, myofibroblasts regress at the wound site and basal conditions are restored [194], although it is unclear whether the myofibroblasts revert to fibroblastic phenotypes [195] or undergo apoptosis [196] followed by repopulation of fibroblasts in the previously injured tissue [180]. In persistent scars [197] and fibrotic tissue disorders such as idiopathic pulmonary fibrosis [198], these cells do not regress but persist. In cancer, a similar persistence of activated fibroblasts occurs at the tumour site [199] with concurrent production of ECM components, comprising the desmoplastic response to the lesion. Cancer-associated fibroblasts are commonly histologically identified by expression of α-SMA [179].

Cancer Associated Fibroblasts

Cancer-associated fibroblasts (CAFs) demonstrate significantly altered gene expression profiles in human specimens with changes in their expression profiles appearing to commence even at the carcinoma *in situ* stage (e.g. human breast cancer specimens) [200]. Intriguingly, CAFs appear to be essential for experimental tumour initiation and not simply proliferation, as shown by separate experiments in cleared mammary fat pads of mice and rats where activated myofibroblasts were required for breast tumour establishment whereas steady state fibroblasts were insufficient [185 201] despite the administration of malignant epithelial cells. These are separate studies to the co-administration of fibroblasts and non-malignant breast epithelial cells into cleared mammary fat pads described in the above paragraph "Fibroblasts in Health and Disease". The precise signals involved in this are as yet incompletely understood but CAFs appear to secrete tumour promoting cytokines including PDGF and HGF that encourage malignant cell growth [202 203]. For example, CAF-derived periostin, (PDGF)-BB, prostaglandin E2 (PGE2) and sphingosine-1-phosphate (S1P) have been identified as mediators of cancer cell survival and chemo therapeutic resistance [204].

Furthermore, CAFs are necessary for the progression of cancer. Although normal fibroblasts both accelerate tumour formation [205] and reduce the cell dose [206]required to form tumours in subcutaneous transplant models, a prostate cancer model has demonstrated the enhanced role of CAFs by directly comparing CAFs with normal fibroblasts: Significant tumour growth occurred when CAFs but not normal fibroblasts were admixed with prostate malignant epithelial cells in a subcutaneous transplant model [207]. A mechanism contributing to this may be the Stromal-cell Derived Factor/ Chemokine (C-X-C motif) ligand 12 (SDF-1/CXCL12) cytokine pathway whereby CAFs recruit endothelial cells into the stroma and direct cancer cell growth (as identified in transplanted MCF-7 breast cancer cells [208].) Chemokines that are known to be produced by CAFs including periostin, HGF, SDF-1, and Wnt-inducible signalling pathway 1v (WISP1v) [209]. These have all been shown to stimulate cell migration and invasion of various human CCA cell lines *in vitro* [204].

Myofibroblasts are one of the major sources of excess ECM deposition, especially collagens [210]. CAFs promote the invasive phenotype of cancer cells by secreting copious quantities of modified scar-associated ECM (that promotes survival in cancer cells) and by remodelling the ECM. For example, CAF-derived MMP1 activates proteinase-activated receptor 1 (PAR1) receptor in breast cancer cells, resulting in cell migration and invasion [211], whilst MMP3 cleaves E-Cadherin and drives epithelial-mesenchymal transition (EMT) in hitherto normal breast epithelial cells that acquire an invasive phenotype [179, 212]. Seprase, a CAF-derived protease that remodels the ECM, has been implicated in cancer progression and represents a cancer-specific potential target for therapy [213, 214]. Although incompletely understood, observations have been made of the enhancing role that fibroblasts play in establishment of successfully engrafted metastatic lesions in distant organs. Separate studies of experimental depletion of CAFs [215] and also a mouse model with attenuated fibroblasts (fibroblast-specific protein-1 (FSP-1) deficient fibroblasts) [216] resulted in reduced primary tumours and metastases.

Intriguingly, it has recently been observed that CAFs play a role in immune regulation of the tumour microenvironment. A subset of CAFs express fibroblast activation protein–α (FAP+). These cells in tumour stroma exhibit powerful immunosuppressive effects despite comprising only 2% of all tumour cells in established Lewis lung carcinomas. Experimental depletion of FAP+ cells caused rapid hypoxic necrosis of both cancer and stromal cells. These findings were replicated by depleting FAP-expressing cells in a subcutaneous model of pancreatic ductal adenocarcinomas [217]. Indeed the observations made in the experimental depletion of CAFs by Liao *et al* [215] found that depletion of CAFs resulted in an immunological polarisation in tumours from a T helpler cell type 2 (Th2) (humoral immunity, considered to be tumour permissive) to a Th1 (cell mediated immunity, cytotoxic to cancer cells)[218] phenotype. This resulted in suppressed recruitment of tumour-associated macrophages, myeloid derived suppressor cells, T regulatory cells, and decreased tumour angiogenesis and lymphangiogenesis. These immune modifications were thought to mediate the observed effects of CAF depletion.

Origins of Cancer Associated Fibroblasts

Cancer associated fibroblasts may be locally derived from adjacent normal tissue, may derive from the bone marrow or may arise as a result of EMT. Resident, or locally derived, cancer associated fibroblasts are mobilised by signalling factors as described above and transdifferentiate from quiescent fibroblasts to an activated myofibroblast phenotype.

Bone marrow derived fibroblasts arise from mesenchymal stem cells (MSC) in the bone marrow. Mesenchymal stem cells are less well understood than haematopoietic stem cells (HSC). Some argue that these cells should preferentially be termed mesenchymal stromal cells since cultured MSCs may comprise a number of cell type subsets and may be derived from other sources including adipose tissue, umbilical cord skin [219, 220] and tissue pericytes [221]. Mesenchymal stem cell characteristics specifically require the demonstrable ability to undergo differentiation into osteoblasts, chondrocytes, adipocytes and fibroblasts [222]. Mesenchymal cells play a regulatory role in the haematopoietic stem cell niche in bone marrow. Mesenchymal stem cells represent an extremely rare cell type within the bone marrow, comprising 0.01% to 0.001% of all mononuclear cells, compared to 1% for the HSC population [223, 224]. There is currently no definitive set of cell surface markers, but human MSCs are considered to be adherent to tissue culture plastic and comprise cluster of differentiation 34- (CD34-), CD45- cells that express a combination of CD44+, CD73+, CD90+ (Thy-1 surface antigen), CD105+, CD106+ (vascular cell adhesion molecule-1 [VCAM-1]), and STRO-1+ markers[225]. Bone marrow derived fibroblasts have been found to contribute to both organ fibrosis [226] and tumour stroma [227, 228] in variable quantities (discussed in more detail below).

Epithelial-mesenchymal transition is a process by which local epithelial cells progressively acquire mesenchymal properties including invasive behaviour and characteristic cell surface markers; it is an important mechanism through which malignant epithelial cells are able to facilitate invasion [229]. A number of triggers for EMT have been identified including hypoxia acting via the Twist pathway [230].

Transforming growth factor β signalling from CAFs appears to orchestrate EMT in established malignant epithelial cells in advanced cancers. These effects contrast with the antiproliferative and pro-apoptotic effect of TGFβ on normal epithelial cells [231]. Epithelial-mesenchymal transition may be a source of fibroblasts in the tumour stroma. The proportional contribution of EMT to the tumour burden of CAFs is likely to be only a fraction of the total cell numbers. Laser capture microdissection studies of epithelial cells and CAFs have shown that although CAFs share a similar frequency of genetic alterations, these are rarely identical, suggesting a common origin for CAFs and epithelial cells in only a small number of cases [179, 232, 233]. Although CCA cells are capable of EMT-like phenotypic changes, evidence in support of their complete transdifferentiation into αSMA+ CAFs is lacking [52].

Macrophages in health and malignancy

Myelomonocytic cells (monocytes and polymorphonuclear granulocytes) are an essential component of innate immunity [234]. Macrophages develop from circulating monocytes and are important residents of all tissues, where they play crucial roles in regulating tissue homeostasis. At steady state, tissue macrophages have intrinsic anti-inflammatory functions [235]. These macrophages assist with the innate response to combating infection, resolving acute inflammation, and regulating the metabolic response to tissue stress [236], such as hypoxic and hyperglycaemic cell injury. Macrophage plasticity is central to their multiple functions and, mirroring the Th1/Th2 nomenclature of T cells, activated macrophages have been broadly categorised as either classically M1 activated or alternatively M2 activated [237].

M1 macrophages are activated by interferon γ (IFNγ) [238, 239] produced by natural killer (NK) cells, as part of the innate immune response, or by CD4+ helper T-lymphocytes. Interferon γ is also released by CD8+ cytotoxic T-lymphocytes and, to a lesser extent B lymphocytes, as adaptive immunity arises. Activation may be in sole response to IFNγ or in concert with lipopolysaccharide (LPS; a component of the outer membrane of Gram negative bacteria), as well as the cytokines TNF-α and

granulocyte-macrophage colony stimulating factor (GM-CSF) produced by a variety of cell types including T cells, macrophages, endothelial cells and fibroblasts upon receiving immune stimuli [237, 240, 241]. M1 macrophages play an important role in acute inflammation and innate immunity, producing effector molecules (reactive oxygen and nitrogen intermediates e.g. superoxide and nitric oxide, NO) and inflammatory cytokines (including IL-1b, TNF-α, IL-6), participating as inducers and effectors in polarized Th1 responses by (e.g. by expressing CXCL9 and CXCL10 [237]) and also mediating immunity to intracellular pathogens and tumour cells [242]. M1 macrophages have high antigen presenting capability with upregulated Major Histocompatibility Complex (MHC) Class II expression [243] and are additionally characterised by an IL-12^{high}, IL-23^{high}, IL-10^{low} cytokine expression phenotype. IL-12 and IL-23 are structurally related, proinflammatory cytokines that activate Th1 and Th17 lymphocytes which further drive inflammatory responses, whereas IL-10 expression is characteristically anti-inflammatory [244].

Although M1 macrophages are essential for immunity, they are implicated in host tissue destruction as part of the inflammatory response [245]. This is because the inflammatory cytokines and mediators, such as superoxide and NO, that are produced may lead to collateral host-tissue damage, for example in rheumatoid arthritis [246] and inflammatory bowel disease [247]. During resolution of an inflammatory episode, therefore, it is necessary to redirect the immune response towards a wound healing or tissue resolution phase. The precise control of the sequential roles of macrophage responses is unclear. Indeed, understanding the underlying mechanisms that restore homeostasis after an inflammatory reaction underpins the research efforts related to chronic inflammatory diseases [235].

M2 macrophages are a group of heterogenous non-classically activated macrophages. In contrast to the pro-inflammatory and antimicrobial profile of M1 macrophage responses, M2 macrophages exhibit potent anti-inflammatory activity and have important roles in wound healing, angiogenesis and fibrosis [235, 248]. They also antagonise M1 macrophage responses, which may be crucial for the switch towards the wound healing response and for tissue homeostasis to be re-established.

Furthermore, recent studies have demonstrated that M1 macrophages may themselves transform into anti-inflammatory macrophages with an M2 wound-healing phenotype [235, 249].

M2 macrophages are subdivided according to their inducing stimuli. M2a macrophages arise after exposure to IL-4 or IL-13 as part of Th2 T cell responses. M2b macrophages are polarised by immune complexes in combination with Toll-like receptor (TLR) or IL-1 receptor agonists IL-1β or LPS. M2c macrophages are driven by exposure to IL-10, TGFβ or glucocorticoids [250]. In converse to M1 macrophages, M2 macrophages are characterised by an anti-inflammatory IL-12^{low}, IL-23^{low}, IL-10^{high} cytokine expression phenotype. Expression of reactive intermediates such as NO is abrogated, whereas, in addition to the expression of M2-specific chemokines such as Chemokine (C-C motif) ligand (CCL22), scavenger receptors such as SR-A and mannose receptor are upregulated [242].

In addition to the above monocyte polarising signals, GM-CSF and macrophage colony stimulating factor (M-CSF) have been found experimentally to polarise monocytes towards an M1 (GM-CSF) and M2 (M-CSF) macrophage phenotype (in terms of expression profiles) [244]. Granulocyte-macrophage colony stimulating factor treated cells express higher levels of pro-inflammatory cytokines such as IL-12 and IL-23 but lower levels of anti-inflammatory cytokines such as IL-10 when compared to M-CSF treated cells [251, 252]. Macrophage polarisation using M-CSF and GM-CSF has experimental utility in that the receptors are exclusively expressed on haematopoietic cells. This ensures that cellular responses to M-CSF and GM-CSF during *in vitro* culture conditions are confined to haematopoietic cells rather than other cells in co-culture conditions.

The above linear model of M1 and M2 macrophages is accepted as an oversimplification and groups differ on how applicable they believe the generalisation to be. Mantovani *et al* are proponents of the model as described whereas Mosser and Edwards argue instead for a classification that recognises the heterogeneity of "alternatively activated macrophages" and instead use the terms

Classically Activated, Wound Healing and Regulatory macrophages. In Mosser's model, classically activated macrophages arise in response to stimuli as described above. Wound-healing macrophages are similar to the descriptions of alternatively-activated macrophages (M2a) as they polarise in response to IL-4. Regulatory macrophages (analogous to M2b and M2c macrophages) are generated in response to various stimuli, including immune complexes, prostaglandins, G-protein coupled receptor (GPCR) ligands, glucocorticoids, apoptotic cells or IL-10. Each of these three populations has a distinct physiology. Classically activated macrophages (M1) have microbicidal activity, whereas regulatory macrophages (M2b and M2c) produce high levels of IL-10 to suppress immune responses. Wound-healing macrophages (M2a) have a role in angiogenesis [247] and tissue repair (secreting TGFβ1 and PDGF6 that stimulate fibroblasts and epithelial cells [253]). Of note, M2/wound healing macrophages have been implicated in TGFβ-controlled fibrotic lung disease [254, 255] and muscular dystrophy [256]. This is thought to be due in part to macrophage-derived expression of pro-fibrotic chemokines that drive fibrosis.

Figure 1.9 – Current models of the phenotypic plasticity of macrophages

Figure 1.9: Phenotypic plasticity of macrophages

A: Linear model of M1/M2 polarisation, popularised by Mantovani**.**
B: Colour wheel model of macrophage activation, proposed by Mosser and Edwards.

A

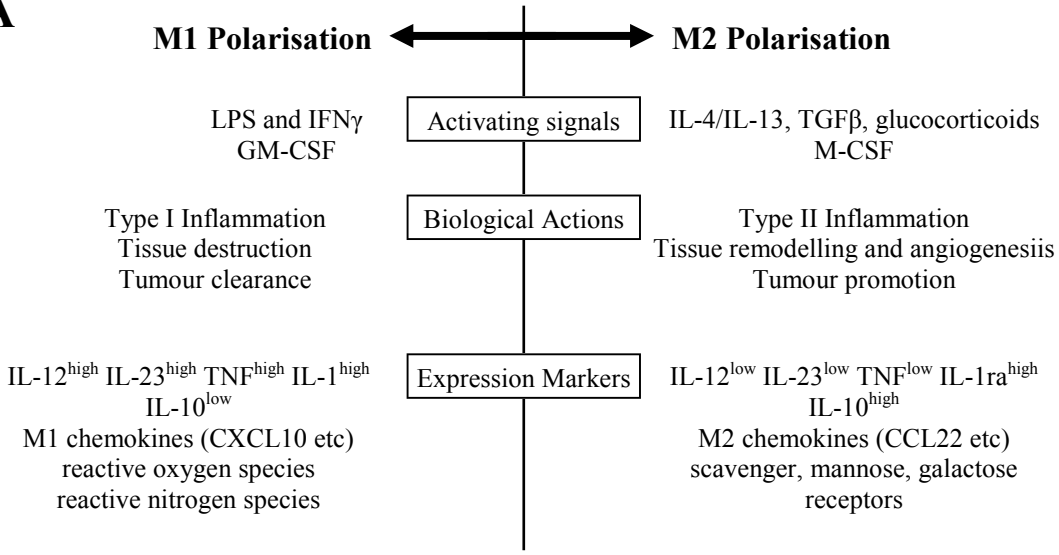

Adapted from Mantovani *et al*, Eur J Immunol 2007;37:14-6.

B

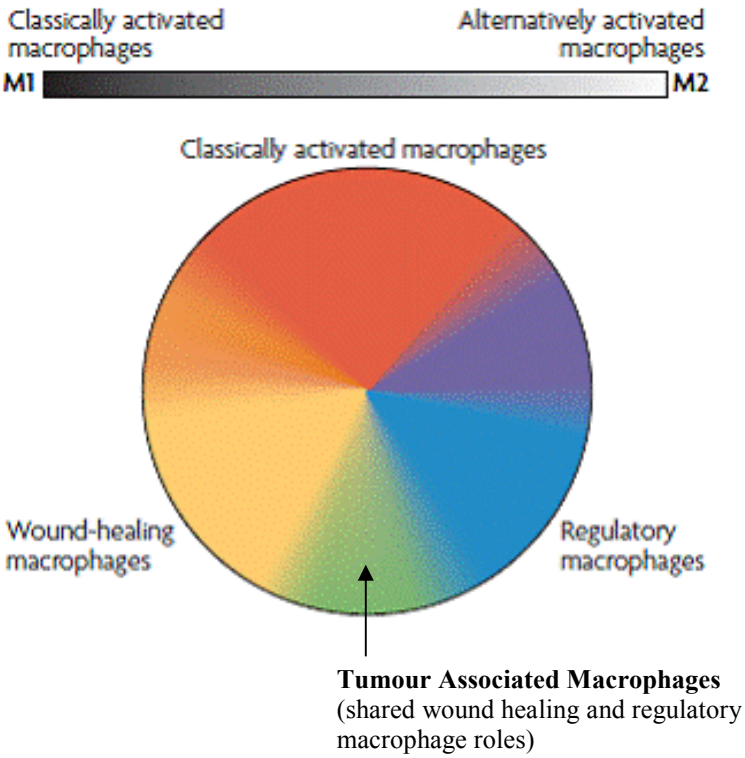

Mosser & Edwards, Nat Rev Immun 2008: 8, 958-969; doi:10.1038/nri2448

Tumour Associated Macrophages

It is increasingly accepted that tumours arise in the context of tissue inflammation. Malignancies that develop within chronic wounds (Marjolin's ulcers)[257] and in patients with chronic inflammatory bowel disease [258] are well recognised clinical examples of this. Infective causes of chronic inflammation are known to increase cancer risk [259]. For example, patients with chronic *H pylori* infection exhibit a 75% increased risk for gastric cancer [260]. Experimental inoculation of mice with *H. influenzae* induces a chronic obstructive airways disease model which, in Kras-activated subjects, results in inflammation-driven development of lung adenocarcinoma [261]. Additional *in vivo* studies in murine models of chronic organ inflammation support a causal relationship between NF-κB signalling and carcinogenesis [262, 263].

Tumour associated macrophages (TAMs) appear to demonstrate multiple, context-dependent phenotyes and roles. M1 macrophages are associated with the early stages of cancer initiation and promotion [264]. Although *in vitro* evidence suggests that M1 macrophages are able to clear cancer cells in preference to normal tissue cells [265-267], this is countered by evidence that these macrophages release inflammatory mediators (such as reactive species) that are implicated in DNA cell damage [268] and carcinogenesis [269]. Direct experimental evidence of this in mice includes macrophage and myeloid cell specific knockout of STAT3, a transcription factor that suppresses macrophage inflammatory responses due to its role as the major target of immunosuppressive cytokine IL-10. This results in upregulated expression of tumour necrosis factor α (TNFα) and IL-6 by macrophages, chronic colitis and colonic adenocarcinomas[270].

Interestingly, the often recognised but incompletely understood phenomenon of male preponderance of certain human malignancies may have, at least in part, a macrophage-related inflammatory cytokine driven mechanism. In an experimental model of hepatocellular carcinoma (HCC) by administration of diethylnitrosamine (DEN), the liver resident macrophages of male mice expressed higher levels of the

inflammatory cytokine IL-6 and a higher incidence of HCC. This sex difference in HCC incidence was abrogated by ablation of IL-6; furthermore IL-6 expression and inflammatory macrophage function was reduced in male mice by oestrogen administration [271].

Established tumours may be considered to be a particular example of a chronic non-healing wound or inflammatory scar [144]. As tumours progress beyond the initial establishment phase, the macrophage population becomes more polarised to the M2 phenotype [272] with, amongst other changes, reduced iNOS and TNFα expression as a result of inhibited NF-κB signalling [273]. The mechanisms that induce this phenotypic switch are multifactorial but include features of the tumour mass itself (such as hypoxia [274] and cell death [275]) and also bi-directional cell signalling (e.g. hyaluronin elements [276]) within the malignant lesions [236]. This modification in the profile of tumour associated macrophages towards an M2 phenotype is a response intended to dampen the immune response, promote tissue healing (including angiogenesis) and re-establish tissue homeostasis. However, in the context of cancer, this is a maladaptive response that instead results in tumour promotion. The M2 phenotype of TAMs allows a permissive environment, as the macrophages attempt to "heal" the malignant lesion rather than destroy it. In this environment cancer cells may evade the immune system and subvert the microenvironment to enhance cancer growth, survival, protection from apoptosis, and promote tumour angiogenesis.

Tumour associated macrophages are major players in the complex process of angiogenesis, critical to tumour progression. The angiogenic switch, a sudden upregulation of pro-angiogenic pathways, such as VEGF-A, occurs during establishment of solid organ lesions and is characterised by large-scale maturation of the tumour vascular network. The importance of macrophages in tumour angiogenesis has been identified in mice lacking the M-CSF-1 gene, in which angiogensis in breast tumours is reduced but then restored with re-expression of M-CSF-1 in mammary epithelium. Furthermore, overexpression of M-CSF-1 in wild type (*wt*) mice drives upregulated macrophage accumulation in breast lesions and an accelerated angiogenic switch [264, 277]. Liposomal clodronate depletion of

macrophages in tumour transplant models has been found to result in similar findings of reduced tumour progression [278]. Macrophage-derived VEGF-A has been suggested as the angiogenic signalling molecule that promotes tumourigenesis [279] but the picture appears more complicated than simply direct tumour proliferation as a result of VEGF-A induction of angiogenesis. Although experimental deletion of inflammatory-cell-derived VEGF-A in murine transgenic breast and isograft tumour models attenuated the formation of typical high-density vessel networks, this resulted in accelerated tumour progression, with less overall tumour cell death and decreased tumour hypoxia. However, the loss of macrophage-derived VEGF-A increased the susceptibility of tumours to chemotherapeutic cytotoxicity [280].

In addition to angiogenesis, tumour associated macrophages play key roles in promoting tumour invasion and metastasis [281]. A well-characterised mechanism through which this is achieved is via tumour cell-derived expression of CSF-1 that attracts macrophages [282, 283] which then express epidermal growth factor (EGF) that activates cancer cell migratory and invasive behaviour [284, 285]. This CSF-1/EGF paracrine signalling loop is necessary for invasion even if promoted by other signalling molecules [286].

Tumour associated macrophages also play a role in tissue remodelling of the ECM, which itself contributes to cancer cell invasion and metastasis since cell migration must occur through the matrix. Macrophages achieve this by direct deposition of ECM components (collagens) and breakdown of these same components via their release of MMPs [287], serine proteases and cathepsins [236, 288]. Separately, macrophage-derived MMP-9 results in release of matrix-bound VEGF-A, promoting tumour angiogenesis [170]. Furthermore, macrophage-derived SPARC (secreted protein, acidic rich in cysteine), involved in deposition of collagen IV and adhesion to other ECM components (such as fibronectin), is required for spontaneous metastasis [289]. Metastasis is an inefficient process from the primary tumour, with most released cells failing to survive in metastatic sites [264]. However, recent studies have identified CD11b+ VEGFR1+ myeloid haematopoietic progenitor cells (similar to macrophages in terms of lineage) as playing an important role in establishing a

metastatic pre-malignant niche into which malignant cells may be seeded [290, 291]. These cells may prepare the metastatic site by releasing factors such as MMP-9 [292] (that mobilises local extracellular stores of VEGF-A) and by providing a local population of monocytes that then differentiate into macrophages to support the establishment of metastatic cells[264, 293].

Macrophages in solid tumours display profound immunoregulatory roles. Direct immunsuppressive mechanisms include IL-10 signalling that activates B7-H1/PD-L1 [294] or B7-H4 [295] suppression of CD8+ T cell cytotoxicity of cancer cells. Indirect, or mediated, examples include TAM expression of the chemokine CCL22 that has been found to control mobilisation of regulatory T cells (T_{reg}) to human ovarian tumours. T_{regs} subsequently reduce cytotoxic T cell activity, and correlate with poor survival outcomes [296]. Reduced direct cytotoxity of cancer cells by macrophages and minimised recruitment of natural killer cells as a result of reduced or absent macrophage-derived IL-12 expression is also well recognised. It remains unclear whether this is due to upregulated NF-κB signalling as reported by some groups [297] or whether defective responses to NF-κB signalling and enhanced interferon regulatory factor-3 (IRF-3)/STAT1 signalling in macrophages are responsible, as identified by Biswas *et al* [298] following transcriptional profiling of tumour associated macrophages.

In established tumours, hetereogeneous populations of both M1 and M2 type macrophages have been isolated from the same tumours depending on the anatomical location within the lesions. For example, in a breast cancer model, macrophages in normoxic regions were found to express markers consistent with an M1 phenotype whereas in hypoxic regions of the tumour, macrophage polarisation was skewed to an M2 phenotype with upregulated pro-angiogenic functions such as expression of VEGF-A [299, 300]. This heterogeneity appears to be primarily controlled by hypoxia-inducible factor (HIF)-1α [274] and, particularly, HIF-2α [301, 302], which are expressed by macrophages in hypoxic conditions and also control their phenotype. (This hypoxia-induced phenotypic control has utility in non-malignant inflammatory pathological environments such as atherosclerosis where tissue healing is beneficial. Of note,

HIFs are additionally induced by inflammatory conditions in normoxic environments but the mechanism of this is incompletely understood [302].) The hypoxia-induced upregulation of M2 phenotype in tumour associated macrophages sends a cautionary note regarding anti-angiogenic therapies as they may result in increased invasive behaviour and metastasis [280, 303].

Therapeutic targeting of the stroma in solid tumours and CCA

Hanahan and Weinberg have postulated six "hallmark characteristics" of cancer: sustained proliferative signalling, evasion of growth suppressors, replicative immortality, resistance to cell death, induction of angiogenesis, and activation of invasion and metastasis [304]. Each of these is regulated by partially redundant signaling pathways, resulting in functional resistance to tumour therapies targeted against only one pathway or hallmark characteristic of cancer. It is arguable that selective, simultaneous targetting of multiple hallmark characteristics will result in more effective and durable therapies for human cancer [305]. The tumour stroma is considerably more genetically stable than malignant epithelial cells and, as such, represents an appealing co-target for anti-cancer therapy. An understanding of the role of the inflammatory stroma in the cancer microenvironment in intrahepatic CCA is critical to the eventual development of therapies. Notably, survival outcomes have been found to be worse in patients with intrahepatic CCA lesions in which there were higher contributions of cancer associated fibroblasts (αSMA) [306] and M2-like macrophages (CD163+) [307]. By modulating the chronic inflammatory microenvironment around CCA cells it may potentially be possible to reduce cancer cell proliferation, cell survival and invasion, and increase responsiveness to chemotherapy and radiotherapy.

Devising therapeutic strategies against CAF elements of the stroma requires identification of pathways that are cancer specific rather than expressed in the physiological context of "normal" fibroblast function elsewhere in the body. Examples of over-expressed pathways in tumour stroma that are involved in tumour

promotion and may represent therapeutic targets include inhibitors of HGF and Met, ERBB2 inhibitors, CXCR4 antagonists, Hh pathway inhibitors [308], PDGFR inhibitors, MMP-7 inhibitors, Galectin-1 inhibitors, therapeutic mono-clonal antibodies directed against tenascin-C and periostin, selected integrin inhibitors, mucin 1 (MUC1) inhibitors, sphingosine kinase-1 inhibitors, antisense aspartate-β-hydroxylase, and antiseprase vaccines [309]. Other potential agents, based on observed interactions between CAFs and CCA cells, include inhibitors of histone H1 and STAT3 kinase activity (reviewed in [204].) Specific depletors of CAFs, such as targeting FAP+ cells has experimental success and may be translateable into a clinical context [310].

Therapeutic strategies currently undergoing development that are directed at TAMs may be categorised into four themes: blocking macrophage effector function, limiting macrophage recruitment, and reprogramming, or preventing M2-like polarization of macrophages [236]. Epidermal growth factor and VEGF pathway inhibitors [311, 312] are designed to target general tumour pathways, but by inference, manipulate the activity of TAMs. Inhibition of macrophage recruitment to tumours in animal models also augments chemotherapeutic strategies against the tumours [313]. An important study that employed administration of CD40 agonists has been shown to regulate the immune reaction and modify the tumour stroma associated with pancreatic cancer in mice and humans by re-education of TAMs [314]. It is likely that future cancer therapeutic strategies will be multimodal, targeting specific cellular and non-cellular elements of the tumour stroma as well as cancer cells themselves, both in the form of daughter cells and cancer stem cells. It may well be that personalised therapy, along the lines of that employed against colorectal liver metastases, will become widespread for multiple cancer types and CCA in particular as the evidence base evolves.

Bone marrow derived stromal components and tumour biology

In health, a steady-state slow turnover of parenchymal and stromal cells occurs. In chronically inflamed organs, bone marrow (BM) derived myofibroblasts functionally contribute to tissue scars [226, 315] and BM-derived macrophages assist in co-ordinating this process [316]. Furthermore, there is evidence that BM-derived elements display migratory capacity towards tumours [317, 318]. Once in the tumours, the cells contribute functionally to the inflammatory stroma of tumours [228, 319].

The proportion of BM-derived contribution to CAFs varies across a range of solid-organ malignancies, contributing 25% of stromal populations in a murine model of pancreatic cancer [228] and up to 30% in xenogeneic tumour engraftment models [320]. Functionally, these cells appear to promote cancer growth [207, 318, 321, 322] with few studies suggesting the converse [323], including proposals that myeloid rather than mesenchymal-derived stromal cells promote tumour growth [324]. Diverse mechanistic pathways have been uncovered including dysregulated TGFβ signalling [325] and stromal modification of tumour neovascularisation [326]. Quante et al [327] have identified that, following generation of 30% BM chimeras, 20% of αSMA myofibroblasts were BM-derived in the stroma of *H. felis* inflammation-induced gastric cancers (that develop over 12-14 months), that the stromal cells appeared to promote tumour cell growth and that the migratory chemotactic axis from the BM may be mediated by CXCR4/SDF-1 tropism. Conversely, Kidd et al [328] studied BM transplant models with subcutaneously engrafted syngeneic ovarian and breast tumour cell lines and suggested there was a subdivision of non-neoplastic cells recruited to the tumour microenvironment. They proposed that BM mesenchyme was recruited into tumours as FSP+/FAP+ CAFs, whereas the vascular stroma (pericytes and fibrovascular structures) defined by αSMA+/NG2+ CAFs, as well as endothelial cells, were recruited from neighbouring adipose tissue.

Experimental studies have also determined that BM-derived cells contribute 10-35% of the endothelial elements of tumour associated vasculature in animal models [329, 330] and 5% of tumour vasculature in human specimens [331]. The propotional contribution

of BM-derived sources to TAM populations is less well characterised with the majority of reports not quantifying BM-derived contribution to lesions. Experimentally, in 16-week-old mice, 38% of TAMs were BM–derived macrophages in a murine model of retinoblastoma [332].

Controversially, it has also been suggested that BM-derived stem cells can transdifferentiate and contribute to the malignant cell component of tumours, possibly by repopulating depleted stem cell niches. In a murine model of gastric cancer (*H. felis* chronic infection), Houghton *et al* [333] demonstrated that BM-derived MSC could repopulate gastric epithelial stem cell niches and subsequently give rise to gastric cancer with almost 100% of malignant cells appearing to be BM-derived. Her group also demonstrated the ability of aged BM-derived MSCs to give rise to fibrosarcomas [334]. Whether this represents a general principle is as yet unclear. Some groups have made similar findings [335] but others have been unable to replicate the principle of the study in alternative models [336].

In human studies, Avital *et al* identified four male patients who developed solid organ cancers (lung adenocarcinoma, laryngeal squamous cell carcinoma, glioblastoma, and Kaposi sarcoma) after myeloablation, total body irradiation, and allogeneic BM transplantation from female donors [337]. Relying on fluorescent *in situ* hybridisation for XX chromosomes (and exclusion of Y chromosomes), 95% of CD45+ cells (lymphocytes) were BM-derived. Additionally, a total of 2.5-6% of malignant cells in lesions were comprised of BM-derived cells. Using similar methodology, Janin *et al* studied 8 patients who developed oropharyngeal squamous cell cancer following therapeutic irradiation and allogeneic BM transplantation [338]. Combined immunostaining and FISH analysis for X and Y chromosomes sequences in sex-mismatched grafts and comparison of microsatellite typing of laser-microdissected cells suggested that in four of eight cases, the tumours were derived from BM sources.

Ando *et al* studied a model of ultraviolet-induced cutaneous squamous cell carcinoma (SCC). Interestingly, they detected a low percentage of BM-derived cells

in the lesions of epidermal dysplasia (0.59%), SCC in situ (0.15%), and SCC (0.03%). There was no evidence of clonal BM cell expansion. Most of the BM-derived cells were tumour-infiltrating haematopoietic cells[339].

Cogle *et al* [340] identified a 1-4% BM contribution to the epithelial compartment of human colon tumours (n=2 specimens) and 20% to lung cancer cells (n=1 patient). When tested in the APCmin female mouse model of colon cancer (n=4 animals) with male transplanted BM, only 1:5000 epithelial cells were found to be BM-derived. In a mouse model of lung cancer, up to 1% of haematopoietic stem cell-derived cells contributed to the malignant cell population. The low contribution of BM-derived cells to cancers prompted the team to propose that, instead of being responsible for forming lesions directly, BM-derived cells may be recruited to epithelial environments by inflammatory cues and then transdifferentiate into malignant cells by a process of developmental mimicry. However, a mechanism for this was not described.

Information regarding hepatic malignancies is lacking. A provocative study by Petersen *et al* [341] was undertaken by carrying out sex-mismatch BM transplants followed by hepatectomy (driving hepatic regeneration) in 2-acetylaminofluorene treated rats (2-AAF blocks hepatic replication). Results suggested that BM-derived cells had the capactity to transdifferentiate into hepatic progenitor cells. To test this, Kubota *et al* [336] studied the choline-deficient ethionine-supplemented diet rat model of hepatic injury and regeneration. They identified that BM-derived cells may fuse with hepatic progenitor cells in rats but do not appear to contribute to HCC pre-neoplastic lesions. Similarly, Ishikawa *et al* [342] used a mouse model of HCC (DEN and phenobarbital administration) and did not identify BM contribution to HCC lesions. Hepatocytes that appeared to be BM derived most likely represented cell fusion events between donor BM and recipient hepatocyte rather than transdifferentiaton events. This has been confirmed by murine studies of tissue-damaged, regenerating liver, where hepatic progenitors (oval cells) were not found to be BM-dervied [343, 344].

There remains controversy as to the exact contribution and clinical significance of BM-derived cells to malignant lesions. What is clear, however, is that experimental parameters must be carefully controlled to minimise experimental error due to inappropriate or insufficient cell tracking techniques.

Stem Cells and the Liver

During development, hepatocytes and intrahepatic bile ducts are derived from bipotential hepatoblastic progenitor cells within the developing hepatic parenchyma (cranial component of the hepatic diverticulum, or pas hepatica). Extrahepatic bile ducts are derived from growth of the pars hepatica whereas the common bile duct, cystic duct and gallbladder are derived from the caudal bud of the hepatic diverticulum (pas cystica) [345].

In adult life, the liver has remarkable capacity to regenerate following injury. However, in times of severe replicate stress (massive liver failure) or hepatocyte senescence (chronic liver disease) there is evidence that bipotential progenitor cells (oval cells in rodents) are able to repopulate injured liver and contribute both to hepatic and biliary cell lineages. These cells are found in the Canals of Hering, adjacent to terminal bile ducts [346]. Cell fate specification is, in part, directed by the stem cell niche, whereby myofibroblasts promote biliary cell phenotypes via Notch signalling and macrophages promote hepatocytic cell fates via Wnt signalling [347]. The component cells in the chronic liver injury regenerative hepatic niche bear a striking similarity to cells comprising the microenvironment of solid organ cancers.

There exists a subset of intrahepatic tumours that appear to demonstrate phenotypic features of both CCA and hepatocellular cancer types and may be derived from bipotential progenitor cells [46, 348-351]. The similarity of risk factors for intrahepatic CCA and hepatocellular carcinoma – factors that mediate their effects by inducing hepatic inflammation – lend support to the concept of an intrahepatic progenitor contribution to these two malignancies. Progenitors in the canals of Hering may be

activated to differentiate while undergoing oncogenic stimulation in the context of chronic hepatic injury. The extent of biliary or hepatic differentiation may be regarded as reflecting the phenotypic nature of the resulting lesion, such as intrahepatic-CCA, hepatocellular carcinoma or an intermediate phenotype [29]. There remains controversy as to whether BM-derived elements functionally contribute to the oval cell population [341] or merely fuse with oval cells [336]. Whether there is a BM-derived contribution to cholangiocarcinoma lesions is unknown.

Stem Cells and Tumour Biology

It is possible that CCA arises from tumour stem cells derived from the bipotential hepatic progenitor cell niche and may include a sub population of malignant stem cells. In this context, CCA lesions might be treated therapeutically by specific targeting of CSC components of the lesions.

The concept that tumours may arise from stem cells is decades old but has only recently become more widely accepted, primarily as a result of studies into haematological malignancies (reviewed in [352]). This was elegantly demonstrated in 1977 by anchorage-independent culture of several cancer types in soft agar [353, 354]. Neoplasms, in the same fashion as normal adult tissues, possess a subpopulation of cancer stem cells (CSCs) essential for tumour propagation. Cancer stem cells themselves are not necessarily derived from normal stem cells. According to a consensus definition [355], a CSC is a cell within a tumour that possesses the capacity to self-renew and to generate the heterogeneous lineages of cancer cells that comprise the tumour. Therefore, CSCs may only be defined experimentally by their ability to recapitulate the generation of a continuously growing lesion [356]. Proliferation of CSCs is considered to be facilitated by dysregulation of normal stem cell self-renewal pathways, such as Wnt/β-catenin, Notch, and Hedgehog [357]. Many organ-restricted adult stem cells and cancer stem cells exhibit few classical stem cell markers [352]. However, recent studies have identified cancer stem cells based on

markers including CD133+ (pancreas [358], colon [359], CNS [360]), CD44+ and the epithelial cell adhesion molecule EpCAM (breast [361], colon [362], pancreas [363]) .

Using haematopoietic stem cell analysis techniques, Goodell *et al.* identified a small, homogeneous population of cells, termed the side population (or SP cells). These cells possess the ability to efflux Hoechst 33342 dye via ATP-binding cassette (ABC) transporters [364] which have been shown to remove chemotherapeutic agents from CSCs and thus participate in multi-drug resistance and improved cancer cell survival [365]. Side population cells exhibit stem-like characteristics [366] and have been found in normal tissues, as well as primary tumours [365] and cell lines established from tumours as diverse as hepatocellular carcinoma [367], lung cancer [368], nasopharyngeal carcinoma [369], glioblastoma [370], neuroblastoma and breast cancer [365].

Current failures of oncological therapies are not primarily due to lack of tumour responsiveness to treatment (although this does occur in cases) but rather due to relapse and tumour progression once treatment has been discontinued. Cancer stem cells may play a role in both treatment resistance and relapse. Clinical studies have identified a correlation between high numbers of CSCs and relapse rates. ATP binding cassette efflux-pump expressing cells correlate with poor outcomes in melanoma [371]. A high frequency of stem cells in acute myeloid leukaemia at diagnosis predicts high minimal residual disease after therapy and poor prognosis [372, 373]. Furthermore, CD44+ CSCs inversely correlate with breast cancer survival and their proportional contribution to tumour burden following chemotherapy increases[374], consistent with CSC resistance to conventional therapies. Tumour initiating cells have been shown to be resistant to conventional therapies and it may be that the multi-drug effluxing capacity of SP cells that are in part responsible for this. Other plausible explanations for CSC resistance to chemotherapy include the cells' slow cycling or quiescent phenotypes, high levels of anti-apoptotic molecules, relative resistance to oxidative or DNA damage, and their efficiency of DNA repair (reviewed in [373]).

Specific therapeutic targeting of CSC may yield translational promise in clinical outcomes. For example, targeting of ABCB5+ myeloma cells in orthotopic transplantation models (with monoclonal antibody therapy) inhibits tumour growth experimentally [371]. Further examples include targeting of CSCs in other malignancies that express markers such as CD90+CD44+ (anti-CD44 antibodies in hepatocellular carcinoma)[375], CD133+ (L1CAM siRNA in glioma)[376] and CD47 (anti-CD47 antibodies in bladder cancer[377]). Therapeutic targeting of dysregulated developmental pathways also appears to have functional relevance. Examples of inhibition across a variety of cancer types [373] of the Wnt [378, 379], Hedgehog [380] and Notch [381] pathways with small molecule inhibitors and monoclonal antibodies support the development of multimodal therapies where combinations of pathway inhibitors are employed in clinical treatments.

3. The Notch Signalling Pathway

The Notch signalling pathway is an evolutionarily conserved local cell signalling mechanism that plays a fundamental role in regulation of both the embryogenesis and adult tissue homeostasis of metazoans (multicellular mitochondrial eukaryotes)[382]. The pathway, which mediates direct cell-cell signalling interactions, was first discovered in *Drosophila melanogaster* flies [383] and has direct homologues in mammals. Notch components play pleiotropic roles in the development and maintenance of structures as diverse as muscle, intestine, pancreas, liver, haematopoietic and nervous systems by both maintaining repopulating stem cell populations and also by involvement in terminal cell fate decisions [384].

Canonical Notch Signalling

The highly conserved Notch system in mammals comprises of four heterodimeric Notch receptors (Notch1-4) and five canonical (or classical) ligands (Jagged1,2 and Delta-like 1,3,4). The ligands belong to the DSL (Delta/Serrate/LAG-2) family of proteins. The receptors and ligands are transmembrane proteins that enable the Notch pathway to transduce signals between immediately neighbouring cells. Of note, recent evidence suggests that in some circumstances, Jagged1 ligand may be secreted and then activate Notch signalling without direct cell-cell contact [385]. Similarly, Delta ligand appears to be released in soluble form and signals to distant cells during neural development [386]. Although deceptively simple, the Notch pathway is subject to multiple levels of regulation, including post-translational modification such as glycosylation and phosphorylation[387], proteolytic processing, endocytosis and membrane trafficking, as well as interaction with other pathways such as Wnt signalling [388].

Following protein translation in the endoplasmic reticulum, the Notch receptor undergoes cleavage (at the S1 cleavage site) by a furin-like protease, resulting in a

mature heterodimer that is non-covalently held together by calcium ions that cause autoinhibition of the receptor [389]. The receptor complex is then transported to the cell membrane. At this point, ubiquitination by Neuralised or Mindbomb E3 ligases enables the receptors to avoid receptor degradation and also efficiently endocytose upon ligand-receptor activation, enabling downstream signalling [390]. Of note, Numb, an antagonist of Notch, inhibits Notch by driving endocytic internalisation of Notch receptors [391].

Ligand engagement induces a conformational change in the Notch receptor that exposes the binding site for S2 cleavage by membrane-bound tumour necrosis factor-α converting enzyme (TACE), which is a member of the A Disintegrin and Metalloprotease enzyme family, and is also known as ADAM10/17 [392]. This is followed by a second cleavage (S3 cleavage) by the γ-secretase complex, that comprises presenilin (the active subunit), nicastrin, anterior-pharynx-defective-1, and presenilin-enhancer-2) [393]. This releases the intracellular part of the Notch receptor (Notch intracellular domain [NICD]) from the cell membrane, allowing it to translocate into the nucleus.

In the nucleus, in the absence of Notch activation, the DNA binding protein RBPJκ (recombination signal binding protein for immunoglobulin J-kappa region, known as CSL in invertebrates), acts as a repressor of Notch target gene transcription [390]. RBPJκ associates with co-repressors (including NcorR and SMRT) [394] and binds to consensus sequences of promoter sites of Notch target genes, preventing transcription.

As a result of Notch receptor activation, NICD enters the nucleus, dissociates the repressor complex and instead assembles a transcriptional activation complex with RBPJκ, the co-activator mastermindlike (MAML) and other co-activators (CoA). The assembly of this transcriptional activation complex on the promoter regions of Notch target genes leads to upregulation of Notch target gene expression [384].

Multiple Notch target genes have been described, and many unidentified Notch targets are likely to exist [395]. These include cyclin D1, NF-κB, p21, Myc, Insulin-like growth factor-1 (IGF1), survivin and SLUG [389]. The best-defined Notch transcriptional targets are the Hairy and enhancer of split (HES) [396] and hairy/enhancer-of-split related with YRPW motif (HEY) [397] families of transcriptional regulators. These act as direct repressors of transcription by binding directly to DNA [398]. In humans, the genes repressed by HES and HEY are responsible for lineage commitment decisions. Consequently, in the majority of cell lineages described to date, Notch signaling maintains an undifferentiated state [399], although there are exceptions in which Notch promotes differentiation, such as in keratinocytes [400] and dendritic cells [401] (reviewed and described in [389]).

Figure 1.10 – The canonical and non-canonical Notch signalling pathway

Figure 1.10: Notch Signalling Pathway

A: Canonical Notch signalling pathway.
B: Non-canonical Notch signalling pathway. Non-canonical signalling is incompletely understood and examples of non-canonical events are illustrated below.

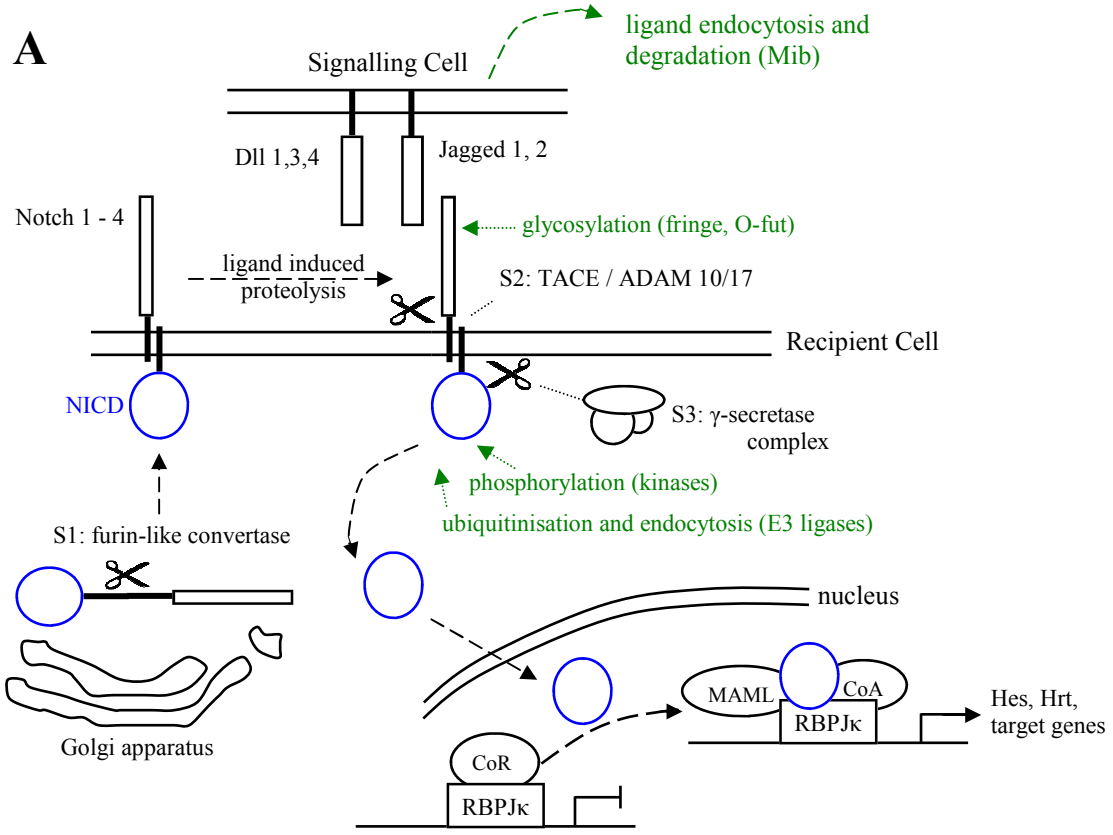

Adapted from Yin L *et al* Biochem Pharmacol 2010;80:690-701; High FA, Nat Rev Genet 2008; 9:49-61 and Koch U *et al* Development 2013;140:689-704

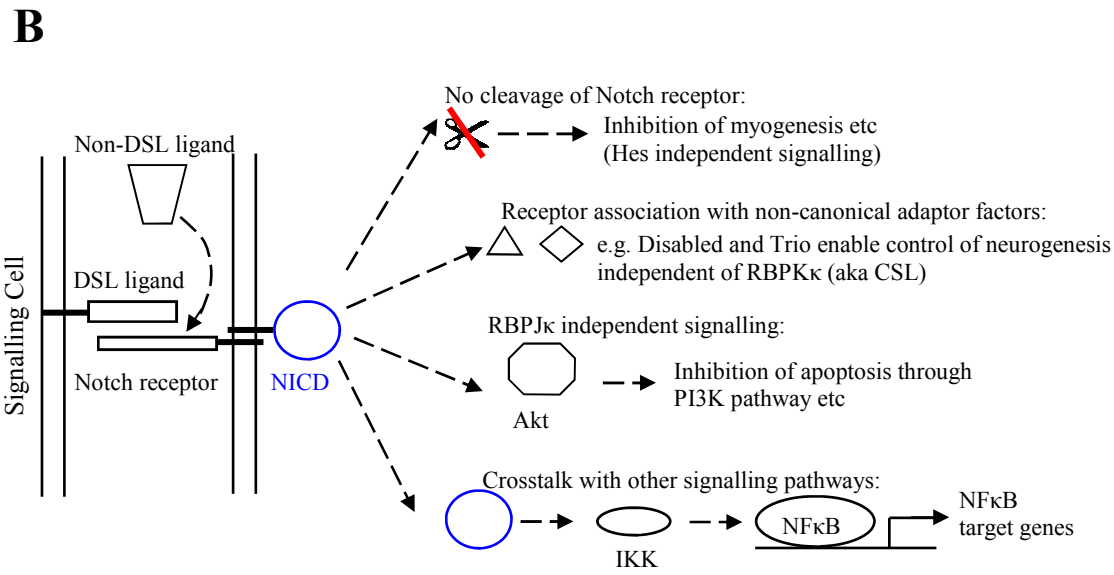

Non-canonical Notch signalling

There is increasing evidence that, in addition to canonical (classical) DSL-family ligand signalling, the Notch pathway appears to be subject to non-canonical signalling. This has been predominantly investigated in the context of embryogenesis and patterning, specifically in *D melanogaster* model systems. The various types of currently recognised non-canonical Notch signalling mechanisms may be broadly categorised as follows: DSL-independent activation of Notch signalling, pathway interactions with non-DSL ligands, RBPJκ-independent transcription events, signal transduction without receptor cleavage, differential post-translational modifications, competition/protection for signalling co-factors, or crosstalk with other signalling pathways (Wnt, BMP etc) [402].

Non-canonical signalling events require neither the classical DSL ligands nor the RBPJκ nuclear mediator [402]. Examples of non-canonical ligands active in vertebrates include membrane-bound molecules that share structural homology to the delta ligand (but lack the DSL domain) such as delta-like1, DNER (Delta/Notch-like EGF-related receptor) and Jedi (Jagged and Delta protein). Membrane-bound molecules that are structurally distinct include cell adhesion molecules F3/contactin1 and NB3/contactin6. Secreted proteins such as CCL3, MAPG-1 and MAPG-2 have also been demonstrated to act as non-canonical ligands (reviewed in [388]).

There is evidence that non-canonical signalling occurs with regard to downstream intracellular signalling cascades, where Notch signalling appears to exert effects independently from the RBP-Jk (CSL) transcription factor cascade. Examples include Notch1 signalling through phosphoinositide 3-kinase (PI3K) to inhibit apoptosis [403]. Furthermore, signalling that is independent of Notch receptor cleavage itself has been demonstrated in a number of systems, including the inhibitory control of muscle differentiation [404, 405]

Examples of non-canonical Notch pathway interactions with other signalling cascades include NFκB. The NICD shares structural features to IκB molecules.

Indeed, the CSL component of the Notch pathway is similar to Rel proteins in NFκB pathway [402]. When overexpressed, NICD can bind NF-κB (with downstream effects) through a poorly conserved region partially overlapping the RBP-Jkappa-associated module (RAM) domain [406]. Functional interactions have been indentified between the two pathways in cancer biology [405, 407-409].

The significance of non-canonical Notch pathway signalling remains unclear but it may explain in part the extraordinary breadth and diversity of biological influence that Notch signalling demonstrates throughout development and adult life, in both health and disease.

The Role of Notch in Liver Development and Homeostasis

In the developing liver, Notch regulates ductal plate formation and intrahepatic bile duct morphogenesis (reviewed in [410]). Notch signalling is crucial for normal biliary system development, as clinically demonstrated by Alagille syndrome, an autosomal dominant mutation in the Notch ligand, Jagged1. The disorder is characterised by a failure of intrahepatic biliary duct formation and mild multisystem defects that include skeletal, cardiac, ocular and craniofacial abnormalities [411]. A subset of patients also have disorders which, whilst displaying similar phenotypes, are due to defects of Notch2 receptor [412].

Evidence from animal studies supports the role of Notch signalling in biliary development. Mice with deleted Hes1 (a major downstream transcription target for canonical Notch signalling) fail to develop intrahepatic bile ducts. Additionally, Jagged1 experimentally drives WB-F344 cells (a rodent hepatic bipotential progenitor or "oval" cell line) to upregulate the Notch pathway and express Cytokeratin 19 (CK19) as a marker of cholangiocyte phenotype [413]. Conversely, small interfering ribonucleic acid (siRNA) against Notch2 and γ-secretase inhibitors drives hepatoblasts towards a hepatocyte phenotype [414]. Furthermore, *in vitro* culture of adult rodent hepatocytes and hepatocytes from adult Ws/Ws mice (deficient in

oval cells) results in hepatocyte "transdifferentiation" into cholangiocyte-like cells (CK19+) and tubular structures associated with upregulated Jagged1, Jagged2, Notch1, and several Notch target genes [415].

Postnatal tissue development and adult tissue maturation throughout the body are also regulated by Notch signalling (reviewed in [416 417]). In the quiescent liver, Notch receptors are expressed exclusively on bile ducts and signalling components are transiently upregulated during oval cell regeneration of the liver following AAF and partial hepatectomy injury [418]. Additionally, in models of surgically induced liver injury and oval cell expansion, Notch signalling has also been shown to be altered, with heterogeneous up-and down-regulation of Notch receptors and ligands over time [419]. Finally, there is evidence that Notch signalling is implicated in biliary inflammation and CCA (see below). Certainly, in the adult liver following chronic injury, myofibroblast-derived Notch ligand directs biliary specification of hepatic progenitor cells within the regenerative niche [347].

The Role of Notch Signalling in Tumour Biology

The Notch pathway has been shown to play dynamic roles in tumour biology, demonstrating both oncogenic and tumour suppressor roles depending on the tumour types and the components of the Notch signalling pathway involved.

In the haematopoietic system, Notch plays a role in maintaining the undifferentiated state in the adult. The majority of studies of Notch pathway mutations in cancer have been undertaken in haematological malignancies. Although activating mutations of Notch1 have been found in more than 50% of human T-cell acute lymphoblastic leukaemias (T-ALL) [420], there is minimal evidence for genetic alterations of Notch genes in solid tumours [421] where upregulation of Notch signalling is commonly observed [422, 423].

The role of the pathway in tumourigenesis is dependent on both tissue type and receptor identity. For example, Notch acts as an oncogene in tissues where it is involved in homeostatic stem cell self-renewal or in cell fate decisions (e.g. breast cancer, gastrointestinal tumours). Notch1 [424] (with a coincident loss of Numb inhibition of Notch in 50% cases [422]) and Notch4 [425] have been implicated in tumour promotion in breast cancer. Notch1 and Notch3 are upregulated in and promote human lung cancer [426-428]. In animal models, Notch2 but not Notch1 is required for development of pancreatic ductal adenocarcinoma [429]. Furthermore, experimental overexpression of Notch3 intracellular domain (but not Notch1 or Notch2) during murine embryogenesis results in invasive intra-ocular (but not intra-cranial) gliomas, reflecting both receptor type and tissue site specificity [430]. Experimental inhibition of the pathway with γ-secretase inhibitors attenuates tumour growth [431]. In contrast, Notch signalling plays tumour suppressor roles in those tissues in which it promotes terminal differentiation events (e.g. keratinocytes). In Notch1 knockout mice, an increase in skin cancers has been noted [432]. Notch may even play both roles within the same tumour. For example, activated Notch is oncogenic to breast cancer cells yet also tumour suppressive by inhibiting angiogenesis [416] . In human mesothelioma cells, Notch1 and Notch2 play opposing roles in tumour progression [433]. Inhibition of Notch signalling may therefore be an effective treatment option for selected tumour types [434].

Table 1.3 – The oncogenic (+) and tumour suppressor (-) roles of dysregulated Notch pathway signalling in malignancies [416]

	Jagged1	Jagged2	Dll-1	Dl-4	Notch1	Notch2	Notch3	Notch4
Haematological :								
AML	+		-	-	+			
B-cell ALL					-	-	-	-
B-cell CLL						+		
Hodgkin lymphoma	+				+ -			
Multiple myeloma	+	+			+ -	+		
T-cell ALL				+	+	+ -	+	
Solid Tumours:								
Brain	+		+		+ -	+		
Breast					+	+ -	+	+
Cervical	+	+	+		+ -	+		
Colon					+	+		
Liver					-			
Lung					+ -	-+		
Pancreas	+	+			+	+	+	+
Prostate	+				-			
Skin					+ -	+	+	+

AML - acute myeloid leukaemia; ALL - acute lymphoblastic leukaemia; CLL – chronic lymphoblastic leukaemia

Multiple separate experimental teams have studied Notch in carcinogenesis. Currently, the pathway is thought to promote malignancies by promoting the CSC phenotype [435, 436], by mediating EMT [437]and by enhancing chemoresistance [438] and radioresistance [439] (reviewed in [389]).

The role of Notch signalling in the tumour stroma

A specific way in which tumour-associated stromal cells may interact with cholangiocarcinoma cells is via the Notch pathway. This relationship may be bidirectional. There is as yet no direct evidence in tumour systems that intercellular signalling via Notch is important in stromal:cancer cell relationships, but there is

evidence from other systems that supports this hypothesis. It is known that stromal cells control dendritic cell fate and proliferation in bone marrow through Notch pathway signalling [440]. Macrophage polarisation appears to be in part mediated by Notch signalling: Notch pathway activation drives cells to an M1 phenotype and downregulation is associated with an M2 phenotype [441]. Additionally, M1 activated macrophages express upregulated levels of Notch1 and Jagged1 [442] and the ligand delta-like 4 [443]. Furthermore, Notch3 mediated signalling increases macrophages' proinflammatory function [443]. Non-canonical Notch signalling mechanisms that theoretically may be active in the tumour:stroma relationship include nitric oxide, as NO production is a recognised feature of activated macrophages [444]. In ovarian cancer, Notch3 and Jagged-1 are expressed both in cell lines and the epithelial compartment of human tumour samples [445] (suggestive of juxtacrine signalling between neighbouring epithelial cells). Jagged-1 is additionally expressed in peritoneal mesothelial cells that may be in direct contact with disseminated ovarian cancer cells in ascitic fluid. Additionally, IGF-1 is a candidate signal for Notch activation via aspartyl asparagynyl beta hydroxylase (AAH) activation in CCA [446, 447] and IGF-1 is produced by tumour associated myofibroblasts [202, 448].

Notch signalling is implicated in Cholangiocarcinoma

Dysregulated Notch signalling has been identified in CCA. Notch1 appears to be upregulated in CCA, and has a role in conferring resistance to apoptosis; iNOS-mediated processes can upregulate Notch1 signalling [79]. Additionally, AAH is highly expressed in cholangiocarcinoma where it translocates from the cytoplasm to the cell membrane and directly upregulates Notch signalling by hydroxylating the extracellular domain of the Notch receptors. This increases CCA invasiveness and cell survival [446, 449, 450].

In CCA, reports have identified receptor elements of the Notch pathway as being over expressed [79]. However, the anatomical distribution of pathway components and therapeutic implications are not clear.

4. Current *in vivo* and *in vitro* models of CCA

In vitro models of CCA

International cell line banks, such as the American Type Culture Center (ATCC), store cell lines derived from the majority of different human cancer types. There are relatively few CCA cell lines that feature in published studies, and even fewer that are deposited in independent cell banks.

Table 1.4 - Published human cholangiocarcinoma cell lines

Table 1.4: Published human cholangiocarcinoma cell lines

Cell lines marked in bold are used in this thesis submission. Cell lines were preferred if they were derived from intrahepatic lesions in patients prior to chemotherapy and were stored in independent cell banks.

Cell Line	Anatomical Location (Intra/Extrahepatic)	Country of Origin	Reference	Notes
YoMi	Unknown	Unknown	Jarnagin 2006[451]	
KKU-MO55	Intra (poorly differentiated)	Thailand	Tepsiri 2005[452]	Contacted
KKU-M156	Intra (moderately diff)	Thailand	Tepsiri 2005	Contacted
KKU-M214	Intra (moderately diff)	Thailand	Tepsiri 2005	Contacted
KKU-OCA17	Intra (well diff)	Thailand	Tepsiri 2005	Contacted
KKU-100	Intra (*O. viverrini*)	Thailand	Tepsiri 2005	Contacted
KKU-M213	Unknown (*O. viverrini*)	Thailand	Juntavee 2005[453]	
HBDCM1-ZSH	Extra	China	Tang 2004[454]	
SNU-245	Extra (distal CBD)	South Korea	Ku 2002[455]	KCLB
SNU-308	Extra (gallbladder)	South Korea	Ku 2002	KCLB
SNU-478	Extra (ampullary)	South Korea	Ku 2002	KCLB
SNU-869	Extra (ampullary)	South Korea	Ku 2002	KCLB
SNU-1079	Intra	South Korea	Ku 2002	KCLB
SNU-1196	Extra (hilar)	South Korea	Ku 2002	KCLB
MZ-Cha-3	Unknown	Germany	Steffen 2001[456]	?SK-Cha-1?
SCK	Intra	South Korea	Kim 2001[457]	Contacted
JCK	Intra (clonorchis)	South Korea	Kim 2001	Contacted
Cho-CK	Intra	South Korea	Kim 2001	Contacted
Choi-CK	Intra	South Korea	Kim 2001	Contacted
HBDC	Extra (hilar)	Japan	Jiao 2000[458]	
ICBD-1	Extra (ascites)	Japan	Takiyama 1998[459]	
OCUG-1	Extra (gallbladder)	Japan	Yamada 1997[460]	
TFK-1	Extra	Japan	Saijyo 1995[461]	DSMZ, Tohoku
OCUCh-LM1	Extra (?liver met)	Japan	Yamada 1995[462]	
GB-CL-1	Extra (gallbladder)	Unknown	Purdum 1993[463]	
KMC-1	Intra	Japan	Iemura 1992[464]	
CC-SW-1	Intra (implicit in article)	USA	Shimizu 1992[465]	
CC-LP-1	Intra (implicit)	USA	Shimizu 1992	
KMBC	Extra (CBD)	Japan	Yano 1992[466]	Derived 1985
PCI-SG231	Unknown	USA	Storto 1990[467]	Contacted
RPMI 7451	Unknown	Unknown	Storto 1990	
HuCCT-1	Unknown	Japan	Miyagiwa 1989[468]	JCRB
HUH-28	Intra (implicit)	Japan	Kusaka 1988[469]	Tohoku
KMCH-1	Intra (combined HCC/CCA)	Japan	Murakami 1987[470]	
EGI-1	Extra	Germany	Scherdin 1987[471]	DSMZ
MZ-Cha-1	Extra (gallbladder)	Germany	Knuth 1985[472]	**(aka: WITT)**
MZ-Cha-2	Extra (gallbladder)	Germany	Knuth 1985	
SK-Cha-1	Extra (ascites)	Germany	Knuth 1985	

KCLB – Korean National Cell Line Bank (Seoul University)
DSMZ – *Deutsche Sammlung von Mikroorganismen und Zellkulturen*:
German Collection of Micro-organisms and Cell Cultures
JCRB – Japanese Collection of Research Bioresources
Tohoku – Cancer Cell Repository, Tohoku, Japan

b) *In vivo* models of CCA

There are few published studies on animal models of CCA. Historical models characteristically demonstrate long latency and variable incidence of tumour formation. For example in 1983, Flavell [473] induced a 10-20% incidence of cholangiocarcinomas in syrian hamsters following a latency of nine months, by administering a single dose of *Opisthorchis viverrini* and N-nitrosodimethylamine. This reprises the aetiological association between liver fluke infestation and CCA in South East Asia and, in principle, would represent an ideal in vivo model. Unfortunately the limited range of biomolecular research tools appropriate for hamster tissue renders this model difficult to experimentally analyse further. Similarly, Elmore (1993) [474] administered 30 mg/kg furan by daily gavage to male Fisher F344 rats for 13 weeks and induced 90% CCAs at 16 months.

Murine models of intrahepatic CCA:

1. dePinho Group (Harvard) [56]:

Farazi (2006) administered carbon tetrachloride (CCl_4) intra-peritoneally to p53 deficient mice three times weekly for four months and then followed up for several months. Only p53+/- and p53-/- mice developed CCAs with P53-/- mice developing significantly more lesions and demonstrating a lower survival than p53+/- mice. Tumours began to form at approximately 26 weeks in p53-/- mice. This model was deemed unsuitable for our studies due to the greater sensitivity of p53 deficient mice to adoptive bone marrow transfer (requiring lethal irradiation and immediate syngeneic transplantation). Furthermore, the available p53 deficient mice (from Dr Jorge Caamano, Birmingham, UK) were derived on a mixed background and hence unsuitable for syngeneic bone marrow transplantation.

2. Deng Group (NIH) [475]

Xu (2006) generated liver-specific disruption of Smad4 and Pten in mice by crossing mice carrying a Smad4 conditional allele and a Pten conditional allele with

transgenic mice carrying a Cre recombinase gene under an albumin promoter. Spontaneous development of multiple tumours occurred from two months with reportedly realistic desmoplastic stroma, and all animals developed tumours by seven months. Additionally, a number of murine cholangiocarcinoma cell lines were developed by this group. The animals and the cell lines were on mixed backgrounds of four strains of mice, rendering it unrealistic to perform syngeneic bone marrow transplantation or syngeneic subcutaneous tumour cell line inoculation into immunocompetent mice.

3. Clarke Group (Cardiff) [476]

Marsh (2008) deleted Pten (Phosphatase and tensin homolog) and APC (Adenomatous Polyposis Coli) genes in mice and identified multiple gastrointestinal tract adenomas and adenocarcinomas by four months. From unpublished data, it also appeared that the animals developed multiple cholangiocarcinomas. Histologically, the tumours more closely represented biliary tract adenomas with minimal stromal contribution.

Rat models of intrahepatic CCA:

1. Sirica Group (Richmond, Virginia) [477]

Sirica (2008) devised a transplantable model of intrahepatic CCA in male Fisher F344 rats. Two CCA rat cell lines were produced: One (BDEneu) by transfection of the rat oncogene neu into an immortalised but non-malignant rat biliary epithelial cell line and one (BDEsp) by spontaneous transformation of the same biliary cell line in selective culture. These cell lines were inoculated into the common bile duct of recipient male rats. BDEneu demonstrated rapid tumour growth with 50% replacement of the liver parenchyma with tumour by 22 days. BDEsp tumours were smaller and developed over the course of approximately 40 days. Furthermore, the lesions themselves recapitulated a prominent stromal component and glandular structure, similar to in situ intrahepatic CCA. NIH regulations proscribed the export of this model to our group.

2. Thioacetamide Model (Various Groups)

Thioacetamide (TAA) is a hydrogen sulphide donor used in industrial chemical processes. It previously served as a preservative of oranges in the 1940s. It has been recognised for a considerable time that TAA has the ability to induce CCA in rats[478, 479]. TAA is currently registered as a Class 2B carcinogen, is a known hepatotoxicant and appears to undergo metabolic activation by mixed-function oxidases, cytochrome P450 2B, 2E1 and flavin monooxygenase. There is evidence that TAA induces toxic effects in the pancreas and kidney. There are no published studies of CCA induction in mice using TAA.

a) Yeh (2004) [480] administered 0.03% TAA in the drinking water of male Sprague Dawley rats and identified a 50% incidence of intrahepatic CCA by 16 weeks rising to 100% by 22 weeks. These tumours appeared histologically similar to human intrahepatic lesions, with invasive features, dense stroma and ductular atypia. A separate paper by the same group using the same schedule identified liver fibrosis in the absence of CCA at the same timepoints [481].

b) Laverman (2007) [482] administered 0.03% TAA drinking water to male Sprague Dawley rats to study the diagnostic utility of (18)F-FDG contrast in PET scanning for CCA detection. He identified subsets of animals with a variable background of cirrhosis demonstrating micro-carcinomas from 10 weeks onwards, increasing in incidence to 100% by 20 weeks.

c) Al-Bader (2000) [483] investigated the dose-response effect of 0.05%, 0.1%, 0.15% TAA drinking water in male Wistar rats. On the lowest dose (0.05%), rats developed CCA by the 13th week and survived to the end of the study period of 14 weeks. Rats on 0.1% TAA developed more marked inflammatory changes, CCA by the 11th week and died by the 14th week. Rats on the highest dose (0.15%) died by the 8th week, presumably of liver failure, before developing CCA.

d) Roskams group (Belgium): Laleman (2006) [484] applied a weight-adjusted variable dosing regime of 0.015% to 0.045% TAA in male Wistar rats to investigate the

potential of TAA in liver fibrosis and portal hypertension models. On a background of fibrosis, dysplastic changes in the biliary epithelium were observable from 12 weeks onwards, increasing in severity by 18 weeks but not representing frankly invasive CCA.

e) Alpini group (Texas): Fava (2008) [485] provided 0.03% TAA to obese (fa/fa) and lean male Zucker rats to investigate the role of leptin in the incidence and progression of CCA. Fa-fa Zucker rats have a mutated long form of the leptin receptor, do not respond to leptin signalling, and so consequently become obese. By 24 weeks of TAA administration, 100% of control lean Zucker rats developed CCA. In contrast, the fa/fa Zucker rats developed a significantly lower incidence of CCA formation.

Conclusion: Current Understanding of CCA:

CCA is recognised as a solid organ tumour with a pronounced desmoplastic component. The tumours arise in the context of chronic inflammation mediated through a variety of sources. The contribution and role of the BM to the stromal and epithelial compartments of the tumours is unknown. Notch signalling has been provisionally identified as playing a role in CCA, with Notch1 upregulation associated with the malignant phenotype [79].

There is suggestive evidence that intrahepatic CCA may in part arise from hepatic progenitors and, inferentially, it is possible that CCA arises from tumour stem cells derived from the bipotential hepatic niche and may include a side population of cells.

Human studies have suggested that the role of stromal cells in CCA may affect prognosis. Notably, survival outcomes have been found to be worse in patients with intrahepatic CCA lesions in which there were higher contributions of cancer associated fibroblasts (aSMA) [306] and M2-like macrophages (CD163+) [307] to the histological lesions. There is as yet no mechanistic understanding of these observations.

CHAPTER TWO

METHODS

Thioacetamide Model of Cholangiocarcinoma

All animal procedures were carried out in accordance with the procedural and ethical guidelines of the United Kingdom Home Office under the Animals (Scientific Procedures) Act 1986. Animals were housed in specific pathogen free conditions with a 12:12 hr light-dark cycle (light from 08:00 to 20:00) at an ambient temperature of 22 +/- 1 °C, with *ad libitum* access to chow and water. Adult male (300-330 g for direct administration studies; 330-350 g for transplant studies) and female (190-210 g; 210-230 g) Sprague dawley rats (Harlan, Hillcrest, UK) were commenced on drinking water supplemented with either 300 mg/L (0.03%) [480] or 600 mg/L (0.06%) thioacetamide (TAA) (Sigma, UK). Water was sweetened with sugar-free drinking squash in a 4:1 ratio. Animals were sacrificed at intervals by CO_2 inhalation, and tissue samples were taken for histology, protein and nucleotide analysis. Age-matched controls were provided with normal water. Similarly, C57bl6 mice (20-25g) were commenced on 300 mg/L or 600 mg/L TAA for up to 52 weeks.

Animal Tissue Acquisition and Storage

Tissues obtained included liver, spleen, lung, blood and bone marrow. Specimens were snap frozen in liquid nitrogen and stored at -80 °C, or fixed in methacarn (70% methanol, 20% chloroform, 10% acetic acid) or neutral-buffered formalin (1 part 37% formaldehyde in 9 parts phosphate buffered saline [PBS]) for 16 hours. Fixed tissues were dehydrated in 70% ethanol followed by mounting in paraffin microtome blocks for histology. For selected studies, whole blood samples (with 100 uL heparin) were taken from the inferior vena cava immediately after the point of sacrifice. Blood samples were pulse centrifuged (9000 revolutions per minute [rpm] for 30 s) to generate a cell pellet and serum supernatant. The serum was snap frozen and stored at -80 °C, whilst circulating cells and platelets were resuspended in PBS and analysed by flow cytometry.

Donor Bone Marrow Transplantation (BMT)

Sprague Dawley rats (female 210-230 g; male 330-350 g) underwent adoptive transfer of syngeneic bone marrow (BM). The enhanced green fluorescent protein (EGFP) transgenic Sprague Dawley rats were a kind gift of Prof Okabe (Genome Information Research Center, Osaka University, Osaka, Japan). These were rederived in our unit from embryo form. The expression of EGFP was under the control of the cytomegalovirus enhancer and the chicken β-actin promoter [486, 487]. Bone marrow transplantation (BMT) was performed with male or female EGFP-expressing BM into male wild type (*wt*) recipients, male EGFP-BM into female *wt* recipients, and male *wt* BM into female *wt* recipients. Rats received whole body γ-irradiation (10.5 Gy in a divided dose 4 hours apart). Under general anaesthesia, irradiated rats immediately received intravenous tail vein injections of $2x10^7$ donor BM cells in single cell suspension. Antibiotic supplementation of the drinking water was started 7 days prior to irradiation and for 28 days after the procedure (0.01% Enrofloxacin, Bayer, UK). For CCA studies, eight weeks after BMT, rats were commenced on either 300 mg/L TAA or control drinking water. Animals were euthanased and tissue harvested at set time points (n=6 each time point for each chimaeric type).

Assessment of Stability of Bone Marrow Transplantation (BMT)

Female *wt* rats underwent BMT with male EGFP-BM to determine stable expression of EGFP following transplantation. Prior to transplantation, whole BM was stained with Vybrant 1,1'-Dioctadecyl-3,3,3',3'-Tetramethylindodicarbocyanine, 4-Chlorobenzenesulfonate (DiD) labelling solution (V-22887, Invitrogen UK), a far-red fluorescent, lipophilic carbocyanine dye that stains cell membranes. This was performed by incubating BM at 37 °C for 30 minutes in a single cell suspension of $1x10^6$ cells/mL in PBS with 5 uL/mL DiD solution. BM was then centrifuged at 1250 rpm for 6 minutes, the supernatant was aspirated and the cells resuspended in 10% foetal calf serum Iscove's modified Dulbecco's medium (10% FCS IMDM). This step utilises the ability of FCS to bind unbound dye. Cells were washed three times in this fashion to remove unbound dye. Prior to transplantation, a sample of cells was

analysed through the flow cytometer to confirm adequate staining. Under general anaesthesia, irradiated rats immediately received intravenous tail vein injections of $2x10^7$ donor BM cells in single cell suspension. Recipients were harvested at 5 minutes, 1 hour, 24 hours, 7 days, 7 weeks, 14 weeks and 32 weeks after BMT (n=3 at each time point.) Bone marrow, spleen and whole blood samples were collected. Blood samples were prepared as single cell suspensions, underwent hypotonic shock in distilled water to remove contaminating erythrocytes and were analysed by flow cytometry to assess EGFP expression and DiD staining. Samples were also snap frozen in liquid nitrogen and stored at -80°C for subsequent quantitative polymerase chain reaction (qPCR).

Hypotonic Shock Treatment of Whole Blood Prior to FACS Analysis

Whole blood samples were centrifuged for 5 minutes at 160 g (rcf). The plasma-containing supernatant was removed by aspiration (as the pellets are loosely adherent to pipette tubes). The pellet was loosened, by flicking the base of the tube, and resuspended in 9 mL of dH_20 then mixed by inversion for 12 seconds to lyse erythrocytes. 1 mL of 10x PBS was added and mixed by inversion. The sample was centrifuged for 5 minutes at 160 g. The supernatant was again removed by aspiration and the pellet washed with 10 mL PBS, centrifuged again for 5 minutes at 160 g, the supernatant removed and the pellet resuspended in 100-500 μL PBS.

Liposomal clodronate macrophage depletion

Liposomal-encapsulated clodronate was a gift of Roche Diagnostics GmbH, Mannheim, Germany, arranged through Dr Nico van Rooijen (Amsterdam, Netherlands) [488]. Liposomal clodronate and control PBS (2-6 μL/g) was administered to Sprague Dawley rats intravenously via the tail vein.

Isolation of Human Peripheral Blood Mononuclear Cells (PBMC)

Freshly drawn blood was collected into 50 mL Falcon tubes containing 4 mLsodium citrate per tube, inverted gently two or three times to mix and then sealed. Samples were centrifuged at 350 g for 20 minutes (with Acc1/Dec0). The top layer of platelet-

rich plasma (PRP) was aspirated into fresh sterile falcons without disturbing the bottom (blood cell) layer. To separate leucocytes from erythrocytes by dextran sedimentation, 6 mL dextran was added to each blood cell layer and filled to the 50 mL mark with pre-warmed saline. (Dextran dose equivalent to 2.5 mL per 10 mL of blood pellet). Samples were inverted gently two or three times and allowed to rest for 20-30 minutes, until the erythrocytes sedimented. The leukocyte-rich upper layer was aspirated and transferred to a 50 mL Falcon tube and topped up to 50 mL with saline. The samples were centrifuged at Bench 350 g (rcf) for 6 minutes (Acc5/Dec5). The supernatant was poured off from pelleted leucocytes which were gently resuspended in 55% percoll. Percoll gradients were made by gently layering 81% percoll (bottom layer), 68% percoll (middle layer) and 55% percoll containing leucocytes (top layer) in 15 mL Falcon tubes at room temperature. The gradients were centrifuged at 720 g (rcf) for 20 minutes (Acc1/Dec0). After percoll centrifugation, peripheral blood mononuclear cells (PBMC) were harvested from the 55:68 interface (upper band) and granulocytes (neutrophils) from the 68:81 interface (lower band) into separate 50 mL Falcon tubes. The tubes were filled to 50 mL with PBS and centrifuged at 230g(rcf) for 6 minutes (Acc5/Dec5). The supernatant was removed, the cells washed again in PBS and re-centrifuged at 230 g (rcf) for 6 minutes (Acc5/Dec5). Cells were resuspended in 50 mL PBS and counted using a nucleocounter. Mononuclear cells were resuspended at a concentration of $4x10^6$/mL in serum-free IMDM. The neutrophils were resuspended at $10x10^6$/mL in Hanks buffered saline solution (HBSS) and provided to other research groups in the institute interested in this cell type.

Generation of Autologous Serum

During the isolation protocol for human PBMCs, autologous recalcified serum was obtained from the whole blood samples by adding 10 mL of platelet-rich plasma (PRP) to glass tubes containing 200 µL 1M $CaCl_2$ and incubating at 37 °C for one hour. After one hour, the clear serum was aspirated from the tubes, leaving the platelet plug in the tubes, which were discarded. The serum was then stored at -20°C.

Enrichment of Macrophages from PBMC - Method 1: Plastic Adherence

Peripheral blood mononuclear cells were counted and then plated on tissue culture plastic (24 or 48 well plates) and incubated for 1 hour. Non-adherent cells were aspirated from the wells and wells were washed twice with PBS. Then 0.5 mL of 10% autologous serum in IMDM ("monofeed") was added to each well. Plates were incubated for 5-7 days to allow differentiation into macrophages.

In a 24-well plate, cells were plated down at a density of $4x10^5$ cells per well. Cells were allowed to adhere in media for 2-3 hours and then washed off twice with HBSS+Ca^{2+}. The Ca^{2+} is necessary as cell adhesion is Ca^{2+} dependent. Once washed, 400 μL media was added to wells. The media included polarising cytokines at the same concentrations as detailed below.

Enrichment of Macrophages from PBMC - Method 2: Negative Selection

Peripheral blood mononuclear cells from the 55:68% percoll interface layer were taken after washing in PBS and purified using magnetic-activated cell sorting (MACS) Human Monocyte Isolation Kit 2 (Miltenyi Biotec, Germany) according to the manufacturer's instructions. This enables isolation of monocytes (CD14+ cells) through magnetic columns by depletion of non-monocytes (negative selection) by indirect magnetic labelling of these cells with microbeads. It is possible to either sort positively for CD14+ cells, negatively for CD14+ by depleting other cell types, or negatively for CD14+ and also positively for CD61+ cells to reduce platelets (but this reduces the yield of CD14+ cells). Negative selection, as chosen here, avoids activation of monocytes. Following isolation, CD14+ cells were resuspended in Roswell Park Memorial Institute (RPMI1640) medium supplemented with 10% FCS at a density of 5-10 $x10^6$/mL and placed in Teflon pots to prevent cell adhesion.

Monocyte Maturation and Polarisation

For method 1 (plastic adherence): Following 7 days maturation of monocytes in autologous monofeed serum and plating on plastic, IFNγ 20 ng/mL was add to the cultured cells for M1 macrophage polarisation, whilst IL-4 20 ng/mL was added to

cultured cells for M2 polarisation. After 18-20 hours of incubation, cells were washed twice with PBS and then used experimentally.

For method 2 (negative selection): During 7 days maturation in Teflon pots (that prevent cell adhesion), cells were incubated with either GM-CSF 50 ng/mL (R&D systems) for 7 days for M1 polarisation or M-CSF 50 ng/mL (R&D systems) for M2 polarisation. Media was changed every 2 days during maturation.

Cholangiocarcinoma (CCA) cell lines and cell culture

SNU-1079, SNU-1196 and SNU-245 cell lines [455] were obtained from the National Korean Cell Bank. LP and SW lines [465] were generous gifts to Professor John Iredale from Whiteside of Mayo Clinic, Rochester USA. HUH-28 [469], WITT/Mz-Cha-1 [472] and TFK-1 [461] were kind gifts of Prof G Alpini, Texas A&M Health Science Center, Temple, Texas, USA. LX2 cells were a resource previously obtained by the Iredale laboratory and used in this study. Cells were maintained in a humidified atmosphere at 37°C with 5% CO_2 and cultured in Dulbecco's modified Eagle medium (DMEM) (E15-009) or IMDM (E15-018) with penicillin (0.1 μ/mL)-streptomycin (0.1 mg/mL) (P11-010) and L-glutamine (2 mM) (M11-004) (all PAA Laboaratories, Yeovil, UK). Culture media was supplemented with heat-inactivated 2.5% - 10% FCS depending on experimental conditions (S1900-500 Biosera, Ringmer, UK). Cells were passaged using 0.25% trypsin with EDTA 1 mmol/L or TrypLE Express at 37 °C (Gibco, UK) no more than 20 times.

Generation of Conditioned Media

Cells were grown in T75 flasks to 80% subconfluence, rinsed twice with PBS and then cultured for a further 36 hours in 0.5% or 0% FCS phenol red-free IMDM. The culture media was then aspirated, centrifuged (500g for 5 minutes) to remove debris, L-glutamine (2 mmol/L) was re-added, filter-sterilised (0.22 μM) and stored at -80°C for experimental use. Experimental target cells were cultured for 24 hours in 96 well plates in 10% FCS media, which was aspirated and cells were washed twice with PBS then serum starved in 0% FCS media for 6 hours before addition of the conditioned media or appropriate control for 24 or 48 hours.

Co-culture of Cells

When using method 1 (cell adhesion), macrophages were plated in wells, matured and then stained (as described below) prior to the addition of stained cancer cells. Cancer cells were stained whilst adherent, trypsinised and then added to adherent macrophages. When using method 2 (negative selection), adherent cancer cells were stained, trypsinised and plated in wells at set densities. Macrophages were stained in Teflon pots and then added to adherent cancer cells at set densities. For example, SNU-1196 was seeded on top of macrophages at a density of $1.5x10^5$ cells per 24 well plate well in polarising media with 500 μL media per well (160 μL SNU-1196 cell suspension with 340 μL polarising media). Cells were allowed to incubate for a further 72 hours and then were fixed and cointerstained with DAPI.

Staining of Cells for Co-culture

Adherent cells of interest were stained with Celltracker dye (Invitrogen). In this case, Celltracker Orange CMTMR (C2927) was used for macrophages and Celltracker Green CMFDA (C2925) was applied to cancer cells. Cultured cells were washed in PBS to remove FCS-containing media and subsequently incubated in FCS-free IMDM culture media with Celltracker dye (20 μL dye in 10 mL media) for 45-60 minutes. The dye was then aspirated and replaced with 10% FCS IMDM for 15 minutes to block non-specific staining. Blocking media was removed and cells were washed twice in PBS and then used for experimental purposes as planned.

Fixation of Co-cultured Cells

Co-culture wells were fixed in 4% formalin and stored at 4 °C for 48 hours. Specifically, for example, in wells containing 500 μL media, 55 μL of 40% formalin was added to each well to a final concentration of 4% formalin. Fixative solution was then aspirated and cells washed gently with PBS. 1 μg/mL Hoescht-3342 was added to counterstain nuclei (300 μL per well in 24 well plates) and incubated at 4 °C for 15 minutes. Cells were washed again with PBS and 4 drops of DABCO were added

to each well. Plates were covered with tinfoil to prevent bleaching and then photographed.

Staining of transplanted BM cells with DiD

$1x10^6$ cells/mL BM cells were made as a single cell suspension in PBS and incubated with 5 μL/mL Vybrant DiD cell-labelling (V-22887, Molecular Probes, UK) solution (the dye is toxic if added neat, so is diluted prior to adding it to cells). The cell suspension was incubated with the dye at 37 °C for 30 minutes. Cells were centrifuged at 1250 rpm for 6 minutes, the supernatant was aspirated and cells were resuspended in 10 mL 10% FCS IMDM. The cells were washed in this manner a total of three times to remove unbound dye. Prior to injection, a sample of cells was assayed by flow cytometry to confirm staining. The stained cells were allowed at least 10 minutes recovery time before injecting into animals.

Side Population (SP) Analysis

Cultured CCA cells or bone marrow cells were resuspended, incubated at a density of $1x10^6$/mL at 37 °C in pre-warmed phenol red-free DMEM+ containing 2% FCS and 10 mM HEPES buffer. Hoechst 33342 dye was added to a final concentration of 5 μg/mL in the absence or presence of 50 μM verapamil. Verapamil blocks ABC cell membrane transporters and so act as controls for Hoechst 33342 dye efflux. Cells were incubated at 37 ºC for 90 minutes and mixed every 30 minutes. The cell suspensions were centrifuged at 4 ºC and resuspended in ice-cold phenol red-free HBSS+ containing 2% FCS and 10 mM HEPES buffer. Cells were filtered through a 40 μm cell screen to remove clumps and placed on ice. Propidium iodide was added at 2 μg/mL for the discrimination of non-viable cells prior to fluorescence-activated cell sorting (FACS). Analyses and sorting were done using FACS Vantage SE using Diva software (Becton-Dickinson). Hoechst 33342 was excited with a UV laser at 350 nm and its fluorescence was measured using optical filters (Hoechst blue, 405 nm; Hoechst red, 570 nm).

Clone Formation

Freshly sorted SP and Non-SP cells were counted and plated in triplicates at different densities (100, 500 and 1000 cells per well) on 6-well plates in 3 mL 10% DMEM. Media was changed every 72 hours and plates were observed for cell growth over a two-month period.

qPCR for Genomic Rat Y-Chromosome

Taqman qPCR probe was designed for a conserved sequence across the six copies of the genomic DNA of the rat y-chromosome - SRY1 (GenBank:AY157669), SRY2 (AY157670), SRY3 (AY157672), SRY3B (AY157996), SRY3B1 (AY157997) and SRY3C (AY157671) [489].

SRY is a single exon gene with untranslated regions at 5 and 3 prime ends. SRY for rattus norvegicus (SRY1 - AY 157669) was identified using the NCBI database. The genomic and mRNA data were then sequence aligned using Ensembl (ebi.ac.uk). The sequence segment that aligned to all six copies of SRY was preferred. The single exon identified by the mRNA sequence was entered into Primer Express 3 (Applied Biosystems Inc.) and primers and probe were designed. The best set was chosen, with penalty factor 54. The designed primers were then searched for using the Basic Local Alignment Search Tool (BLAST) against the NCBI database (Nucleotide setting - refseq_rna database) and self-adjusted for short sequences (by inserting both primers into the database search box with a space between the two sequences.) Rattus norvegicus SRY was positively identified with highest sequence homology ("at the top of the list") (reference: NM_012772.1); lower order SRY included drosophila etc. The reference generated was an mRNA sequence but, as SRY is a single exon gene, the sequence was equivalent to genomic DNA.

The TaqMan primer sequences were as follows –
Forward: TACGGACAGGACTGGGCTAGAG
Reverse: TGTTTCTGCTGTAGTGGGTATCC
Probe: TGCACACCGTCCTCCAGAACCGAA – VIC/BHQ

Taqman qPCR uses a fluorogenic probe to detect specific DNA sequences as they are generated by the qPCR reaction. The probe comprises a fluorescent reporter dye at the 5' end together with a quencher at the 3' end. Binding of the probe to the target strand results in cleavage of the probe by polymerase in the reaction mix that separates the reporter from the quencher, generating a measurable fluorescent readout. Multiplex qPCR entails the simultaneous amplification of more than one primer pair in the same reaction mixture. Different reporter dyes are used which are analysed by qPCR detection software that analyses the spectral output and derives the proportional contribution to this from the separate reporter dyes. Competition for common reagents in the reaction tube is prevented by limiting the concentrations of primers used to ensure that reagents are not exhausted by the more abundant species present in the sample [490]. In this series, efficiency was determined at greater than 90% and validity of multiplex qPCR was confirmed when run with control qPCR primer-limiting taqman primer/probe for rat GAPDH (ABI) (according to manufacturer's instructions). qPCR was performed on BM, spleen and whole blood of female rats transplanted with male EGFP or male *wt* BM to confirm chimaerism.

Reconstitution of Haematopoeitic and Mesenchymal compartments

The contribution of donor EGFP-BM to haematopoietic tissues of recipients was determined by flow cytometry and fluorescence activated cell sorting. Data was acquired and analysed on a FACSAria using Diva Software (Becton Dickinson). Forward and side scatter characteristics were used to apply an electronic gate before acquisition of data and sorting to exclude red cells, dead cells and debris. Acquired data was analysed for the contribution of EGFP+ cells to BM, spleen and blood. Lymphocyte and granulocyte sub-populations were identified and gated based on their scatter characteristics, before measuring the percentage of EGFP+ cells in each. EGFP+ cells were gated compared to cells from the same tissue derived from a wild type control.

To characterise EGFP-BM chimaerism of the mesenchymal stem cell compartment, BM from transplant recipients was collected by flushing femurs with PBS following incubation in collagenase 1A (Sigma) (100µl in 10ml 0% FCS RPMI) for 30 minutes

at 37°C. Recovered cells were washed and resuspended in Mesencult MSC basal medium (Stem Cell Technologies) supplemented with 10% HyClone FCS (Fisher Scientific), Cells recovered from 1 femur after flushing were plated into a 1 well of a 6 well plate and passaged up to 4 times using TRYPLE (Invitrogen). The phenotype of cultured cells was assessed by flow cytometry using a FACSCaliber and CellQuest software (Becton Dickinson) for data acquisiton and FloJo software (TreeStar Inc) for analysis. Briefly, cells were incubated with fluorochrome-conjugated monoclonal antibody for 30 minutes and washed before data acquisition. An electronic gate was used to exclude dead cells. Unstained cells from wild type and EGFP+ BM, together with appropriate isotypes were used as controls to set gates to identify EGFP+ cells co-expressing specific markers. Monoclonal antibodies used included CD45 (PECy5.5) [Caltag] and STRO-1 (APC) [R&D]. Endogenous cellular expression of EGFP did not require antibody staining to be detectable by the flow cytometer. Cells were deemed to be mesenchymal stem cells (MSCs) if they expressed STRO-1$^{491\text{-}493}$ and were donor-derived if they co-expressed EGFP. Transplanted animals were compared to untransplanted positive control EGFP rats.

Cell tracking in Cholangiocarcinoma experimental design

Male chimaeric rats: Male rats transplanted with either female EGFP-BM or male EGFP-BM were commenced on oral TAA ten weeks after BMT. These were harvested following 14, 26 and 38 weeks of TAA dosing (n=6 TAA for each transplant group at each timepoint.) Controls consisted of transplanted chimaeras on drinking water alone (n=3 at each timepoint). Cell tracking was performed by immunohistochemistry for GFP and fluorescent *in situ* hybridisation for the Y-chromosome (YChr-FISH).

Female chimaeric rats: Similarly, female rats underwent BMT with male *wt* BM and were treated with oral TAA. These were harvested 12, 18, 32 and 52 weeks later (n=6 TAA and n=3 water controls at each timepoint.) Cell tracking was performed in these animals by means of YChr-FISH.

Immunohistochemistry and Immunofluorescence

Antibody Types

Primary antibodies for cell-specific markers were used in antibody diluent (003218, Invitrogen): CK19 (1:50 dilution, NCL-CK19, Novocastra), PanCK (1:200, Z0622, Dako), ED1 and ED2 (1:100, MCA341R and MCA342R, AbD Serotec), α-SMA (1:2000, A5228, Sigma), desmin (1:50, Z0097, Dako), AFP (1:400, A0008, Dako), laminin (1:25, Z0097, Dako). Primary antibodies for Notch pathway components were similarly diluted and comprised: Notch1 (1:50, sc6014, Santa Cruz and 1:50, btan20/ab79972, Abcam), Notch2 (1:50, sc7423, Santa Cruz), Notch3 (1:50, sc7424, Santa Cruz), Notch4 (1:50, ab23427, Abcam), Delta-like 1 (1:50, ab10554, Abcam), Jagged1 (1:50, sc8303, Santa Cruz), Jagged2 (1:50, sc5604, Santa Cruz). Secondary antibodies included swine antirabbit IgG/biotin (E0431, Dako); rabbit antimouse IgG/biotin (E0464, Dako); rabbit antirat IgG/biotin (E0468, Dako), and rabbit antigoat (E0466, Dako) all used at 1:400. Appropriate isotype controls were used for each primary antibody.

Immunohistochemistry

Immunohistochemistry was performed on paraffin sections. 5 μm methacarn- or formalin-fixed sections were de-waxed in xylene for 10 minutes, serially rehydrated through graded alcohol to distilled water (5 minutes) and washed in PBS. Antigen retrieval was performed using the appropriate method for the primary antibody of interest (citrate, ethylenediaminetetraacetic acid [EDTA], trypsin or proteinase-K). Slides were then washed in PBS for five minutes. To block endogenous peroxidase activity, slides were treated with 3% H_20_2 (Sigma) in PBS for 20 minutes at room temperature on a rocker. Slides were then washed in PBS and mounted in sequenza racks. Avidin and biotin blocks were then performed for 15 minutes each (SP-2001, Vector), with two rinses of PBS between each step. Sections were then blocked with serum-free protein block (X0909, Dako) for 30 minutes. Without PBS washing, sections were immediately incubated with appropriate primary antibody dilutions in blocking buffer for either one hour (room temperature) or overnight (4 °C). Primary

antibody concentrations and incubations were as detailed in "Primary Antibody Types" above. Following rinsing in PBS, slides were incubated with 1:400 biotinylated secondary antibody (Rabbit anti-mouse, E0354, Dako) for 30 minutes. Following treatment with ABC-reagent (Vector PK-7100) for 30 minutes and PBS washing, sections were developed using 3,3′-diaminobenzidine (Dako K3468) for 4-10 minutes in the dark then counterstained with Harris' hematoxylin and blued in Scott's tap water for 25 seconds each. Slides were then dehydrated through graded alcohol, cleared in xylene and mounted with Pertex mount medium.

Immunofluorescence

For immunofluorescence, following rehydration of slides into PBS as described above, sections were immediately blocked with serum-free protein block (X0909, Dako) for 30 minutes and then incubated with appropriate primary antibody dilutions in blocking buffer for either one hour (room temperature) or overnight (4°C). Sections were then washed with PBS and re-incubated with appropriate secondary antibody for 30 minutes at room temperature in the dark. Secondary antibodies included Alexa ®Fluor 488 (green), Alexa® Fluor 594 (red) and Alexa® Fluor 647 (red) fluorescent dye conjugated antibodies. Slides were subsequently washed with PBS and mounted using Vectashield with DAPI to counterstain the nuclei (Vector, Burlingame, CA, USA).

Dual Immunofluorescence – Two Step

For dual immunofluorescence, dependent on the stability and signal strength of the antibody complexes, staining was undertaken either as two-step immunofluorescence staining or by use of Perkin Elmer Tyramide Signal Amplification (TSA) Plus systems that stabilise the first antigen signal of interest prior to application of second antigen staining.

For two-step dual immunofluorescence, following incubation with secondary antibody for the first antigen-recognising primary antibody, slides were washed with PBS. They were then re-blocked with serum-free protein block (X0909, Dako) for 30 minutes and incubated directly with appropriate primary antibody dilutions (for the

second antigen of interest) in blocking buffer for either one hour (room temperature) or overnight (4 °C). Sections were then washed with PBS and re-incubated with appropriate secondary antibody for 30 minutes at room temperature in the dark. Slides were subsequently washed with PBS and mounted using Vectashield with DAPI to counterstain the nuclei (Vector, Burlingame, CA, USA).

Dual Immunofluorescence – Tyramide Signal Amplification (TSA)

Perkin Elmer TSA Plus systems were used according to the manufacturer's instructions (Cy3 Nel744001KT, Cy5 etc). Briefly, immunostaining was carried out by rehydrating slides, blocking endogenous peroxidase with H_20_2, washing with PBS, blocking with serum-free protein block, incubating with primary antibody (1 hour room temperature or overnight at 4 °C), washing, and incubating with 1:500 diluted Fab Peroxidase-conjugated secondary antibody for 30 minutes (Goat anti-Mouse or Goat anti-Rabbit depending on primary antibody species). Slides were then washed and incubated with 1:50 diluted Tyramide Cy3/Cy5 for 10 minutes. Following this, sections were washed and mounted using Vectashield with DAPI (Vector, Burlingame, CA, USA). Primary antibody concentrations were reduced to minimise signal:noise ratio (CK19 1:4000, αSMA 1:16000, ED1 1:2000, ED2 1:400, EGFP 1:10,000). To further reduce background, sections were incubated in hot 0.01 M sodium citrate pH 6.0 for two minutes between the first and second primary antibodies.

For immunofluorescence prior to YChr-FISH, the sections were treated according to the TSA protocol above to ensure stability of signal prior to exposure of sections to the YChr-FISH protocol. Sections were then washed and entered into the YChr-FISH protocol.

Fluorescent *In Situ* Hybridization (FISH) analysis of transplanted tissue

The BM origin of cells was tested by YChr-FISH using STAR* FISH Rat 12/Y Cy3 labelled Paint (#CA-1631, Cambio, Cambridge, UK). To determine the chromosomal complement of the cells with a myofibroblast phenotype and

cholangiocyte phenotype, YChr-FISH was combined with immunohistochemistry for α-SMA or CK19 using an indirectly labelled Cy5 signal. Cell nuclei were analysed using microscopy for the Y chromosomes.

Sections were dewaxed in xylene, rehydrated in graded alcohols and then immunofluoresence for cellular antigens was performed as detailed above, with the addition of tyramide amplification and stabilisation of the antigen signal on the sections. Following addition of tyramide amplification, slides were immediately incubated in 1 mol/L sodium thiocyanate for 10 minutes at 80 °C, washed in PBS, and (for formalin-fixed tissues) digested in pepsin (0.4% wt/vol) in 0.1 mol/L HCl at 37°C for two minutes. The protease was quenched in glycine (0.2% vol/wt) in double-concentration PBS, and the sections were then rinsed in PBS, post-fixed for two minutes in paraformaldehyde (4% wt/vol) in PBS, dehydrated through graded alcohols, and air-dried. The chromosome paint was added to the sections (10 μL per slide), sealed under glass with rubber cement, heated to 80 °C for 30 minutes, and incubated overnight at 37 °C. The slides were then rinsed three times in Formamide wash solution at 37 °C, three times in 2×SSC at 37 °C, detergent wash solution for 10 minutes and then PBS. The slides were mounted using Vectashield with DAPI (Vector, Burlingame, CA, USA).

Antigen Retrieval

In rat tissue, trypsin antigen retrieval was performed to enable detection of CK19 and ED2 epitopes. ED1, αSMA, MPO and desmin required antigen retrieval with boiling sodium citrate. In human tissue, no antigen retrieval was necessary. PanCK was antigen retrieved by means of Proteinase K. For Notch pathway components, no antigen retrieval was performed and sections were permeabilised with 3% TritonX for 30 minutes.

Sodium Citrate: Sections were incubated in citrate buffer (10 mM sodium citrate, 0.05% Tween20, pH 6.0), in a microwave on full power, heated for 5 minutes three times, topping up the level every time. Slides were then allowed to cool for 10

minutes with running water. For Notch components, sodium citrate antigen retrieval was performed using a pressure cooker for five minutes (timed from when incubation pressure had been reached), and then cooled for 20 minutes in the cooker.

EDTA: Sections were treated in the same fashion as for sodium citrate, using 1 mM EDTA, 0.05% Tween 20, pH 8.0.

Trypsin: Sections were incubated at 37°C with 0.01% Trypsin in 0.1% $CaCl_2$ in dH_20 for either 15 minutes (formalin fixed tissues) or eight minutes (methacarn fixed tissues). The pH was adjusted to 7.8 using 1 M NaOH.

Proteinase K: Sections were incubated with Proteinase K for 8 minutes (methacarn) or 15 minutes (formalin) at 37 °C. For the retrieval, 12.5 mg of Proteinase K was added to 100 mL of PBS and pH balanced to pH 8.0.

Cytospins

Cell suspensions were created in a solution of 0.1% bovine serum albumin in PBS (A7906, Sigma, UK). Cell number counts were performed with a nucleocounter (941-0002 Nucleocassettes and SCC-100 Nucleocounter, Chemotec, Denmark). 20-50,000 cells were pipetted into a cytofunnel (cytoclip, slide and filter card – 3120110, Thermo Scientific) and centrifuged at 300 rpm for 3 minutes (Shandon Cytospin 4 centrifuge, Thermo Scientific). Slides were fixed in ice cold methanol for 5 minutes, allowed to air dry and stored at -20 °C before use. In separate experiments for immunocytochemistry studies, cells were cultured in 4 well LabTek II Chamber Slides (177399, Thermo Scientific, UK) for 72 hours and then used for immunocytochemistry studies.

Immunocytochemistry

Slides with adherent cultured cells (80% confluence following 72 hours of culture) or cytospun cells were washed in PBS and fixed in ice-cold methanol for 10 minutes.

Slides were then processed in a similar fashion as for the immunohistochemistry protocol starting from the endogenous peroxidase-blocking step as antigen retrieval was not required.

Picrosirius Red Staining for Quantification of Liver Fibrosis

Picosirius red (PSR) stains collagens, a marker of fibrosis. Picrosirius red staining was performed on 5 μm liver sections. Slides were deparaffinised in xylene and rehydrated in graded ethanol (100-50%) and distilled water followed by incubation for 2 hours in saturated picric acid solution containing 0.1% Sirius red and 0.1% Fast green. Slides were subsequently rinsed in distilled water to remove excess dye and dehydrated in graded ethanol (50-100%) and cleared in xylene. The slides were mounted on glass cover slips with aqueous PermountTM mounting media (Fisher Scientific, Loughborough, UK). Picrosirius red staining of liver specimens was quantified by digital image analysis (Photoshop, Adobe, San Francisco, USA) of 30 randomly selected and blinded high magnification (x200) photomicrographs. Detection thresholds were set for the red colour of PSR stained collagen from an area of intense staining and an arbitrary colour threshold range was applied.

Microscopy and Image Capture

For light and fluorescent microscopy, a Nikon Eclipse E600 microscope (Nikon UK Ltd., Surrey, UK) was used with a DXM 1200F digital camera. Image processing was performed using Adobe Photoshop software (Adobe Systems UK, Uxbridge, Middlesex, UK).

RNA extraction from cultured cells and tissue samples

RNA was isolated from snap-frozen tissue (rat and human CCA and normal liver tissue samples) by using Trizol or Trireagent (Invitrogen, UK) and a RNeasy RNA extraction kit (74104, Qiagen, UK) according to the manufacturers' instructions.

For *in vitro* cell line culture, Trizol RNA isolation was used. Culture medium was removed from wells and cells were washed in ice-cold PBS. Cells were harvested into Trizol (100 µL for 24 well, 250 µL for 12 well and 500 µL for 6 well plates), ensuring plates were thoroughly scraped and samples pipetted up and down several times. (Samples could be stored at -20 °C at this stage.) Specimens were then incubated at 25 °C for 5 minutes, followed by addition of 200 µL chloroform/1 mL Trizol. Eppendorf tubes were then shaken vigorously for 15 seconds and re-incubated at 25 °C for 2 minutes. Samples were centrifuged at 12,000 g for 15 minutes at 4 °C. The aqueous phase of the sample was transferred to a fresh tube and 500 µL isopropanol/1mL original Trizol volume was added. Reincubation at 25 °C for 10 minutes was followed by centrifugation at 12,000 g for 10 minutes at 4 °C. The supernatant of each sample was gently aspirated, leaving the pellet in the Eppendorf tube which was then vortex-washed with 250 µL 75% ethanol and re-centrifuged at 7,500 g for 5 minutes at 4 °C. The ethanol was aspirated, the pellet was air dried for 10 minutes at room temperature and then resuspended in 10 µL sdH_2O and incubated at 55 °C for 10 minutes prior to DNAse treatment or direct reverse transcription.

DNAse treatment was undertaken to remove contaminating genomic DNA from RNA. To the RNA sample in 10 µL sdH_2O, as yielded above, 2 µL 5x RT buffer and 0.5 µL RNAse-free DNAse I (5 units) was added. This was incubated at 37 °C for 15 minutes followed by incubation at 70 °C for 10 minutes. The resulting pure RNA sample was then quantified using a Nanodrop (ND-1000) prior to reverse transcription into first-strand cDNA.

Reverse Transcription

1 µg RNA was added to RNAse/DNAse free water to a final volume of 9 µL in 0.2 mL Eppendorf tubes (on ice). Alternatively, if the RNA extraction protocol yielded a dilute concentration of RNA such that this volume was not possible, then 0.1 µg RNA was used and made up to 9 µL. 2 µL (50 ng/µL) random hexamers (272166-0.5ku pd(N)6 Na salt 50 u) was added to the lid of the Eppendorf tube and pulse spun

to mix. Samples were then heated at 70 °C for 10 minutes in the PCR microplate incubator and chilled on ice. Mastermix was made up of the following components for each sample to be reverse transcribed: 4 µL 5x RT buffer, 2 µL 0.1 M DTT, 0.5 µL 10 mM dNTp mix (10 mM each), 0.5 µL Superscript II (added last), 0.5 µL RNAse inhibitor and 1.5 µL H_2O. Mastermix was added to each sample to be reverse-transcribed, ensuring controls were undertaken: One control without Superscript II and one control without RNA (negative control). The samples were incubated at 42 °C for one hour in the PCR microplate incubator, then pulse spun and stored at 20 °C.

qPCR for Notch pathway and macrophage markers

Notch pathway qPCR analysis was undertaken using the human and rat Notch RT^2 SYBR Green/ROX Profiler PCR arrays (Ref: PAHS-059C-12 and PARN-059Z, SABioscience, Frederick, MD) to study expression profiling of the Notch pathway's binding and receptor processing genes, putative targets and main crosstalk pathways in normal liver and CCA specimens. In essence, SYBR Green qPCR generates a quantitative fluorescent signal as SYBR green dye binds to double-stranded DNA sequences (amplicon) produced by the qPCR reaction. qPCR was performed with the ABI Prism 7500 fast real-time PCR system (Applied Biosystems, Foster City, CA) according to the manufacturer's instructions (two step cycling programme). Each PCR tube comprised 12.5µl RT^2 SYBR Green/ROX qPCR master mix, 10.5 µl ddH_20, 1.0 µl template cDNA, 1.0 µl gene-specific 10 µM PCR primer pair stock (25 µl total volume). The ΔΔCt method was used to analyze the relative expression level of each gene. A threshold of three-times greater expression was set to identify upregulation.

Separately, qPCR for individual macrophage receptors and markers were undertaken using QuantiTect SYBR Green primer assays (Qiagen, Crawley, UK) for CSFR1 (QT00073276), CSFR2a (QT00046298), CSFR2b (QT01676962). qPCR for IL-10 was undertaken with a primer designed in-house: IL-10 Fw: TGC-CCT-CAG-CAG-AGT-GAA-GA and IL-10 Rv: GGT-CTT-GGT-TCT-CAG-CTT-GG. Each PCR

tube contained 10.0 µl Express SYBR mastermix, 0.4 µl forward primer and 0.4 µl reverse primer (10 µM stock), 1.2 µl ddH_20 and 8.0 µl template cDNA (20 µl total volume). qPCR was performed with the ABI Prism 7500 fast real-time PCR system (Applied Biosystems, Foster City, CA).

Cytotoxicity assays and inhibition of Notch signalling

Cells were plated in 96-well plates at 80% confluence. For each cell line, the cell numbers were as follows: SNU-1079 $2.0x10^3$, SNU-1196 $2.0\ 10^3$, CC-SW-1 $1.0x10^4$, CC-LP-1 $1.0x10^4$. Cells were plated and allowed to adhere overnight before medium was changed and culture continued for 24-48 hours with chemotherapeutic drugs (1.0-160 µM 5-fluorouracil, 0.2-320 µM cisplatin [Sigma, UK]) and/or 1-50 µM of the γ-secretase inhibitor DAPT (565784, Calbiochem). These agents were reconstituted in dimethyl sulphoxide (DMSO; Sigma). Cytotoxicity was determined using 3-(4,5-dimethylthiazol-2-yl)-2,5-diphenyltetrazolium bromide (MTT) assay as described below.

Luciferase Reporter Assays

For Notch reporter gene assays, CCA cell lines were seeded in 12- and 48-well plates. After 24 hours cells were transiently transfected using Lipofectamine 2000 (Invitrogen) according to the manufacturer's instructions. Transfection of dual-luciferase reporters was performed with up to 0.5 µg of a 12xRBPJk-luciferase Notch reporter construct (gift from U. Lendahl and E. Hansson to S Lowell [494]) together with up to 0.1 µg of a SV40-renilla plasmid. As a positive control, additional transfection of up to 0.5 µg of the constitutively activated Notch intracellular domain (NICD) was performed. Following transfection, cells were allowed to recover for 8 hours and subsequently treated with DAPT and chemotherapy for 48 hours. Cells were then harvested, and lysates prepared and analyzed for luciferase activity using a Dual-Glo® Luciferase Reporter Assay System (Promega, Madison, Wisconsin, USA) according to the manufacturer's instructions. Luminescence was measured using an Orion II Microplate

Luminometer (Titertek-Berthold, Pforzheim, Germany): luciferase luminescence was read followed by addition of a quencher and substrate for renilla with re-measurement of renilla luminescence. Luciferase expression was calculated as a ratio of the two readings (luciferase:renilla).

Human tissue samples

Samples of normal and neoplastic tissues were obtained from patients who underwent elective resection of CCA tumours at the Royal Infirmary of Edinburgh between 2008 and 2010 under ethics code 08/S1101/41 (Edinburgh Experimental Cancer Medicine Centre protocol) and 10/S1402/33 (NHS Research Scotland Bioscience protocol.)

Age	Sex	Hepatectomy	TNM	CCA Risk Factors
69	F	Extended Right	T3 N0	No
67	M	Extended Right	T3 Nx	No
53	F	Extended Right	T2 N1 M0	Ulcerative Colitis
59	F	Extended Right	T1 N0	No
53	M	Extended Left	T3 N0	No

MTS and MTT Cell Proliferation Assays

MTT and MTS assays were used to determine the proliferation of cells. MTT [3-(4,5-dimethylthiazol-2-yl)-2,5-diphenyltetrazolium bromide] is a yellow tetrazole which is reduced to a purple formazan in living cells by mitochondrial dehydrogenase in viable cells. The formazan salt is insoluble and must be resolubilised by DMSO before being colorimetrically quantified [495]. Similarly, MTS [3-(4,5-dimethylthiazol-2-yl)-5-(3carboxymethoxyphenyl)-2-(4-sulfophenyl)-2H-tetrazolium] is reduced from the yellow tetrazolium salt to a purple formazan salt in the presence of phenazine methosulfate (PMS). This enables “one-step” colorimetric analysis.

Experiments were carried out in 24-well plates (doublets or triplicates) and 96-well plates (triplicates or sextriplicates). Differing volumes (20 µL for 96 wells -130 µL for 24 wells) of either MTT or MTS reagent (Promega-G3580) were added to wells

and plates were incubated at 37 ºC for 30 to 120 minutes, dependent on the assay. For MTS assay, cells were cultured in phenol-red free media (to reduce colorimetric interference) whereas for MTT assay, cells were cultured in standared media. MTS-treated cells were analysed immediately whereas MTT-treated cells were dried and the insoluble formazan salt was resolubilised with 100-300 µL DMSO prior to analysis.

Plates were shaken for 10 seconds to ensure uniform distribution of MTT/MTS before spectrophotometry by a Biotek Synergy HT Multi-Detection Microplate Reader. Plates were read at 570 nm optical density and expressed relative to background at 690 nm. Gen5 data collection software was used for analysis. Controls comprised incubation of MTT/MTS with wells that contained either no cells (media only) or wells that contained lysed cells (treated with Triton X).

Lactate Dehydrogenase (LDH) Assay

The MTT/MTS proliferation assay was performed concurrently with the lactate dehydrogenase (LDH) Cytotoxicity Assay. Lactate deydrogenase is released from cells during cell death (apoptosis and necrosis). Consequently, absence of LDH *in vitro* indicates that MTT/MTS assay results represent cellular proliferation rates rather than metabolic cell death pathways. Cell culture supernatant was centrifuged at 500 g for 3 minutes to remove cellular debris then plated in triplicate (50 µL) in 96 well plates. 50 µL of LDH reagent (Promega-G1781) was added to each well. Plates were incubated at room temperature in a microplate incubator at 600 rpm in the dark for 20 minutes to ensure even distribution of substrate. Optical density was read at 570 nm and expressed relative to background at 690 nm on a Biotek Synergy HT Multi-Detection Microplate Reader.

^{3}H-Thymidine Incorporation Assay

^{3}H-thymidine ("tritiated thymidine") is incorporated into DNA in new cells and thus is a measure of proliferation. Cultured cells in 96 well plates were incubated with 2 µm (in 10 µL) ^{3}H-thymidine (1:14 dilution in DMEM) for 16 hours. Experiments were carried out in sextuplicate. Following incubation, plates were frozen at -20 °C

to permeabilise cell membranes and enable efficient acquisition of ^{3}H-thymidine. The cells were transferred onto filter paper (Wallac-1205-401) using an automated harvester. The filter paper was then dried in an oven for 20 minutes and heat-sealed in a sample bag (Wallac-1205-411) with scintillation fluid (9 mL). A Betaplate scintillation counter (Wallac-SC/9200/21) was used for analysis.

Collagen and Laminin Plating

Plates were either pre-coated with collagen I (354407), collagen IV (354429) or laminin (354410) (all Sigma) or were coated prior to use. Coating was undertaken using collagen I (from rat tail), collagen IV (from human placenta) or laminin (all Sigma, UK) and were dissolved in 0.1M Acetic acid to a concentration of 1.0 mg/mL then diluted in distilled water to 0.1 mg/mL and plated out at a concentration of 15 μg/cm^2 on to 96 well culture plates. Poly-D-lysine (Sigma, UK) was disolved in distilled water to a stock concentration of 0.1 mg/ml, further diluted to a final concentration of 10 μg/ml then applied to 96-well plates in a similar manner to the ECM components. The coated culture plates were left to dry in a class II microbiological safety cabinet for 1 hour then moved to 4 °C for 24 hours. Residual acid was neutralised with 0% FCS DMEM and then 0.1% bovine serum albumin (BSA) in 0% DMEM was applied for one hour in order to block non-specific binding. Cells were then cultured on these coated plates in appropriate media for 24-48 hours before the MTT assay was performed.

Flow Cytometry

Flow cytometry and flourescence activated cell sorting (FACS, FACSVantage, Becton and Dickinson) was performed to analyse and collect different cell populations within cancer cell lines and bone marrow samples. For side population analysis, cells were stained using Hoechst 33342 and propidium iodide (to enable targeted gating of viable cells). For EGFP bone marrow studies, cells were gated according to their intrinsic fluorescent properties. For epitope-specific cells sorting, the following pre-conjugated antibodies were used: STRO-1, CD133, Thy-1 (Company – eBiosciences, Biolegend, BD Pharmingen etc) with the appropriate isotype control.

Growth of Plasmids

The plasmids obtained from Dr Sally Lowell were transformed and expanded for use within our laboratory. The plasmids were as follows:

1. Sel35-12CSL luciferase (Notch signalling pathway reportor plasmid with 12xCSL repeats to amplify the signal)
2. GFP Plasmid AGS445
3. Sel67 SV40-renilla
4. pNotchIC Sel39 (pCAG-NotchIC-ires)
5. Empty vector AGS-564 (564-pPyCAGIP)

All of these plasmids possess ampicillin-resistance cassettes to enable colony growth and selection. The GFP plasmid, empty vector and PNotchIC also contain puromycin resistance to enable the creation of stably transfected cell lines. Note that luciferase and renilla are not appropriate for stable transfection.

Plasmids were transformed into MAX efficiency® DH5α competent cells (Invitrogen 18258-012) and then expanded using ampicillin resistance growth cultures. Plasmid DNA was then extracted from the cultured cells using MidiPrep (Qiagen 12243) and stored at -70 °C.

Day One:

Plasmids to be transfected were made up into 10 ng/mL solutions. 100 µL samples of DH5α cells were thawed on wet ice from -70 °C and placed in chilled polypropylene tubes, one sample for each plasmid. 1 µL plasmid was added to 100 µL cell sample and heat-shock transformed as described in the Invitrogen protocol (Cat No: 18258-012). Briefly, this entailed incubation of the suspension on wet ice for 30 minutes, followed by heat-shock for 45 seconds at 42 °C in a water bath, then placement on ice for 2 minutes, addition of 0.9 mL S.O.C. medium (15544-034 Invitrogen). Cell suspensions were shaken at 225 rpm at 37 °C for 1 hour and then spread in 10-100 µL aliquots onto agar plates containing 100 µg/mL ampicillin. Plates were incubated overnight.

Agar plates were made by melting the pre-prepared solid agar in a microwave, and were then allowed to cool until it was possible to hold the bottle with bare hands. Appropriate antibiotics for resistance were then added. In this case, ampicillin 100 μg/mL was used (stock solution 50 mg/mL so 1 mL added to a 500 mL bottle of agar). The agar was then poured into plates and allowed to set, avoiding condensation on the lids that can increase contamination (by setting the plates in cell culture hoods). Following setting, cells were spread onto plates and incubated upside down in the bacterial incubator (37 °C) overnight.

Day Two:

Colony growth was checked on each plate, and the plates were wrapped in parafilm and store in the fridge until the afternoon. Single colonies were selected from each plate for each plasmid. In this case, single colonies from the 10 μL aliquot plates were used. A pipette tip was used to lift the colonies and transfer them to 4 mL of Lysogeny (LB) broth supplemented with 100 μg/mL ampicillin. The control comprised broth with no added cells. The broth was stored overnight at 37 °C at 225 rpm.

Day Three:

The 4 mL tubes were inspected and appeared cloudy due to cell growth. These were placed in the fridge to await the afternoon. In the afternoon, 400 μL of broth culture from each tube was added to 100 mL LB broth containing 100 μg/mL ampicillin. This was incubated overnight at 37 °C at 180 rpm in 500 mL conical flasks with sponge bungs.

Day Four:

The bacterial cells were harvested by placing 50 mL suspensions into Corese tubes and then centrifugation at 6000 g for 15 minutes at 4 °C to create cell pellets. Plasmid extraction was undertaken using QIAfilter Plasmid Midi kits according to the manufacturers instructions In essence, this results in purified pellets of plasmid

DNA that is then redissolved in TE buffer (pH 8.0). Quantification of plasmid yield was then performed by nanodrop.

Glycerol stocks of transformed cells were also stored at -70 °C, to avoid having to re-transform cells in the future if further plasmid stocks are required. This was performed by mixing 500 µL sterile autoclaved glycerol to 500 µL cells grown in selective LB broth and storage at -70 °C. When defrosted, these cells may be added to 100 mL LB broth containing 100 µg/mL ampicillin, incubated overnight at 37 °C at 180 rpm in 500 mL conical flasks with sponge bungs, prior to harvesting and purification of plasmid DNA.

Test of Plasmids

In order to test the plasmids, PNotchIC Sel39 plasmid was sequenced to confirm the correct inclusion of the NotchIC component in the plasmid (see below for details). A functional test of the ability of this plasmid to drive the 12CSL luciferase reporter was then undertaken. Following confirmation of the sequence, co-transfection of the PNotchIC Sel39 plasmid, empty vector plasmid and Sel35-12CSL luciferase reporter plasmid into CCA cell lines. Luciferase signal was then measured and found to be elevated in cells with PNotchIC Sel39 but not in cells with empty vector. This confirmed that the plasmids functioned appropriately.

Transfection of CCA cell lines with Notch reporter constructs

Transient transfection of Notch reporter constructs into CCA cell lines comprised the following category sets:

1. SV40-renilla + 12CSL-luciferase + pGFP (with subsequent treatment with γ-secretase inhibitor or chemotherapy)
2. SV40-renilla + 12CSL-luciferase + pNotchIC

SV40-renilla functions as an equaliser for transfection efficiency (vector tagged to renilla fluorescent protein), whilst 12CSL-Luciferase responds to Notch pathway

signalling and produces a measureable signal, that may be quantified relative to SV40-renilla. pGFP functions as a visual signal to confirm successful transfection as GFP may be directly visualised by fluorescent live cell photomicroscopy. Finally, pNotchIC acts as a positive control for Notch pathway signalling by comprising the internal portion of the Notch receptor, with the result that transfected cells demonstrate constitutively Notch pathway activation.

Transient transfection was performed in 24 or 48 well plates. Cells were grown to 70-90% confluence (seeding numbers characteristically required 0.5 to 2.0 $x10^5$ cells per well in 24 well plates to enable transfection 24 hours after plating). Cells were washed with cell culture media (not PBS as phosphate may inhibit transfection) and cultured for six hours in antibiotic-free 10% FCS L-glutamine-enriched culture media (IMDM/RPMI-1640).

Lipofectamine-plasmid suspensions were generated, with a total volume of 100 µl per well in a 24 well plate and 50 µl per well in a 48 well plate. The suspensions were generated as follows (quantities described below are for one well in a 24 well plate and should be scaled appropriately to the number of wells transfected):

A: 50 µL RPMI + 0.1 µg SV40-renilla + 0.5 µg 12CSL-luc + 0.5 µg pNotchIC Sel39 (or 0.5 µg pGFP)
B: 50 µL RPMI + 1.5 µL lipofectamine

These mixtures were allowed to stand for 5 minutes, then A and B were mixed (by adding dropwise) and left to stand for a further 35 minutes, then the appropriate volume added to each well for transfection.

After 18 hours, wells were washed with antibiotic-free culture media to remove transfection suspension, then cultured for a further six hours in antibiotic-free 10% FCS media reverting to ongoing culture in antibiotic-containing 10% FCS cell culture media thereafter. To confirm transfection, live cells were visualised under a microscope through the FITC filter to identify cells that expressed GFP signal. Cells

were then treated experimentally for up to 48 hours, for example with γ-secretase inhibitor or chemotherapeutic drugs prior to analysis of Notch pathway activation.

Wells were then washed with with PBS and analysed using Dual-Glo® Luciferase Reporter Assay System (Promega, Madison, Wisconsin, USA) according to the manufacturer's instructions. Briefly, this entailed addition of passive lysis buffer (Dual-Glo ® Luciferase Assay Reagent) - 50 µl for 48 wells or 100 µl for 24 wells - and storage of the plates at -20°C prior to analysis. Plates were brought back to room temperature and analysed within two hours. Cell lysates were transferred to opaque 96 well plates (to remove signal interference between wells) and 12CSL-luciferase luminescence of the wells was measured in a semi-automated plate reader An equal volume of Stop and Glo ® Reagent (quenches the luciferase signal and provides substrate for the renilla) was added to the wells by the semi-automated plate reader , incubated for 10 minutes and then the renilla luminescence was measured. Results expressed as ratio of the two readings.

Sanger Sequencing of pNotchIC Sel39 plasmid

The full sequence of Notch1 was obtained from Dr Sally Lowell (MRC Scottish Centre for Regenerative Medicine) as a CM5 file. This was opened in Notepad (to create a continuous sequence), put into BLAST to compare it to the murine form of Notch1 (mus musculus). This sequence encodes for the Notch intracellular domain region. The identified sequence was copied into the GenScript sequencing primer design tool (http://www.genscript.com/cgi-bin/tools/sequencing_primer_design).

In designing primers to sequence the NICD plasmid, the primer design software was set to allow for base pair gaps between the primers to be 500 or 650 base pairs, with a Tm 60 °C (+/-5 °C).

Sequence inserted for Notch1:

TCGTGCATCTGTTAGCGGCCGCTCGACCCGGCGCCAGCATGGCCAGCTCT
GGTTCCCTGAGGGTTTCAAAGTGTCAGAGGCCAGCAAGAAGAAGCGGAG

AGAGCCCCTCGGCGAGGACTCAGTCGGCCTCAAGCCCCTGAAGAATGCC
TCAGATGGTGCTCTGATGGACGACAATCAGAACGAGTGGGGAGACGAAG
ACCTGGAGACCAAGAAGTTCCGGTTTGAGGAGCCAGTAGTTCTCCCTGAC
CTGAGTGATCAGACTGACCACAGACAGTGGACCCAGCAGCACCTGGACG
CTGCTGACCTGCGCATGTCTGCCATGGCCCCAACACCGCCTCAGGGGGAG
GTGGATGCTGACTGCATGGATGTCAATGTTCGAGGACCAGATGGCTTCAC
ACCCCTCATGATTGCCTCCTGCAGTGGAGGGGGCCTTGAGACAGGCAAC
AGTGAAGAAGAAGAAGATGCACCTGCTGTCATCTCTGACTTCATCTACCA
GGGCGCCAGCTTGCACAACCAGACAGACCGCACCGGGGAGACCGCCTTG
CACTTGGCTGCCCGATACTCTCGTTCAGATGCTGCAAAGCGCTTGCTGGA
GGCCAGTGCAGATGCCAACATCCAGGACAACATGGGCCGTACTCCGTTA
CATGCAGCAGTTTCTGCAGATGCTCAGGGTGTCTTCCAGATCCTGCTCCG
GAACAGGGCCACAGATCTGGATGCCCGAATGCATGATGGCACAACTCCA
CTGATCCTGGCTGCGCGCCTGGCCGTGGAGGGCATGCTGGAGGACCTCAT
CAACTCACATGCTGACGTCAATGCCGTGGATGACCTAGGCAAGTCGGCTT
TGCATTGGGCGGCCGCGGTGAACAATGTGGATGCTGCTGTTGTGCTCCTG
AAGAACGGAGCCAACAAGGACATGCAGAACAACAAGGAGGAGACTCCC
CTGTTCCTGGCCGCCCGTGAGGGCAGCTATGAGACTGCCAAAGTGTTGCT
GGACCACTTTGCCAACCGGGACATCACGGATCACATGGACCGATTGCCG
CGGGACATCGCACAGGAGCGTATGCACCACGATATCGTGCGGCTTTTGG
ATGAGTACAACCTGGTGCGCAGCCCACAGCTGCATGGCACTGCCCTGGGT
GGCACACCCACTCTGTCTCCCACACTCTGCTCGCCCAATGGCTACCTGGG
CAATCTCAAGTCTGCCACACAGGGCAAGAAGGCCCGCAAGCCCAGCACC
AAAGGGCTGGCTTGTGGTAGCAAGGAAGCTAAGGACCTCAAGGCACGGA
GGAAGAAGTCCCAGGATGGCAAGGGCTGCCTGTTGGACAGCTCGAGCAT
GCTGTCGCCTGTGGACTCCCTCGAGTCACCCCATGGCTACTTGTCAGATG
TGGCCTCGCCACCCCTCCTCCCCTCCCCATTCCAGCAGTCTCCATCCATGC
CTCTCAGCCACCTGCCTGGTATGCCTGACACTCACCTGGGCATCAGCCAC
TTGAATGTGGCAGCCAAGCCTGAGATGGCAGCACTGGCTGGAGGTAGCC
GGTTGGCCTTTGAGCCACCCCCGCCACGCCTCTCCCACCTGCCTGTAGCC
TCCAGTGCCAGCACAGTGCTGAGTACCAATGGCACGGGGGCTATGAATTT
CACCGTGGGTGCACCGGCAAGCTTGAATGGCCAGTGTGAGTGGCTTCCCC

GGCTCCAGAATGGCATGGTGCCCAGCCAGTACAACCCACTACGGCCGGG
TGTGACGCCGGGCACACTGAGCACACAGGCAGCTGGCCTCCAGCATAGC
ATGATGGGGCCACTACACAGCAGCCTCTCCACCAATACCTTGTCCCCGAT
TATTTACCAGGGCCTGCCCAACACACGGCTGGCAACACAGCCTCACCTGG
TGCAGACCCAGCAGGTGCAGCCACAGAACTTACAGCTCCAGCCTCATAA
CCTGCATCCACCATCACAGCCACACCTCAGTGTGAGCTCGGCAGCCAATG
GGCACCTGGGCCGGAGCTTCTTGAGTGGGGAGCCCAGTCAGGCAGATGT
ACAACCGCTGGGCCCCAGCAGTCTGCCTGTGCACACCATTCTGCCCCAGG
AAAGCCAGGCCCTGCCCACATCACTGCCATCCTCCATGGTCCCACCCATG
ACCACTACCCAGTTCCTGACCCCTCCTTCCCAGCACAGTTACTCCTCCTCC
CCTGTGGACAACACCCCCAGCCACCAGCTGCAGGTGCCAGAGCACCCCTT
CCTCACCCCATCCCCTGAGTCCCCTGACCAGTGGTCCAGCTCCTCCCCGC
ATTCCAACATCTCTGATTGGTCCGAGGGCATCTCCAGCCCGCCCACCACC
ATGCCGTCCCAGATCACCCACATTCCAGAGGCATTTTGAATTTCGACTAG
CTAGAGCGGCCGCTCGAT

A number of primer sets were generated by the primer design software. To ensure optimum characteristics in terms of temperature conditions and primer length, forward primers were selected to span 500 base pair gap sets whilst reverse primers spanned 650 gap sets:

Table 2.1: NICD Plasmid Primers

Primer No.	Sequencing Range	Start Site	5'-Sequence-3'	Tm (°C)	Length
FOR_1	501-1000	457	AGAAGATGCACCTGCTGTCA	59.577	20
FOR_2	1001-1500	956	CGTGAGGGCAGCTATGAGAC	60.966	20
FOR_3	1501-2000	1456	TATGCCTGACACTCACCTGG	59.701	20
FOR_4	2001-2400	1954	ACACCTCAGTGTGAGCTCGG	61.502	20
REV_1	650-1	692	GGAGCAGGATCTGGAAGACA	60.349	20
REV_2	1300-651	1354	GGAGTCCACAGGCGACAG	60.415	18
REV_3	1950-1301	2005	CAAGAAGCTCCGGCCCAG	64.342	18

The NICD plasmid was sequenced by expanding the reporter constructs obtained as a kind gift from Dr Sally Lowell.

For sequencing, 3.2 pmol primer was added to 420 nmol of template generated from plasmid expansion and delivered to the sequencing institute as a 6 μL reaction sample in 0.2 mL Eppendorf.

Primers were supplied as 100 μmol stock solution by Eurogentec. These were made into 6 μL samples in 0.2 mL Eppendorf tubes comprising 3.2 pmol primer and 430 nmol pNotchIC Sel39 plasmid DNA and delivered to the sequencing facility. In total, 7 samples were generated, one for each primer. Briefly, this was performed by diluting 3.2 μL of stock primer solution with 96.8 μL H_2O then adding 1 μL of this to the reaction sample. The pNotchIC Sel39 plasmid DNA sample was generated at 860 nmol/L concentration (as assessed by spectrometry). This was diluted tenfold by adding 45 μL H_2O to 5 μL plasmid DNA. 5 μL (430 nmol) was then added to the reaction sample to comprise a total volume of 6 μL.
Sequencing was performed by the University of Edinburgh School of Biological Sciences Sequencing Service (SBSSS) using an ABI3730 sequencer (Applied Biosystems, UK) and the sequencing results were provided for analysis.

The sequences generated by the primers were analysed using sequence assembly software provided by Pôle Rhône-Alpes de Bioinformatique Site Doua (http://pbil.univ-lyon1.fr). In brief, the software assigned the seven separately generated primer sequences to homologous regions of the NICD sequence. This confirmed that the entire sequence (exons) of NICD was encoded within the plasmid DNA sequence generated.

On this basis, the sequencing of the 12CSL reporter was not required as a test of function could be performed: if the reporter responded to NICD signalling appropriately then this was considered to be sufficient proof of principle that the system worked

Small Animal High Frequency Ultrasound

Rats were anaesthetised by isoflourane inhalation with monitoring of body temperature, cardiac profile (electrocardiogram; ECG) and respiration (pulse oximeter) during ultrasound scanning using the Vevo 770 scanner (Visualsonics inc, Toronto, Canada). The abdomen was shaved and images of the liver were taken with the lowest frequency probe to obtain maximum ultrasound penetration (RMV 710B centred at 30 MHz with a 15 mm focal depth). The portal vein and porta hepatis were used as anatomical markers of location. Image acquisition was performed with and without intravenously injected microbubble contrast imaging agents (Vevo MicroMarker®) delivered via the tail vein. These microbubbles delineate the vasculature and are not specifically targeted to any structures. Ultrasound images were obtained of control non-fibrotic and TAA-treated fibrotic/cancer bearing animals.

Small Animal Magnetic Resonance Imaging

All MRI experiments were performed using a 7 T horizontal bore NMR spectrometer (Agilent, Yarnton, UK), equipped with a high-performance gradient insert (12 cm inner diameter, maximum gradient strength 400 mT/m). The rat was anaesthetized with 1.5–2% isoflurane in oxygen/air (50/50, 1 L/min), placed in a cradle (Rapid Biomedical GmbH, Rimpar, Germany), and the skull was fixed with plastic ear bars. Rectal temperature and respiration rate were monitored throughout the experiments, and body temperature was maintained at 37.0 °C with a heat fan. A birdcage coil (72-mm diameter) was used for radio frequency transmission and signal reception. All sequences were acquired using respiratory gating and the following parameters: field-of-view 80 mm×80 mm, matrix 256×256 (i.e. 312 μm in-plane resolution), slice thickness 1 mm.

T1-weighted MRI:

Twenty contiguous axial fast spin echo images (echo train length 4) were collected with the following parameters: repetition time (TR) = 1 respiratory cycle (~1000 ms),

effective echo time = 9 ms; 2 signal averages. This scan was acquired at baseline and following injection of Dotarem (gadolinium contrast agent).

T2-weighted MRI:

Twenty contiguous axial fast spin echo images (echo train length 4) were collected with the following parameters: TR = 2 respiratory cycles (~2000 ms), effective echo time = 36 ms; 4 signal averages. This scan was acquired at baseline.

T2*-weighted MRI:

Ten contiguous axial gradient echo images were collected with the following parameters: TR = 40 ms, echo time = 3.5 ms; flip angle 30°, 1 signal average. This scan was acquired at baseline and, following injection of Dotarem, interleaved with the T1-weighted scan.

Small Animal Fluorescent Imaging

Fresh tissue was obtained from *wt* and EGFP transgenic SD rats and imaged using the Olympus OV100 fluorescent imager. Acquisition settings were adjusted to obtain brightfield and fluorescent images which were overlaid to determine EGFP *in vivo* signal tissue depth penetrance.

Statistical Analysis

Where appropriate, statistical analyses were calculated using Student's two-tailed t test by GraphPad Prism v5.00 for Windows (GraphPad Software, San Diego, USA) or by means of one-way and two-way ANOVA with post-hoc Bonferroni testing. Significance was defined as $P<0.05$.

CHAPTER THREE

MODELS OF CHOLANGIOCARCINOMA

Introduction

A range of animal model systems of human malignancies have been developed that provide essential information regarding *in vivo* behaviour of cancer cells. Examples of these include subcutaneous administration of human cancer cells to immunodeficient mice with subsequent tumour formation (xenogeneic), and administration of animal cancer cells into immunocompetent host animals that are able to mount a typical tumour immune response without inducing transplant rejection (syngeneic). Other animal models are generated by dysregulation of specific genes that result in spontaneous *in vivo* tumour formation. A final model type entails administration of carcinogenic substances to wild type (*wt*) animals that then develop progressive lesions.

A limitation of many model systems is that the induced tumours comprise primarily of cancer cells; neither tumour associated stroma nor pre-malignant stem cell niche cells are readily apparent in the lesions or precursor stages. In the case of cancer cell transplant models, this is due to administration of a bolus of tumour cells that are not penetrated by immune cells. In the case of spontaneous tumours, this occurs due to the rapidity of tumour formation and inexorable tumour progression.

In order to study the *in vivo* stepwise development of CCA and tumour-stroma interactions in established intrahepatic CCA lesions, I investigated the feasibility of all CCA tumour models described in the literature, as detailed in the Introduction (Chapter 1). Common to most of the systems identified was the absence of tumour-associated stroma and a failure to realistically recapitulate the tumour microenvironment. One model considered was from the Clarke group [476] in which combined Pten and Apc deletion resulted in intestinal adenocarcinomas and additional intrahepatic lesions. Specimen blocks were kindly provided by Professor Alan Clarke and Dr Victoria Marsh. At the time of investigating the model, the intrahepatic biliary lesions more clearly represented biliary polyps or intraepithelial neoplasia rather than carcinomas. Furthermore, the tumour-associated stroma was minimal, as identified by αSMA staining of lesions. In view of this, the model was not pursued further at this stage (**Figure 3.1**).

No satisfactory mouse models of intrahepatic CCA were found in pure background mice that would allow adoptive transfer of bone marrow (a core element of planned studies) without causing an immunological reaction. It was deemed impractical to perform adoptive transfer studies on DePinho's model of induced CCA by administration of intraperitoneal CCl_4 to p53-deficient mice [56]. This was because p53- deficient mice are particularly sensitive to irradiation protocols.

Figure 3.1: Clarke mouse model of intrahepatic CCA

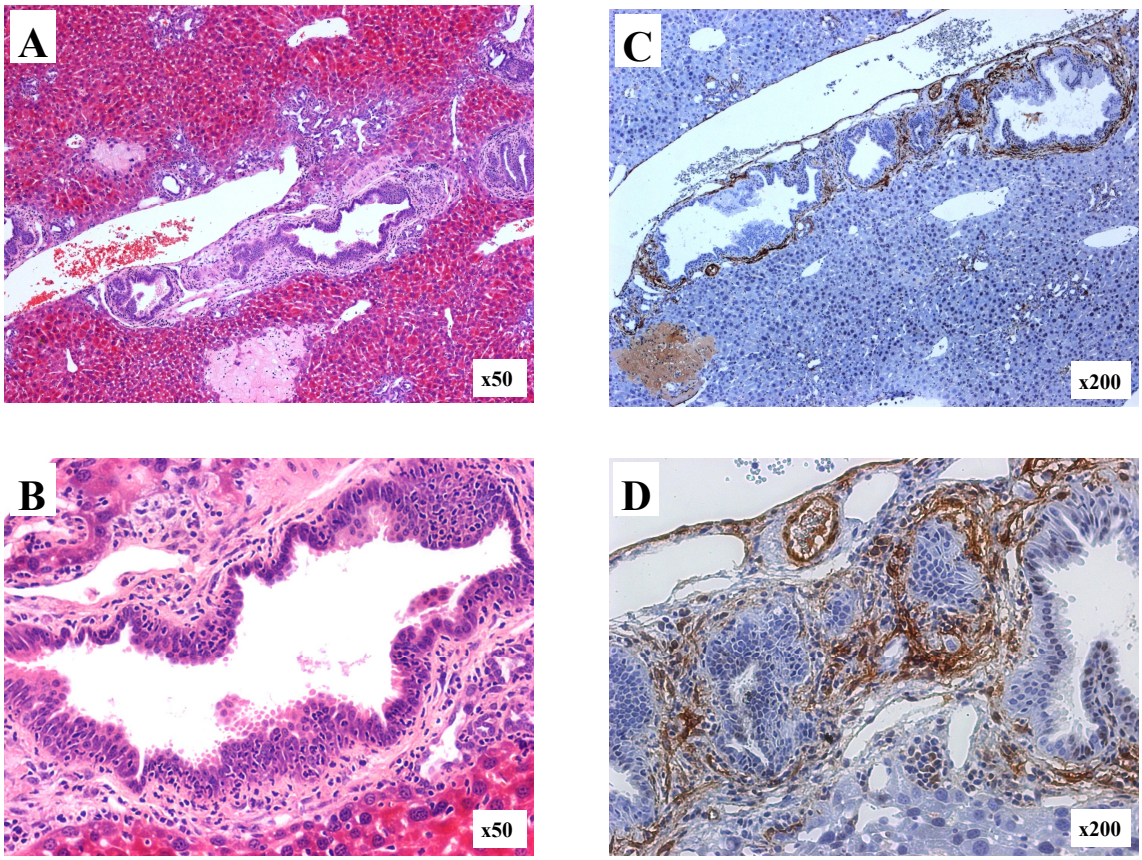

A: Proliferative biliary epithelium of medium and small bile ducts at 16 weeks. (haematoxylin and eosin stain).

B: Proliferative but not neoplastic features of biliary epithelium with no evidence of nuclear atypia or invasion through basemement membrane. (H&E stain).

C: A thin layer of myofibroblasts invests the bile ducts.
(αSMA immunohistochemistry).

D: Myofibroblasts ensheathe bile ducts but do not comprise a dense stromal mass. (αSMA).

CCA lesions develop in rats with prolonged administration of TAA

In view of current histological limitations of CCA models, and in light of the intention to perform adoptive transfer (bone marrow transplant) studies, a trial was undertaken of the administration of thioacetamide (TAA) in drinking water to adult Sprague Dawley (SD) rats in order to induce intrahepatic CCA.

To identify the timecourse of intrahepatic CCA induction in rats and to specifically identify a timepoint when 100% of animals would reliably have tumours, cholangiocarcinogenesis was induced by oral administration of low dose TAA (0.03%) in drinking water in male SD rats. Animals were sacrificed and liver tissue analysed at 4, 8, 10, 14, 18, 20, 26, 28 and 80 weeks (n=4 each timepoint except 28 and 80 weeks where n=2). Two rats were sacrificed at 80 weeks to investigate whether metastatic lesions developed. Comparison was made to tissue derived from age-matched, untreated control animals (n=1 each timepoint).

No tumours were identified until 14 weeks, when one of four livers demonstrated pale, firm hepatic nodules that were histologically confirmed as CCAs. However, at 16 and 20 weeks, no further animals had CCA despite continued development of inflammatory fibrotic changes in the liver parenchyma. At 26 weeks, all four animals exhibited CCA. Conversely, at 28 weeks, neither of the two animals sacrificed had lesions. Due to this finding, the remaining two animals in the planned cull cohort were not sacrificed as it became clear that it was not possible to identify reliably a timepoint when all animals consistently bore tumours. These two animals were instead sacrificed at 80 weeks and displayed intrahepatic CCA but no macroscopically identifiable metastases in the lungs or abdominal compartment (**Figure 3.2**).

Figure 3.2: TAA model of intrahepatic CCA in SD rats. Rodents were treated with 0.03% TAA for up to 80 weeks.

A Macroscopic features at 26 weeks.

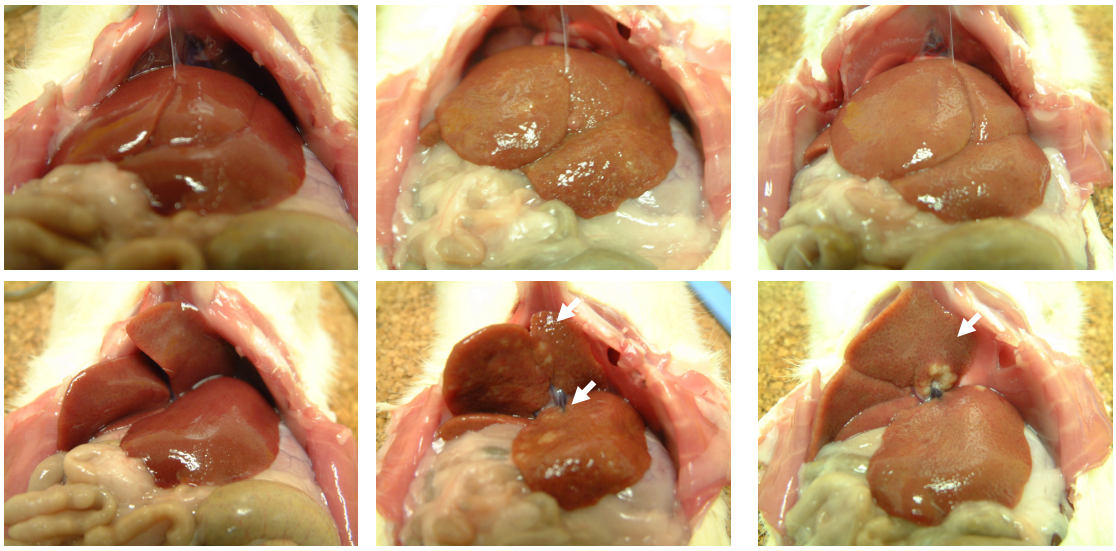

Control | Multiple Small Tumours | Single Large Tumour

B The 0.03% TAA diet did not yield a reliable timepoint for tumour formation.

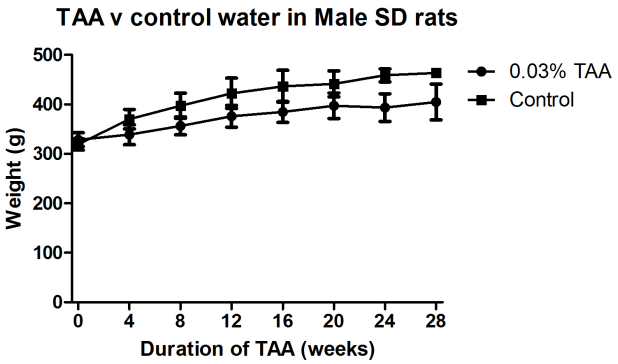

TAA (wks)	CCA	Group size
4	0	4
8	0	4
10	0	4
14	1	4
16	0	4
20	0	4
26	4	4
28	0	2

C At 80 weeks, tumours had grown significantly in size although there was no macroscopic evidence of systemic metastases.

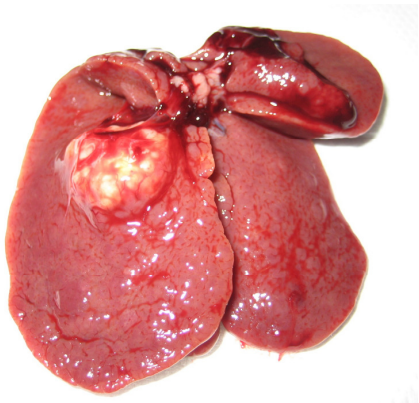

Human and TAA rat sections of cholangiocarcinoma show excellent phenotypic similarity.

CCA lesions in TAA-treated rats were found to display histological congruency with human tumours with very similar distribution of epithelial and stromal elements. Immunohistochemistry was performed for CK19+, CD68+, CD163+, αSMA+ cells and laminin extracellular matrix component.

CK19 expression in hepatic tissue identifies biliary epithelial cells, progenitor cells in the Canals of Hering and malignant epithelial cells in CCA [350, 496]. Progenitor cells in the periportal niche have the potential to differentiate into either biliary or hepatic phenotypes and are often referred to as oval cells based on their morphology. CD68+ (termed ED1+ in rat tissue) staining identifies migratory macrophages and monocytes, CD163+ (ED2+ in rat) identifies tissue resident macrophages (including Kupffer cells in the liver) [497], and αSMA expression delineates myofibroblasts [186]. The distribution of all these cellular and extra-cellular elements of the tumour associated stroma was found to be notably similar between human and rat lesions (**Figure 3.3**).

Figure 3.3: Comparative histology of human and rat intrahepatic CCA lesions

A

Both human and rat intrahepatic CCA lesions comprise disordered glandular epithelial cells surrounded by a dense stroma of extracellular and cellular elements (H&E stain).

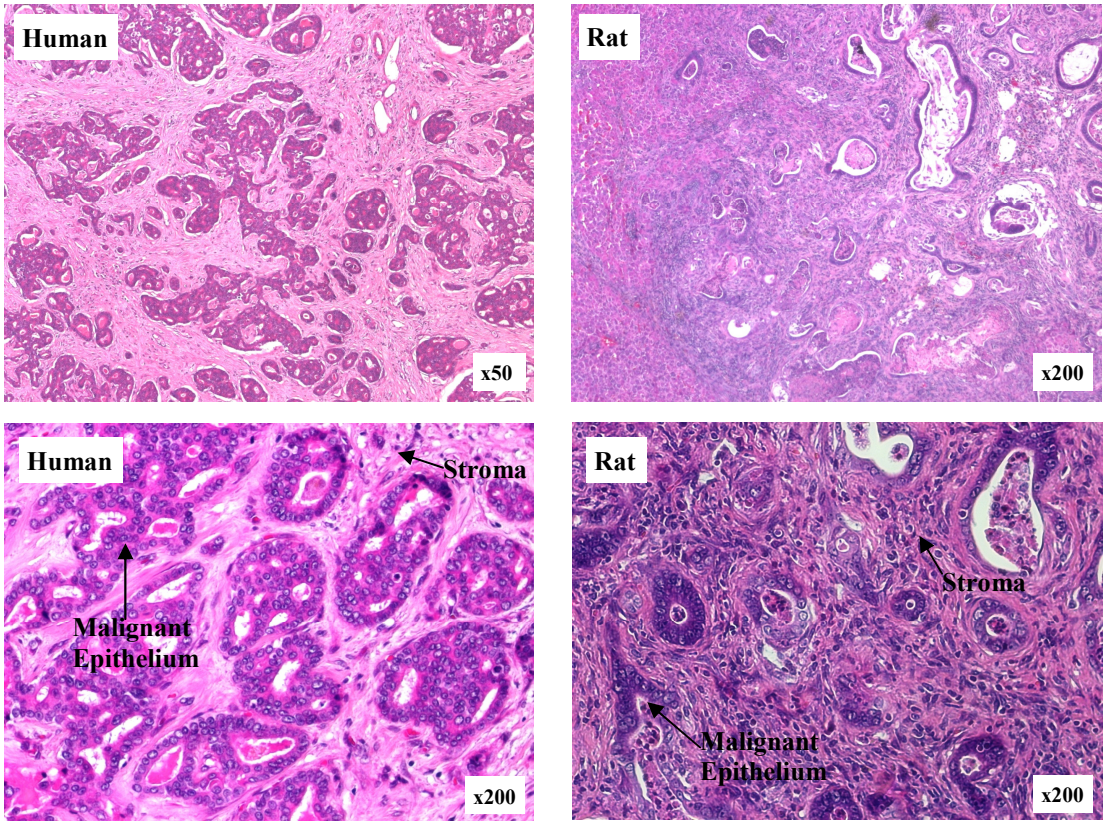

B

The pattern of expression of CK19+ malignant epithelial cells is similar in rats and humans (CK19 immunohistochemistry):

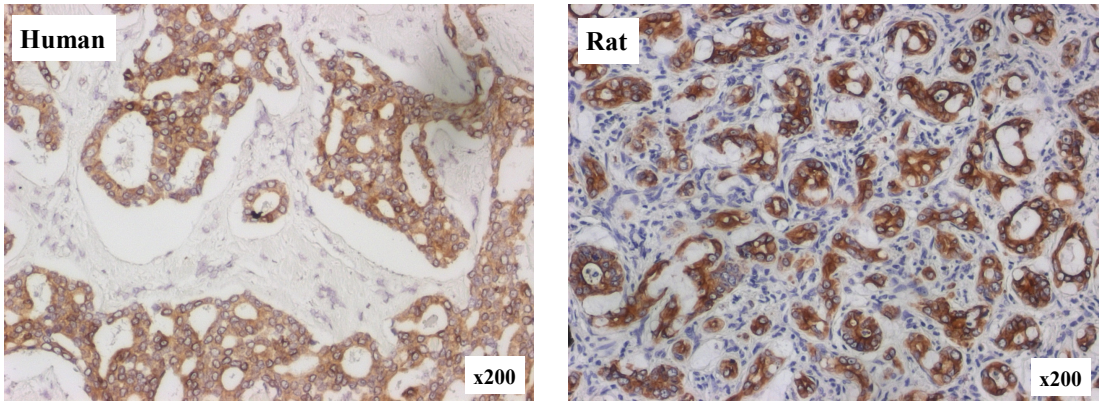

C

1: Migrating macrophages/monocytes (CD68/ED1) are distributed throughout the stroma (**1**), whereas tissue resident macrophages (CD163/ED2) are minimally present (**2**). Laminin surrounds all bile ducts (**3**). Myofibroblasts (αSMA) juxtapose bile ducts in an apparently direct cell contact mediated fashion (**4**).

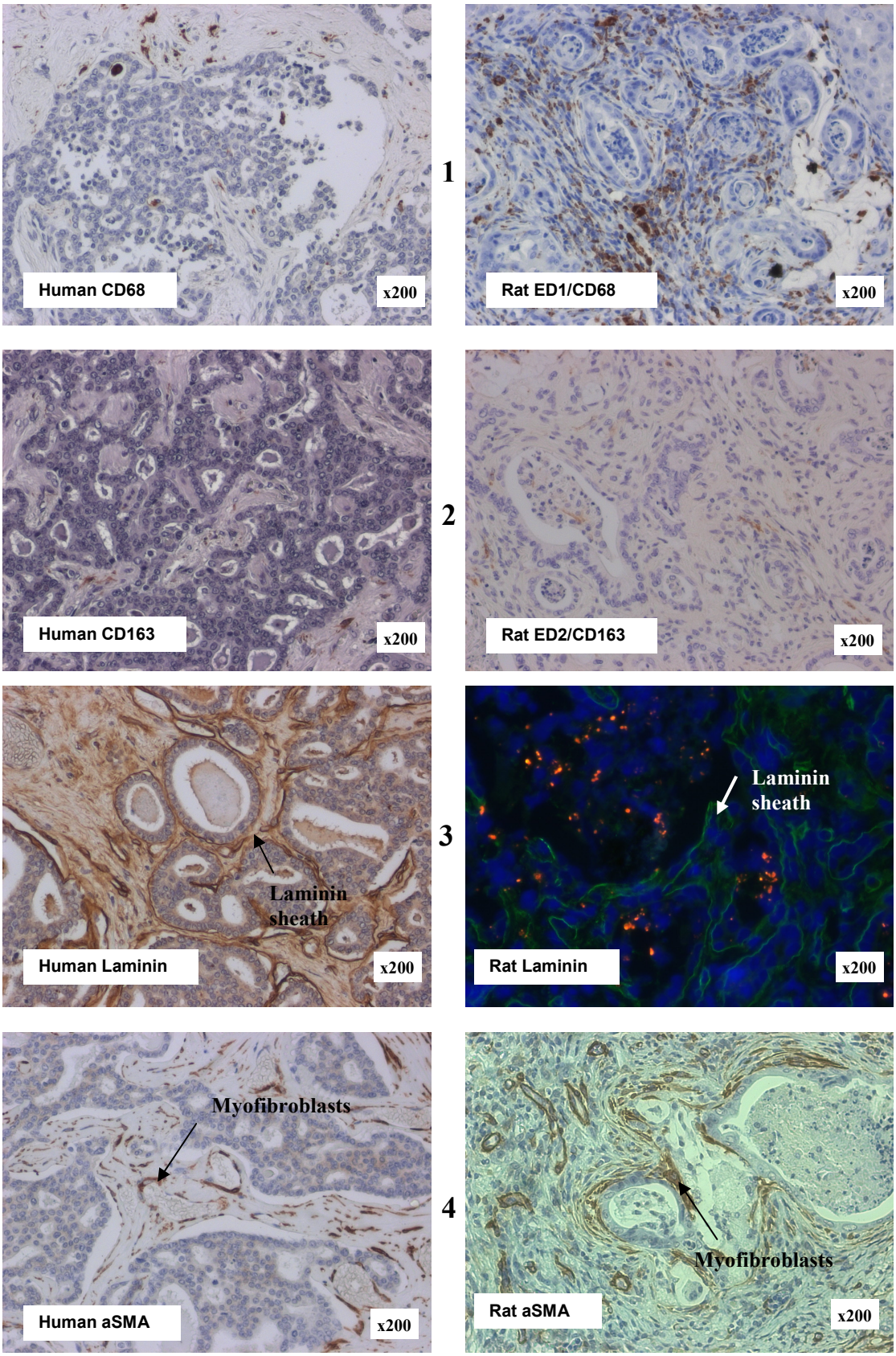

The TAA model demonstrates a stepwise progression of histological changes during carcinogenesis:

Early inflammatory changes appear in rat liver tissue from the fourth week of TAA administration. A niche of inflammatory cells and extracellular matrix (ECM) forms in the periportal regions where bile ductules and progenitor cells are located. Migratory ED1/CD68+ macrophages (**Figure 3.4**) aggregate at the periportal space and interlobular plates in a progressive fashion in the premalignant hepatic environment and are particularly prominent in CCA tumour stroma. Similarly, αSMA+ myofibroblasts accumulate at the "invading edge" of fibrosis in the periportal and interlobular plate regions and are also very prominent in tumour stroma (**Figure 3.5**). In contrast, the distribution of tissue resident ED2/CD163+ macrophages does not change during the treatment regime and these cells are not present in CCA tumour stroma in significant numbers **(Figure 3.6)**.

In both healthy and inflamed/premalignant liver and also in CCA lesions, the ECM protein laminin closely invests bile ducts, oval cells and the epithelial component of CCA lesions **(Figure 3.7)**. In CCA, the laminin basement membrane continues to encircle malignant bile ducts despite the invasive phenotype of the cancer cells.

Oval cells (CK19+) proliferate during hepatic inflammation and are found to accumulate during the prolonged TAA regime. Additionally, CCA lesions show strong CK19+ staining (**Figure 3.8)**.

Figure 3.4: The TAA rat model of CCA demonstrates a stepwise progression of histological and inflammatory changes

CD68/ED1 macrophages (MΦ) migrate to peri-portal regions during the TAA regime and are prominent in CCA tumour stroma.

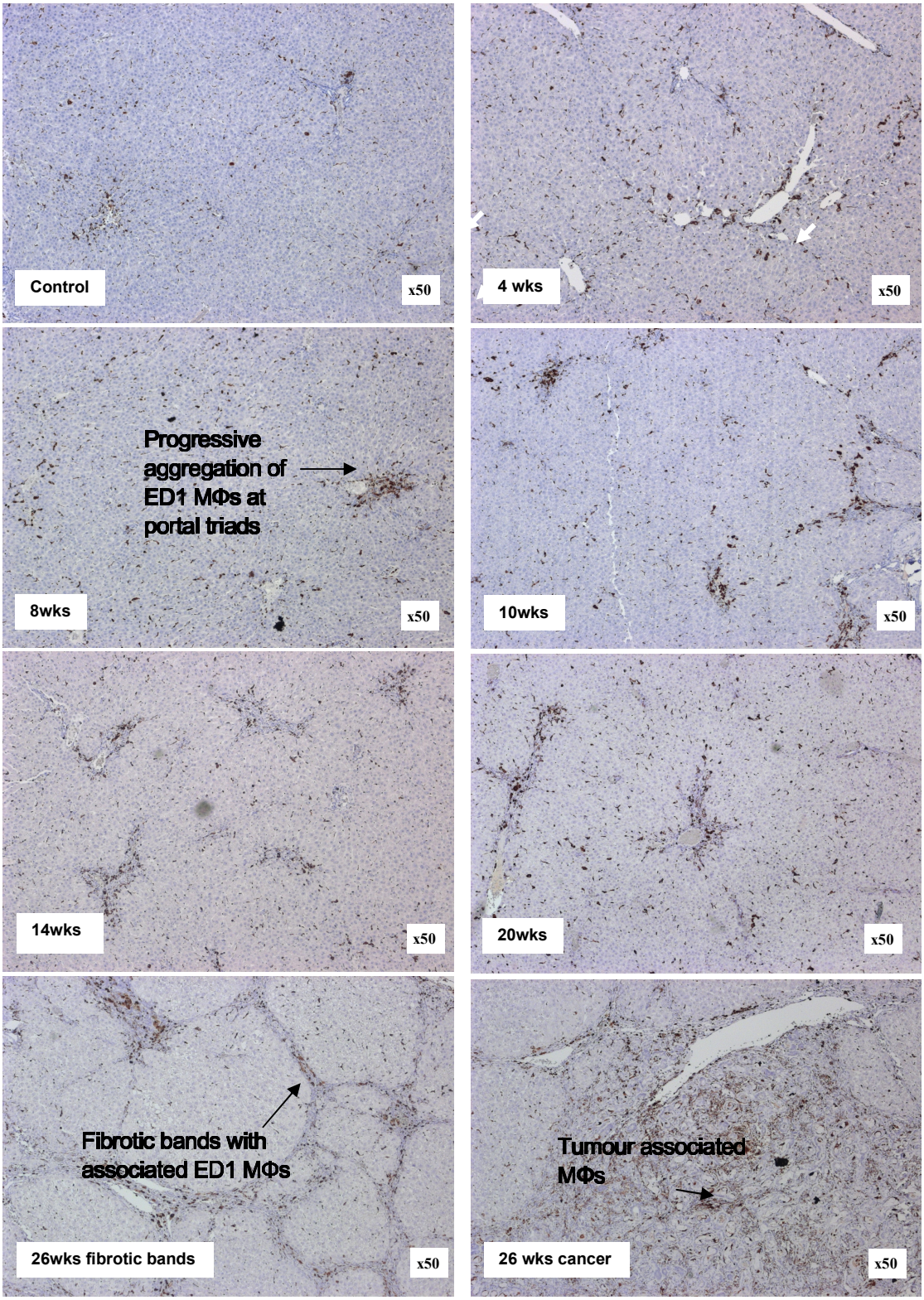

Figure 3.5: Distribution of αSMA+ myofibroblasts

αSMA+ cells accumulate at the "invading edge" of liver fibrosis during TAA administration and are prominent in tumour stroma.

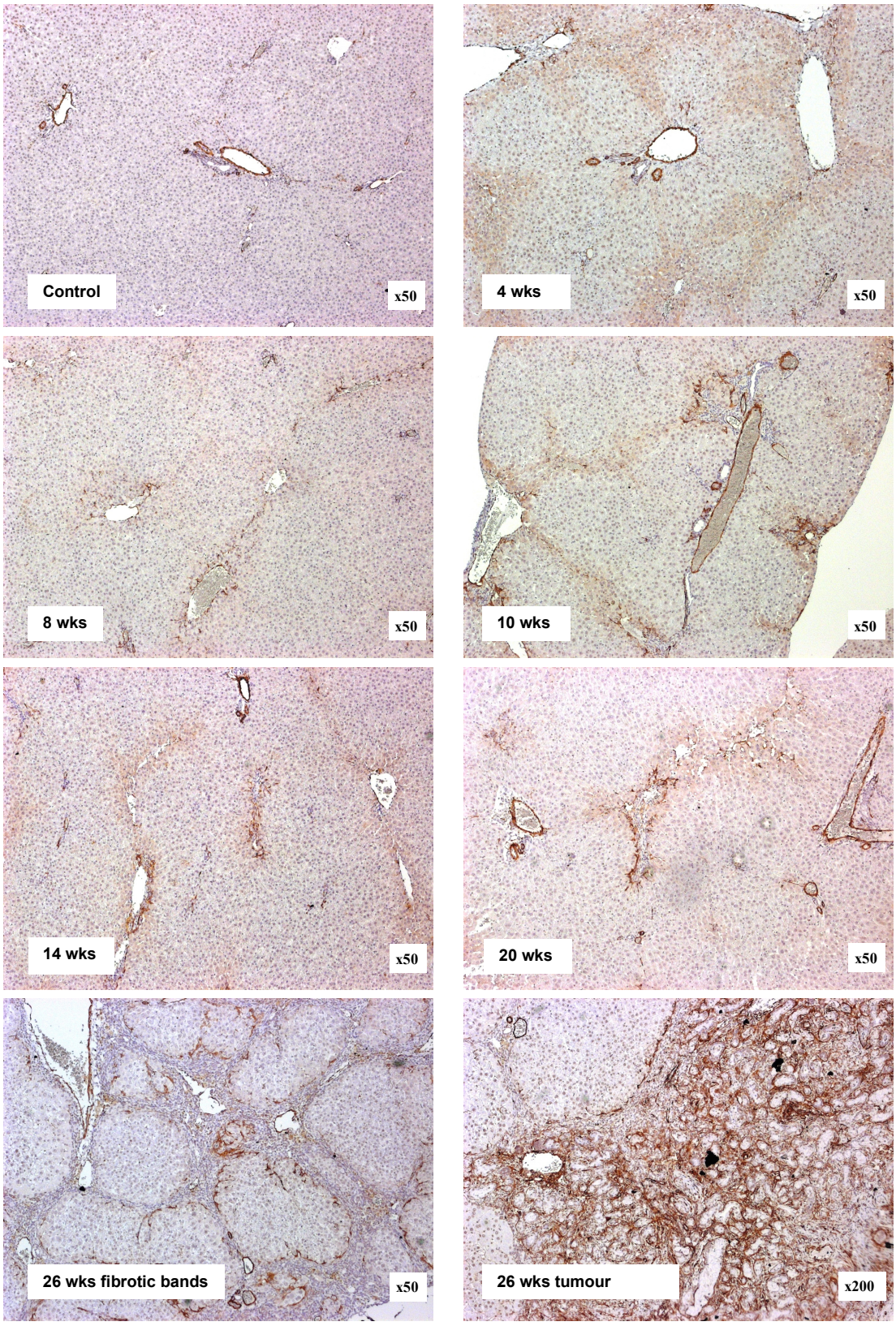

Figure 3.6: Distribution of CD163/ED2 tissue resident macrophages

CD163/ED2 distribution does not change significantly during TAA administration regime and these cells are not present in CCA tumour stroma.

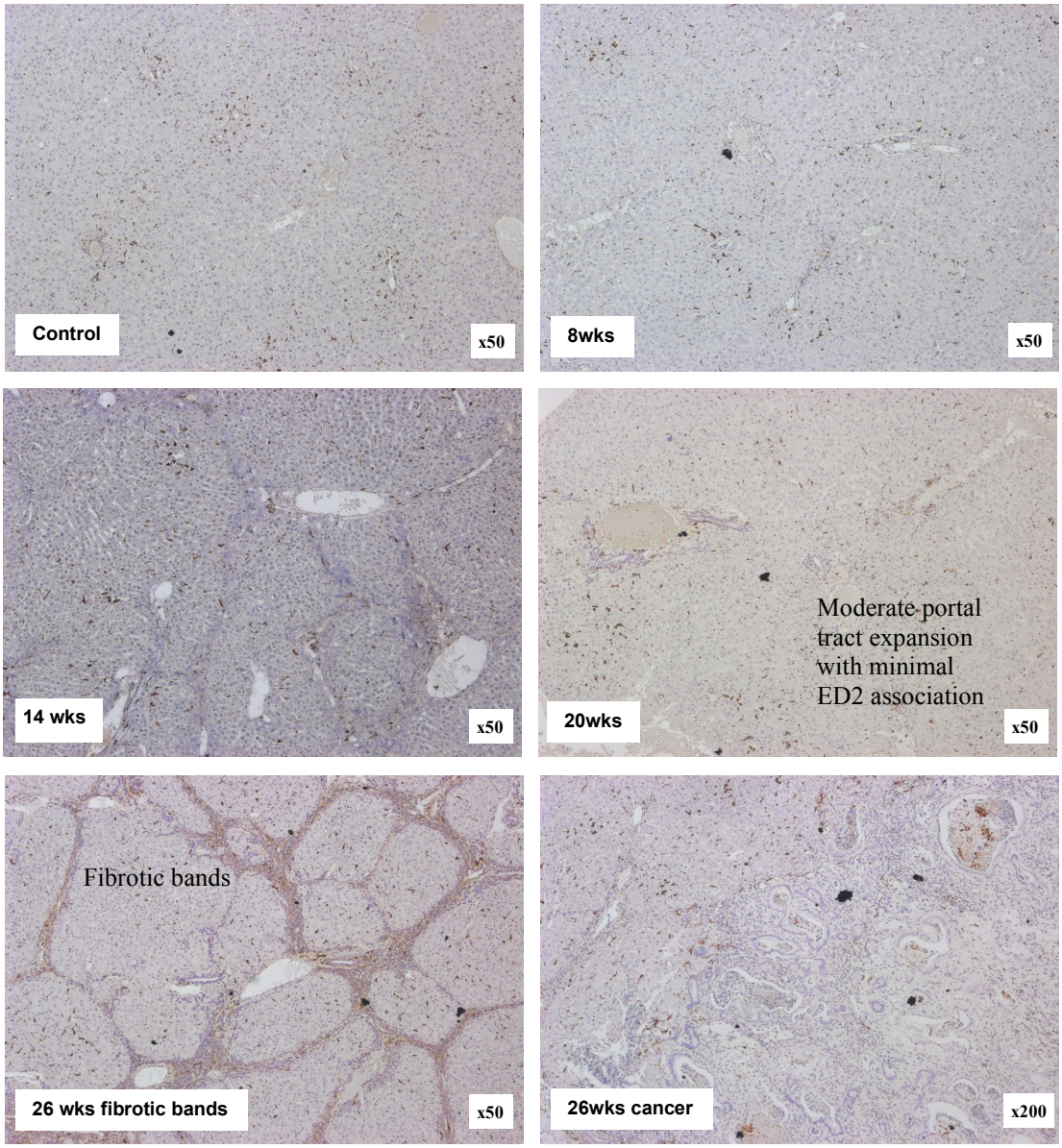

Figure 3.7: **Laminin closely invests bile ducts, oval cells and CCA lesions**

A Laminin distribution does not change during TAA cholangiocarcinogenesis.

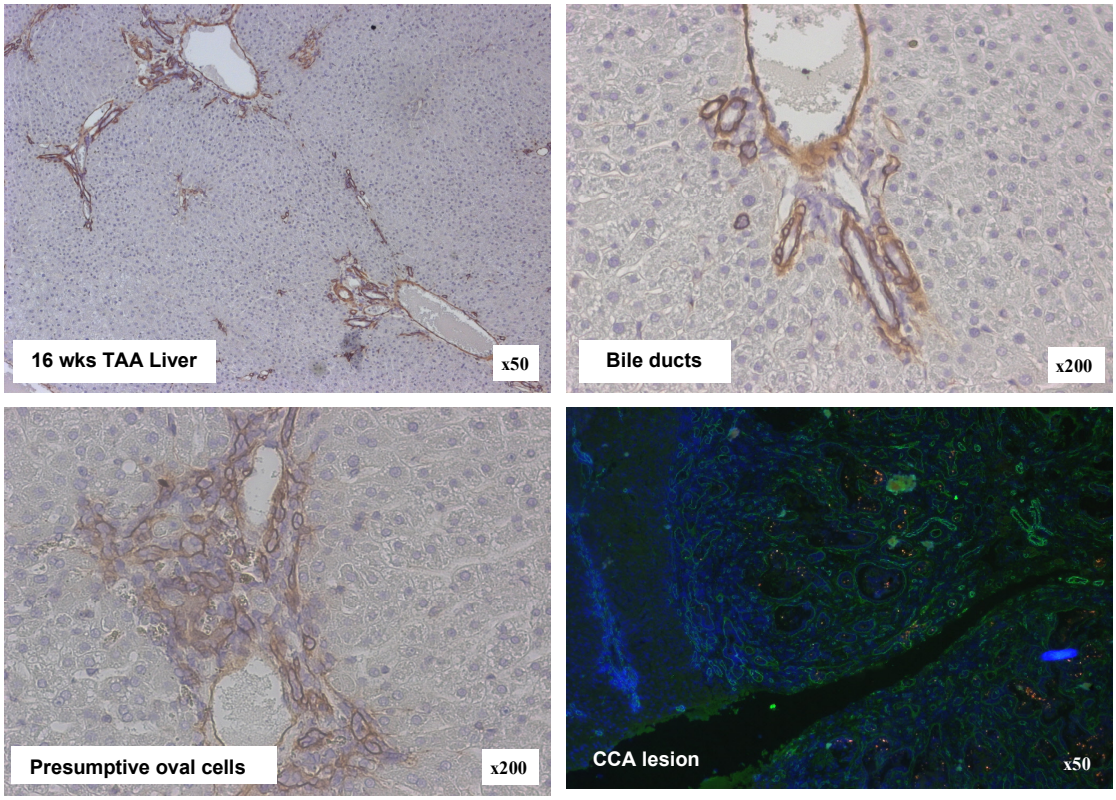

B Laminin ensheathes proliferating oval cells in TAA-treated rats: dual immunofluorescence for CK19 (red) and Laminin (Green) after 16 weeks TAA.

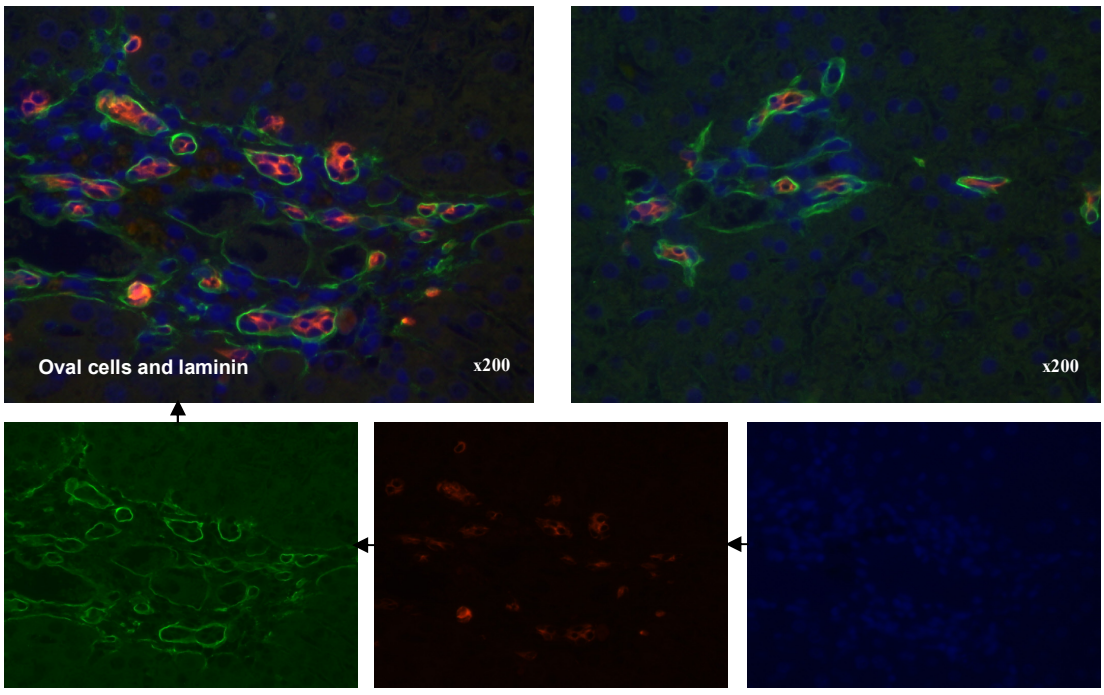

Figure 3.8: Oval cells (CK19+) behaviour
CK19+ cells accumulate after prolonged TAA treatment and CCA lesions demonstrate strong CK19+ staining.

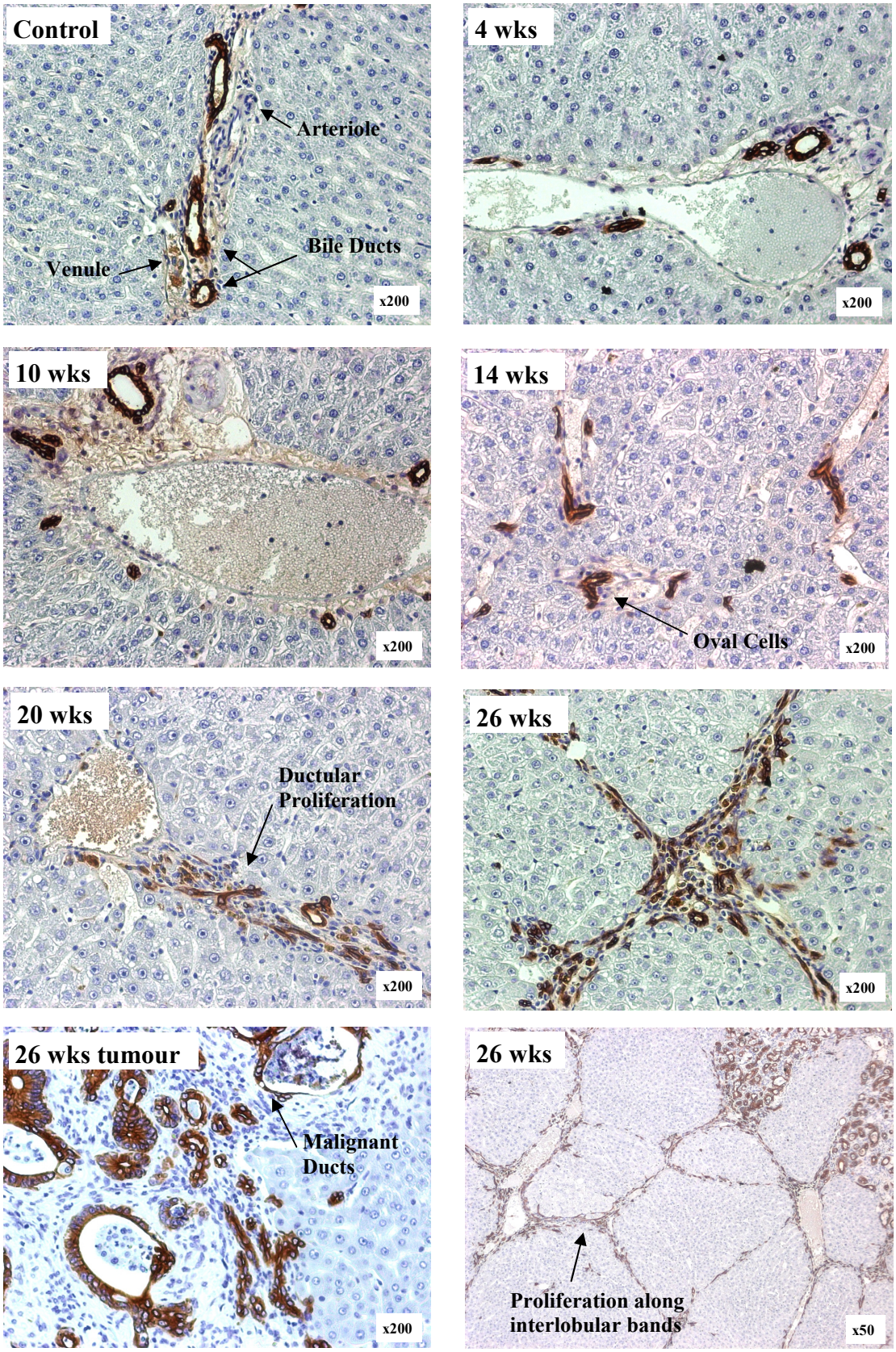

Liver fibrosis and progenitor cell proliferation in the TAA model precedes CCA formation

The relationship between the development of inflammatory liver fibrosis and oval cell proliferation was studied during the time period prior to the onset of CCA. The oval/progenitor cell response to TAA-induced hepatic inflammation was measured by counting CK-19+ cells that were not part of established bile ductular structures. Liver fibrosis was characterised by quantitative analysis of picrosirius red (PSR) staining. Oval cells numbers were found to increase in a progressive manner with prolonged TAA administration, when compared to untreated controls. Compared to untreated controls, oval cell numbers doubled from 4 weeks (2.0 fold, $p=0.07$), with a statistically significant increase from 10 weeks onwards (2.1-fold, $p=0.01$). The oval cell response was markedly increased following 26 weeks of TAA (25.6-fold, $p=0.03$) **(Figure 3.9A**).

Histological analysis of PSR-stained liver sections from the same TAA-treated rats identified bridging fibrosis between portal triads along interlobular plates from 20 weeks onwards. By 26 weeks, this had progressed to established liver cirrhosis, with dense bridging fibrosis and regenerative nodules. Liver fibrosis was quantified by digital image analysis of PSR-stained sections. Until week 20, there was no significant increase in liver fibrosis in comparison to untreated controls. Following 20 weeks of low dose TAA treatment there was a modest but significant increase in PSR-staining (1.7 fold, $p=0.01$). At 26 weeks there was a marked increase in liver fibrosis (6.3-fold, $p<0.0001$) relative to untreated controls **(Figure 3.9B**).

The major expansion in oval cell numbers at 26 weeks corresponded to a similar increase in PSR-staining at this time point. Regression analysis identified a positive correlation between oval cell numbers and liver fibrosis as identified by PSR staining ($R=0.665$, $p<0.001$). The more modest early increase in oval cell numbers from week 4 onwards (2.0 fold increase) preceded the development of significant liver fibrosis and intrahepatic CCA lesions **(Figure 3.9C**).

Figure 3.9 Liver fibrosis and oval cell (CK19+) proliferation during TAA induced cholangiocarcinogenesis

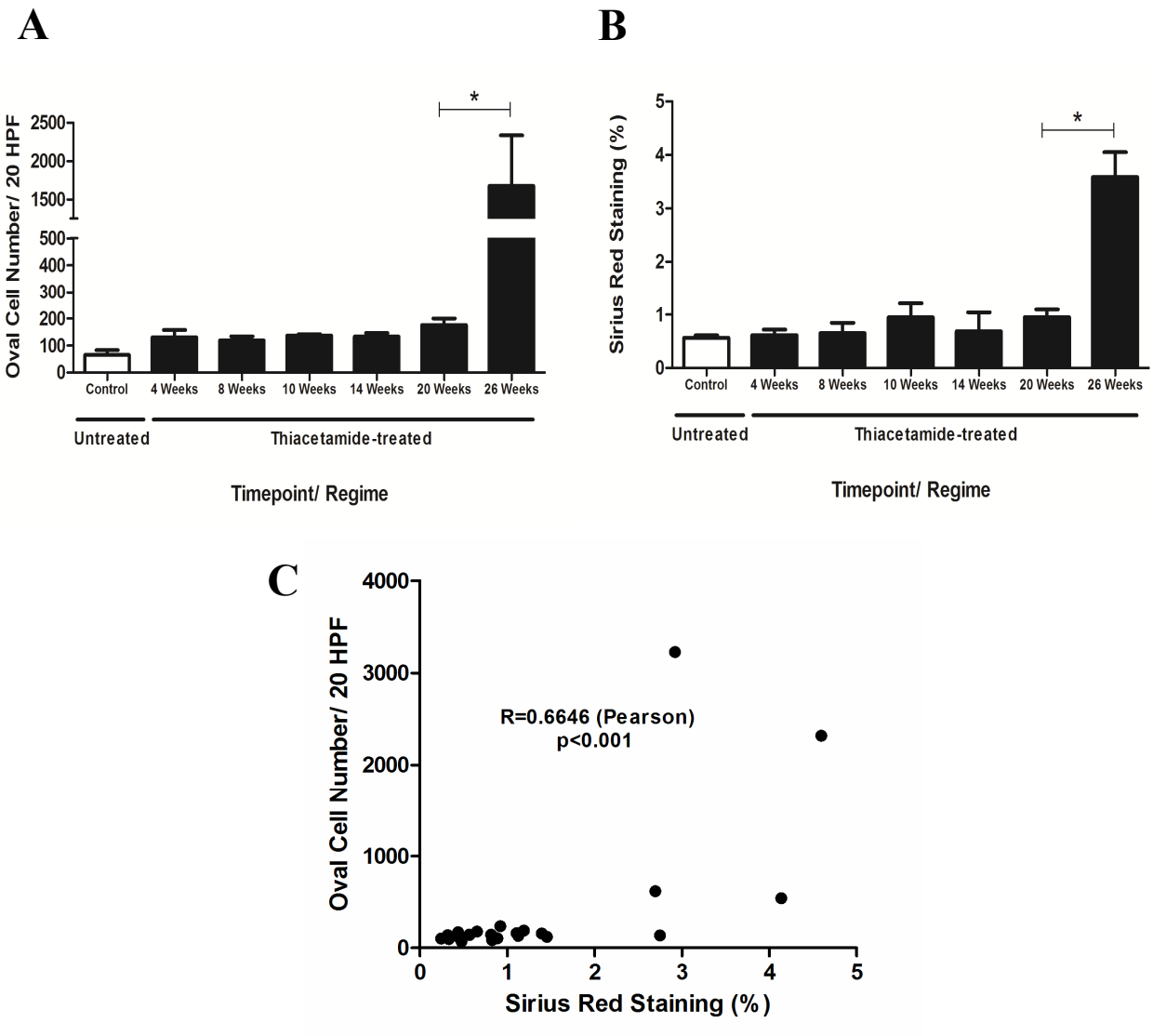

(**A**) Quantification of CK-19+ cells in liver sections. Each bar represents the mean number of non-bile duct associated CK-19+ cells per high power field (x200) from 3-6 animals (n=6 controls, n=3 at 14weeks, otherwise n=4). (**B**) Liver fibrosis quantification by digital analysis of PSR-staining of liver sections from the same rats. Each bar represents the mean percentage area of PSR-staining per high power field (x200) field from 3-6 animals. (**C**) Statistical correlation between oval cell number and liver fibrosis (% PSR staining) (R= Pearson correlation co-efficient). In each case error bars represent SEM, *p<0.05 (t-test).

The TAA model, tissue processing, CK19+ immunohistochemistry, oval cell counting and PSR staining were performed by myself. Dr Timothy Gordon-Walker undertook the PSR digital image analysis and the regression statistical analysis between oval cell numbers and PSR staining.

***In vivo* tumour imaging with ultrasound scanning is currently unsuitable for TAA induced rat CCA lesions**

In view of the unpredictable appearance of CCA lesions in the 0.03% TAA model, the use of small animal imaging modalities was investigated to identify lesions and to measure tumour size *in vivo* prior to harvest. The Home Office license was rewritten to include the use of high-frequency ultrasound and small animal 7-Tesla MRI to identify animals with lesions *in vivo* and to measure tumour dimensions in live animals. Ultrasound was selected as the favoured modality to identify tumours in animals due to relative analysis speed and lower costs than MRI.

A pilot ultrasound scan on two rats was performed. One rat received 40 weeks TAA and was compared to an age-matched control rat that received normal water. Scans were performed with the addition of intravenously administered microbubble contrast agent to enhance the hepatic vasculature. The process was time-consuming, taking longer than one hour per rat under anaesthesia, expensive (greater than £100 per contrast aliquot) and the area of assessable liver was only $1cm^3$ per ultrasound scan session. This equates to less than 20% of the liver volume of an adult SD rat. The resulting ultrasound scan images were of insufficiently high resolution for small lesion detection, and it was not possible to identify either intrahepatic lesions or liver fibrosis. No tumours were positively identified (**Figure 3.10**).

Figure 3.10: High frequency liver ultrasound of TAA and control SD rats

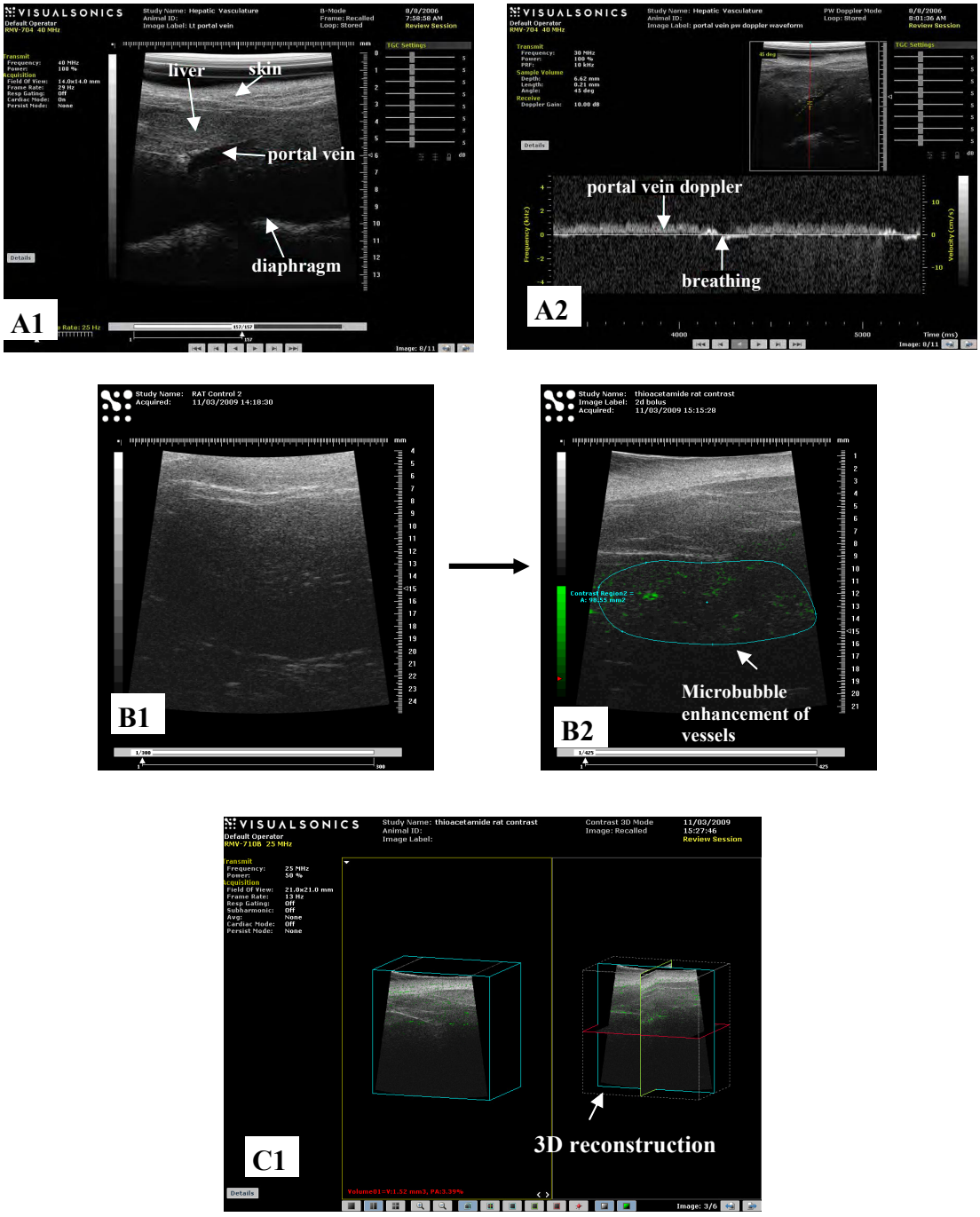

A1: Representative ultrasound image of portal vein and liver parenchyma of rat provided by Visualsonics **A2:** Representative Doppler waveform signal from portal vein **B1:** Cross-sectional ultrasound of rat liver **B2:** Enhanced microbubble contrast ultrasound of TAA-treated liver section, with region of interest (highlighted in blue) identifying intrahepatic vasculature **C1:** Three dimensional reconstruction of serially collected trans-sectional ultrasound images of TAA-treated liver with microbubble enhancement. No evidence of liver tumours seen.

***In vivo* tumour imaging with Magnetic Resonance Imaging identifies TAA induced rat CCA lesions**

MRI imaging provides the most accurate assessment of tumour dimensions and temporal growth. However, the technique is expensive and labour intensive. A pilot study was undertaken using a 7-Tesla horizontal bore NMR spectrometer of the feasibility of using the technology. MRI scanning with intravenous gadolinium contrast was undertaken to sequentially acquire T1, T2, T2* perfusion weighted and gradient echo multislice (GEMS) MRI images of the same TAA treated rat as used in the above ultrasound study. At 40 weeks, tumours were identified in the liver with high anatomical accuracy.

The TAA-treated animal was harvested following 80 weeks TAA administration and found to have a large 1cm CCA on the under surface of the liver together with multiple intrahepatic tumours, corresponding to the lesions identified on MRI scanning but not visualised with ultrasound imaging (**Figure 3.11**).

Figure 3.11: MRI with gadolinium contrast of TAA-treated compared to control rat

Gadolinium contrast enhancement reliably identified CCA lesions in TAA-treated rat tissue in T1 weighted images, with additional peritumoral vasculature on T2* weighted perfusion scanning. In the Gradient Echo Multislice imaging, TAA-treated rat liver is nodular in comparison to control rat liver.

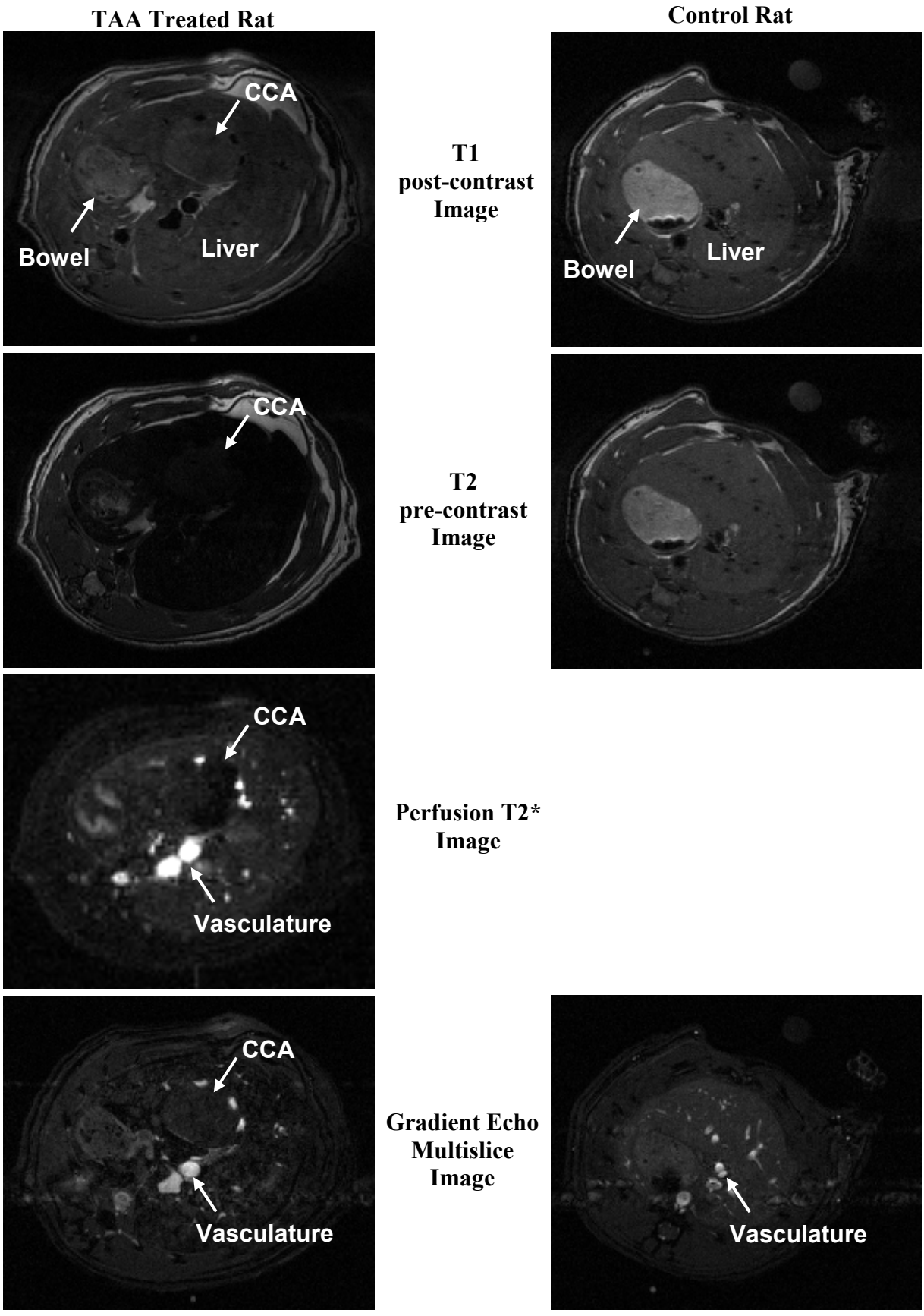

***In vivo* tumour imaging with live fluorescent imaging is currently not possible for TAA induced rat CCA lesions**

In view of the EGFP+ BM adoptive transfer experiments being undertaken (see Chapter 5), an investigation was undertaken of the feasibility of imaging fluorescent intrahepatic CCA lesions in live *wt* SD rats following EGFP+ BM adoptive transfer and subsequent TAA treatment. The liver of an EGFP+ SD rat was overlaid with a section of abdominal wall from a *wt SD* rat and imaged with an Olympus OV100 fluorescent camera. This resulted in complete obliteration of fluorescent signal from the liver and demonstrated that, in rats, the depth penetrance sensitivity of currently available fluorescent cameras is insufficient for detection of EGFP signal through tissue. Consequently, this technology was not pursued as a method for identifying EGFP+ CCA tumours in rats (**Figure 3.12**).

Figure 3.12: Fluorescent Imaging of EGFP+ and *wt* SD rat tissue

A1: Brightfield image of *wt* and EGFP skin. **A2:** Fluorescent image of *wt* and EGFP skin. **A3:** Overlay of brightfield and fluorescent image with green highlight of fluorescent image. **B1:** Brightfield image of *wt* organs. **B2:** Fluorescent image of *wt* organs. **B3:** Fluorescent image of EGFP organs. **C1:** Brightfield image of *wt* liver. **C2:** Fluorescent image of *wt* liver. **D1:** Fluorescent image of EGFP liver. **D2**: Fluorescent image of EGFP liver overlaid with *wt* skin, that results in loss of detection of EGFP signal by fluorescent camera.

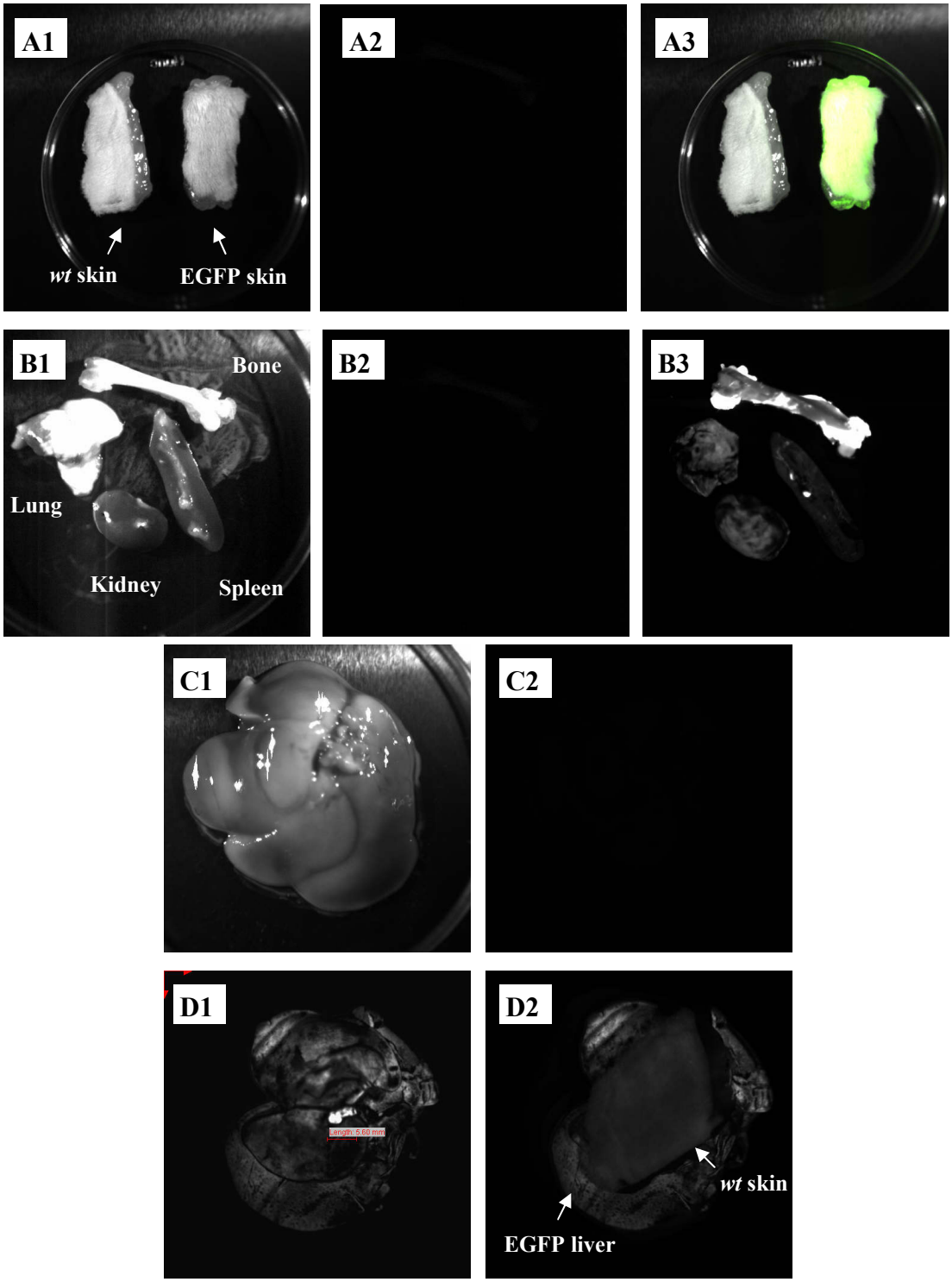

A higher dosage of TAA treatment accelerates CCA development in rats

In view of the latency period associated with 0.03% TAA administration, the unpredictability of developing CCA lesions and the various obstacles to detecting tumours *in vivo*, a second group of rats were commenced on a doubled dose of TAA (0.06%), following modification of the Home Office project license. Animals were sacrificed at 10, 14, 16, 18, 20, 22, 24 and 26 weeks to identify whether tumours could be induced at an earlier stage (n=3 each timepoint). These animals developed more rapid histological and fibrotic changes than the 0.03% group and developed lesions from 18 weeks with 100% penetrance. The macroscopic features and histological architecture of the CCA lesions were similar to those induced in the 0.03% TAA group (data not shown). This higher dosage was used for liposomal clodronate macrophage depletion studies (as described in Chapter 4).

Murine models of TAA liver disease and cholangiocarcinonogenesis

Whilst establishing the rat model of cholangiocarcinogenesis, the effect of TAA administration on mice was investigated. This was undertaken with the aim of identifying the development of CCA lesions and liver fibrosis. Male C57bl6 mice were commenced on 0.03% or 0.06% TAA drinking water. Control mice received water. Animals were sacrificed at 8, 12, 16, 20, 24, 28, 40 and 52 weeks. Slides were analysed for histological evidence of CCA and of liver fibrosis. PSR staining confirmed the formation of bridging, irreversible liver fibrosis from week 24 at 0.06% TAA dosing. This represents a potential new model of irreversible liver fibrosis and is the subject of further investigation within the laboratory. However, at all time points, despite underlying hepatic inflammation and proliferation of progenitor cells, no evidence of intrahepatic CCA was found in mice (**Figure 3.13**).

Figure 3.13: TAA administration to mice results in progressive, irreversible fibrosis but not CCA

A

Male C57bl6 mice were administered 0.03% or 0.06% TAA for up to 52 weeks (n=3 each timepoint). Liver fibrosis quantification was undertaken by digital analysis of PSR-staining of liver sections. Each bar represents the mean percentage area of PSR-staining per high power field (x200) field from 3 animals. Significantly elevated collagen deposition was noted in the 0.06% group from 8 weeks with formation of bridging fibrosis from 24 weeks. CCA lesions were not identified. (*p<0.05, t-test).

PSR Staining:

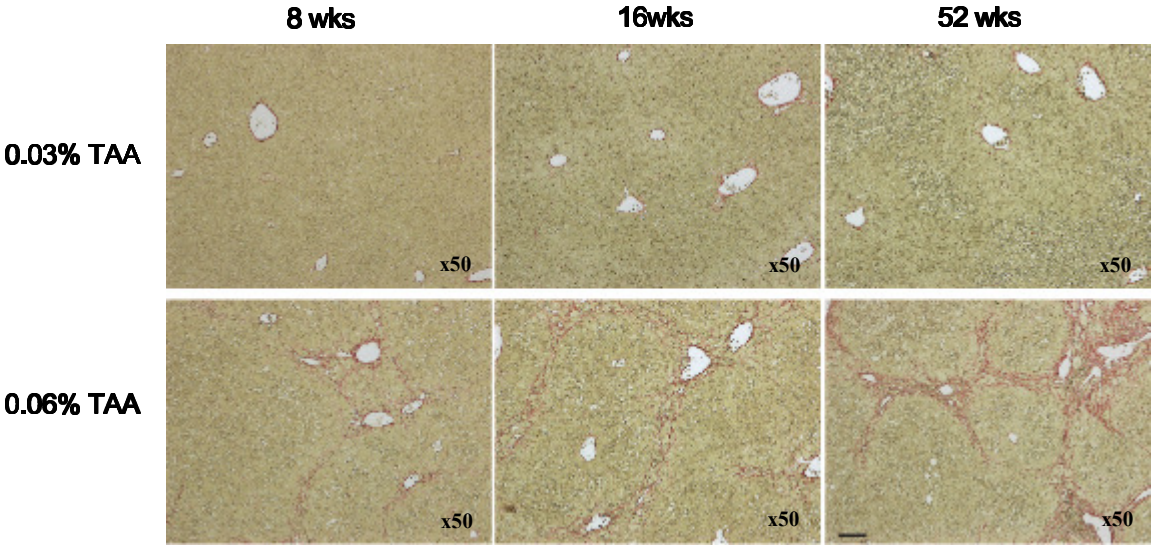

Digital Analysis Quantification:

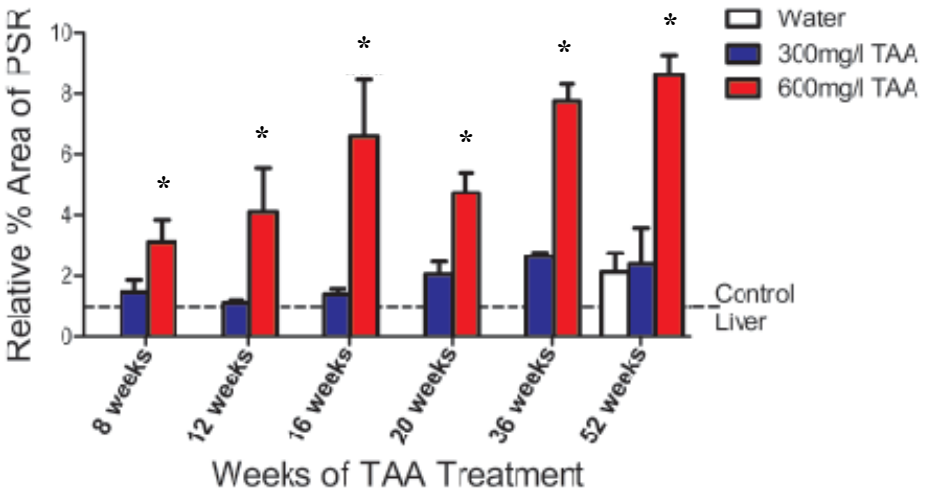

B

The notable liver fibrosis that arose following administration of 0.06% TAA.was found to be non-reversible upon withdrawal of TAA with persistence of fibrosis (as measured by PSR staining digital quantification) during recovery periods of up to eight weeks. (*p<0.05, t-test).

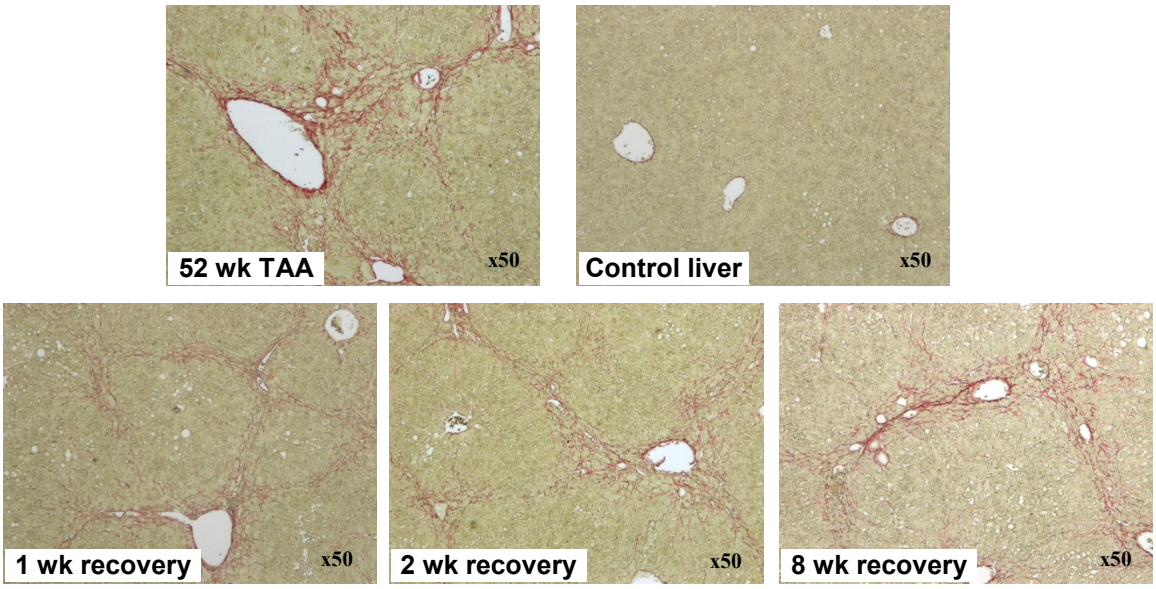

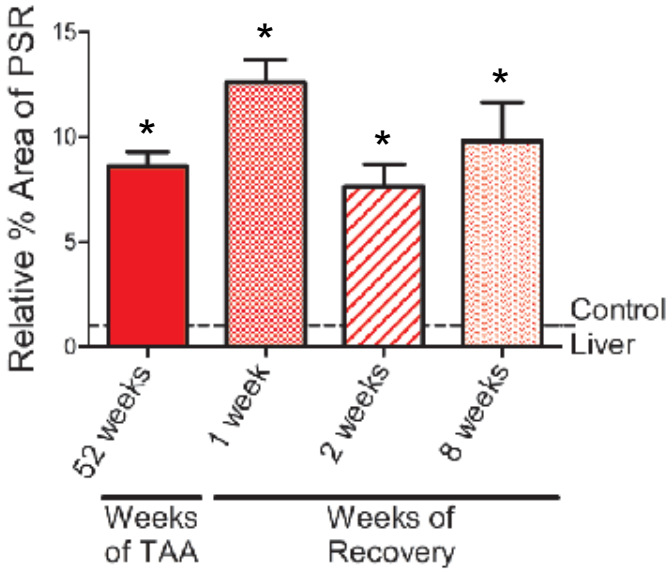

This study was carried out in conjunction between Dr P Ramachandran, Dr A Pellicoro and myself. Dr Pellicoro undertook the image acquisition and Dr Ramachandran performed the data analysis as detailed above.

Discussion

The TAA rat model of CCA results in liver fibrosis, oval cell activation, dysplasia and tumourigenesis. The model produces intrahepatic CCA lesions that are histologically consistent with human tumours and recapitulate their phenotype. A high dose TAA regime (0.06%) is required for homogeneous, consistent and timely tumour development. Migrating monocyte/macrophages (ED1) and myofibroblasts (αSMA) are prominent components of the tumour stroma. Oval cells (CK19+) proliferate in parallel with liver fibrosis and predate formation of CCA lesions. Macrophages and myofibroblasts accumulate at the periportal region prior to the formation of invasive CCA. This represents what appears to be a histological pre-malignant tumour niche of proliferating progenitor cells and inflammatory macrophages and myofibroblasts. Currently available small animal imaging modalities (ultrasound, fluorescence) have significant limitations in rats rendering them infeasible for *in vivo* CCA tumour detection. The lesions may be imaged by MRI but it became apparent, due to the incomplete penetrance of CCA lesions after adoptive transfer following 38 weeks of TAA (as detailed in Chapter Five), that serial MRI analysis would not improve the detection rate of CCA in vivo. Neither the low dose nor high dose TAA model produces CCA lesions in mice but is a useful model of irreversible liver fibrosis.

CHAPTER FOUR

IN VITRO CHARACTERISATION OF CHOLANGIOCARCINOMA: DEFINING THE FUNCTIONAL ROLE OF THE STROMAL:CHOLANGIOCYTE INTERACTION

Introduction

Solid organ epithelial cancers arise in the context of inflammation and develop in concert with a progressive desmoplastic reaction of activated cancer-associated fibroblasts, accumulation of inflammatory cells (predominantly tumour associated macrophages) and the deposition of modified extracellular matrix (ECM) components. In the tumour associated ECM, fibrillar collagen types I and III are typically over-represented at the expense of collagen IV (basement membrane) [166]. The cancer-promoting role of the stroma in cancer biology has been discussed in the introduction (Chapter 1). Upregulation of collagen elements I and III within the ECM is associated with poorer clinical outcomes in certain malignancies such as the pancreas [166], ovary [498] and lung [165] although this has not been quantified in CCA. In solid organ tumours, the normal production and assembly of the basement membrane is dysregulated during malignant cancer progression with disruption of collagen IV which itself might otherwise provide protective effects in determining the rate of cancer progression [499, 500] Previous studies of human intrahepatic CCA have confirmed a rich distribution of collagen I and collagen III fibrils in CCA lesions [501]. Furthermore, we have identified persistence of laminin around the malignant bile ducts throughout the progression from normal to neoplastic tissue.

As described in the introduction (Chapter 1), tumours possess a subpopulation of cancer stem cells (CSCs) that is essential for propagating the lesions. Many organ-restricted adult stem cells and CSC exhibit few classical stem cell markers [352]. However, recent studies have identified cancer stem cells based on markers including CD133+ (pancreas [358], colon [359], CNS [360]), CD44+ and EpCAM (breast [361], colon [362], pancreas [363]). Side population (SP) cells exhibit stem-like characteristics [366] and have been found in normal tissues, as well as primary tumours [365] and cell lines established from tumours as diverse as hepatocellular carcinoma [367], lung cancer [368], nasopharyngeal carcinoma [369], glioblastoma [370], neuroblastoma and breast cancer [365]. SP cells possess the ability to efflux Hoechst 33342 dye via ATP-binding cassette (ABC) transporters [364] which have been shown to remove chemotherapeutic agents

from CSCs and thus participate in multi-drug resistance and improved cancer cell survival [365].

In this chapter, a characterisation was undertaken of the roles of the stromal elements in CCA together with an assessment of the *in vitro* evidence for the existence of cancer stem cells in CCA by studying whether CCA cell lines possess stem-cell like compartments, comprising specifically of SP cells. Furthermore, I aimed to elucidate the role of stromal ECM components laminin and collagen types I and IV in the growth of CCA cells. An assessment of the role of cell:cell interactions within the tumour stroma was made by assessing the role of polarised macrophages in cancer cell behaviour.

Acquisition of cholangiocarcinoma (CCA) cell lines for experimental use

There are few published studies using *in vitro* models (cell lines) of CCA. To identify cell lines, the databases of all major international cell line banks (including ATCC, DSMZ, KCLB, JCRB) were interrogated and a literature search was performed. Human cell lines were identified as detailed in the introduction (Chapter 1). Specifically, cell lines were preferred if they were derived from intrahepatic sources from patients prior to chemotherapy and were stored in independent cell line banks. In cases where lines appeared appropriate but were not in a cell line bank, I contacted the principal investigators involved to request their lines. This was unsuccessful.

Through Professor Iredale (JPI), CC-LP-1 and CC-SW-1 lines were obtained from Professor Whiteside, University of Pittsburgh, and TFK-1, HUH-28 and MZ-Cha-1 (WITT) lines were obtained from Professor Alpini, Texas College of Medicine, Temple, USA. I subsequently purchased SNU-245, SNU-1079 and SNU-1196 lines from the Korean National Cell Line Bank (KCLB). These lines formed the basis of future studies.

CCA cell lines contain a resident side population (SP) of cells that efflux Hoechst 33342 dye and exhibit stem cell like properties

SP cells represent a subpopulation in tumours that are able to efflux Hoechst 33342 dye. This ability is abrogated by administration of verapamil, which inhibits ABC efflux pumps, and acts as an experimental control. In order to characterise and identify whether a subpopulation of stem-like cells exists within the CCA cell lines, the ability of the cell lines to efflux Hoechst 33342 was assessed. Following exposure to Hoechst 33342 and verapamil controls, the cells were analysed using flow cytometry (gated for viable cells as defined by propidium iodide staining) to identify the side population.

Five out of seven CCA cell lines and one hepatic stellate cell line (LX2) [502] exhibited the presence of a side population. The proportional contributions varied and two out of seven cell lines did not appear to comprise a side population (**Figure 4.1**).

The HUH cell line was chosen for further analysis due to relatively high SP fraction compared to other cell lines. The HUH line was studied for co-expression of CD133+ (a recognised stem cell marker in cancer stem cells) within the SP fraction by treating cells with Hoechst, then washing with HBSS+ and incubating with CD133 antibody or IgG isotype control antibody for one hour followed by flow cytometric analysis. Initial high background binding of IgG1 isotype rendered analysis unsuccessful. Repeated analysis with an alternative isotype, a smaller number of target cells, completely fresh reagents and the addition of extra washes did not identify CD133+ staining in SP cells relative to non-SP cells. The absence of positive control tissue rendered this an incomplete result and thus no firm conclusions may be drawn from this. The study would need to be repeated with a fresh anti-CD133 antibody and positive control cells, such as the human colorectal cancer cell line, CaCo-2, which contains uniformly high levels of CD133+ cells [503].

Figure 4.1: Characterisation of the Side Population (SP) in CCA cell lines
Flow cytometry of cell lines treated with Hoechst 33342 and verapamil controls identified a fraction of cells that were able to efflux the dye in a characteristic fashion.

A

HUH cell line displayed 4.11% SP cells in flow cytometry analysis. SP cells are identified by reduced blue-red fluorescent dye signal compared to non-SP cells stained with Hoechst 33342. 4.11% SP fraction is derived from 4.143% cells in P2 gate minus 0.033% in P2 gate in verapamil-treated controls.

HUH cell line with SP fraction highlighted in P2 gate

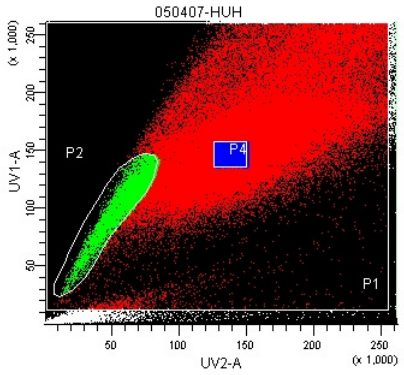

Experiment Name:	SP sort_006
Specimen Name:	050407
Tube Name:	HUH
Record Date:	Apr 5, 2007 2:16:20 PM
$OP:	Administrator

Population	#Events	%Parent	%Total
All Events	158,140	####	100.000
P1	100,000	63.235	63.235
P3	37,301	23.587	23.587
P4	6,599	4.173	4.173
P2	6,551	4.143	4.143

HUH cell line with SP fraction highlighted in P2 gate following verapamil administration

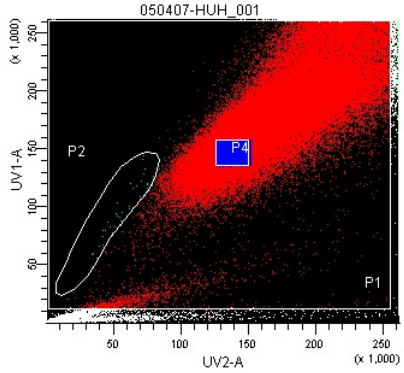

Experiment Name:	SP sort_006
Specimen Name:	050407
Tube Name:	HUH_001
Record Date:	Apr 5, 2007 2:19:31 PM
$OP:	Administrator

Population	#Events	%Parent	%Total
All Events	174,042	####	100.000
P1	100,000	57.457	57.457
P3	52,647	30.250	30.250
P4	8,638	4.963	4.963
P2	55	0.032	0.032

B

Seven CCA cell lines and one hepatic stellate cell line (LX2) were analysed for the presence of the side population. 5/7 CCA lines and LX2 line expressed the SP fraction, whereas 2/7 CCA lines did not possess the SP fraction.

Cell Line	Side Population (SP)	Percentage SP
WITT	Y	1.449
TFK-1	Y	2.208
HUH-28	Y	4.140
LP	N	0
SW	N	0
SNU-245	Y	5.200
SNU-1079	Y	0.600
SNU-1196	Not tested	Not tested
LX2(HSC line)	Y	0.731

Characterising SP cell activity *in vitro*

HUH cells were treated with Hoechst 33342 and sorted into SP and non-SP fractions. Analysis was made of the proliferative capacity and clonogenicity of these sorted cells, together with the ability of the SP cells to regenerate SP and non-SP progeny.

Proliferation of SP vs. non-SP cells

SP and non-SP cell *in vitro* proliferation was measured at serial timepoints following culture for 48 hours and 28 days using MTS assay. Optimal cell number seeding density and MTS incubation time calibrations were performed using unsorted cells (data not shown). Cells were plated in 96 well plates in sextriplicates at high (5000 cells/well) and low (500 cells/well) densities for analysis over 48 hours and 28 days, respectively.

The MTS assay signal absorbance of HUH SP cells (5000 cells/well) was found to be significantly greater with respect to non-SP cells at 24 hours and 48 hours (t-test $P<0.0005$) (**Figure 4.2A**). However, MTS absorbance of both SP cells and non-SP cells at 48 hours was not significantly greater with respect to their corresponding measurements at 24 hours (SP: $P=0.58$; non-SP: $P=0.39$). This suggests that the SP cell fraction displayed higher metabolic activity compared to non-SP cells, rather than actual growth of the cell populations occurring in the first 48 hours after cell sorting.

In the long-term (28 day) assay (500 cells/well), MTS absorbance for both SP and non-SP were similar to each other, with no increase in absorbance from day 3 to day 28 (**Figure 4.2B**). Morphologically, cells remained small and were poorly adherent to tissue culture well plates. It was concluded that growth of these cells did not occur over the 28-day time period. Despite the most gentle flow cytometer sorting parameters possible, it is likely that this finding reflects the strain put upon the SP and non-SP cells during the Hoechst treatment and cell sorting protocol leading to cell injury. Certainly it has been recognised that exposure of Hoechst-treated cells to

ultraviolet lasers reduces their viability by 20% [504] and this pattern of cellular injury may explain their poor proliferation post-sorting.

Clonogenicity

In vitro clonogenic assays were performed to identify whether HUH SP and non-SP cells differed in their abilities to form colonies over eight weeks. SP and non-SP cells were plated at 100, 500, or 1000 cells/well in 6 well plates. No morphological growth changes were noted during this time period in either SP or non-SP populations, at any plating density. Cells remained adherent to tissue culture plastic but did not appear to increase in number. This may have been due to cell trauma incurred during flow cytometry. Alternatively, it is possible that the cell densities plated were too low to support viable growth as it was observed that SP clone formation and proliferation was achieved when plated at 20,000 cells in 25cm^2 flasks in a separate experiment investigating the ability of HUH SP and non-SP cells to regenerate (described below).

Characterisation of SP and non-SP cell progeny: SP cells regenerate both SP and non-SP cells

HUH SP and non-SP cells were plated at a density of 20,000 cells in two 25cm^2 flasks and cultured for eight weeks until sufficient cell growth had occurred to re-sort the populations using flow cytometry. Considerable colony growth occurred in the SP flask over eight weeks whereas non-SP cells exhibited minimal growth. Consequently, only the SP population was available for re-analysis and was found to give rise to both SP (3.76%) and non-SP cells (**Figure 4.2C**).

Figure 4.2: Characterisation of the Side Population (SP) in HUH cell lines

A: SP cells have significantly higher metabolic activity than non-SP cells over 48 hours

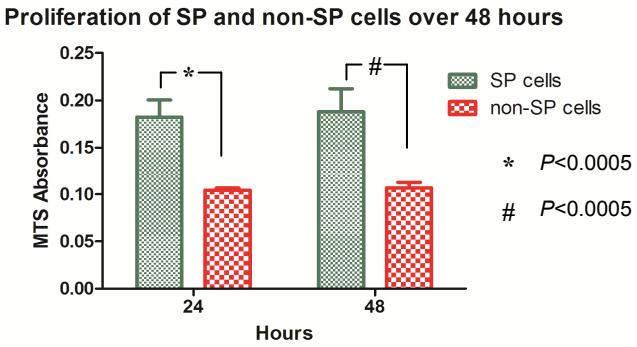

B: SP and non-SP cells demonstrate no proliferation over 28 days (500 cells/well)

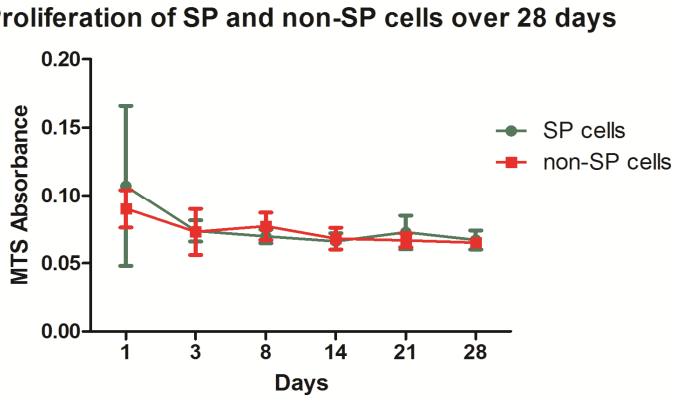

C: HUH SP cell progeny following re-treatment with Hoechst 33342. SP cells produce both SP (3.76%) and non-SP progeny.

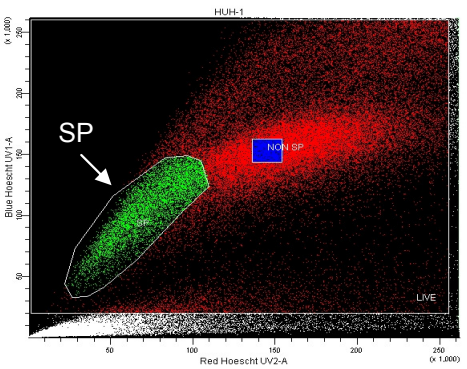

Experiment Name:	SP sort Sep 07
Specimen Name:	HUH
Tube Name:	1
Record Date:	Sep 26, 2007 12:33:22 PM
$OP:	Administrator

Population	#Events	%Parent	%Total
All Events	148,005	####	100.000
LIVE	50,000	33.783	33.783
DEAD	51,310	34.668	34.668
SP	7,214	4.874	4.874
NON SP	2,938	1.985	1.985

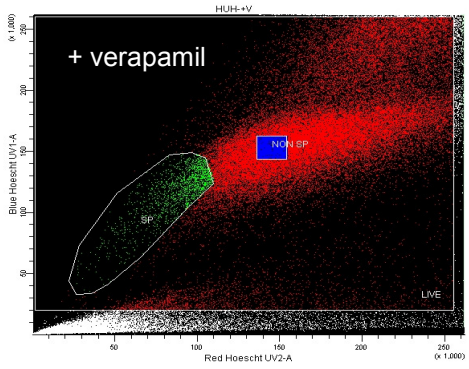

Experiment Name:	SP sort Sep 07
Specimen Name:	HUH
Tube Name:	+V
Record Date:	Sep 26, 2007 12:38:15 PM
$OP:	Administrator

Population	#Events	%Parent	%Total
All Events	153,506	####	100.000
LIVE	50,000	32.572	32.572
DEAD	62,611	40.787	40.787
SP	1,704	1.110	1.110
NON SP	3,478	2.266	2.266

SP cells in CCA express both hepatic and biliary markers

Following sorting, SP and non-SP cells were cultured on glass slides and underwent immunohistochemistry for alpha fetoprotein (AFP), characteristically a marker of hepatoblasts and hepatocellular lesions, and CK19, a marker of biliary epithelium. (**Figure 4.3**). SP cells expressed AFP and CK19 whereas non-SP cells did not express AFP, consistent with biliary fate type specification. This is suggestive of SP cells maintaining a stem cell phenotype in CCA, unlike non-SP cells that are relatively "differentiated" and express only CK19.

From the outset, initial experimental plans included the aim of identifying a stem cell like population in CCA cell lines, and then investigating whether there was differential expression of Notch pathway components and whether Notch pathway inhibition affected SP and non-SP cell behaviour. However, due to the technical complexities encountered in SP cell sorting and subsequent growth, this was not feasible. Analysis of the effect of pre-incubation of SP cells with Notch pathway inhibitors (γ-secretase inhibitors) or overexpression of the Notch pathway (transfection with Notch Intracellular Domain - NICD) or the effect of repeated administration of Notch pathway inhibitors were not undertaken. Further analysis, such as *in vivo* studies of tumour forming capacity in *in vivo* xenograft models, were also impracticable.

Figure 4.3 Expression of AFP and CK19 in SP and Non-SP Cells

A

TFK cell line immunocytochemistry: SP cells express AFP (marker of hepatic type stem cells) and CK19 (marker of biliary epithelium) whereas non-SP cells do not express AFP, consistent with biliary fate type specification.

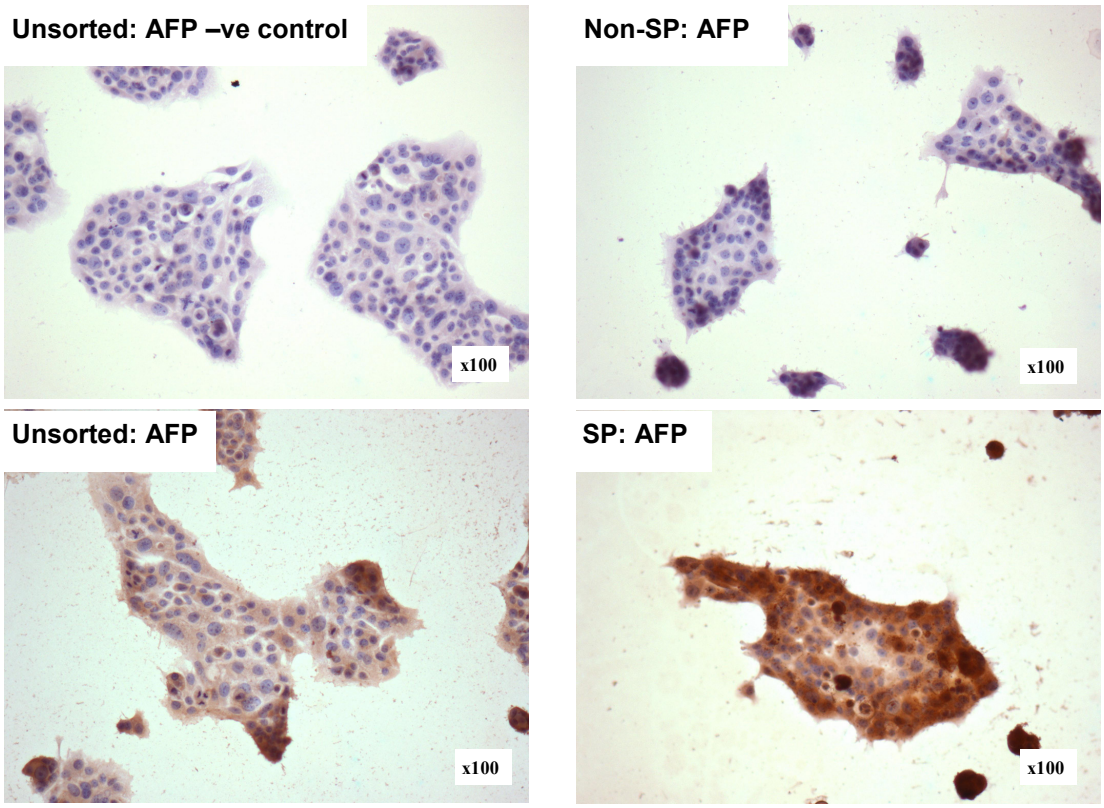

B

CK19 (biliary epithelial marker) is expressed in unsorted, SP and non-SP cells in TFK cell line.

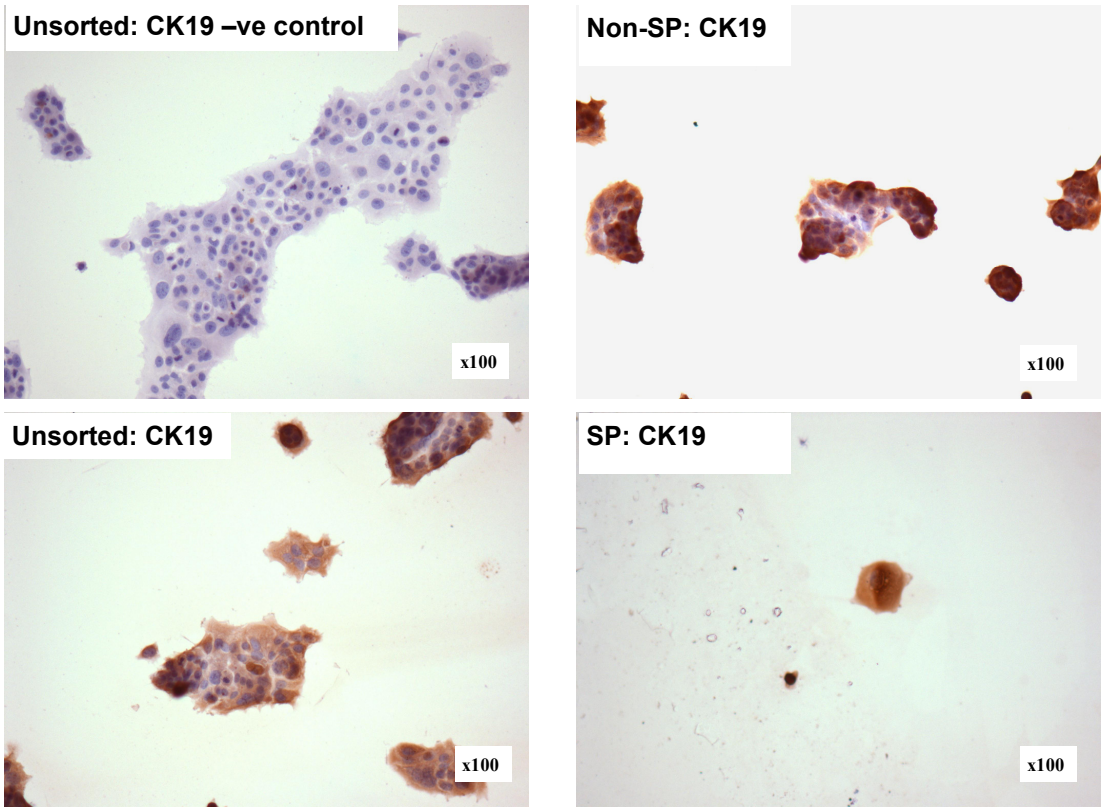

Direct Contact with Extracellular Matrix affects Growth Morphology of CCA *in vitro*

In view of the anatomical distribution of ECM components in CCA, with laminin remaining a consistent presence around malignant bile ducts in invasive CCA, cell lines were cultured on tissue culture plastic (TCP), collagen I (fibrillar collagen upregulated in desmoplasia and fibrosis), collagen IV (basement membrane collagen) and laminin. Morphologically, cell line growth rate appeared more clumped and inhibited (to the eye) on laminin compared to other ECM components and control TCP (**Figure 4.4**).

Figure 4.4: Morphologic Growth Characteristics of TFK and WITT cell lines on ECM Components

WITT and TFK1 CCA cell lines demonstrate morphologically different growth patterns and growth rate on laminin compared to tissue culture plastic, (TCP) collagen I and collagen IV.

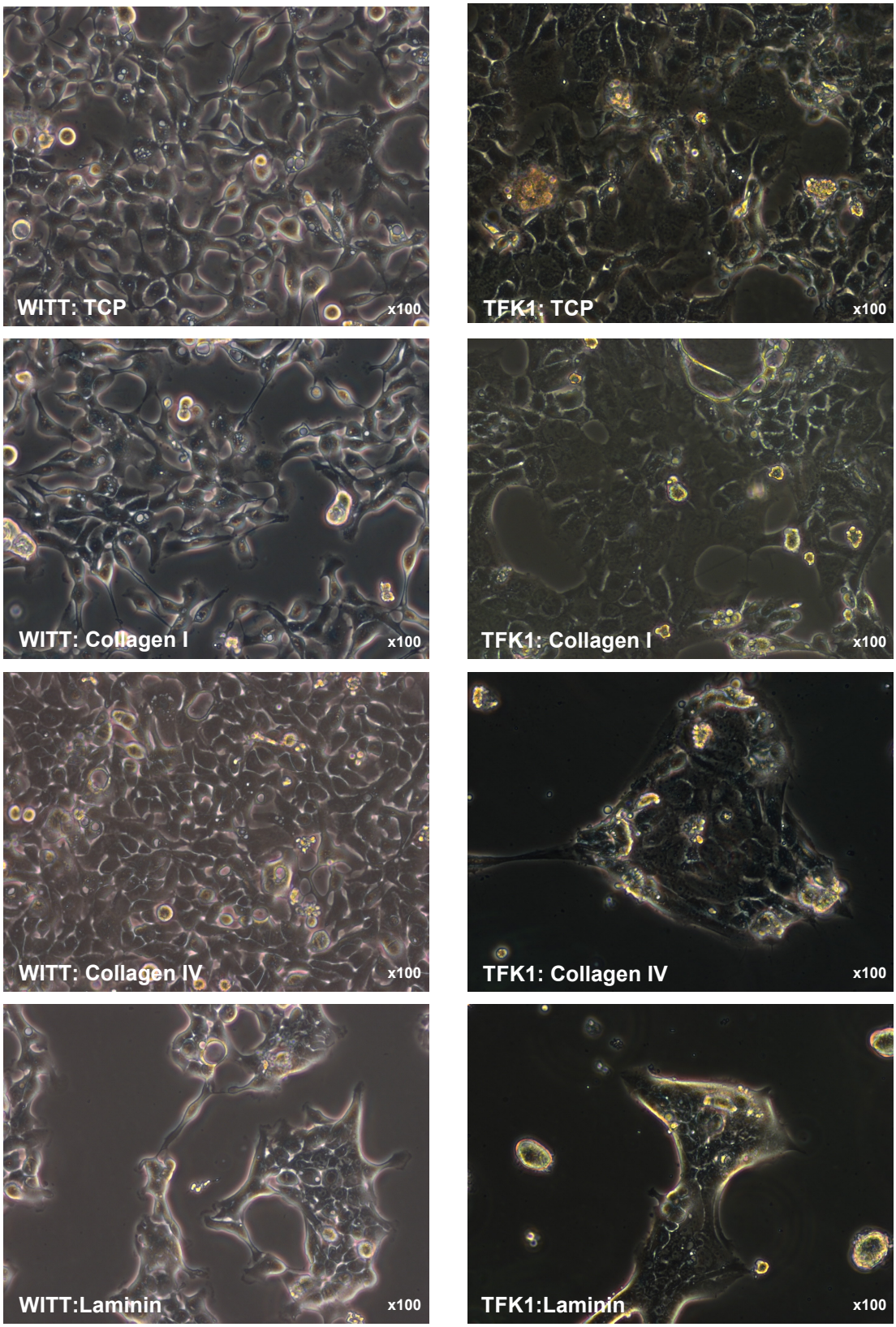

CCA growth rate is inhibited on ^{3}H-thymidine DNA incorporation analysis

^{3}H-thymidine DNA incorporation assay was used to quantify the effect of ECM components on tumour cell proliferation. CCA cell lines (SW, LP, WITT) were plated on TCP, collagen I, collagen IV and laminin 96 well plates at a seeding density of 5,000 cells per well for 24 hours. ^{3}H-thymidine was then added to cells, which were incubated for a further 16 hours. Cellular proliferation on ECM components was expressed relative to control TCP (as measured by ^{3}H-thymidine DNA incorporation).

Initial extremely variable experimental results were identified as being due to incomplete collection of cultured cell line DNA by the semi-automated harvester (which is designed to collect DNA from non-adherent cells in round-bottomed plates). The assay was optimised for adherent cells on 96-well flat-bottomed plates by trypsining the cells and then freezing and defrosting the plates prior to harvest, which enabled complete uptake of material by the harvester device.

The behaviour of the three cell types was broadly similar but the magnitude effect of matrix components appeared to depend in part on the cancer cell line as well as the ECM components themselves. Collagen I and particularly collagen IV significantly upregulated growth. In contrast, laminin effected moderate upregulation, had no effect, or inhibited growth *in vitro* dependent on the cell line (**Figure 4.5A**).

ECM Components do not affect cisplatin chemosensitivity of CCA cell lines

In view of the different growth morphologies and growth rates of CCA cell lines on the ECM components, the effect of chemotherapy was studied. Two cell lines (s1079 and s1196, with similar morphological changes on the ECM components as Figure 4.4 (data not shown) were cultured in sextuplicate at 5,000 cells/well in 96 well plates on collagen I, collagen IV, laminin, TCP or wells coated with poly-D-lysine (synthetic positively-charged amino acid that increases electrostatic cell binding to

surfaces). Cells were grown for up to 96 hours and treated concurrently with cisplatin.

When considering s1079 cell line, two way ANOVA with post-hoc Bonferroni testing identified no significant differences between ECM growth conditions for each chemotherapeutic dose ($p>0.05$ for each dose-condition). For s1196 cell line, although an overall apparent effect of matrix conditions was identified on two way ANOVA ($p<0.001$), post-hoc Bonferroni testing identified no consistent dose-matrix effect. For example, apparent significant differences ($p<0.05$) arose between TCP and Collagen I at 20μM and 320μM and Laminin at 320μM but not intervening doses or compared to other conditions. Accordingly, it was considered that no experimentally significant result was demonstrated. (**Figure 4.5B**).

Figure 4.5: ECM growth: Laminin inhibits growth rate but does not affect chemosensitivity *in vitro*

A

Collagen I and IV promoted cancer cell line growth with variable magnitude dependent on cell type. Laminin promoted proliferation of LP cell line, but inhibited SW and oval cell growth, whilst having no effect on WITT.

For each cell line, all data points in the chart are significantly different to control TCP ($p<0.05$) except for WITT growth on laminin where p=NS compared to TCP (ANOVA).

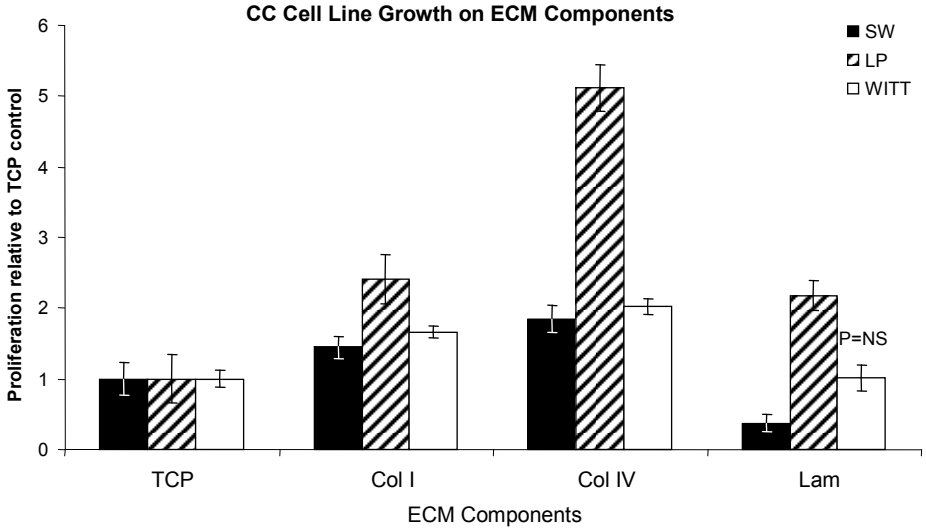

B

CCA cell lines (s1079 and s1196) were cultured on TCP, poly-lD-lysine (promotes binding of cells), collagen I, collagen IV and laminin. Cells were treated with cisplatin for up to 96 hours.

When considering s1079 cell line, two way ANOVA with post-hoc Bonferroni testing identified no significant differences between ECM growth conditions for each chemotherapeutic dose ($p>0.05$ for each dose-condition). For s1196 cell line, although an overall apparent effect of matrix conditions was identified on two way ANOVA ($p<0.001$), post-hoc Bonferroni testing identified no consistent dose-matrix effect. For example, apparent significant differences ($p<0.05$) arose between TCP and Collagen I at 20µM and 320µM and Laminin at 320µM but not intervening doses or compared to other conditions. Accordingly, it was considered that no experimentally significant result was demonstrated.

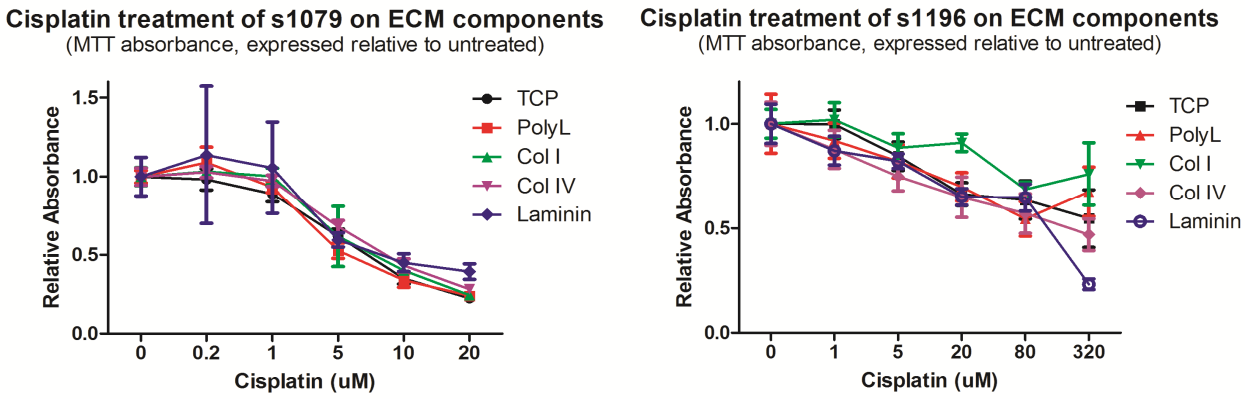

In vitro Soluble factor signalling: Bidirectional signalling exists between CCA cell lines and fibroblasts

To study further the potential effects of the microenvironment in CCA, an investigation was undertaken to identify potential soluble cell-derived factors mediating a relationship between CCA cell lines and myofibroblasts. Optimal cell number, seeding density and MTS incubation time calibrations were performed using cell lines (data not shown). Optimisation of the conditioned media protocol was subsequently undertaken as described in **Figure 4.6**.

Conditioned media (CM) was generated from tumour cell lines (LP, SW) and LX2 cells (hepatic stellate cell myofibroblast line) as described in the Methods (Chapter 2). LP, SW and LX2 cells were then cultured for 24 hours in sextuplet in 96 well plates at a starting density of 20,000 cells per well in FCS-free CM generated from LX2 cells and from the tumour cell lines themselves. The MTS assay was used to measure cellular proliferation. Proliferation of cell lines in CM was measured relative to 15% FBS and 0% FBS unconditioned media. Paracrine and autocrine growth-promoting effects on tumour cell line growth and LX2 cells were identified. Conditioned media from the LP, SW and LX2 cells significantly increased LX2 cell proliferation when compared to serum free (0% FBS) unconditioned media. Additionally, a significant increase in proliferation was observed, compared to serum free (0% FBS) unconditioned media, when LP cells were grown with CM from LP and LX2 cells, and SW cells were grown with LX2 cell CM (**Figure 4.7A,B**). The autocrine effect in CCA cells was only identified in the LP cell line but not SW line. The SW cell line was very slow growing and 24 hours may not have allowed for proliferation changes to be seen. The assay was continued to 48 hours in order to allow for this, but at 48 hours cellular proliferation was reduced in all cell lines, likely representing exhaustion of other factors necessary for growth in the 0% FBS media.

To confirm that cells cultured in CM did not undergo apoptosis or necrosis in response to soluble factors in CM and that observed changes in MTS levels were a

result of changes in proliferation, LDH cytotoxicity assays were performed in parallel to determine evidence for cell death. Cell death in the CM samples, as measured by LDH levels in the cell culture supernatants, was significantly lower than the positive control samples (addition of triton X resulting in cell death), and there was no significant difference when FCS-free control media was used (**Figure 4.7C**).

Figure 4.6: Optimisation of the conditioned media (CM) transfer protocol

Comparison was made of the effect of 0% and 0.5% FBS CM at "100%" concentration or "50%" concentration, and the replenishment of fresh L-glutamine to CM.

A

"100%" CM was generated by culturing 7ml 0% or 0.5% FBS media with subconfluent conditioning cells per T75 flask. Conversely, "50%" CM was generated from 14ml media in subconfluent T75 flasks. LX2 and LP cell CM was transferred onto LP cells (LX2 cell data not shown). No significant difference was found between the 0% FBS and 0.5% FBS CM, as shown below. In a proportion of the "100%" CM transfers (*) there was a significant increase in growth when compared to the "50%"CM. Therefore "100%" CM was used in subsequent experiments.

* = P<0.05, when compared to [50%] CM of the same type (t-test).

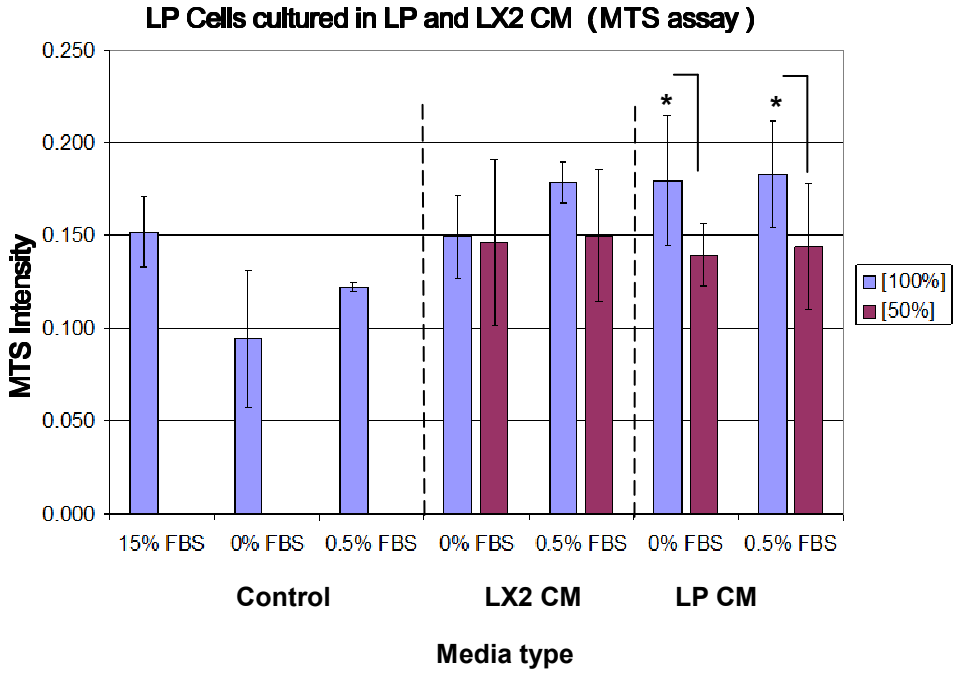

B

L-glutamine is recognised as a rapidly exhausted component of cell culture media, with a short half life. LP cells were cultured in LX2 and LP cell 0% FBS CM. (Similarly, LX2 and SW cells were cultured in LX2 and SW CM - data not shown here). Comparison of the effect of replenishing 1% L-glutamine to 0% FBS CM was made. Cells cultured in CM with replenished L-Glutamine demonstrated either a trend increase (LX2) or a significant increase (LP) in growth compared to the unreplenished CM. Therefore L-Glutamine was added to the conditioned media in subsequent experiments.

* = P<0.05, when compared to CM, minus L-Glutamine, of the same type (t-test).

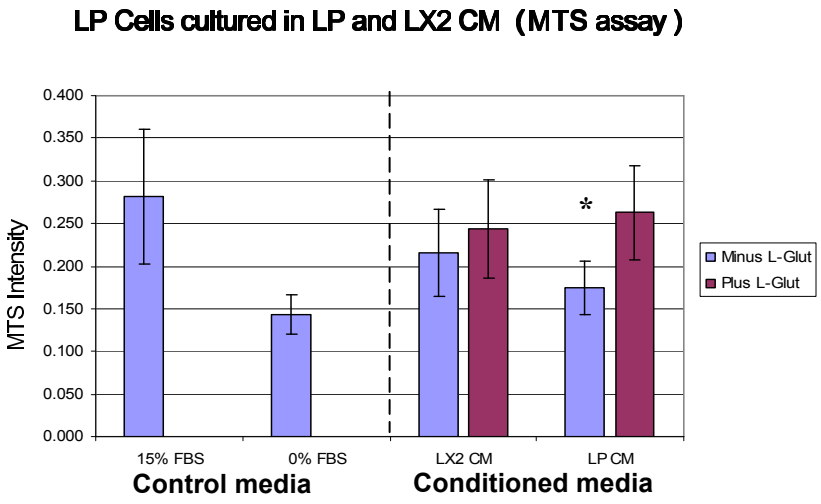

Figure 4.7: Paracrine and autocrine soluble factors promote cellular proliferation in an *in vitro* model of the CCA:myofibroblast microenvironment

A

LP and SW CCA cell lines were cultured for 24 hours in CM from "paracrine" hepatic stellate cell (LX2) and "autocrine" CCA cell lines (SW, LP). This resulted in increased proliferation of CCA cell lines (MTS assay).
* = P<0.05 (relative to 0% FBS media control), ANOVA. [CM= conditioned media]

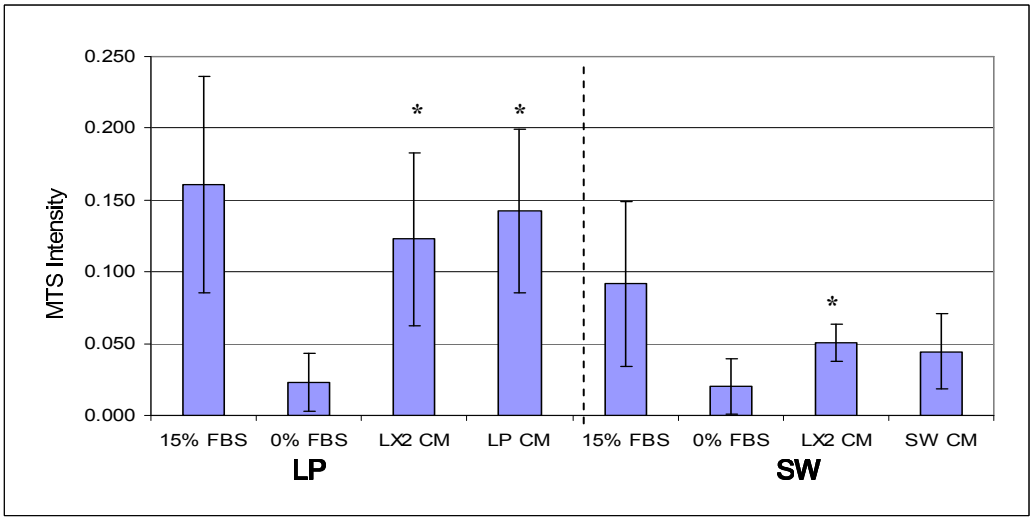

B

Hepatic stellate cells (LX2) were cultured for 24 hours in CM from "autocrine" LX2 and "paracrine" CCA cell lines (SW, LP). This resulted in significantly increased proliferation (MTS assay).
* = P<0.05 (relative to 0% FBS media control), ANOVA. [CM=conditioned media]

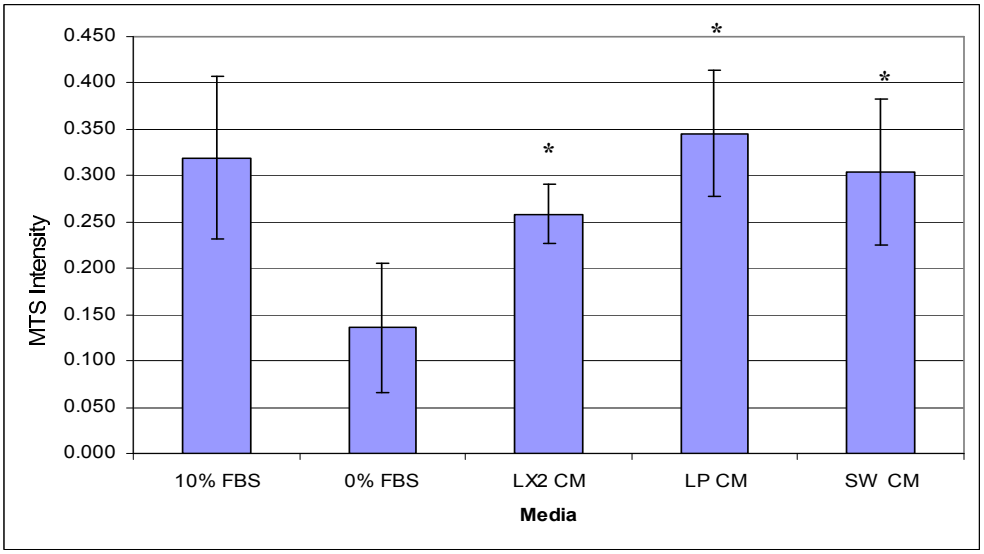

C

Analysis of cell death on the supernatant following CM transfer: LDH assay was performed on supernatant from the LX2, LP and SW cells following culture in LX2, LP and SW cell 0% FBS CM. MTS values for all the CM supernatants were significantly lower than the positive control (Triton X causing cell death).

* = P<0.05, when compared to the positive control (ANOVA).

LX2 Cell line

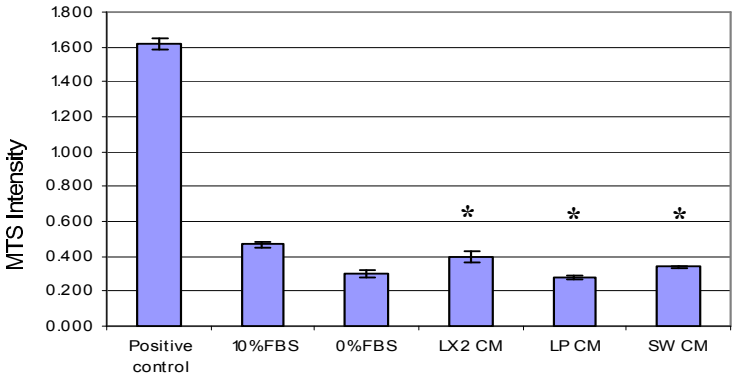

LP Cell line

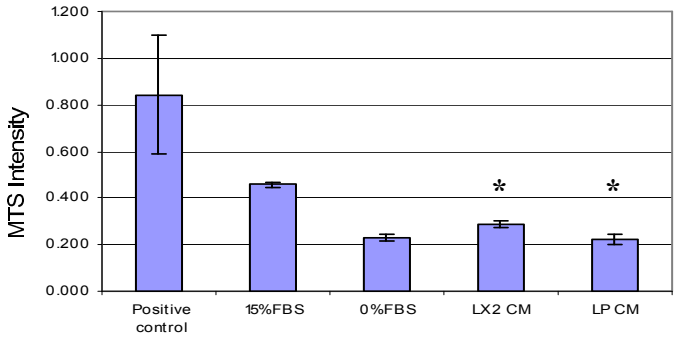

SW Cell line

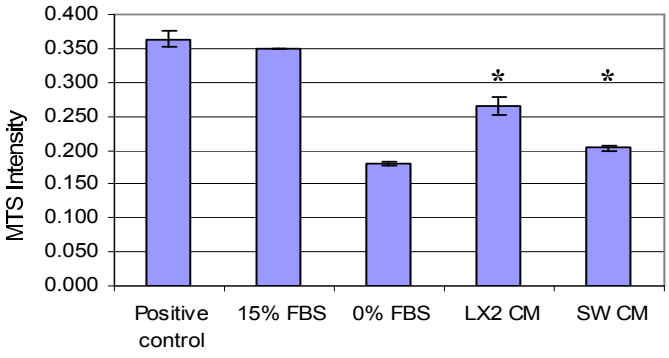

in vitro Direct cell:cell interaction - The effect of direct co-culture with human primary macrophages

In order to identify whether a functional relationship exists between CCA cells and tumour-associated macrophages, a direct co-culture system was devised consisting of human primary macrophages that were either M1 (classically) or M2 (alternatively) polarised co-cultured with CCA cell lines. M2 polarisation represents the tumour-associated macrophage phenotype, as described in the introduction (Chapter 1).

Two methods of *in vitro* macrophage polarisation were used and adapted for the purpose of the model – the plastic adherence and the negative selection protocols. Using the plastic adherence macrophage maturation protocol, peripheral blood monocytes ($2x10^6$) were plated in 24 well plates and allowed to mature into macrophages for six days. Following this, they were M1/classically (LPS/IFNg) and M2/alternatively (IL4/IL13) activated and then co-cultured for 24 hours with LP CCA cell lines ($15x10^3$ per well). Experiments were performed in triplicate and cells were stained with Celltracker fluorescent dye to enable discrimination between macrophages and cancer cells (**Figure 4.8)**.

Cell counting of 20 x320 magnification sequential fields per well was carried out to quantify CCA cell number and phagocytosed CCA cell debris within macrophages. CCA cell proliferation was significantly greater when cultured with M2 macrophages compared to non-polarised/naïve macrophages (P=0.028) and trended to be greater than M1 polarised macrophages (P=NS). Conversely, in co-culture with CCA cells, M1 macrophages displayed significantly greater phagocytic behaviour than M2 polarised or non-polarised/naïve macrophages (P<0.05) (**Figure 4.9)**.

I then modified the plastic adherence protocol of macrophage maturation and polarisation to the negative selection protocol to produce a more purified phenotype of macrophage polarisation (**Figure 4.10A**). To assess the purity of cells generated by this technique, flow cytometry of purified cells was undertaken and confirmed that greater than 90% of viable cells were CD14+ monocytes (**Figure 4.10B**). These

cells were matured in Teflon pots and polarised with M-CSF or GM-CSF for seven days. qPCR was performed on cultured cells to test macrophage polarisation (**Figure 4.10C**) and also to confirm the absence of expression of receptors to M-CSF and GM-CSF by cancer cells (**Figure 4.10D**). Furthermore, proliferation of CCA cell lines was tested whilst in culture with M-CSF and GM-CSF polarising media and this confirmed that neither M-CSF nor GM-CSF administration significantly affect CCA proliferation (**Figure 4.10E**).

The negative selection and Teflon culture technique was used for the Notch signalling studies reported in Chapter 6 but was not used experimentally in co-culture counting as described in Figure 4.9 due to limitations of experimental time. However, this remains a viable technique for cancer cell co-culture in experimental studies**.**

Figure 4.8: Schematic representation of *in vitro* co-culture model for macrophages and CCA cells

Polarisation to M1 or M2 phenotypes was performed following maturation of macrophages for six days. Macrophages were generated through either plastic adherence or negative selection protocols as described. Fluorescent microscopy was undertaken with merged images. Representative images are shown.

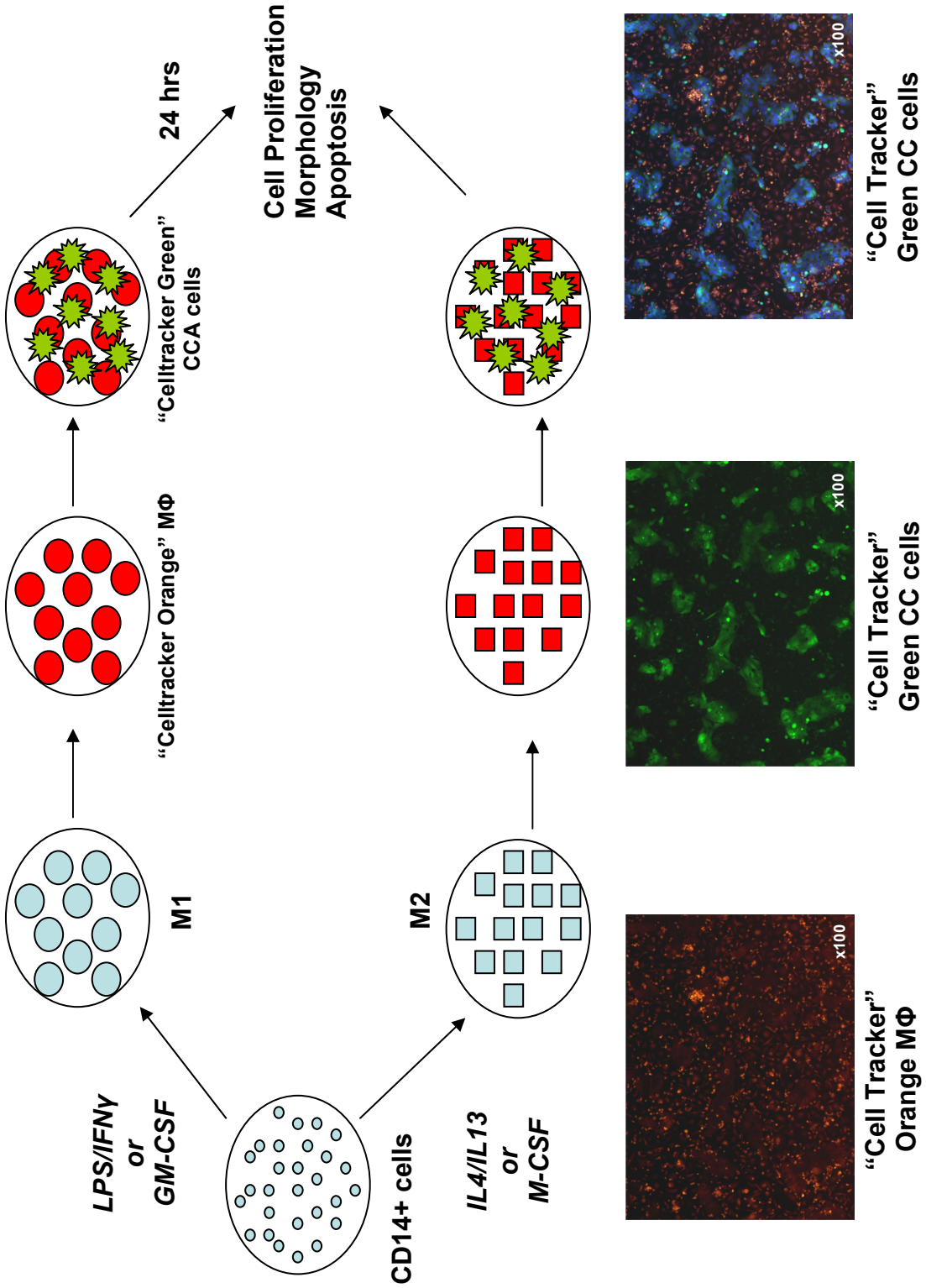

Figure 4.9: *In vitro* co-culture of M1 and M2 polarised human macrophages (MΦ) with LP CCA cell line

A

At 24 hours, CCA cell line growth trends to be greater when co-cultured with M2 alternatively activated MΦs than M1 classical MΦs (*P*=NS, t-test)

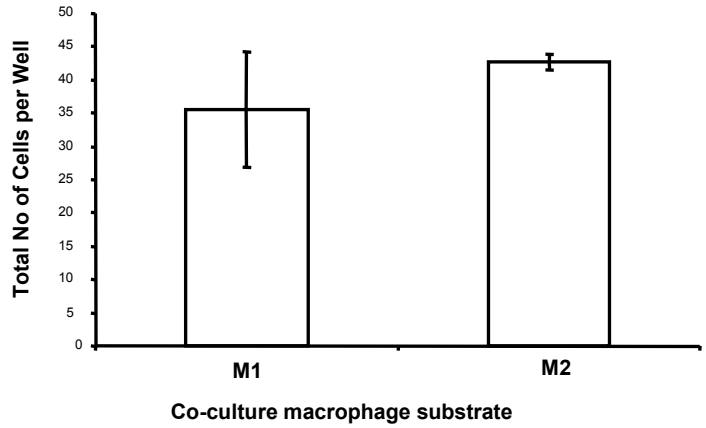

B

In co-culture with CCA cells, phagocytosis of tumour cells and debris is significantly greater by M1 MΦs. In CCA co-culture, phagocytosis of tumour cells and debris appear significantly reduced in M2 MΦs (*p<0.05, t-test).

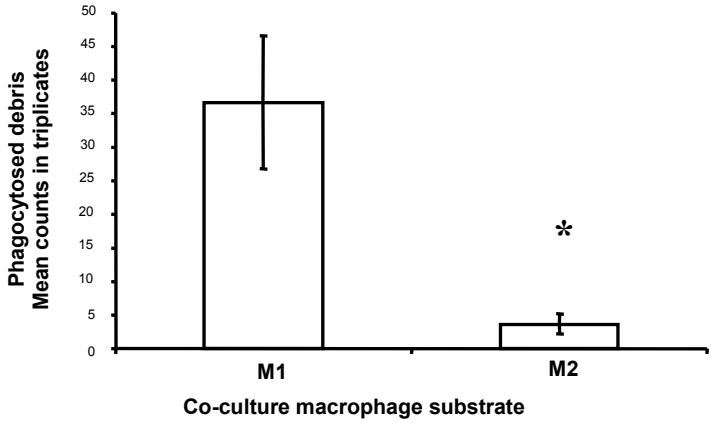

C

Illustrative photomicrograph of M1 MΦ and CCA cell line co-culture. Phagocytosed cellular debris is identifiable within MΦs.

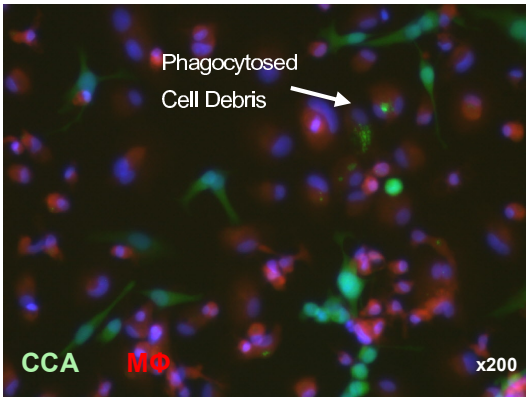

D

M1 MΦ/CCA and M2 MΦ/CCA cell line co-cultures. CCA cells grow in larger clumps and display less phagocytic attack when cultured with M2 MΦs.

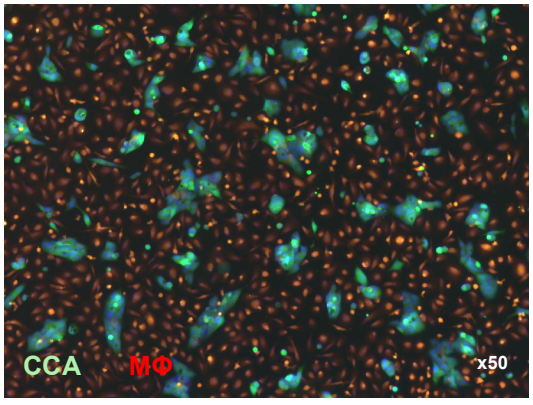

M1 co-culture

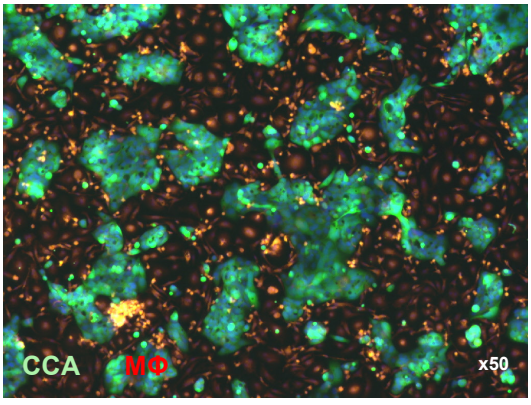

M2 co-culture

Figure 4.10: Development and validation of negative selection tool for macrophage polarisation

A

Human blood was purified using Percoll gradients to yield PBMCs that were then passed through negative selection columns (magnetic activated cell sorting - MACS) to enrich for CD14+ cells (monocytes). These cells were then cultured for 7 days in Teflon pots with polarising media: GM-CSF media for M1 macrophages and M-CSF media for M2 macrophages.

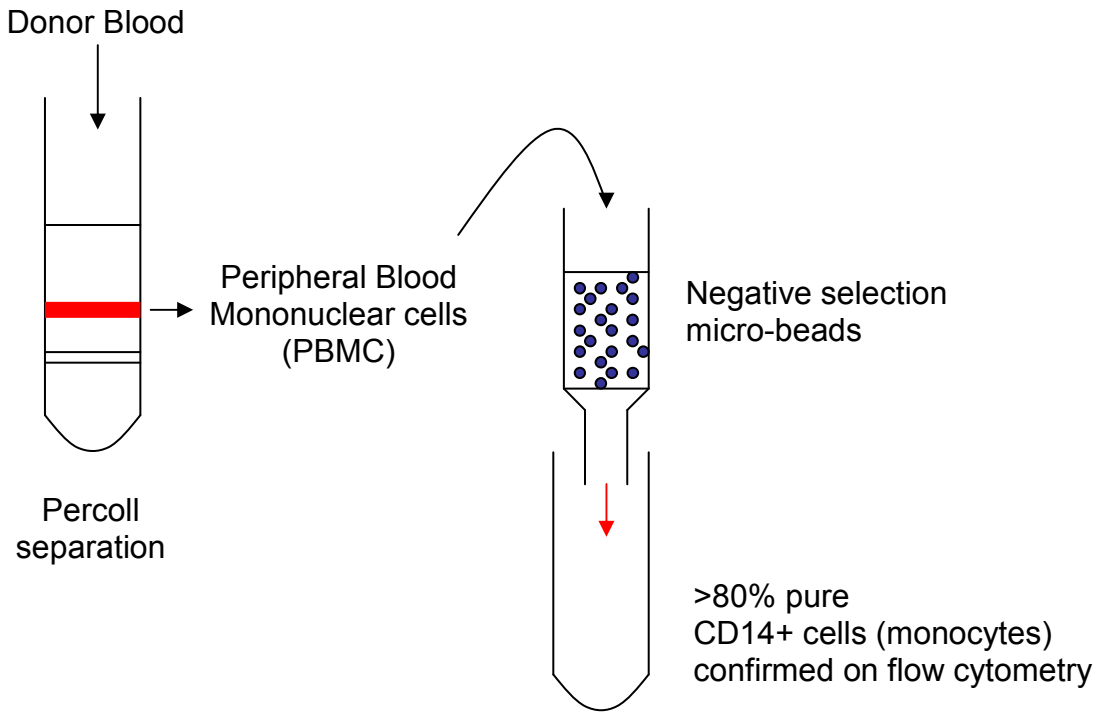

B

Cells obtained from MACS column were incubated overnight in Teflon pots with either 10%FCS RPMI (Panels A and C) or 10% FCS RPMI with additional M-CSF (Panels B and D) and then analysed by flow cytometry (two biological replicates and three technical replicates).

Panels A and B: Gates were set around viable cells, lymphocyte and monocyte subpopulations based on their scatter characteristics.

Panels C and D: Only viable cells were displayed. This enabled comparison of proportions of lymphocyte and monocyte subpopulations based on scatter characteristics. 79.7% and 81.9% of viable cells in the two analysed sample groups had the scatter properties of monocytes.

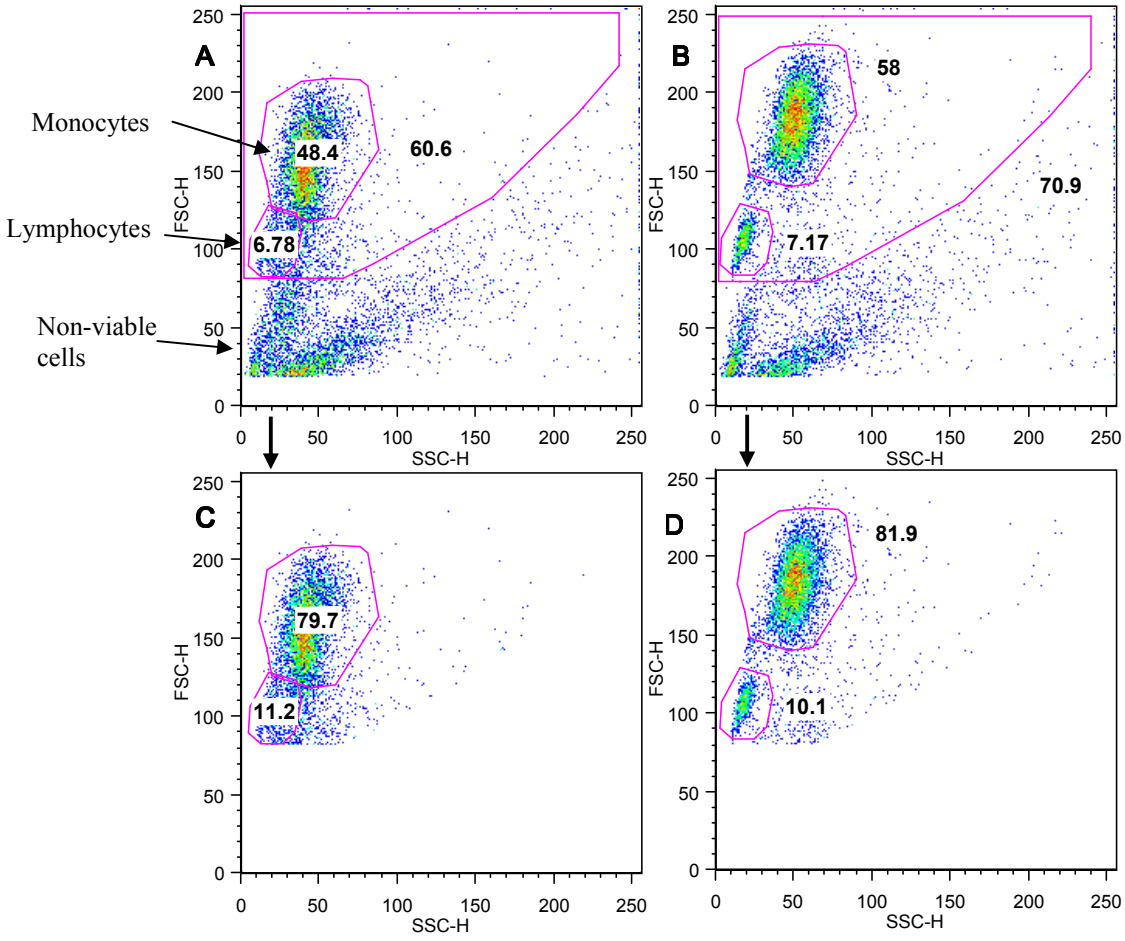

The same cell samples were analysed for CD14+ expression. The cells obtained from MACS column were incubated overnight in Teflon pots with either 10%FCS RPMI (Panels E and G) or 10% FCS RPMI with additional M-CSF (Panels F and H) and then analysed by flow cytometry.

Panels E and F: Cells were gated to display only viable cells: showing CD14 staining of both lymphocytes(lower quadrants) and monocytes (upper quadrants). This demonstrates that 80.3% and 82.9% of viable cells were CD14+.

Panels G and H: Gated to display only viable cells: showing unstained control used to place the quadrants to define CD14 +ve cells.

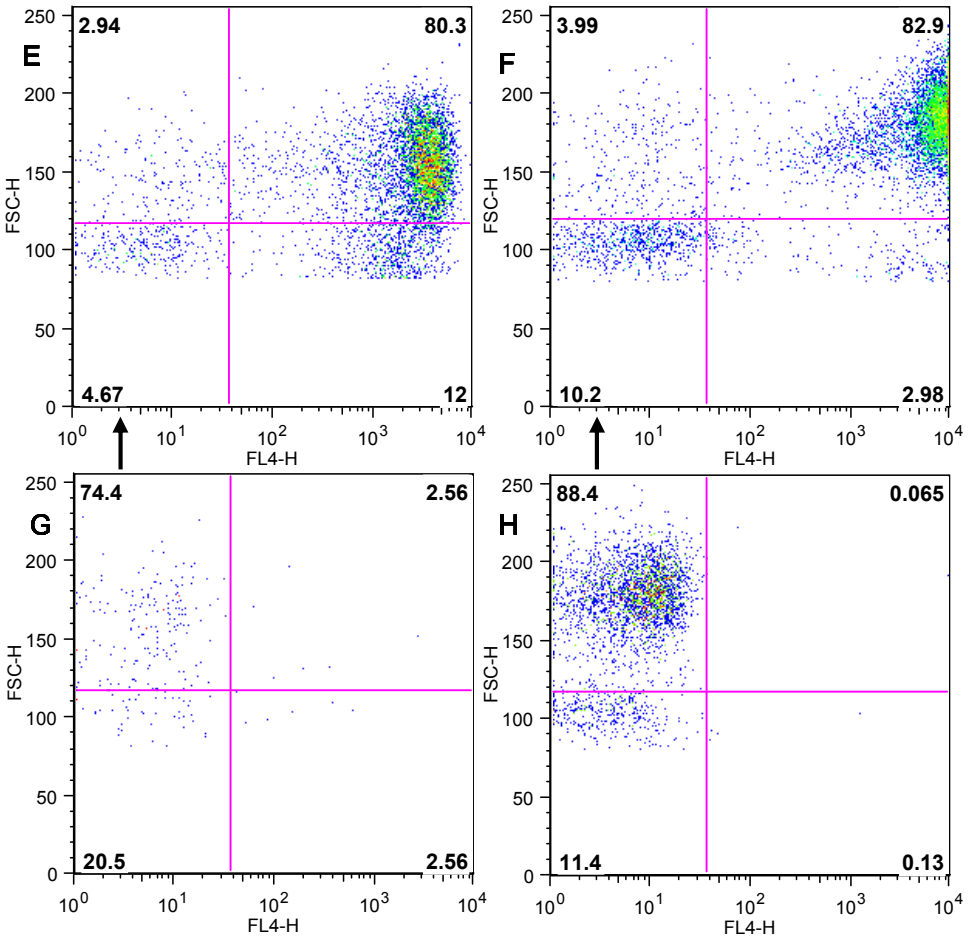

C

M1 polarisation by GM-CSF and M2 polarisation of macrophages by M-CSF was confirmed by qPCR for IL-10 in the two macrophage populations. IL-10 expression was low in M1 macrophages and high in M2 polarised macrophages (triplicates).

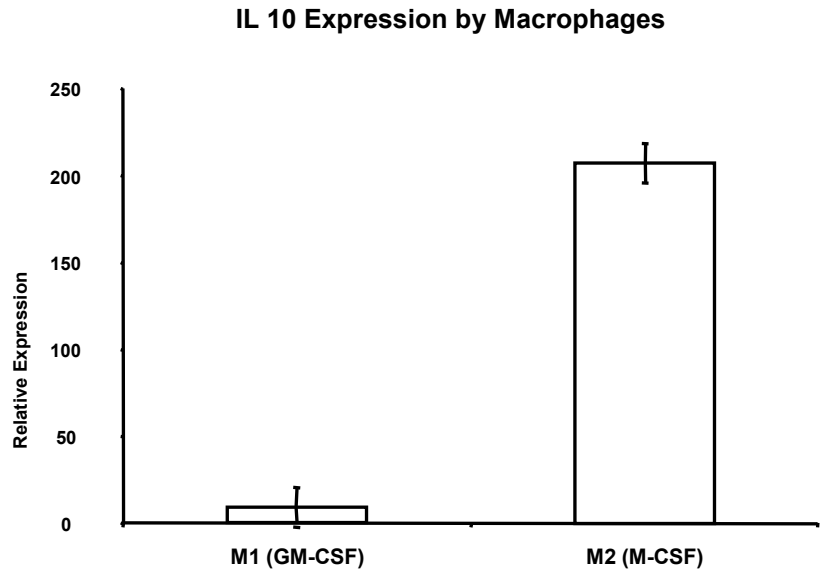

D

Macrophages generated by the sorting protocol express appropriate receptors: CSFR1 (M-CSF receptor), CSFR2a and CSFR2b (GM-CSF receptors), which are determining features of macrophage populations. CCA cell lines (S-1079, S-1196 and S245) do not express these receptors. Human solid organ CCA specimen shows expression of receptors in the tissue, consistent with a multi-cellular stroma that includes macrophages. (qPCR results expressed relative to GM-CSF treated macrophages).

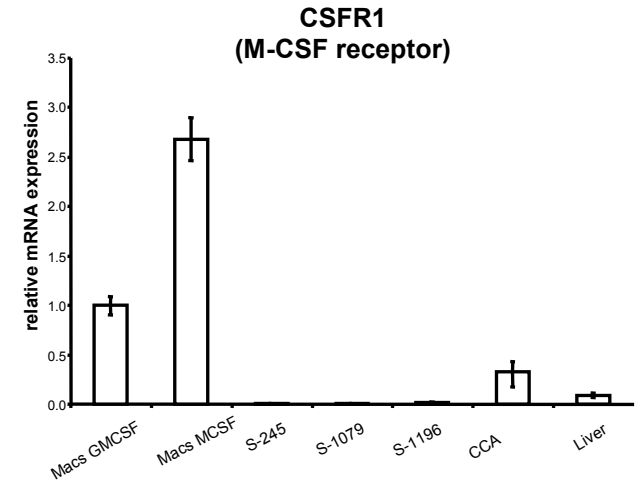

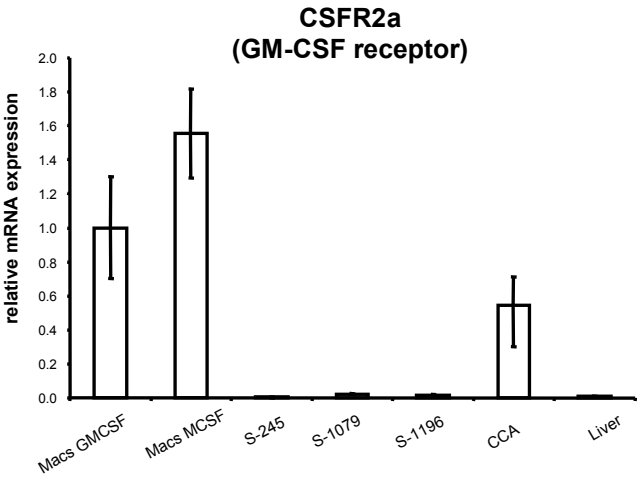

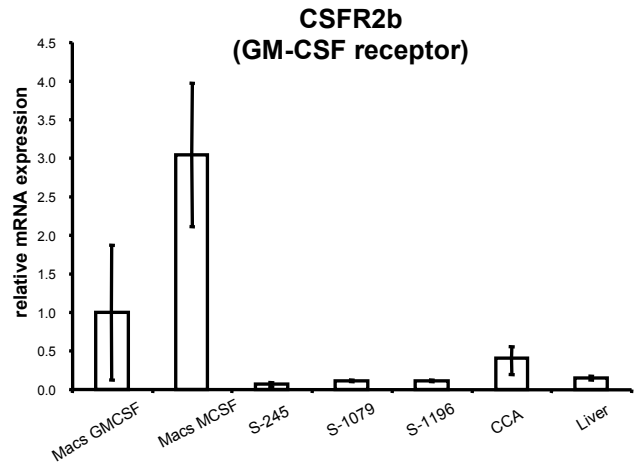

E

M-CSF and GM-CSF do not affect *in vitro* cell proliferation of CCA cell lines (S-1196, S-1079), as measured by MTT assay (sextuplets). Cells were cultured in 0%, 1% and 10% FCS IMDM with and without supplemental M-CSF or GM-CSF. There were variable effects on proliferation in 1% and 10% FCS compared to 0% FCS IMDM. However, there was no significant difference in proliferation of cells when cultured in either M-CSF or GM-CSF in all conditions (ANOVA with post-hoc Bonferroni).

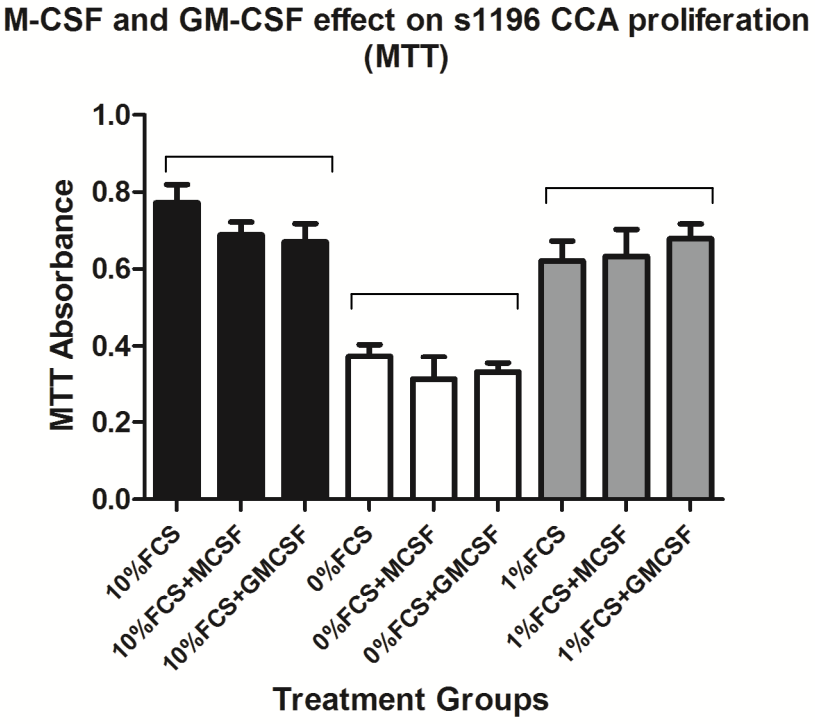

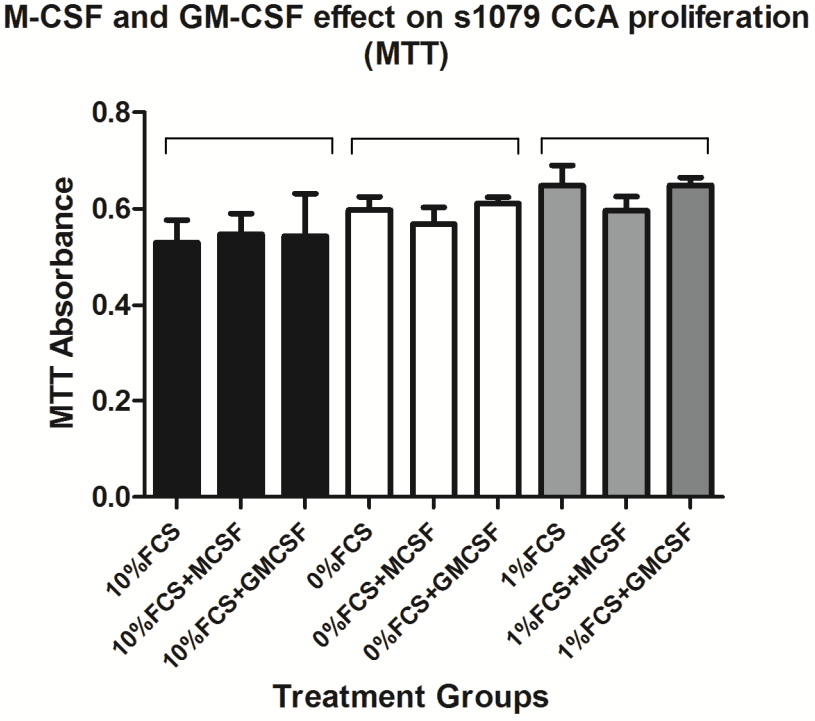

Liposomal Clodronate depletes macrophage *in vivo* but is not feasible in the rat model of CCA

To test the validity of *in vitro* findings that M2 macrophages promote tumour progression and are associated with reduced tumour cell phagocytosis than M1 macrophages, macrophage depletion *in vivo* was developed to assess the role of CCA tumour-associated macrophages in controlling the phenotype of tumours. Furthermore, we aimed to address whether altering the stem cell niche (by depleting macrophages) during the premalignant, cholangiocarcinogenesis phase would delay the onset of CCA lesions.

Liposomal clodronate comprises the bisphosphonate drug clondronate encapsulated within lipid vesicles [505]. These vesicles are phagocytosed by macrophages and, once an intracellular concentration threshold is achieved, macrophage apoptosis occurs [488]. Liposomal clodronate was tested in the rat as a mechanism of macrophage depletion. The dosing regime and frequency was established by intravenous administration of liposomal clodronate 4-6 μL/g body weight with repeat dosing at 5 and 7 days. This resulted in complete depletion of ED2/CD163 macrophages and 60% depletion of ED1/CD68 macrophages. A dosing regime of 5 μL/g every 7 days was selected.

Figure 4.11

It was planned to treat rats with 0.06% TAA for 24 weeks with commencement of intravenous dosing of liposomal clodronate at week 12 and continued treatment for a further 12 weeks. This proved impractical and so was not completed.

Figure 4.11 Optimisation and validation of liposomal clodronate administration to rats

A

To deplete macrophages in the pre-malignant stem cell niche and within CCA lesions, the experimental intention was to use the TAA model to induce CCA and, from 12 weeks, administer liposomal clodronate for up to a further twelve weeks during CCA induction.

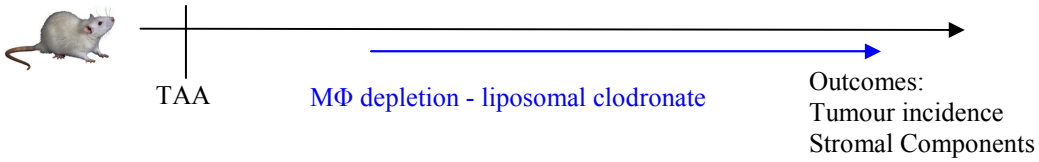

B

Liposomal clodronate dose calibration and assessment of the effect on liver MΦ depletion was performed. Rats were treated with 4µl/g or 6µl/g body weight intravenous liposomal clodronate or control intravenous PBS. Animals were culled 1, 3, 5, and 7 days after injection to assess duration of MΦ depletion. The effect of repeat dosing was also checked with rats that received a repeat dose of liposomal clodronate either 5 or 7 days apart.

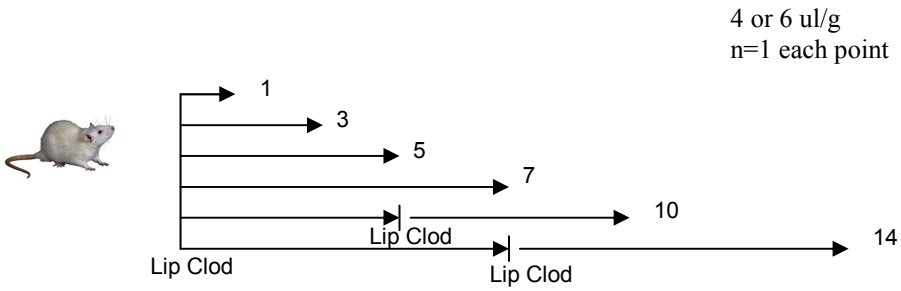

C

Lipsomal clodronate almost completely depleted ED2/CD163 MΦ (resident kuppffer cells and mature MΦ) in adult rats at both 4µl/g or 6µl/g dosing. The effect is complete by 3 days after administration and is preserved on repeated dosing:

Paraffin-embedded sections of liver and spleen from treated rats were stained for ED2/CD163 immunoreactivity and cell counts were made of 40 sequential fields of the stained rat liver sections.

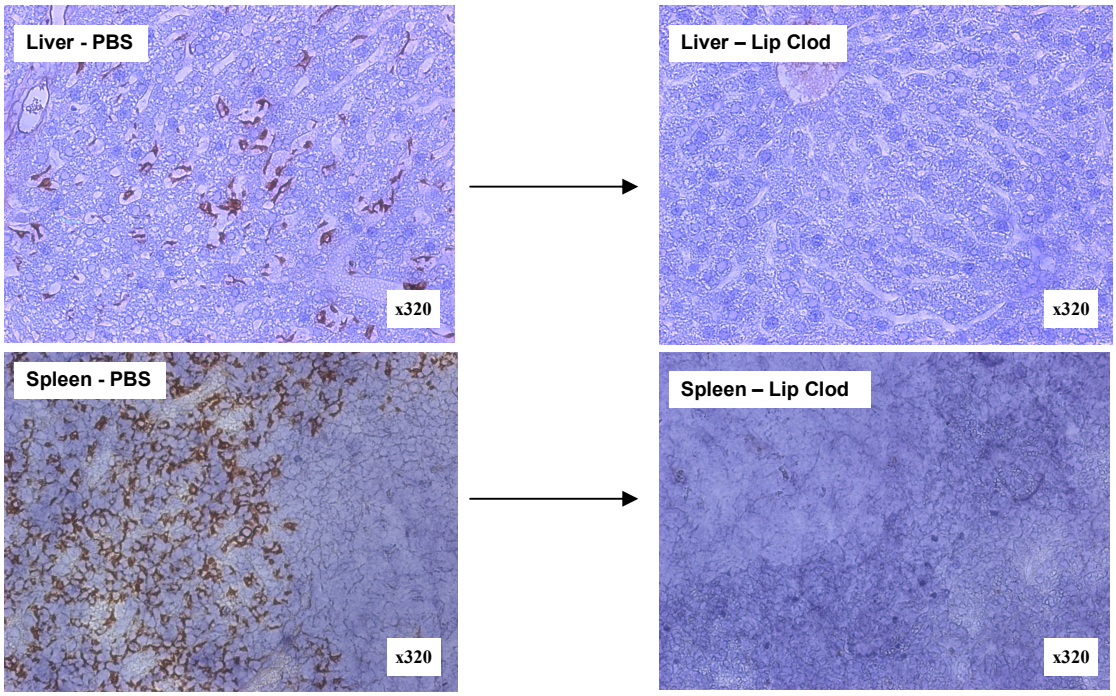

40 x320 sequential field cell counting of ED2 stained rat liver sections. Almost total depletion for all time points, at both doses, including repeated dosing 7 days apart:

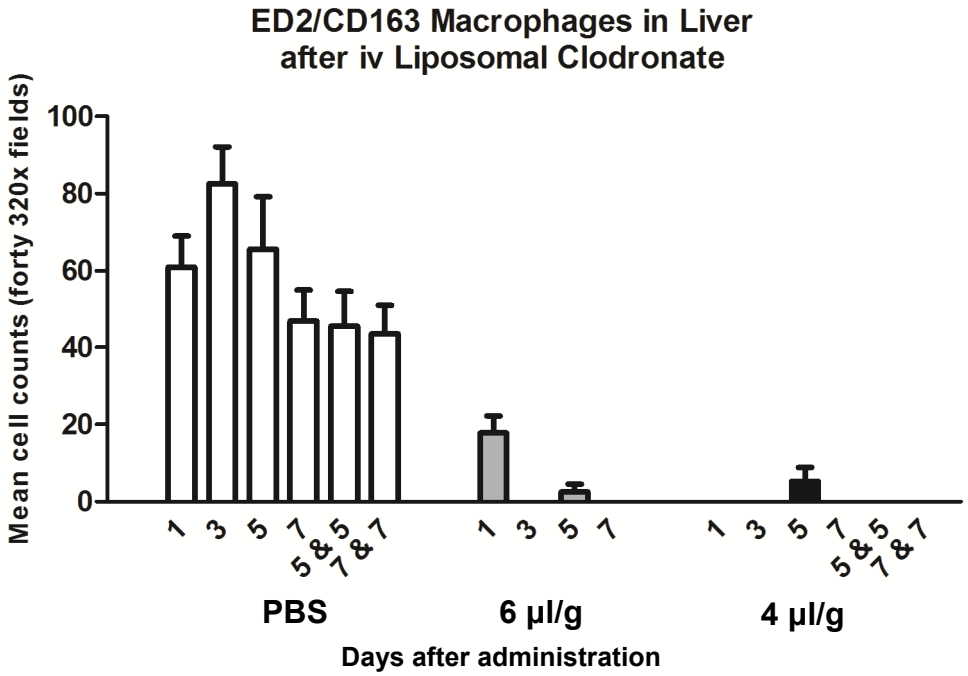

D

Liposomal clodronate depletes 60% of ED1/CD68 MΦ (migrating MΦ and monocytes) in adult rats at both 4µl/g or 6µl/g dosing. Maximal effect is complete by 3 days after administration and is preserved but not augmented by repeated dosing:

Paraffin-embedded sections of liver and spleen from treated rats were stained for ED1/CD68 immunoreactivity and cell counts were made of 40 sequential fields of the stained rat liver sections.

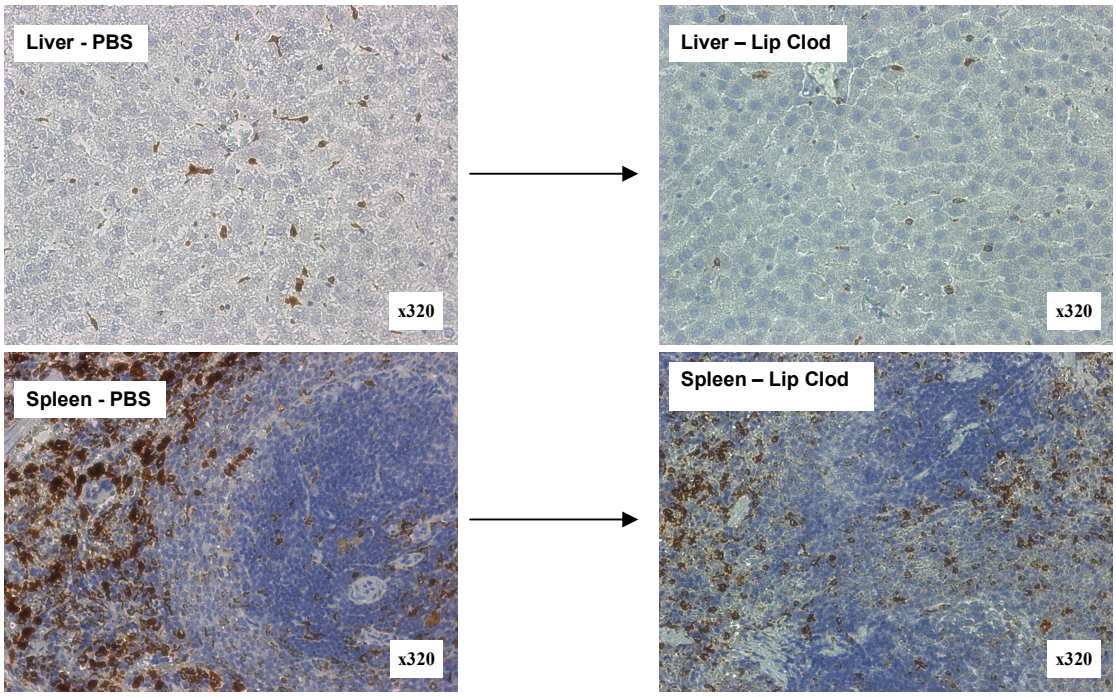

Forty x320 magnification sequential field cell counting of ED1-stained rat liver sections. Approximately 50% depletion for all time points including repeated dosing 5 and 7 days apart:

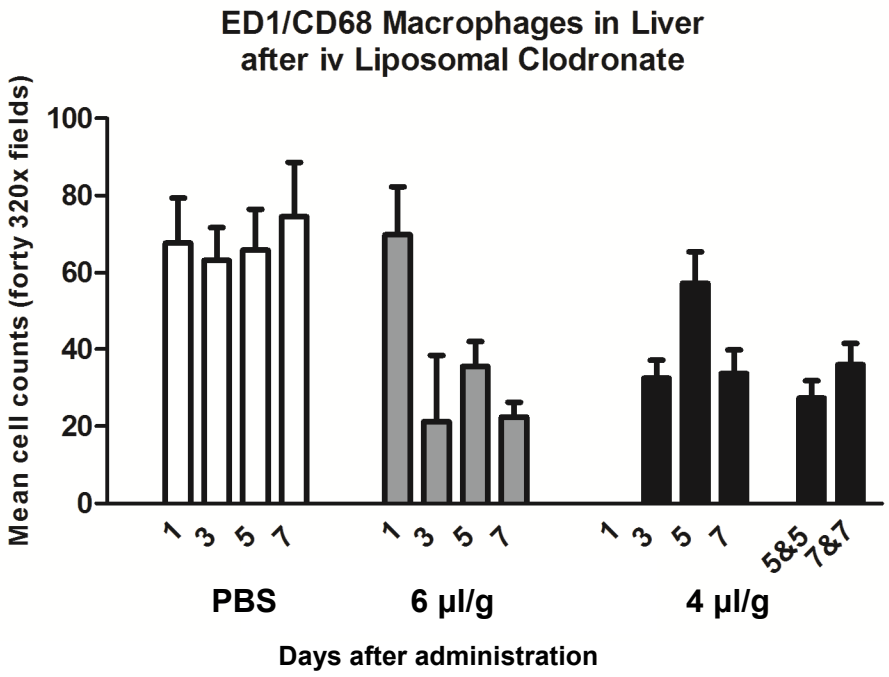

Discussion

In vitro, the majority of CCA cell lines possess SP cells, which are known to have stem cell like properties. We were unable to propagate these quantitatively, presumably due to the harshness of the protocol that rendered cells difficult to grow after cell sorting. However, CCA SP cells generated both SP and non-SP cells, and expressed markers (CK19 and AFP) consisted with maintenance of the non-differentiated state, unlike non-SP cells that expressed only CK19. The role of stromal ECM components in regulating proliferation of HSCs and CCA was also investigated. ECM components induce characteristic cell proliferation patterns with enhancement of growth of cancer cells on collagen I and IV, but reduced growth on laminin (the ECM component that ensheathes CCA cells *in vivo*). However, no *in vitro* evidence of variable cell sensitivity to chemotherapy was identified. There was no protective effect of ECM components on chemosensitivity in vitro. Stromal cell:CCA interactions were studied and we found evidence for soluble factor bidirectional interaction between CCA cells and hepatic stellate cells, together with autocrine stimulation of CCA growth. Macrophage polarisation appears to play a role in CCA tumour progression with M2 polarised macrophages appearing to both enhance cell proliferation and be associated with an *in vitro* environment in which cell phagocytosis is reduced compared to M1 macrophages. Typically, M2 macrophages phagocytose cell debris whilst M1 macrophages mediate a cytotoxic effect on target cells. In this instance, it appears that the M2-polarised *in vitro* tumour microenvironment creates a more permissive environment for CCA cell proliferation which results in less debris available for M2 macrophages to phagocytose. Separately, an optimised form of macrophage:CCA co-culture system was developed and validated which shows experimental promise.

When considering strategies for *in vivo* depletion of stromal cells, the fungal metabolite gliotoxin, a member of the epipolythiodioxopiperazine family, induced apoptosis of myofibroblasts. Gliotoxin administration has been shown to destroy hepatic stellate cells and reduce liver fibrosis [506]. However, gliotoxin has pleiotropic effects on inducing hepatocyte apoptosis (albeit at non-clinical levels during *in vivo*

experiments) and inhibiting the immune system (reviewed in [507].) Consequently, it was deemed an inappropriate tool for use with concurrent TAA cholangiocarcinogenesis. Recently, a more targeted form of gliotoxin has been developed whereby gliotoxin is conjugated to mannose-6-phosphate-modified human serum albumin (GTX-M6P-HSA) which accumulates selectively in liver fibrogenic cells [507]. The targeted gliotoxin shows promise in inhibiting hepatic myofibroblasts with significantly reduced off-target effects and may have been an appropriate alternative myofibroblast depletion tool in this series of studies.

An alternative *in vivo* macrophage depletion strategy to liposomal clodronate was considered: administration of anti c-fms neutralising antibody. This would entail regular dosing of blocking antibody against the receptor of macrophage colony-stimulating factor (CSF-1), which is a type III integral membrane protein tyrosine kinase encoded by the c-fms protooncogene (csf1r). This receptor is expressed exclusively on mononuclear phagocytes and results in profound macrophage depletion [508]. However, this was deemed impractical due to the significantly larger quantities of antibody that would be required from collaborators for rat as opposed to mouse dosing and so was not pursued.

When considering chemotherapeutic treatments for the *in vitro* chemosensitivity assays, cisplatin, 5-Fluorouracil (5-FU) and gemcitabine represented the most cogent choice of agents to study. Cisplatin is a platinum-based alkylating agent that binds to genomic DNA in nuclei with three main effects: the DNA is fragmented by repair enzymes, DNA is directly damaged by the formation of cross-links, and mispairing of the DNA nucleotides occurs which leads to mutations [509]. These effects lead to disrupted transcriptional events, including apoptosis. 5-FU is a pyrimidine analogue that is an antineoplastic antimetabolite. It interferes with DNA synthesis by blocking the thymidylate synthetase conversion of deoxyuridylic acid to thymidylic acid and hence inhibits cellular proliferation [509, 510]. Cisplatin was chosen for *in vitro* treatment of CCA cell lines in this experiment as, although 5-FU is currently being investigated by the BILCAP trial (surgery alone versus surgery with adjuvant capecitabine – oral 5-FU), cisplatin is recognised as having a higher cancer cell toxicity profile.

Furthermore, the ABC-02 trial of cisplatin with gemcitabine was shown to provide a survival advantage of 3.6 months over gemcitabine alone for patients with locally advanced or metastatic biliary tract cancer (11.7 v 8.1 months) [132]. Gemcitabine would have represented an acceptable alternative choice of chemotherapy drug to test in this instance.

CHAPTER FIVE

HAEMATOPOIETIC BUT NOT MESENCHYMAL STEM CELLS CONTRIBUTE TO THE MICROENVIRONMENT IN SOLID ORGAN TUMOURS AND DO NOT DIFFERENTIATE INTO EPITHELIAL CELLS

Introduction

Solid organ tumours such as CCA are typified by malignant cancer cells surrounded by a pronounced micro-environment of inflammatory cells such as cancer-associated fibroblasts (CAFs), tumour-associated macrophages (TAMs), immune cells (neutrophils, dendritic cells) and neovasculature embedded in a modified extracellular matrix with a preponderance of fibrillar collagens 1 and 3 [159]. This specialised microenvironment bears a striking similarity to the periportal regenerative niche that exists in the context of chronic liver injury [347]. The vast majority of CCAs are moderately differentiated adenocarcinomas (90%)[12] and intrahepatic CCA is characterised by the presence of an extensive tumour stroma[147].

A contribution of bone marrow (BM) derived cells to fibrosis has been found to occur in chronic injury in several organs [226, 315]. The migration of BM-derived cells into tumours is also described [317, 318], with the proportion of CAFs being variable across a range of models of solid-organ malignancies. Cancer-associated fibroblasts were reported as contributing 25% of stromal populations in a murine model of pancreatic cancer [228] and up to 30% in xenogeneic tumour engraftment models [320].

It has been suggested that BM-derived stem cells may contribute to the malignant epithelial cell component of tumours, possibly by repopulating depleted stem cell niches. In an elegant murine model of gastric cancer (*H. felis* chronic infection), Houghton [333] demonstrated that BM-derived mesenchymal stem cells (MSC) could repopulate gastric epithelial stem cell niches and subsequently give rise to gastric cancer with almost 100% of malignant cells appearing to be BM-derived. This group also demonstrated that aged BM-derived MSCs (generated by prolonged culture *in vitro*) give rise to fibrosarcomas when administered to mice *in vivo* [334]. Whether this represents a general principle is as yet unclear. Some groups have reported similar findings [335] but others have been unable to replicate the principle of the study in alternative models [336].

Here we investigate the contribution of BM-derived cells to both the tumour associated stroma and the epithelial component in the TAA rat model of intrahepatic CCA. We demonstrate that tumour-associated cells of the haematopoietic lineage (monocytes, macrophages, neutrophils) are overwhelmingly derived from the BM. In contrast, cells from the mesenchymal lineage (activated myofibroblasts and fibroblasts), despite being a major component of the tumour burden, do not derive from BM sources. Furthermore, we were unable to identify evidence to support the principle of either BM-derived mesenchymal or haematopoeitic stem cell contribution to the epithelial component of tumours. These findings were corroborated in spontaneous breast, skin and colon tumours found in, lethally irradiated and reconstituted but otherwise untreated chimeric rats.

Sex mismatched adoptive transfer of wild type (*wt*) BM into *wt* recipients and enhanced green fluorescent protein (EGFP+) transgenic BM into *wt* recipients allowed two independent methods to be used for tracking transplanted BM-derived cells following treatment with TAA to induce CCA. Adoptive transfer of sex-mismatched *wt* BM into *wt* recipients. enabled tracking using the sex determining region Y (SRY) component of the Y Chromosome in transplant recipients. In parallel, immunohistochemistry for EGFP enabled independent tracking of EGFP-expressing cells in wt recipients of EGFP+ transgenic BM.

Due to the relatively long TAA treatment periods required to induce CCA, a number of simultaneous studies were embarked upon following rederivation of EGFP+ transgenic rats from frozen embryos kindly provided by Professor Okabe. These included pilot studies to confirm whether EGFP+ BM was stably expressed following adoptive transfer and studies to verify whether both the haematopoietic and mesenchymal components of the BM fraction were transplanted and functionally propagated. Concurrently, adoptive transfer of EGFP+ sex-mismatched BM into male rats was performed followed by tumour induction. In addition, in case EGFP expression was silenced, rendering transplanted cells unidentifiable, adoptive transfer of *wt* male BM into *wt* female was undertaken followed by TAA exposure.

Following establishment of CCA lesions in experimental chimeras, cell tracking was undertaken.

A summary of the BM transplants and acquisition timepoints that were undertaken is listed (**Table 5.1**). These are described in more detail below.

Table 5.1: BM transplants undertaken in experimental series

Male *wt* to Female *wt*			**Male EGFP to Male *wt***			**Female EGFP to Male *wt***	
Time	***TAA***	***Control***	***Time***	***TAA***	***Control***	***Time***	***TAA***
18wks	6	2	12wks	6	3	12wks	6
32wks	6	3	26wks	6	3	26wks	6
52wks	6	3	32wks	6	3	32wks	6

Quantifiable detection of SRY in SD rats

In order to quantify the degree of chimerism in sex-mismatched BM transplant recipients, qPCR primers were designed (as described in the Chapter 2: Methods) for the rat Y chromosome (SRY). The primers were selected to identify a homologous region across the six copies of the SRY gene in rat (SRY1, SRY2, SRY3, SRY3B, SRY3B1, SRY3C). The efficiency of SRY qPCR in multiplex was ascertained to be greater than 90% with good correlation with GAPDH gDNA endogenous control. Multiplexing did not affect the efficiency of the qPCR assay (**Figure 5.1A** and **5.1B**).

To quantify the contribution of male cells in male to female BM transplants a standard curve was produced using qPCR of serial dilutions of genomic DNA using control male BM and control female BM of Sprague Dawley (SD) rats. Five-fold dilutions were made from 100% male, to 20%, 4%, 0.8%, 0.16%, 0.032%, 0.0064%, 0.00128% and eventually 0% male (100% female). The SRY:GAPDH ratio for each sample was ascertained by multiplex qPCR. The equation describing the resulting curve was then used to derive the proportion of male cell contribution per experimental sample in transplanted animals (**Figure 5.1C**).

Figure 5.1: Quantifiable detection of SRY in SD rats

A: Efficiency of SRY and GAPDH multiplex PCR of genomic DNA. $R^2 > 90\%$ for both SRY and GAPDH slopes, confirming >90% efficiency, non-saturability of the primers in multiplex, and good correlation of SRY with GAPDH gDNA endogenous control.

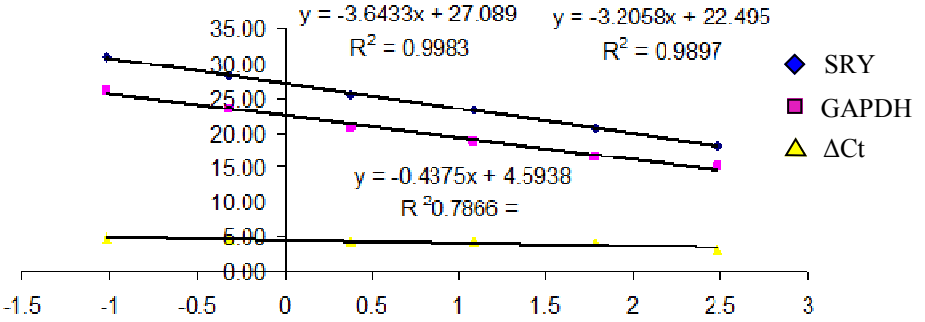

B: Rat SRY genomic DNA alignment of the six copies on the Y chromosome SRY1 (AY157669), SRY2 (AY157670), SRY3 (AY157672), SRY3B (AY157996), SRY3B1 (AY157997), SRY3C (AY157671). Primers and Probe as highlighted (amplicon 107bp).

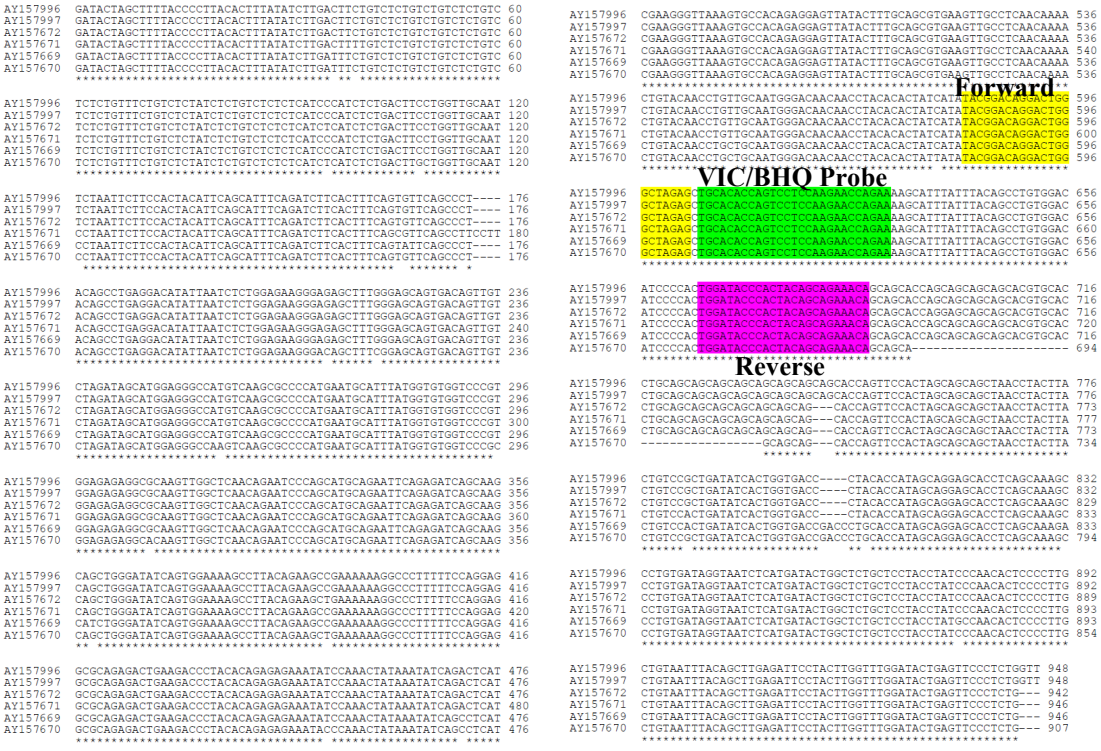

C: Serial dilutions of male into female BM (x axis) with calculation of SRY:GAPDH ratio for each sample by qPCR. The equation describing the curve was then used to derive the proportion of male cell contribution per experimental sample in transplanted animals.

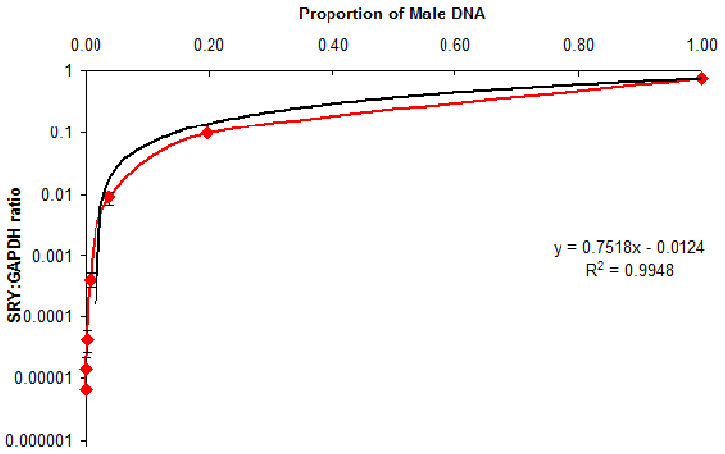

Adoptive transfer protocol establishes chimeras with persistent EGFP expression

The irradiation regime for adoptive transfer of BM in SD rats was derived from the literature [487, 511, 512]. Home Office regulations do not provide for dose testing protocols outwith specifically permitted schedules. Consequently, it was necessary to ascertain that adoptive transfer resulted in functional cellular adoptive transfer rather than endogenous repopulation from the recipients' BM. Furthermore, reports have suggested variable occurrence of GFP silencing following adoptive transfer in inbred syngeneic murine studies [513, 514]. As the TAA cholangiocarcinogenesis protocol utilises SD rats, which are outbred, it was necessary to determine whether EGFP silencing occurred. Consequently, the origin of BM reconstitution (whether donor derived or endogenous cellular repopulation) and assessment of the stability of EGFP expression following adoptive transfer was studied.

The EGFP+ transgenic SD rats were a kind gift of Prof Okabe (Osaka)[486, 487]. The colony of EGFP+ SD rats was rederived from frozen embryos in the Edinburgh University BRR. These rats ubiquitously express enhanced GFP under control of the cytomegalovirus enhancer and the chicken ß-actin promoter.

In a control experiment, chimerism was measured over time in female recipients of male EGFP+ BM. In order to investigate silencing and the timeframe for cellular regeneration, adult female SD rats underwent adoptive transfer of male EGFP+ BM as detailed in **Figure 5.2A**. The transplanted male BM was additionally stained with CellTracker DiD to enable independent flow cytometry detection of "red" stained BM if EGFP+ signal was immediately undetectable or silenced upon injection. Bone marrow, spleen and blood samples were obtained 5 minutes, 18 hours, 7 weeks and 14 weeks after adoptive transfer. The duration of DiD staining would enable detection of cells in the 5 minutes and 18 hour samples. Successful stable transplantation of male EGFP+ BM into *wt* female rats was confirmed in BM, spleen and blood as identified by flow cytometry and qPCR for genomic DNA. Additionally, to determine the persistence of expression of EGFP+ BM during

induction of CCA, female *wt* SD rats that underwent adoptive transfer with male EGFP+ BM were commenced on TAA after 10 weeks recovery. These were harvested after a total of 42 weeks (10 weeks recovery, 32 weeks TAA) **Figure 5.2B**.

Eighteen hours post BM transplantation, only 1.95% (BM), 2.17% (spleen) and 1.93% (blood) were transplanted male cells as measured by qPCR for SRY (**Figure 5.2C**). Flow cytometry was performed and cells of interest were considered to be DiD+EGFP+, DiD+EGFP- or DiD-EGFP-. No transplanted cells were detected on flow cytometry for EGFP+ expression and only a very small number were found on flow cytometry for DiD cell staining (data not shown). It is likely that a large number of transplanted cells were cleared via the lungs (and liver and kidney) following intravenous administration and hence were not detected by flow cytometry.

Seven weeks following adoptive transfer, only two of the three transplanted rats expressed SRY in BM and splenic tissue (blood not tested) (**Figure 5.2D**). These two rats possessed EGFP+ cell populations on flow cytometry (A representative example of EGFP flow cytometry analysis is shown in Figure 5.3D panels B and C that demonstrates chimerism of lymphocyte and granulocyte subpopulations). The rat that did not express SRY on qPCR also did not express EGFP+ cells on flow cytometry. This indicated that the irradiation and BM transplant protocol successfully achieved chimerism for transplanted BM, but that it was also possible for a subset of individuals to reconstitute their BM from endogenous sources. There was no evidence for silencing of EGFP+ transplanted cells, which would have been evidenced by EGFP- SRY+ chimeras. These findings were similar at 14 weeks where chimerism for transplanted BM comprised 100%, 63.95% and 58.80% male cells in BM, spleen and blood respectively as measured by qPCR (**Figure 5.2E**). When considering the timecourse of reconstitution, the plateau of chimerism was maximal by 7 weeks following adoptive transfer (**Figure 5.2F**). Two of the three female *wt* rats were found to be chimeric for male EGFP+ (qPCR and flow cytometry of BM, spleen and blood). The third rat had endogenously repopulated, as identified by the observation that BM, spleen and blood were EGFP- SRY-.

It was then confirmed that cellular expression of EGFP by the EGFP+ chimeras was persistent and unaffected by the TAA treatment schedule. Forty-two weeks after adoptive transfer (10 weeks recovery and 32 weeks 0.03% TAA administration), of the two rats that received this schedule, one was EGFP+ SRY+ whilst the other was EGFP- SRY- (**Figure 5.2G**).

In view of the timeframes necessary for rederivation of the EGFP+ SD rat colony and the possibility of EGFP silencing following transplantation rendering donor cells unidentifiable, it was decided to pursue concurrently the feasibility of male *wt* to female *w*t BM adoptive transfers, using SRY expression to identify donated cells. Female rats underwent adoptive transfer with male *wt* BM and were treated with oral TAA for 18, 32 and 52 weeks (n=6 TAA and n=3 water controls at each timepoint). To confirm that BM reconstitution was successful (and functional) in male to female sex-mismatch transplants, cells from whole BM, sorted lymphocytes and granulocytes (CD11b+ and CD45+ staining) and spleen were collected by Fluorescence-activated cell sorting (FACS). The intention was to then undertake qPCR for SRY on the male to *wt* female chimeras to identify the proportion of cells that were male donor-derived. These samples were collected whilst the EGFP+ protocol was being developed but there was no requirement to analyse them in further detail as the EGFP+ transplant chimera system was successful, demonstrating success of the protocol. The BM of all male to female wt chimeras was tested for SRY (qPCR) to exclude individuals that had reconstituted from endogenous cell sources rather than from donor BM.

Figure 5.2: Adoptive transfer protocol establishes chimeras with persistent EGFP expression

A

Determination of whether EGFP was stably expressed following adoptive transfer to outbred *wt* SD rats.

Male EGFP BM was stained with DiD ("red" on flow cytometry) and transplanted into female *wt* recipients. Subjects were harvested at serial timepoints and flow cytometry for EGFP with DiD and qPCR for SRY were performed.

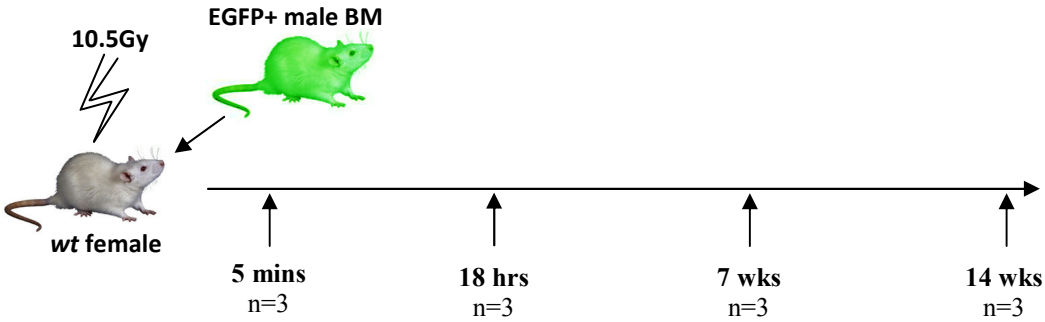

B

Determination of persistence of EGFP stable expression in the context of 0.03% TAA administration.

Male EGFP BM was transplanted into female *wt* recipients then administered TAA after 10 weeks of recovery.

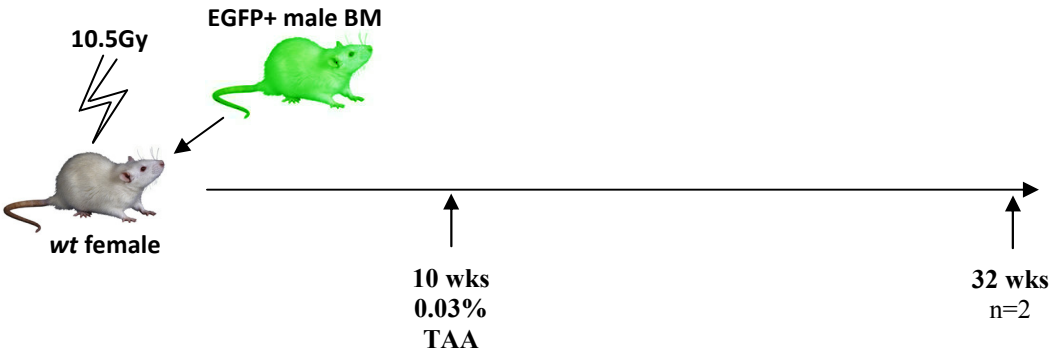

C

Eighteen hours after adoptive transfer, no EGFP signal was identified on flow cytometry. qPCR for SRY identified a mean of 1.95% (in BM), 2.17% (spleen, SP) and 1.93% (blood, BL) transplanted male cells comprising the cellular fraction in the three subjects. (Five minute data not shown).

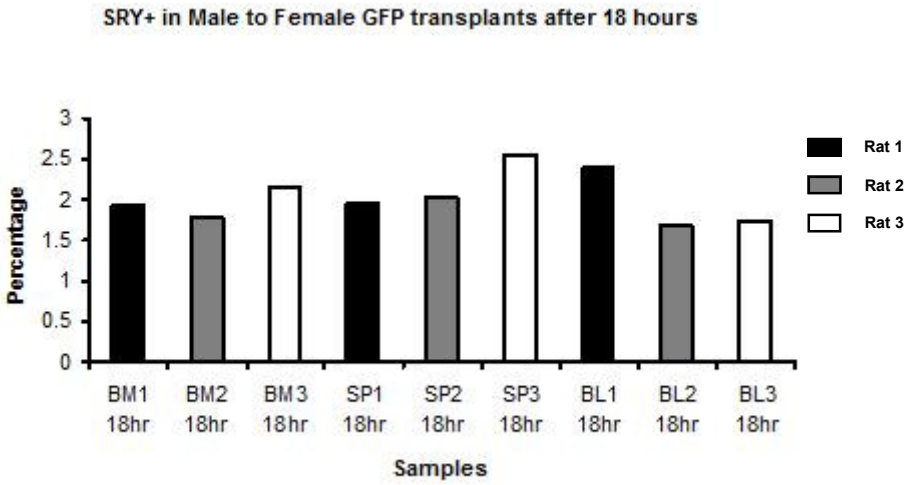

D

Seven weeks after adoptive transfer, there was a positive relationship between SRY expression and EGFP patterns. Rats 2 and 3 demonstrated SRY expression as detailed below. Furthermore, rats 2 and 3 also possessed high EGFP chimerism on flow cytometry. (An example of flow cytometry analysis is shown in Figure 5.3D). Conversely, rat 1 displayed no EGFP or SRY expression. The absence of SRY indicates endogenous repopulation rather than EGFP silencing and exogenous reconstitution. (BM and spleen data shown, blood not shown).

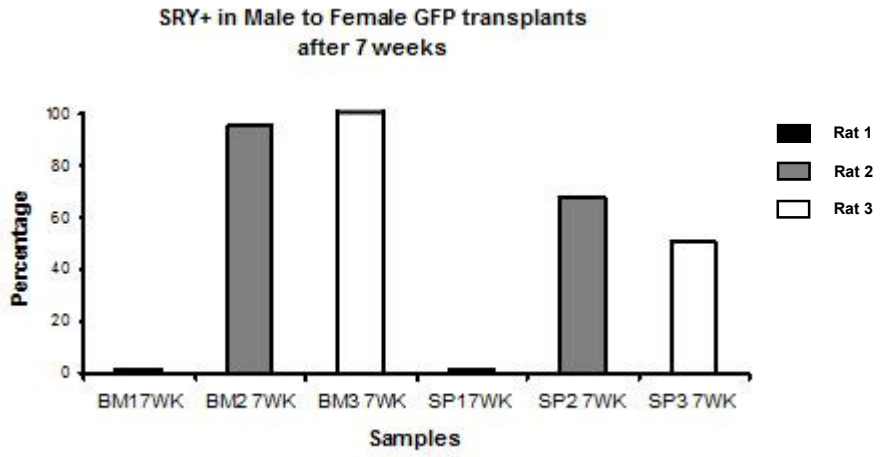

E

Fourteen weeks after adoptive transfer, there was a positive relationship between SRY expression and EGFP patterns with apparent maximal reconstitution by 7 weeks since the proportional contributions did not increase significantly at week 14. At 14 weeks,rats 1 and 2 (but not rat 3) demonstrated both EGFP expression and SRY expression.

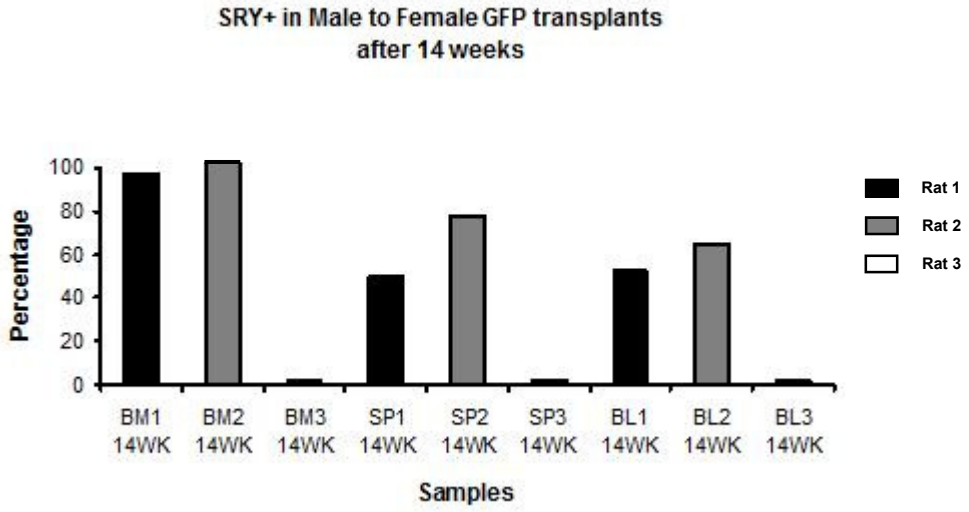

F

The plateau of maximal reconstitution was reached by 7 weeks.

qPCR of BM, spleen and blood (n=2 at each timepoint as non reconstituted specimens were excluded).

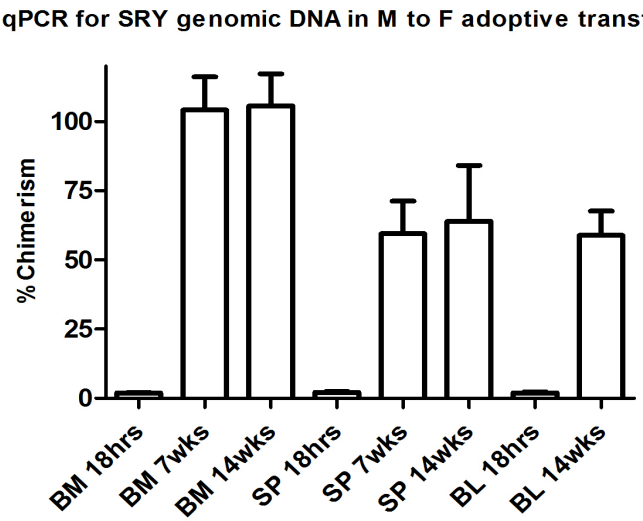

G

After 32 weeks of 0.03% TAA, EGFP expression was maintained. Rat 1 expressed both EGFP on flow cytometry and SRY on qPCR in BM and spleen. Rat 2 expressed neither EGFP or SRY, consistent with endogenous reconstitution in this instance rather than depletion or silencing of successfully transplanted EGFP+ BM.

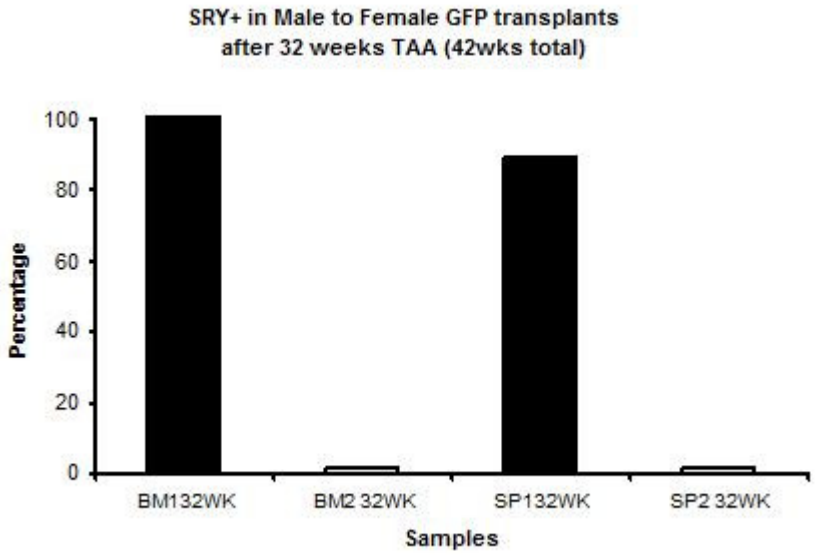

Stable chimerism of haematopoietic stem cell compartments in recipient rats following administration of TAA

Adoptive transfer of male and female EGFP+ BM into male *wt* recipients was followed 10 weeks later by TAA administration. The EGFP+ chimeras were then serially harvested after 14, 26 and 38 weeks of TAA administration. Transplants comprised n=6 male EGFP to male *wt* and n=6 female EGFP to male *wt* recipients at each timepoint (**Figure 5.3A**). The contribution of donor EGFP-BM to haematopoietic tissues of recipients was determined by flow cytometry. Data were acquired and analysed on a FACSAria cell sorter using Diva Software (Becton Dickinson). Forward and side scatter characteristics were used to apply an electronic gate before acquisition of data and sorting to exclude red cells, dead cells and debris. Acquired data were analysed for the contribution of EGFP+ cells to BM, spleen and blood in *wt* recipients. Persistent EGFP chimerism was observed within the haematopoeitic compartments of BM (57.10%), spleen (85.10%) and blood (73.70%) (**Figure 5.3B**).

Functional reconstitution of the haematopoeitic compartment after adoptive transfer and 38 weeks TAA administration was confirmed using flow cytometry to identify EGFP+ lymphocytes and granulocytes in chimeras. Lymphocyte and granulocyte sub-populations were identified and gated based on their scatter characteristics, before measuring the percentage of EGFP+ cells in each subpopulation. EGFP+ cells were gated compared to cells from the same tissue derived from a wild type control (**Figure 5.3C**). Samples of sorted cells were re-aquired to confirm the experimental purity of collected sub-populations (**Figure 5.3D**). Of note, sex-mismatched male to female *wt* chimeric BM, spleen and blood was collected and sorted in the same fashion as shown in Figure 5.3D, using scatter properties to identify lymphocyte and granulocyte subtypes (data not shown) in case EGFP SD rat colony rederivation failed.

The apparent difference in proportional reconstitution detected by flow cytometry (70%) and qPCR (100%BM) may be explained by the effect of using a derived

equation to determine chimerism on qPCR, whereas flow cytometry allowed direct detection of EGFP fluorescence in each cell. Alternative explanations may include the argument that more than one (ideally three) housekeeping genes are strictly required for qPCR quantification; however this is very rarely undertaken in practice. A single housekeeping gene, GAPDH, was used in this study for multiplexing because to multiplex more than two genes was not indicated in the absence of methodological flaws that would otherwise render results difficult to interpret. It is unlikely that male/female differences in endogenous GAPDH expression explain the above findings as the mean Ct vales for GAPDH for male and female BM were found to be very similar (male BM Ct 16.049 and female BM Ct 16.300). Additionally, minimal sex differences in GAPDH expression have been identified in other species [515].

In the EGFP chimeras it was observed that a proportion of cells were EGFP- on flow cytometry. This may represent either the persistence of endogenous (non-EGFP) cells or silencing of EGFP in a subpopulation of transplanted cells. To determine the origin of the EGFP- cells, it would be necessary to sort the cells within the chimeric tissue into EGFP+ and EGFP- fractions using FACS, and then undertake qPCR for SRY. EGFP- SRY+ cells would represent silenced, transplanted cells whereas EGFP- SRY- cells would be derived from endogenous sources. This experiment was not undertaken due to time constraints and also because it is widely recognised in the literature that adoptive transfer protocols generate chimeras comprising transplanted cell types and endogenous cell types [516, 517].

Figure 5.3: Stable EGFP chimerism of blood, spleen and BM in wt rats following adoptive transfer of syngeneic EGFP+ BM

A

Male rats underwent adoptive transfer of either male or female EGFP+ BM, recovered for 10 weeks and then received TAA for up to 38 weeks.

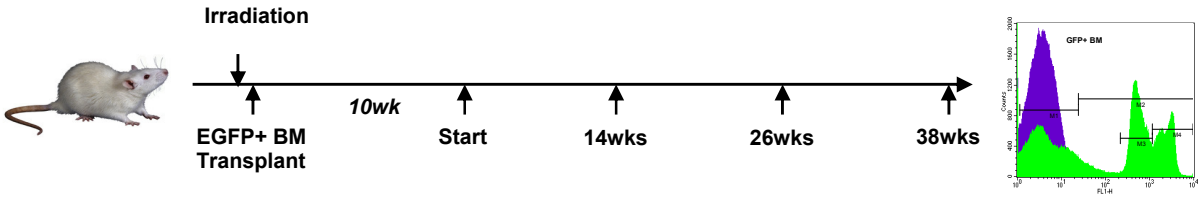

B

Following adoptive transfer, flow cytometry confirmed EGFP+ chimerism of the haematopoeitic compartment of BM, spleen and blood at 38 weeks of TAA, N=6.

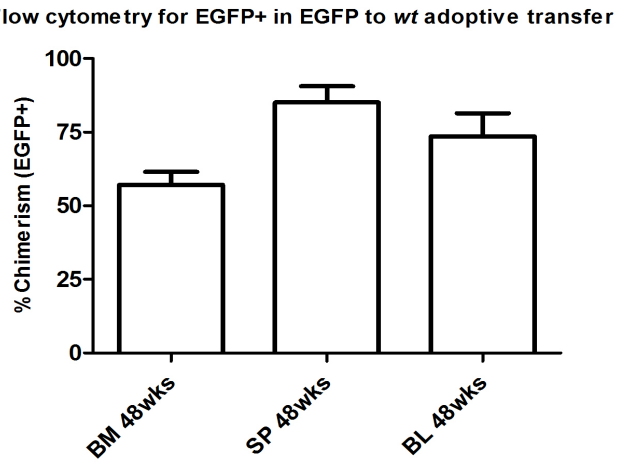

C

Functional reconstitution of the haematopoeitic compartment after 38 weeks of TAA and adoptive transfer, with EGFP+ mononuclear cells and granulocytes identified in chimeras.

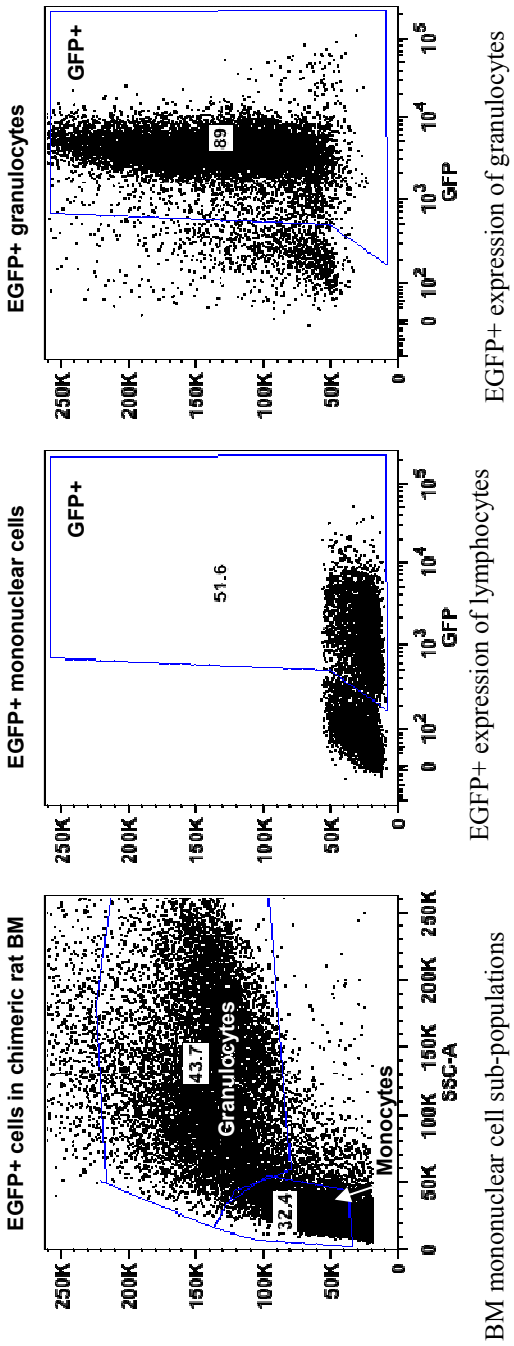

D

Example of sorting strategy used to isolate cell populations from a chimeric recipient of EGFP+BM, showing purity of recovered cells.

Cells were labelled with PE conjugated anti-CD45 antibody to confirm haematopoietic lineage and cells were sorted based on EGFP and CD45 expression. Panel A: unsorted BM after gating to exclude cell aggregates, red cells, dead cells and debris, showing gates defining lymphocyte and granulocyte sub-populations. Panel B: unsorted lymphocytes gated for EGFP+CD45- cells (P6) and EGFP+CD45+ cells (P7). Panel C: unsorted granulocytes gated for EGFP+CD45- cells (P9) and EGFP+CD45+ cells (P8). Panel D and E: reacquisition of sorted lymphocytes from P6 and P7. Panel J and K: : reacquisition of sorted granulocytes from P8 and P9. Panels F and G; sorted lymphoctes were absent from granulocyte sort gates P8 and P9. Panels H and I: sorted granulocytes were absent from lymphocyte sort gates P6 and P7. Figures in gates are % of cells falling within the gate.

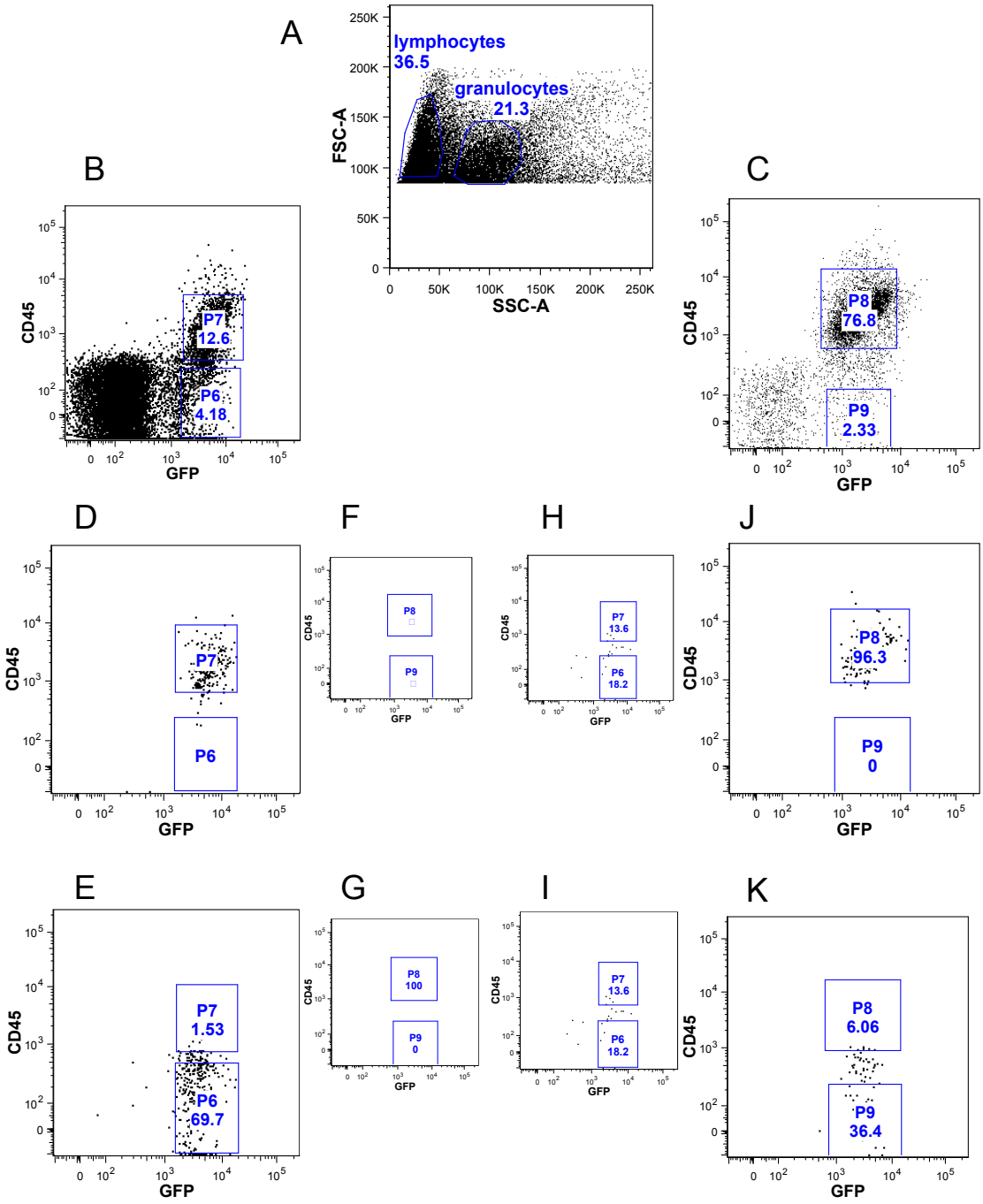

Stable chimerism of mesenchymal stem cell compartments in recipient rats following adoptive transfer

Mesenchymal stem cells (MSC) are extremely rare, comprising 0.01%-0.001% of all mononuclear cells, compared to 0.1% for the haematopoietic stem cell (HSC) population [223]. Some argue that these cells should preferentially be termed mesenchymal stromal cells since cultured MSCs may comprise a number of cell type subsets and may be derived from other sources including adipose tissue, umbilical cord skin [219, 220] and tissue pericytes [221]. Mesenchymal stem cells are considered to be more radio-resistant than HSCs [518-520] and the degree of chimerism achieved in the MSC compartment by adoptive transfer was investigated. To characterise EGFP-BM chimerism of the mesenchymal stem cell compartment, BM from transplant recipients was collected by flushing femurs with PBS following incubation in collagenase 1A[521]. Recovered cells were washed and resuspended in Mesencult MSC basal medium supplemented with 10% HyClone FCS. Cells recovered from 1 femur after flushing were plated into a 1 well of a 6 well plate and passaged up to 4 times using TRYPLE. (**Figure 5.4A**). Live cell fluorescent microscopy of BM MSC cultures demonstrated abundant EGFP+ MSC (**Figure 5.4B**). The phenotype of cultured cells was assessed by flow cytometry. Briefly, cells were incubated with fluorochrome-conjugated monoclonal antibody for 30 minutes and washed before data acquisition. An electronic gate was used to exclude dead cells. Unstained cells from wild type and EGFP+ BM, together with appropriate isotypes were used as controls to set gates to identify EGFP+ cells co-expressing specific markers. Monoclonal antibodies used included CD45 (PECy5.5) and STRO-1 (APC). Cells were deemed to be mesenchymal stem cells (MSCs) if they expressed STRO-1 [491-493] and were donor-derived if they co-expressed EGFP. In addition, the cells were gated to be non-haematopoeitic, by gating for CD45- (data not shown). Transplanted animals were compared to non-transplanted positive control EGFP+ rats. Flow cytometry identified that the proportion of STRO-1+/EGFP+ cells was comparable between transplanted animals and non-transplanted positive control EGFP rats (**Figure 5.4C**), n=5 transplants and n=2 controls.

The currently accepted definitive test for MSCs is the ability of plastic-adherent cultured cells to undergo tridirectional differentiation into bone, fat and cartilage [223, 522]. Due to the prolonged timecourse involved (months) for clonal expansion of cultured cells, a decision was made to phenotype mesenchymal-like cells using cell surface markers. The use of cell surface markers is widely used in published studies of MSCs. These markers have been well characterised for humans and mice. Human MSC typically express CD44 (H cell adhesion molecule), CD73 (5'-nucleotidase), CD90 (Thy-1 surface antigen), CD105 (endoglin), CD106 (vascular cell adhesion molecule) and STRO-1[223, 225]. Mice express the same markers except for STRO-1. Conversely, STRO-1 represents the current validated MSC cell surface marker in rats[491-493, 523, 524] whereas the other markers above have not yet been found to be replicated in rat MSC phenotypes.

Figure 5.4: EGFP chimerism of mesenchymal component of BM

A

Protocol for enrichment of MSCs from EGFP+ chimeras.

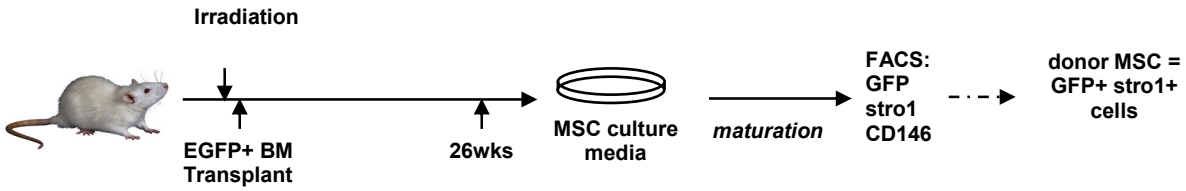

B

Live cell fluorescent microscopy identifies abundant EGFP+ cells in MSC selective culture.

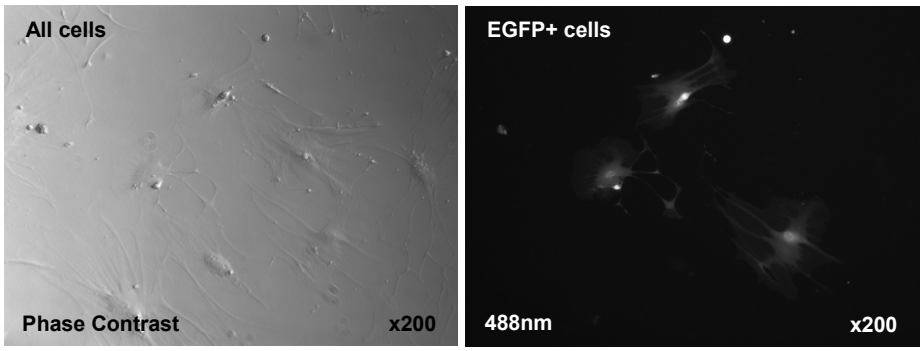

C

Flow cytometry for co-expression of stro-1 and EGFP confirms similar chimerism to positive control rats with a similar proportion of stro-1+ EGFP+ cultured cells up to the fourth culture passage (73.5 and 70.2%).

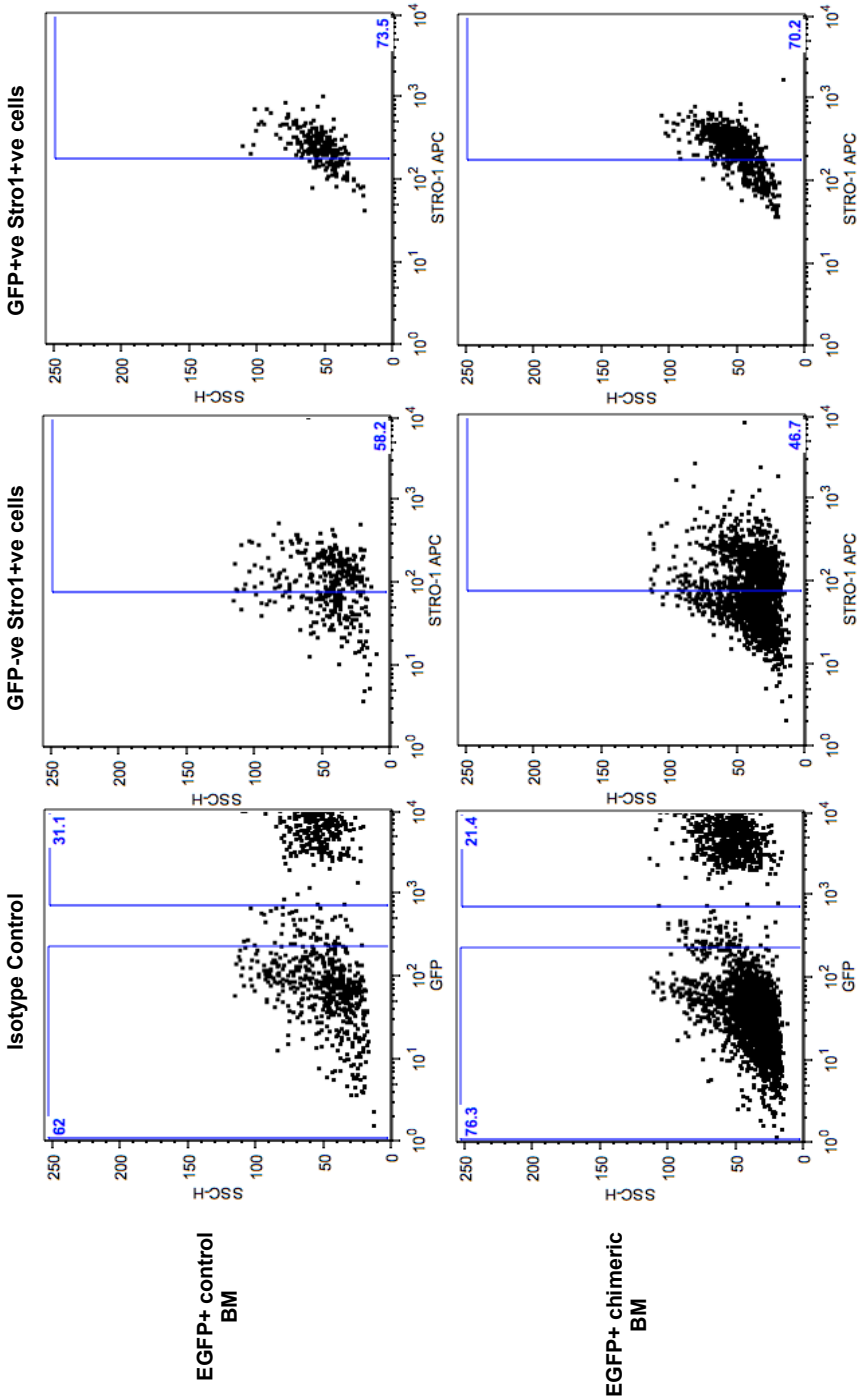

Haematopoeitic cells but not mesenchymal cells are recruited from BM-derived sources

Ten weeks following bone marrow transplantation (BMT), chimeric rats (male recipients of either female EGFP-BM or male EGFP-BM) were commenced on drinking water supplemented with 300 mg/L thioacetamide (TAA) (Sigma)[480]. These were harvested following 14, 26 and 38 weeks of TAA dosing; n=6 TAA for each transplant group at each timepoint. Age-matched chimeric controls were provided with unsupplemented drinking water (n=3 at each timepoint). Cells of BM origin were tracked in liver using immunohistochemistry for EGFP and fluorescent *in situ* hybridisation for the Y-chromosome (YChr-FISH) together with immunofluorescence for cell specific antigens. For anti-EGFP immunofluorescence combined with YChr-FISH, Tyramide Signal Amplification (TSA) was performed to stabilise the EGFP epitope signal.

Following 38 weeks of TAA treatment, multiple intrahepatic CCA lesions developed in five animals (two male *wt* recipients of male EGFP+ BM and three male *wt* recipients of female EGFP+ BM). These lesions accurately reprised the histological architecture of human intrahepatic CCA tumours with a similar distribution of biliary epithelial and stromal cells. See **Figure 3.3** for details.

EGFP+ cells comprised a large component of the cellular compartment of the tumour stroma. The origin of haematopoietic-derived cells was tracked using dual immunofluorescence for EGFP and cell specific antibodies: ED1/CD68 migrating monocyte/macrophages, ED2/CD163 tissue resident macrophages and myeloperoxidase (MPO) neutrophils. These cells were predominantly from BM-derived sources, as characterised by dual EGFP+/cell specific marker+ immunofluorescence (**Figure 5.5A**).

In contrast, dual immunofluorescence for EGFP and αSMA (myofibroblasts) and desmin (fibroblasts) identified that cancer associated fibroblasts (CAFs) and

perivascular fibroblasts were not derived from transplanted BM sources (**Figure 5.5B**).

Figure 5.5: Haematopoeitic and mesenchymal stem cell derived stromal elements in intrahepatic CCA

Dual immunofluorescence of haematopoeitic cells and EGFP identifies BM-derived cells in tumour associated stroma in the rat TAA model of intrahepatic CCA.

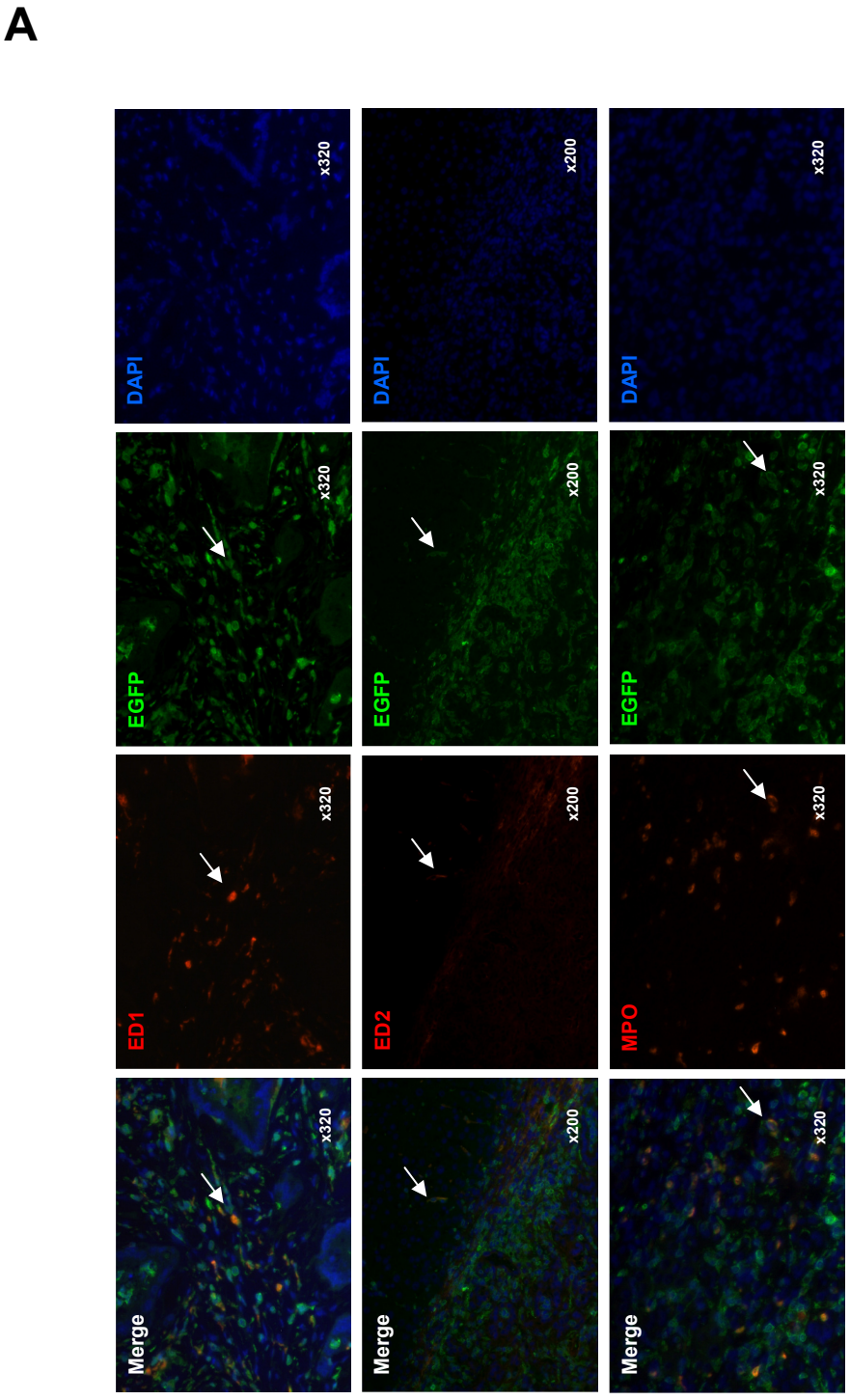

ED1+ macrophages, ED2 macrophages and MPO+ neutrophils are BM-derived as demonstrated by co-expression of EGFP (green) and epitope markers (red). ED1 macrophages and MPO neutrophils are distributed throughout the tumour stroma whereas ED2+ macrophages are tissue resident and not associated with tumour stroma.

B

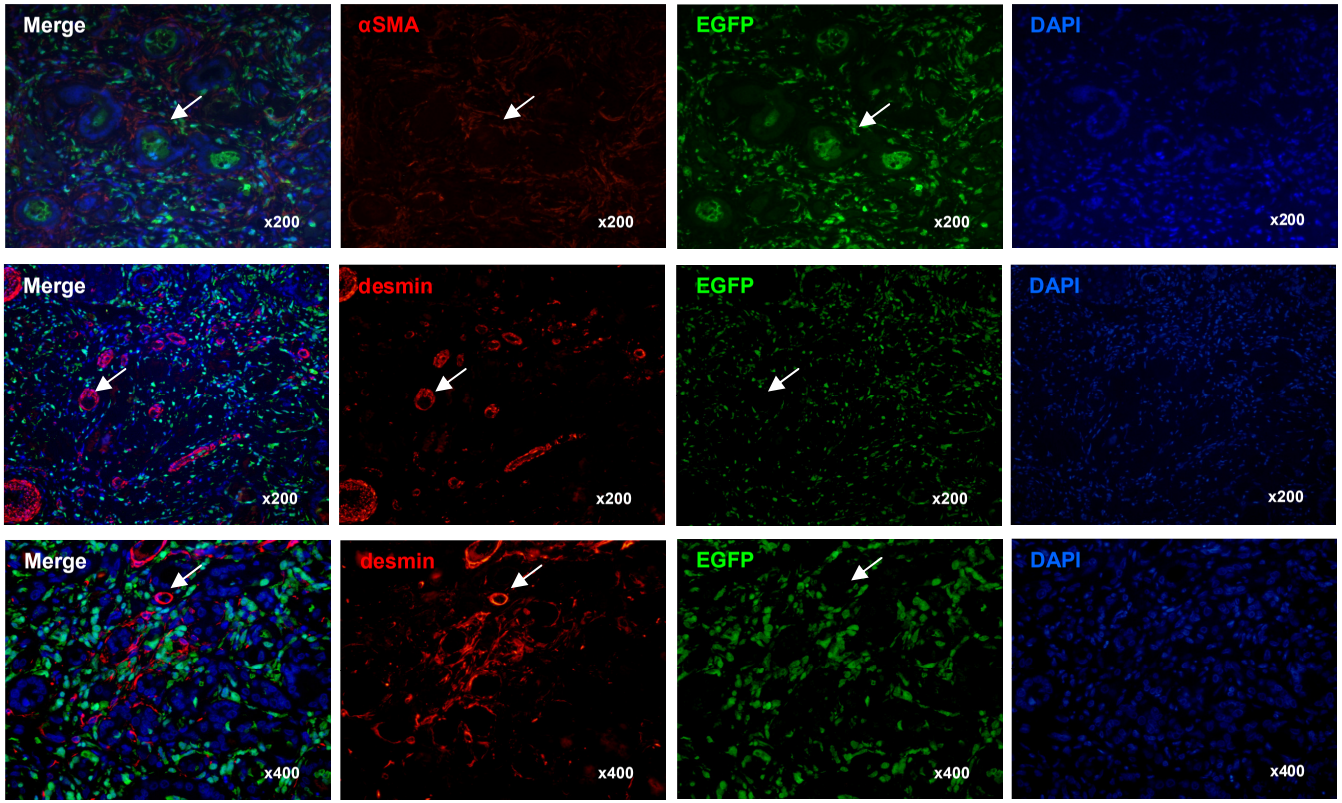

αSMA+ and desmin+ myofibroblasts are distributed throughout tumour stroma and are not bone marrow derived, as evidenced by the absence of dual EGFP/epitope staining.

Epithelial cells are not BM-derived in the TAA model of intrahepatic CCA

Dual immunofluorescence for EGFP and epithelial cell markers (CK19 or PanCK) identified disordered, glandular, malignant epithelial cells. However, there was no evidence of EGFP+CK19+ or EGFP+PanCK+ cells, suggesting that malignant epithelial cells were not BM derived (**Figure 5.6**).

Figure 5.6: Epithelial cells in intrahepatic CCA are not BM-derived

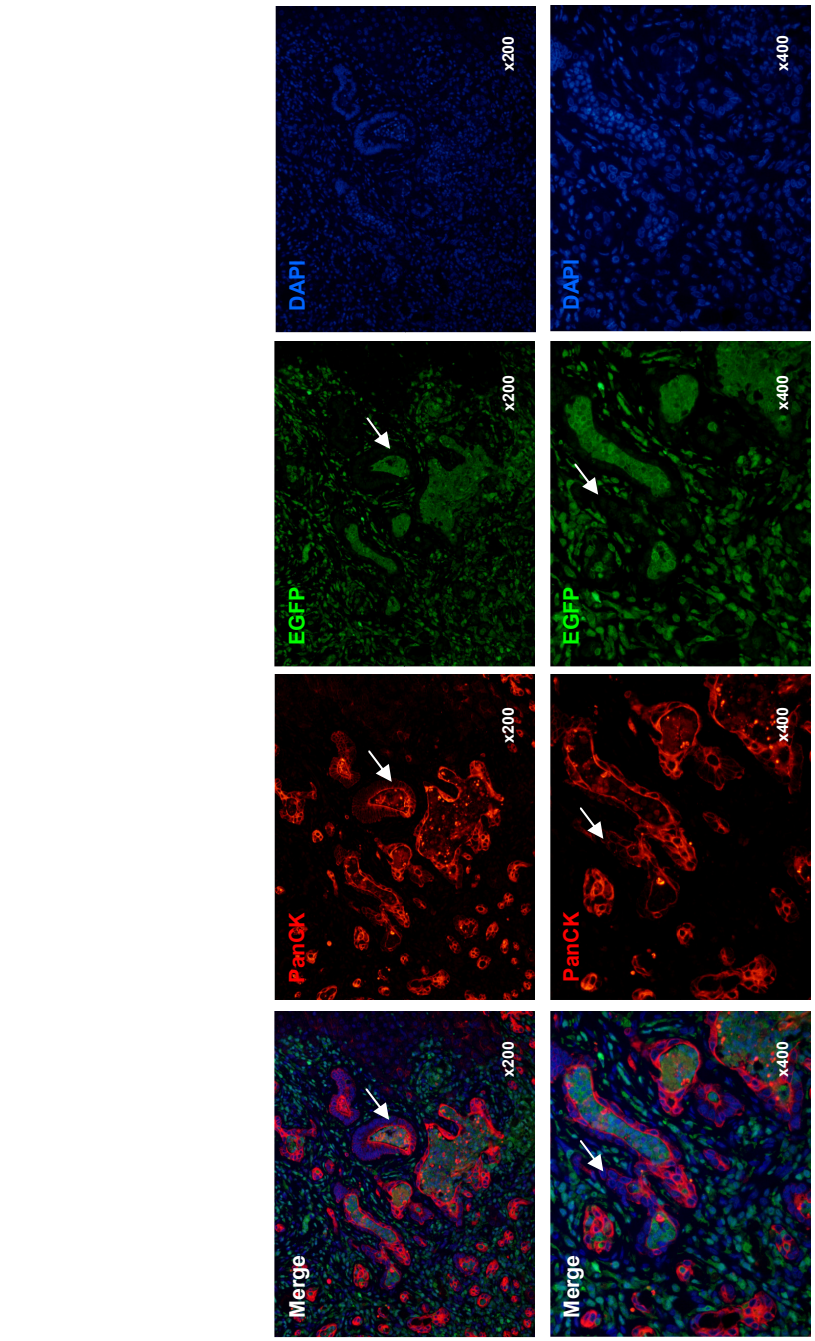

Dual immunofluorescence for PanCK and EGFP does not identify co-expression of PanCK19+ and EGFP+. This indicates that BM-derived cells in tumour associated stroma in the rat TAA model of intrahepatic CCA are not contributing to the malignant epithelium. Arrows mark epithelial cells that are PanCK+ EGFP-.

B

Dual immunfluorescence for CK19 and EGFP identifies that BM-derived cells in tumour associated stroma in the rat TAA model of intrahepatic CCA are not contributing to the malignant epithelium of intrahepatic CCA. Arrows mark epithelial cells that are CK19+ EGFP-.

No evidence for significant rate of cell fusion or EGFP silencing in CCA

To identify whether BM-derived cells transdifferentiated into epithelial-type cells and, in so doing, silenced EGFP expression, the incidence of EGFP- Y-Chr- epithelial cells of tumours in the female EGFP+ BM to male *wt* chimeras was studied. The BM origin of cells within the lesions was traced by YChr-FISH using STAR* FISH Rat 12/Y Cy3 labelled paint. This technique paints the Y-chromosome red and also identifies homology in chromosome 12 (that paints green) and chromosome 3 (that paints orange). The combination of immunohistochemistry and Y-Chr immunofluorescence of serial sections was used to track the epithelial cells within the lesions. Histological sections are of finite thickness and the Y chromosome is not detectable in all cells even in male control tissue, as the nucleus may be only partially included in the tissue sections, Hence, there is a detection rate of the Y-Chr based on section thickness and nuclear. For example, studies in the literature have identified 42-63% cells in male control tissue to contain Y-Chr on FISH analysis [315, 331]. All malignant bile ducts analysed in this series were found to have greater than 30% Y-Chr+ cells, and the majority were greater than 60%. These findings fit within the Y-Chr detection rate for cells that would be identified as male cells in control serial sections. Conversely, EGFP is a cytoplasmic protein and should be detectable in all EGFP+ cells on the section as it is unaffected by section thickness.

To address whether BM-derived cells fused with epithelial cells to a significant degree, dual EGFP+ immunofluorescence and YChr-FISH was performed on both the female EGFP+ to male *wt* male tumour-bearing chimeras following 38 weeks of TAA. No evidence of fusion was observed with no GFP+Y+Chr cells seen in female-to-male chimeras **Figure 5.7A**.

Over the time course of TAA administration in the male to female *wt* BM transplants, marked cirrhosis developed with evidence of biliary duct dysplasia and microinvasive carcinomas (oral TAA for 18, 32 or 52 weeks; n=6 TAA and n=3 water controls at each timepoint). Male BM-derived cells were identifiable in the

fibrotic scars of these animals by 32 weeks **Figure 5.7B**. Following 52 weeks of TAA administration, CK19+ cells were Y-FISH- indicating that malignant biliary epithelial cells arose within the liver rather than being BM-derived **Figure 5.7C**. These results confirmed the results from EGFP chimeras.

Figure 5.7: **Tracking of Y-Chromosome in transplant chimeras using FISH**

A

Y-Chr FISH and dual immunofluorescence for EGFP in female EGFP to male *wt* BM chimeras identify no female malignant bile ducts and no EGFP+ bile ducts.

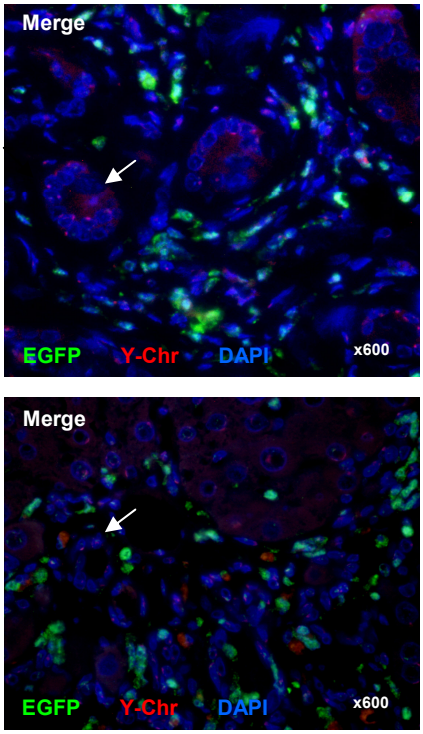

B

Timecourse of the male to female *wt* BM transplants. At 18 weeks minimal hepatic abnormalities were noted with no evidence of biliary duct abnormalities. At 32 weeks, cirrhosis was marked with evidence of biliary duct dysplasia and microinvasive carcinomas. Male derived cells were identified by FISH in the fibrotic scar tissue of female livers at 32 weeks. The arrows in the figure mark male chromosomes.

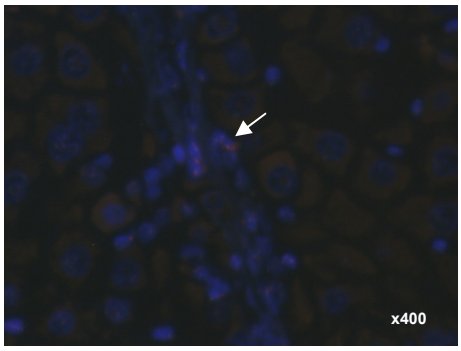

Male derived cells in female liver fibrotic scar tissue

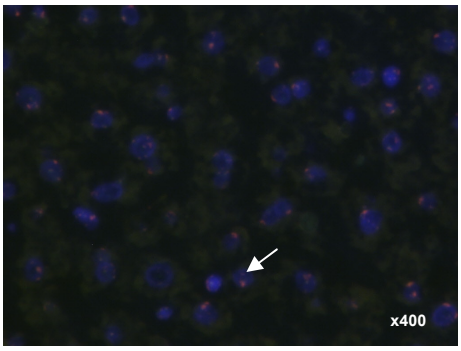

Male liver positive control tissue

C

Y-Chr FISH and CK19 serial sections in male to female *wt* BM chimeras after 52 weeks TAA identify no male cells in malignant biliary epithelia.

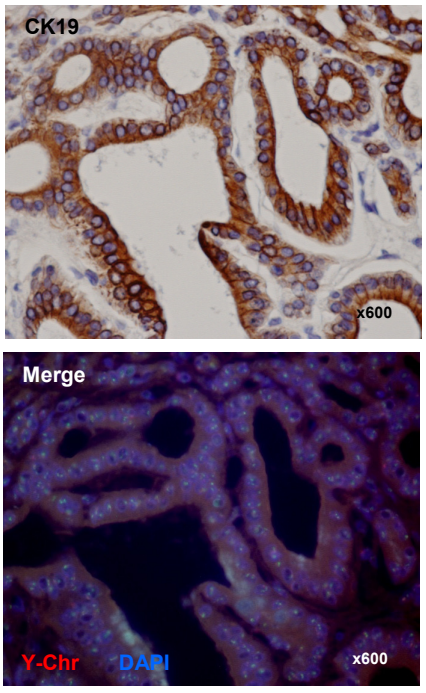

Progressive accumulation of BM-derived haematopoietic cells occurs in the liver during TAA-driven cholangiocarcinogenesis

The developmental timecourse was investigated in the TAA CCA model over 14 and 26 weeks prior to tumour formation at 38 weeks. Using dual immunofluorescence, ED1, ED2 and MPO cells in the liver were, over the studied timepoints, seen to display increasing proportions of cells expressing both cell-secific markers (ED1, ED2, MPO) and EGFP as cells migrated from the BM to the liver and replaced. ED1 macrophages and MPO neutrophils demonstrated relatively early co-expression of EGFP and cell-specific markers by 14 weeks. Conversely, ED2 macrophages displayed later apparent changes insofar as minimal co-expression of EGFP was noted by 26 weeks (**Figure 5.8A**). It was previously demonstrated that full BM chimerism was achieved in this model by 7 weeks (see **Figure 5.2F**). Consequently, the observed differences here may be explained by the fact that ED1 and MPO cells are migratory immunoregulatory cells whereas ED2 cells are tissue resident and hence more sessile and therefore less prone to rapid turnover. These cell types were distributed throughout the liver as turnover occurred.

When considering MSC-derived cells, αSMA myofibroblasts were distributed in vascular walls and were not BM derived at any time point. Similarly, epithelial cells (CK19 and panCK) displayed non-chimeric qualities (no co-expression of EGFP) during the entire TAA carcinogenesis regime (**Figure 5.8B**).

Figure 5.8: Haematopoeitic and mesenchymal stem cell derived stromal elements in liver during TAA carcinogenesis

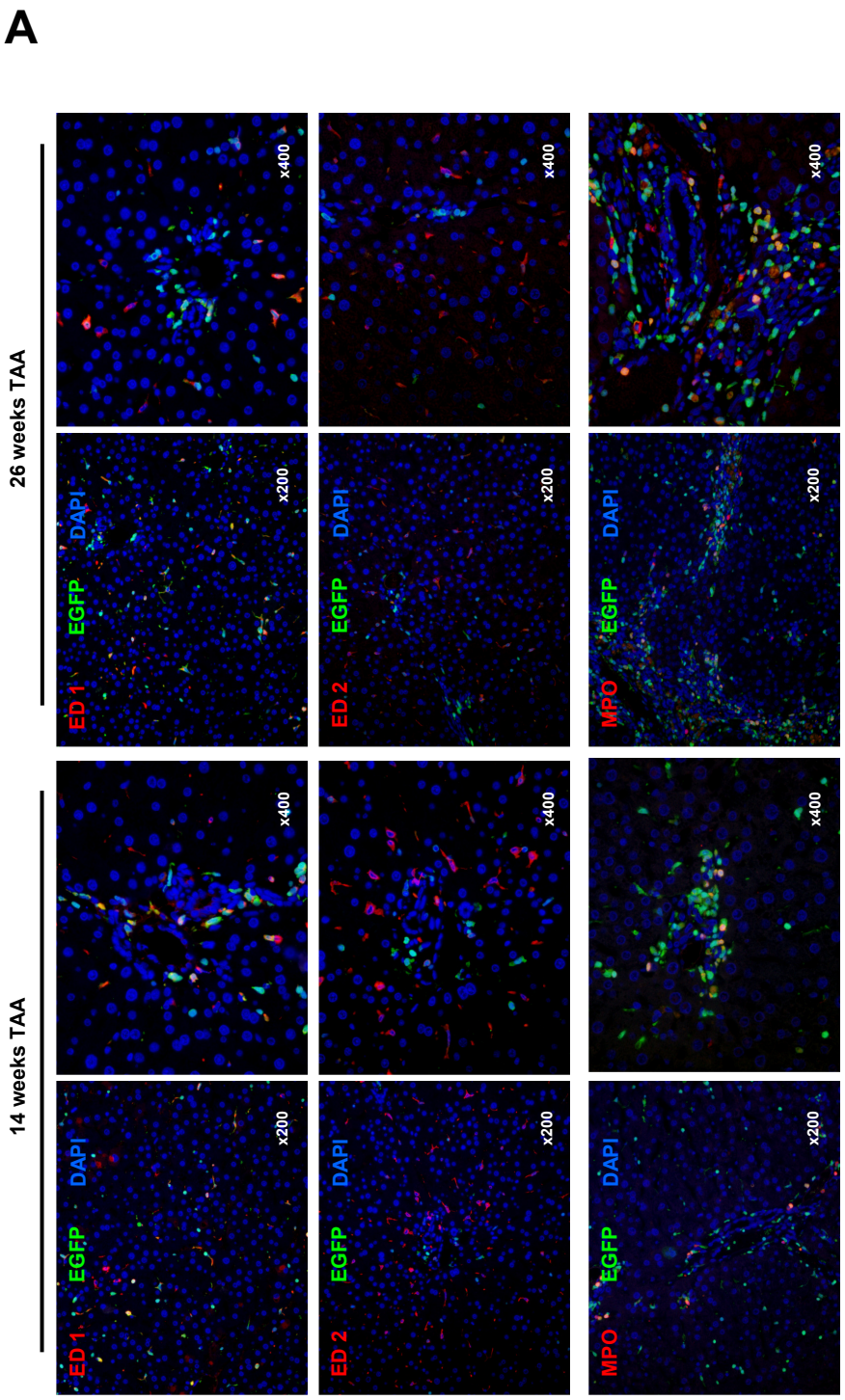

Dual immunofluorescence of haematopoeitic cells and EGFP identifies BM-derived cells in periportal niches and interlobular fibrotic bands in the rat TAA model of intrahepatic CCA. ED1 macrophaes and MPO neutrophils demonstrate earlier apparent chimerism when compared to ED2 macrophages.

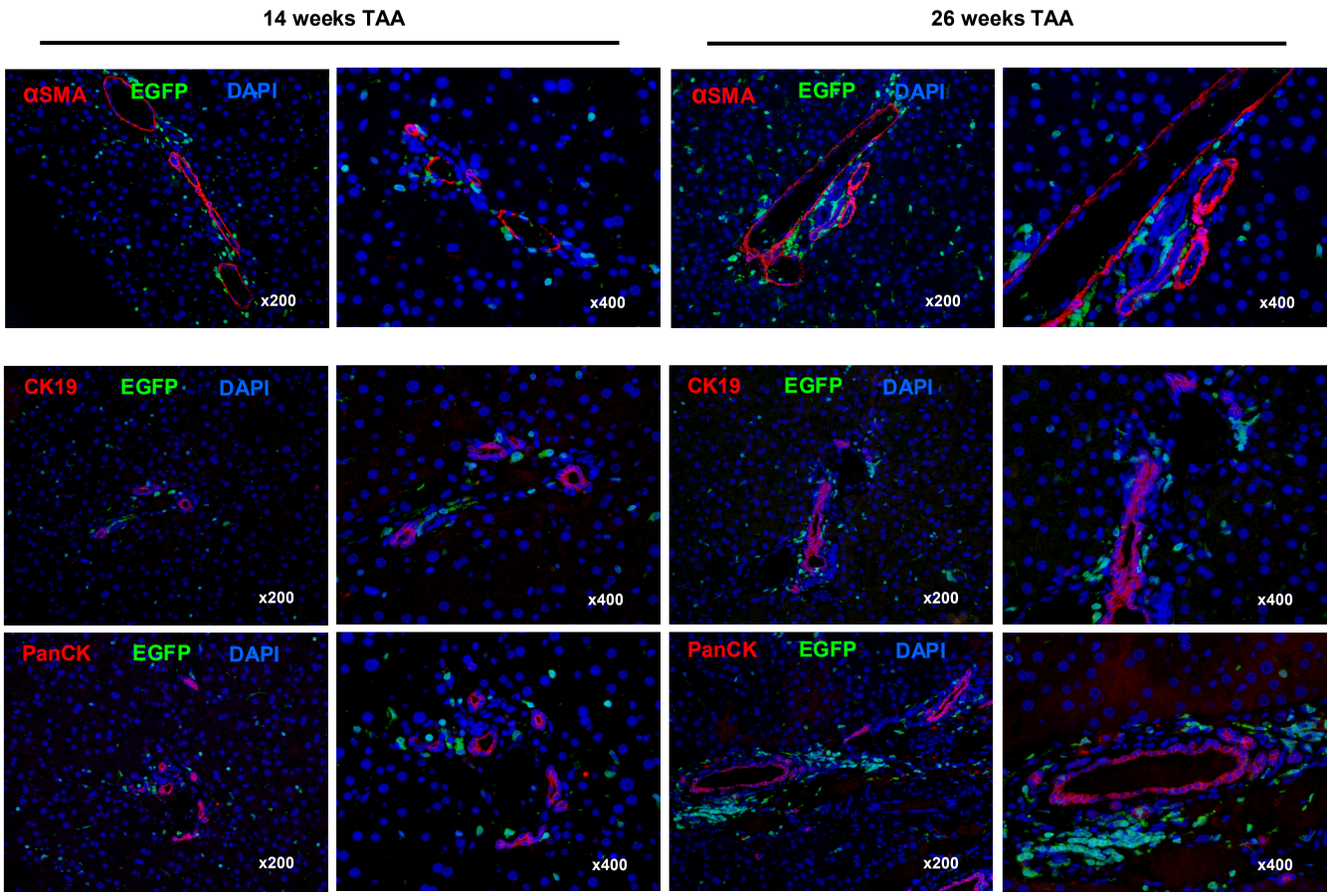

αSMA myofibroblasts are distributed in vascular walls and do not co-express EGFP. These cells are not BM derived at any time point. Similarly, epithelial cells (CK19 and panCK) do not co-express EGFP during the entire TAA carcinogenesis regime.

A similar pattern of cell origin is noted in other solid organ lesions compared to CCA

Spontaneous tumours are known to occur in irradiated rats [525]. In female rats that underwent adoptive transfer of male EGFP+ BM but received no further treatment (specifically, no TAA), spontaneous breast (n=8), skin (n=6) and colon (n=1) lesions developed between 26 and 38 weeks. The histological subtypes of these lesions comprised: Breast [fibroadenoma (3), infiltrating duct adenocarcinomas of tubular, papillary or cribriform types (4), adenocarcinoma with lymphosarcoma (1)]; skin [basal cell carcinoma (6)]; colon [adenocarcinoma with osteoclastic malignant components (1)].

The spontaneous tumours were studied in the same fashion as the CCA lesions by means of dual-fluorescence immunohistochemistry. A similar pattern of cell distribution was seen in breast, colon and skin malignancies as compared to CCA in rat. Desmin and αSMA- expressing cells originating from MSC-derived were not BM-derived(**Figure 5.9A and 5.9B**). Similarly, PanCK+ cells all displayed no evidence of BM-derivation (**Figure 5.9C**). Conversely, ED1 cells displayed more heterogeneity than in the CCA lesions, with more cells being EGFP- than in CCA (**Figure 5.9D**). This may be explained by the spontaneous lesions forming earlier and so resident ED1 macrophages still being present at the time of tumour formation. In a similar fashion, ED2 cell heterogeneity followed the same pattern as ED1+ cells (**Figure 5.9E**). Separately, MPO cells were overwhelmingly EGFP+, explained perhaps by the shorter lifespan of these cells and so a more rapid turnover from the BM driving replacement of endogenous neutrophils prior to tumour onset (**Figure 5.9F**).

Figure 5.9: A similar pattern of cell distribution is seen in breast, colon and skin malignancies in rat as compared to CCA

A

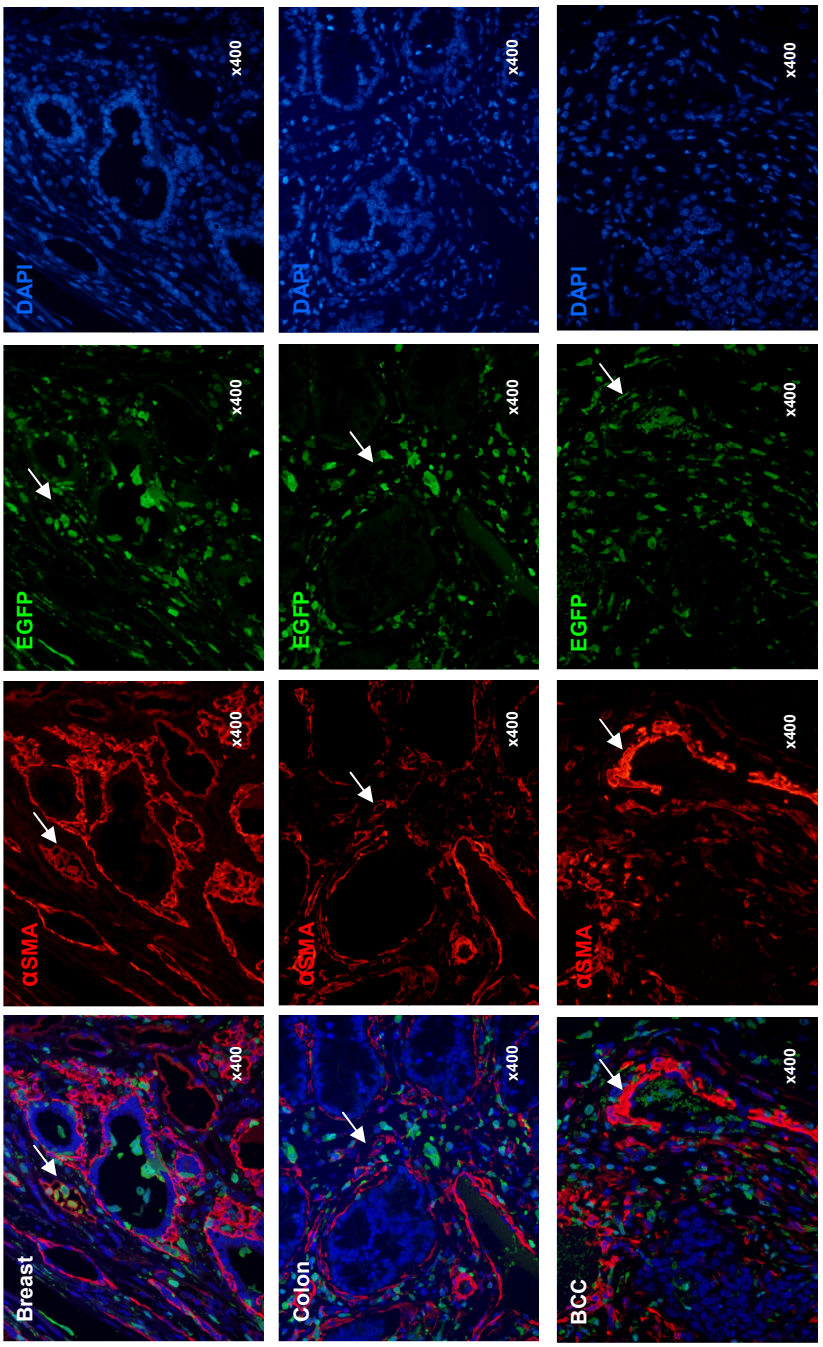

αSMA+ cells do not co-express EGFP in breast, colon and skin (BCC) lesions. White arrows identify αSMA+ EGFP- cells.

B

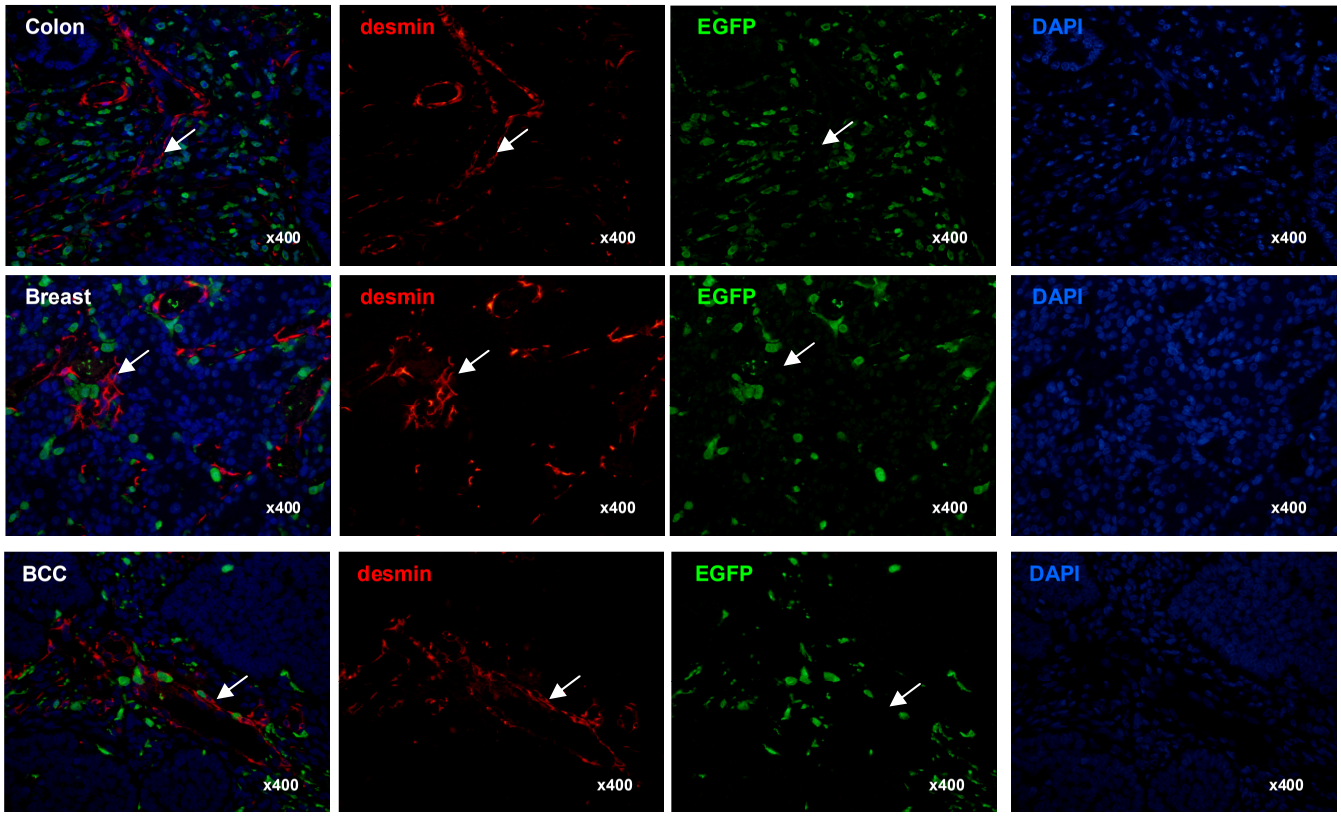

Desmin+ cells do not co-express EGFP in breast, colon and skin (BCC) lesions. White arrows identify Desmin+ EGFP- cells.

C

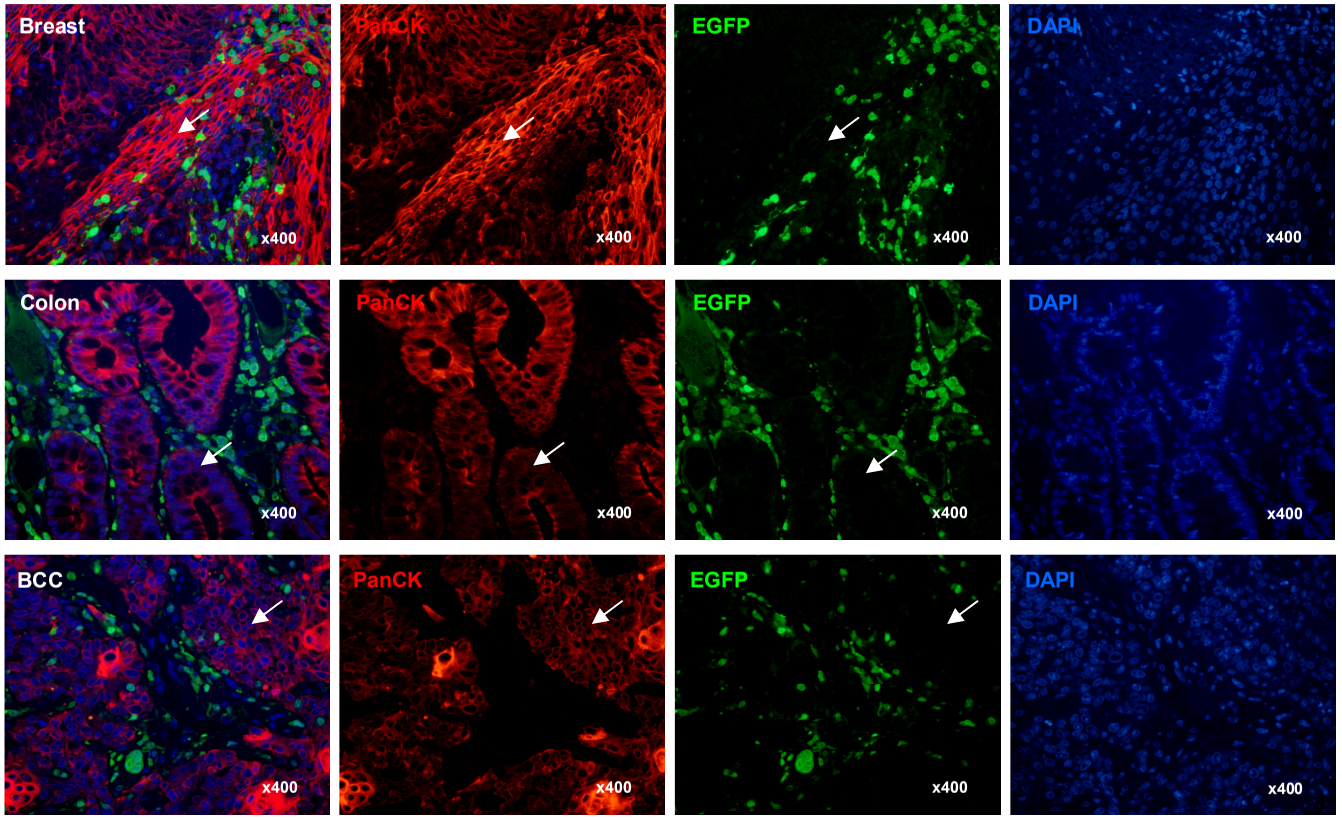

PanCK+ cells do not co-express EGFP in breast, colon and skin (BCC) lesions. White arrows identify PanCK+ EGFP- cells.

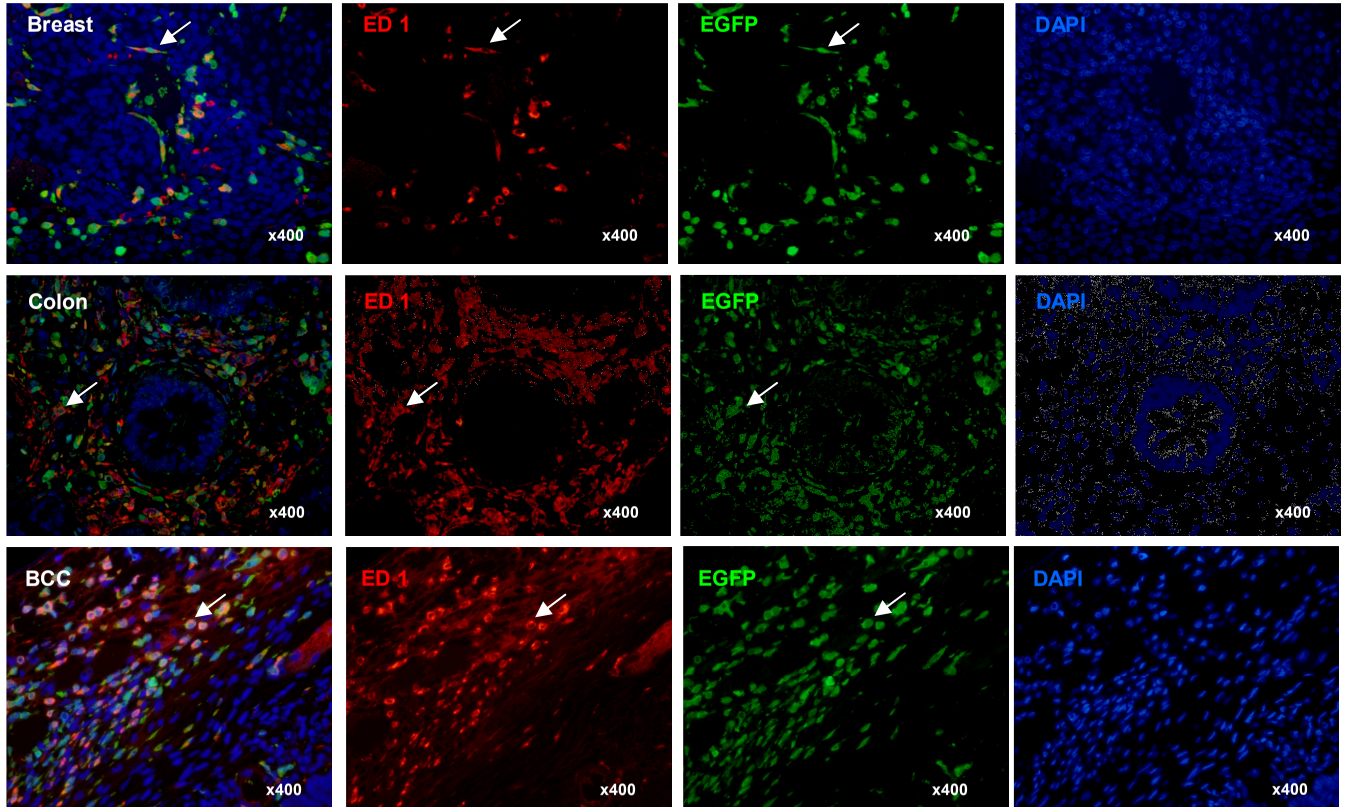

ED1+ cells display a mixed pattern of co-expression of EGFP. More ED1+ cells appear to be EGFP– in these tumours than compared to CCA lesions.

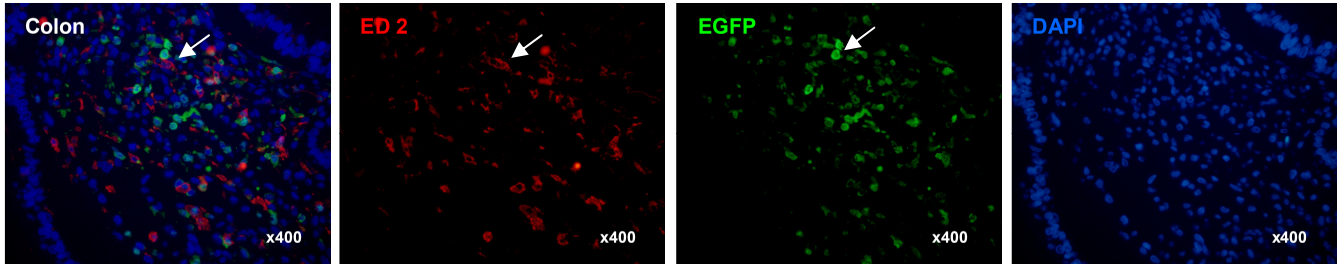

E

ED2+ cells do not express EGFP in malignant colon tissue (breast and skin not shown).

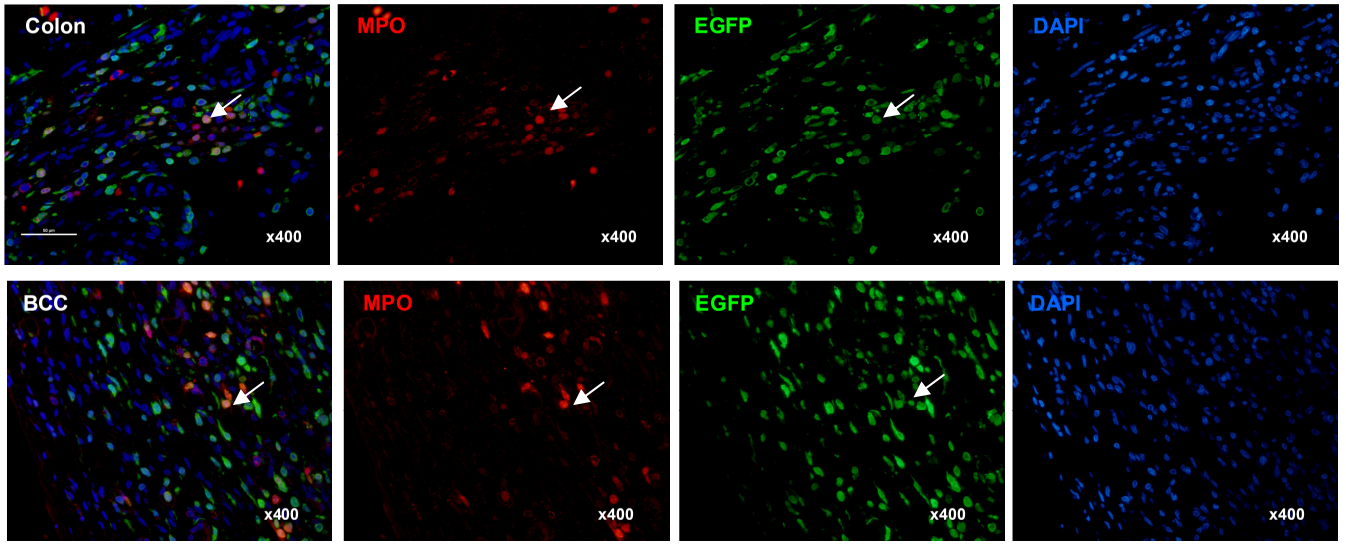

F

MPO+ cells display high co-expression of EGFP in colon and skin tumours (breast not shown).

Discussion

There are conflicting reports regarding the contribution of BM-derived stem cells to the cellular composition of distant organs and also the role played in tumour initiation and propagation. In health, a steady-state slow turnover of parenchymal and stromal cells occurs. Engrafted transdifferentiation into the epithelial compartment of distant organs by BM-derived haematopoietic stem cells occurs at very low levels under physiological conditions, if at all [526].

In chronic inflammation, studies that appear to demonstrate transdifferentiation of BM-derived stem cells into epithelial cells include examples of sex-mismatched BM transplants followed by hepatectomy (that drives hepatic regeneration) in 2-acetylaminofluorene treated rats (2-AAF blocks replication of hepatocytes). Results suggested that BM-derived cells had the capacity to transdifferentiate into hepatic progenitor cells [341]. Other examples include sub-acute organ injury such as radiation induced pneumonitis [527], where apparently whole alveoli appeared to be populated with epithelial cells derived from bone marrow. Limitations of these studies include the reliance on a single marker, the Y-chromosome, rather than addressing cell fusion events. To test this, Kubota *et al* [336] studied the choline-deficient ethionine-supplemented diet rat model of hepatic injury and regeneration. They identified that BM-derived cells may fuse with hepatic progenitor cells in rats but do not appear to contribute to hepatocellular carcinoma (HCC) preneoplastic lesions. Similarly, Ishikawa *et al* [342] employed a mouse model of HCC (diethylnitrosamine and phenobarbital administration) and did not identify BM contribution to HCC lesions (cells were tracked by x-gal staining and Y-FISH). Hepatocytes that appeared to be BM- derived most likely represented cell fusion events between donor bone marrow and recipient hepatocyte rather than transdifferentiaton events. This has been confirmed by murine studies of tissue-damaged, regenerating liver, where hepatic progenitors (oval cells) were not found to be BM-dervied [343, 344].

Contemporary experimental studies of the role of BM-derived cells in tumour biology have been extensively detailed in Chapter One – Introduction: Bone Marrow Derived

Stromal Components and Tumour Biology. There is evidence that BM-derived elements display migratory capacity towards tumours [317, 318] where the cells contribute functionally to the inflammatory stroma of lesions [228, 319]; these cells appear to promote cancer growth [207, 318, 321, 322] with few studies suggesting the converse [323, 324]. Studies by Quante *et al* [327] and Kidd *et al* [328], have suggested a proportional BM-contribution to mesenchymal elements (myofibroblasts) of tumour stroma in H felis gastric cancer models and subcutaneous synegeneic tumour bolus models. The BM-derivation of haematopoeitic elements (macrophages and endothelial cells) are less well studied but appear to comprise 10-35% of the endothelial elements of tumour associated vasculature in animal models [329, 330], 5% of tumour vasculature in human specimens [331] and 38% of TAMs in a murine model of retinoblastoma [332].

As discussed in Chapter One - Introduction, when considering the possible role of BM-derived cells and malignant tumour cells themselves, Houghton's provocative study of *H. felis*-induced gastric cancer suggests that BM derived cells may differentiate into tissue stem or mature cells to reconstitute the damaged tissue and contribute to carcinoma formation[333]. Entire epithelial gastrointestinal crypts were identified as being BM-derived, with a suggestion that these cells were mesenchymal in origin. Separately, their group also demonstrated the ability of aged BM-derived MSCs that were aged by culture *in vitro* to give rise to fibrosarcomas when administered *in vivo* [334]. As detailed in the Introduction, human studies have identified cancers with apparent small-volume BM cell contribution to the epithelial compartments of larynx and brain tumours [337 338]. Other murine studies similar to the *H. felis* gastic cancer model have suggested that BM-derived cells can contribute to tumours of small intestine, colon and lung [340] whereas this does not appear to be the case in squamous cell carcinomas of the skin [339].

In this study, we have not found evidence that epithelial compartments of tumours, or indeed, regenerating hepatic progenitor cells, are BM-derived. Cogle *et al* [340] suggest (from their findings in the APCmin mouse model of colon cancer of minimal BM-contribution to epithelial elements of tumours) that individual cells that appear to be donor-BM derived in the context of an overwhelmingly locally-derived tumour may

represent developmental mimicry on the part of circulating haematological stem cells whereby BM-derived cells may be recruited to malignant lesions by inflammatory cues and then transdifferentiate into malignant cells themselves. We suggest that the inherent variability and data interpretation required to identify such isolated cells renders it possible that these findings of small numbers of cells are potentially subject to a Type One error. Certainly these isolated cells do not appear to be functionally significant, unlike studies in the gastric cancer model where whole epithelial crypts were identified as being donor derived [333].

Another possible explanation for our findings that differ from published studies focusing on the intestine in the absence of radioprotection may include different radiosensitivity of target organs. The gastrointestinal tract is exquisitely radiosensitive, routinely sloughing and regenerating the epithelial lining following total body irradiation. It may be that these tissue stem cell niches are ablated and thus rendered experimentally available to occupation and repopulation by circulating stem cells. Conversely, the liver is a relatively radioresistant gastroenterological organ with low turnover of hepatocytes and biliary cells in the liver in healthy adult mice and rats [528, 529]. There are very few *in vivo* models of CCA, with the majority of models employing induced genetic abnormalities with rapidly forming lesions in the absence of tumour associated stromal elements [475], or by transplanting malignant cells in either the xenogeneic [530] or syngeneic context [477]. We elected to study chemically induced carcinogenesis in an outbred species of rodent with a model that generates tumours in a relatively indolent fashion. Furthermore, adult organs possess their own MSC in the tissues [531] and this may explain the failure of myofibroblasts to migrate from the BM in this model. It may be that a combination of these features of the TAA CCA model and the spontaneous breast, skin and colon tumours that makes this study more comparable to the human setting and hence more similar to the human studies that have shown either no or minimal BM involvement in the epithelial component of tumours.

In conclusion, in a rodent model of intrahepatic CCA that realistically recapitulates human lesions, there is evidence of overwhelming BM contribution to the

haematopoietic component of the tumour-associated inflammatory stroma. However, there is minimal or no contribution to the mesenchymal lineage of tumour associated stroma. Furthermore, we have found no evidence for bone-marrow derived contribution to the epithelial element of this tumour. There remains controversy as to the exact contribution and clinical significance of BM-derived cells to malignant lesions. What is clear, however, is that experimental parameters must be carefully controlled to minimise experimental error due to inappropriate or insufficiently sensitive cell tracking techniques.

CHAPTER SIX

NOTCH SIGNALLING AND CHOLANGIOCARCINOMA

Introduction

The Notch signalling pathway is an evolutionarily conserved local cell signalling mechanism that plays a fundamental role in regulation of both embryogenesis and adult tissue homeostasis[382]. The pathway is dysregulated in diverse haematological and solid organ tumours, demonstrating both oncogenic and tumour suppressor roles depending on the tumour types and the components of the Notch signalling system involved. These are covered in detail in Chapter One – Introduction: The Notch Signalling Pathway.

In the developing liver, Notch signalling is crucial for normal biliary system development, as clinically demonstrated by Alagille syndrome, an autosomal dominant mutation in the Notch ligand, Jagged1. The disorder is characterised by a failure of intrahepatic biliary duct formation and mild multisystem defects that include skeletal, cardiac, ocular and craniofacial abnormalities [411]. Adult tissue homeostasis is also regulated by Notch signalling (reviewed in [416] [417]). In the quiescent liver, Notch receptors are expressed exclusively on bile ducts whilst signalling components are transiently upregulated during oval cell regeneration of the liver following AAF and partial hepatectomy injury [418]. Furthermore, there is evidence that Notch signalling is implicated in biliary inflammation and CCA. Certainly, in the adult liver following chronic injury, myofibroblast-derived Notch ligand directs biliary specification of hepatic progenitor cells within the regenerative niche [347].

Dysregulated Notch signalling has been identified in CCA. Notch1 appears to be upregulated in CCA, and has a role in conferring resistance to apoptosis; this appears to be via iNOS-mediated processes that upregulate Notch1 signalling [79]. Non-canonical Notch signalling mechanisms that theoretically may be active in the tumour:stroma relationship include iNOS signalling mechanisms, as NO production is a recognised feature of activated macrophages [444]. Additionally, IGF-1 is a candidate signal for Notch activation via AAH activation in CCA [446, 447] and IGF-1 is produced by tumour associated myofibroblasts [202, 448]. AAH is overexpressed in CCA

and directly upregulates Notch signalling. This in turn increases CCA invasiveness and cell survival [446, 449, 450]. In CCA, reports have identified receptor elements of the Notch pathway as being over expressed [79]. However, the anatomical distribution of pathway components and therapeutic implications are not yet clear.

We hypothesised that the canonical signalling elements of the Notch pathway may drive CCA carcinogenesis, compartmentalise across the epithelial and stromal compartments of lesions and serve to enhance tumour progression. Furthermore, it was hypothesised that manipulating this pathway may enhance chemosensitivity. Data are presented demonstrating that, in CCA, Notch signalling promotes tumour growth and, in *in vivo* models, is upregulated in a sequential fashion during cholangiocarcinogenesis. Within the tumour microenvironment, Notch ligands are expressed by the biliary epithelia which in principle may be responsive to signalling from the tumour stroma. Inhibition of the Notch pathway reduces proliferation and appears to enhance chemosensitivity *in vitro*.

Notch Pathway components are upregulated in human CCA lesions

Although there is limited information regarding canonical Notch ligand expression, Notch1 receptor has been found to be upregulated in human CCA [79, 532]. Accordingly, a series of human CCA lesions was collated to study the expression patterns of the main elements of the Notch signalling pathway using qPCR array. Human CCA lesions were obtained from resection specimens of patients undergoing hepatectomy for CCA with curative intent. These patients had not received prior neoadjuvant chemotherapy or radiotherapy. qPCR Notch pathway array (commercially obtained) was undertaken on five human CCA lesions with matched control liver from elsewhere in the resection specimen. Compared to normal liver, upregulation of Notch pathway elements were noted in CCA lesions. Namely, Notch-2 and Notch-3 receptors together with the canonical ligands Jagged-1 and Jagged-2 and downstream targets HeyL and Hey1 but not Delta-like ligands were upregulated in human CCA. (**Figure 6.1**).

Ideally, this observation would have been confirmed with individual qPCR for each gene on the individual tissues. Unfortunately, I designed in-house primers for the Notch pathway rather than obtaining commercially available primers (Qiagen) and consequently did not perform this assay due to time limitations.

Figure 6.1: Notch pathway signalling is active in human CCA

Clustergram and volcano plot: Upregulation (>4-fold) of Notch3 receptor, Jagged1 and Jagged2 ligands occurs in malignant CCA lesions (n=5) compared to control tissue (n=6) (qPCR array). Downstream elements HeyL and Hey1 are also upregulated as illustrated by the data points highlighted in red.

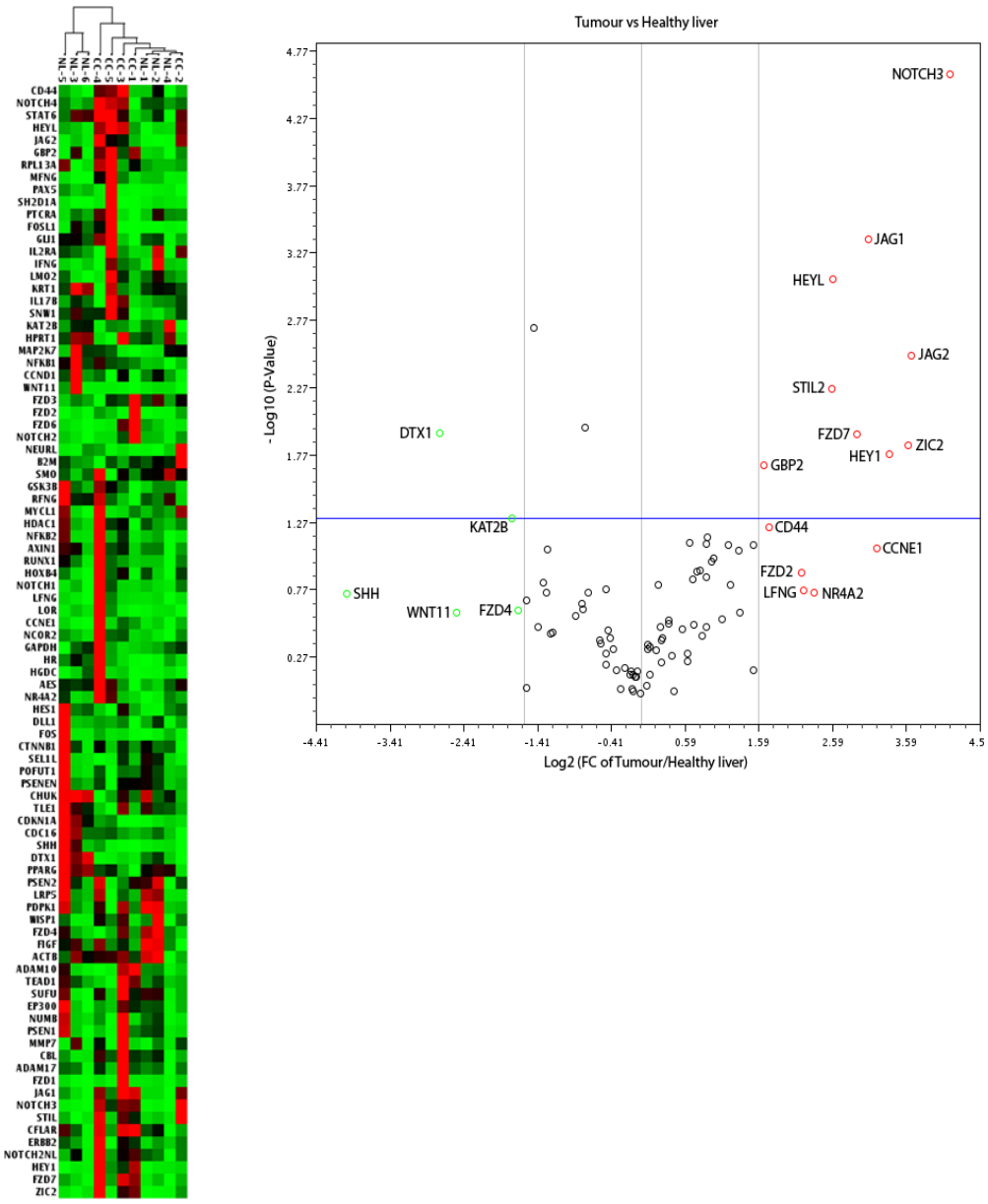

I obtained the tissue specimens, purchased the array, performed the first three tumours and three controls and Dr Luke Boulter performed the subsequent two tumours and three controls and produced the images above.

Notch Pathway components are upregulated in cholangiocarcinogenesis and in CCA lesions

To study the timecourse of Notch pathway signalling, the TAA rat model of CCA was used to analyse Notch pathway components in the premalignant environment of the liver during cholangiocarcinogenesis. Animals treated with 0.06% TAA were grouped according to the duration of TAA exposure and the histological appearances of the tissue. Pooled mRNA was analysed with a commercially acquired qPCR rat Notch pathway array.

Animal tissue was pooled and described as follows:
Control: Described as t=0 weeks (n=6 age-matched animals that did not receive TAA)
Inflamed Liver: t=12 weeks, comprising 10 and 14 weeks TAA, (n=3 at each timepoint), total n=6
Fibrotic Liver: t=17 weeks, comprising 16 and 18 weeks TAA, (n=3 at each timepoint), total n=6
Early Malignancy: t=21 weeks, comprising 20 and 22 weeks TAA, (n=3 at each timepoint), total n=6
Late/Established Malignancy: t=25 weeks, comprising 24 and 26 weeks TAA, (n=3 at each timepoint), total n=6

An increase in Notch signalling components was noted after 17 weeks of TAA treatment compared to controls, with particular upregulation identified in established lesions (week 25). Of note in the qPCR array, Notch3 receptor, Jagged1 and Jagged2 ligands and downstream components HeyL were upregulated more than four-fold by 25 weeks. (**Figure 6.2**).

Figure 6.2: Notch pathway elements are progressively upregulated in the TAA rat model of cholangiocarcinogenesis

A

qPCR array of pooled mRNA from rats treated with 0.06% TAA. Upregulation of Notch signalling components is pronounced following the formation of established malignant lesions. In particular, Jagged1, HeyL, Jagged2 and Notch3 (marked as *) represent the most upregulated components, with Notch1, Notch2, Notch4 and Hey1 (#) not demonstrating upregulation. Data shown as fold-change relative to untreated controls.

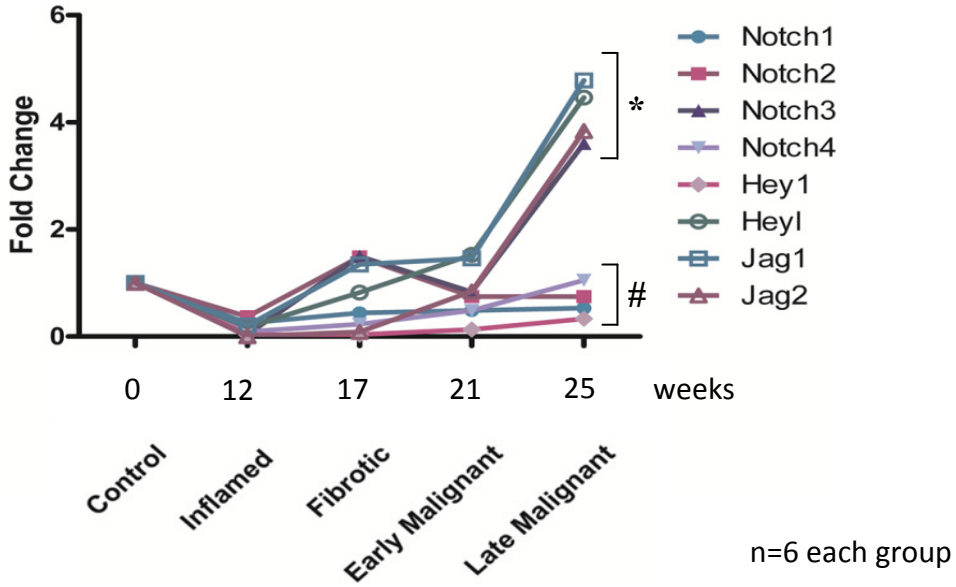

Tissue was generated and grouped into histological sets by myself, then Dr Luke Boulter (LB) and I discussed timepoints. LB carried out the qPCR array, data analysis and generated the above figure and the figure overleaf.

B

qPCR array comparison of malignant liver (25 weeks TAA) versus control liver tissue. Scatterplot data points in red identify at least four-fold upregulation whereas green data points denote at least four-fold downregulation compared to control tissue.

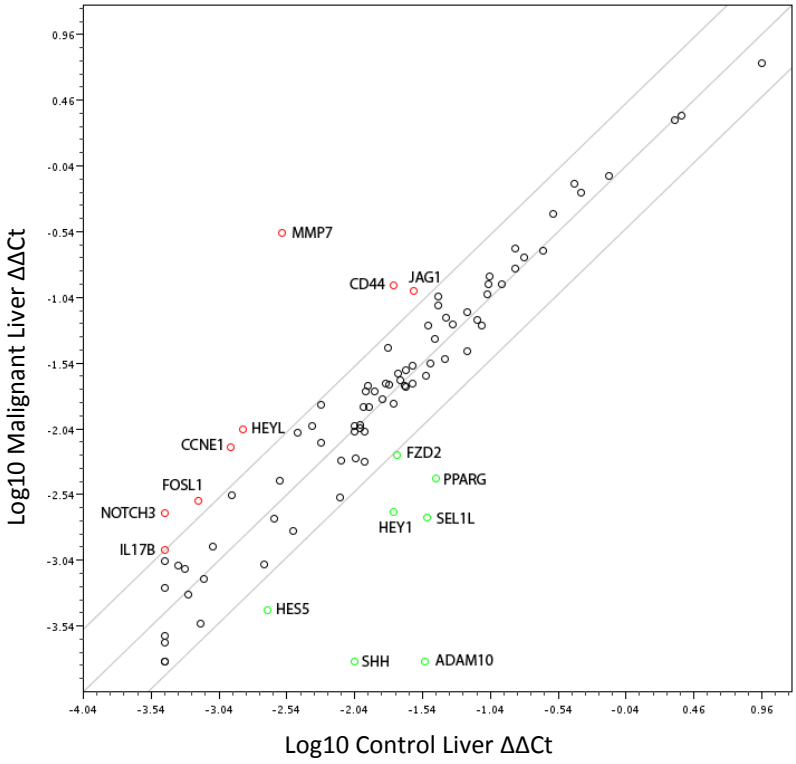

Notch Pathway elements are distributed at a protein level in the CCA lesions

To identify the anatomical distribution of Notch signalling components in CCA lesions, antibodies were purchased from Santa Cruz. These proved to be labour and resource intensive to optimise. A wide range of tissue fixations (frozen section, formalin- and methacarn-fixed paraffin-mounted) were trialled. Protocol variations were undertaken, including antigen retrieval strategies (heat treatment with sodium citrate and enzymatic digestion with proteinase K or trypsin) and different antibody incubation durations (from one hour up to 72 hours). Signal amplification and stabilisation was performed with antibody agents such as Tyramide Signal Amplification (Perkin Elmer) and Alexa Fluor® 555 streptavidin (Molecular Probes). Mouse embryo tissue was used as positive control, since the Notch pathway is highly expressed during development.

Using immunofluorescence it was identified that Notch1 was expressed on malignant biliary epithelial cells whilst Jagged 1 was expressed in the stroma of human CCA lesons. Specifically, myofibroblasts (αSMA+ve) in the stroma expressed jagged1 ligand (**Figure 6.3 A** and **B**).

Optimisation of DAB immunohistochemistry for human CCA lesions was unsuccessful. However, using human liver, Notch1 Notch2 and Notch3 receptors were found to be expressed weakly by blood vessels, whilst Notch2, Notch 3, Notch4 receptors and delta-like1 ligand were expressed by bile ducts. **Figure 6.3 C**.

As an illustration of the optimisation process, Notch 1, Notch2 and Jagged2 protein distribution was studied in rat tissue (premalignant inflamed liver and CCA lesions) using rat embryo as positive control tissue (**Figure 6.3 D**, **E**, **F**). Apparent Notch1 staining was identified in venules, stroma surrounding bile ducts and also larger order bile ducts themselves (Figure 6.3 D). Apparent Notch2 staining was noted of venules, stroma surrounding proliferating bile ducts, larger order bile ducts and vessels and also malignant bile ducts in tumours. Jagged2 staining was unsuccessful

with no staining noted, even in positive control tissue, most likely representing protocol optimisation failure. These findings suggested that Notch1 and 2 are expressed in non-biliary elements of tumour stroma which conflicts with the finding that Notch1 is expressed only in bile ducts whilst staining with immunfluourescence (Figure 6.3 A). The technical hurdles encountered with DAB protocols suggest that the immunfluorescence results represent more cogent data.

Of note, the qPCR array of human lesions identified upregulation of Notch2 and Notch3 (in particular) together with Jagged2 which is in keeping with the immunofluorescence findings. So, it would appear that although the immunohistochemistry has not indicated upregulation of Notch1 or Jagged1 in CCA lesions, this is perhaps not surprising in the context of the findings of the qPCR array.

Figure 6.3: Notch pathway component expression patterns in human and rat liver tissue

A

Notch1 receptor is expressed on malignant bile ducts whilst Jagged1 ligand is expressed within the stroma of CCA lesions (human tissue).

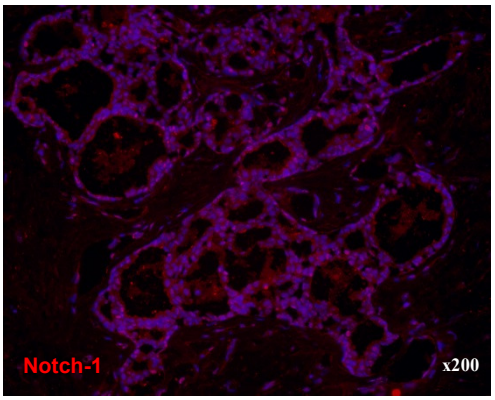

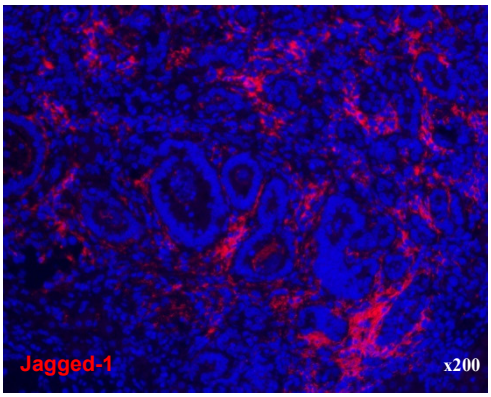

B

Dual immunofluorescence identifies expression of Jagged1 ligand by myofibroblasts (αSMA) in tumour stroma (human tissue).

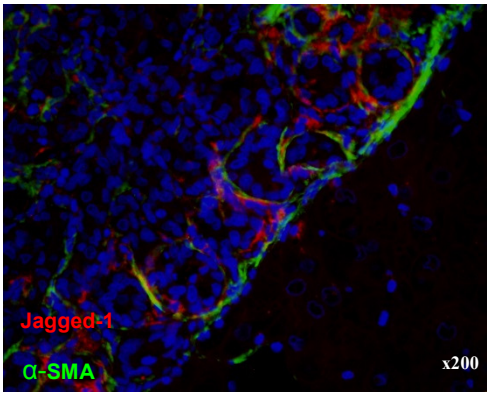

The above immunohistochemical stains were performed by Dr Luke Boulter on tissue that I generated.

C

Notch receptor and delta-like 1 ligand expression profiles were studied in human liver using the original purchased antibodies (Santa Cruz Biotechnology, USA). A variable expression pattern was noted.

Notch 1

Weak vessel staining

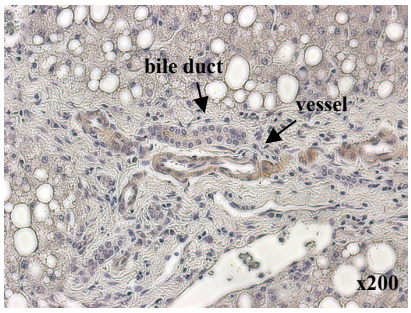

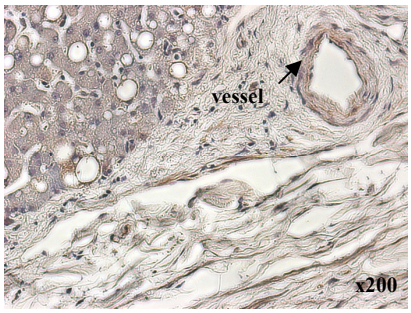

Notch 2

Strong Ducts and vessel staining

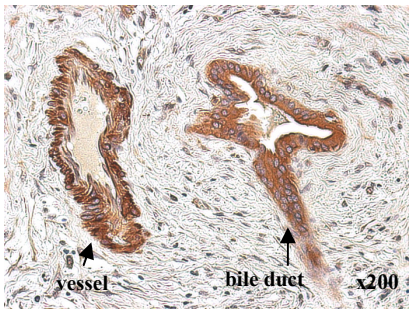

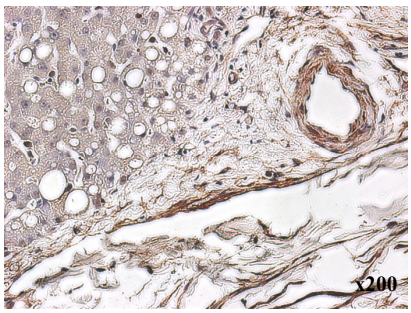

Notch 3

Weak Ducts and vessels staining

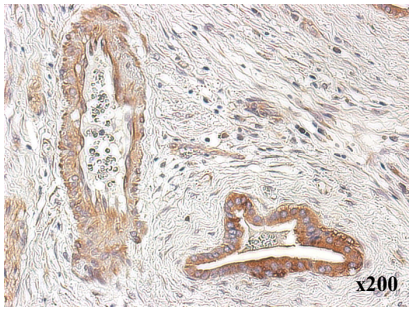

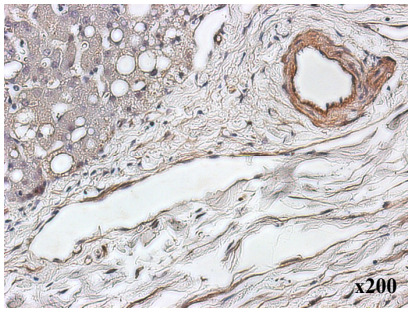

Notch 4

Ducts but not vessels staining

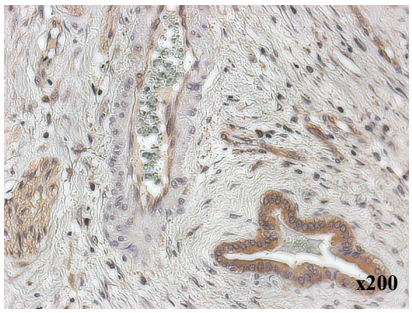

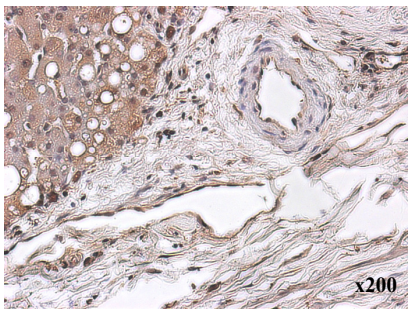

Delta-like 1

Weak ducts but not vessels staining

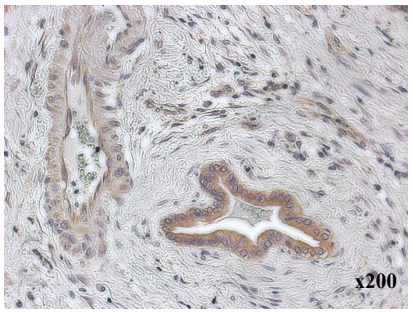

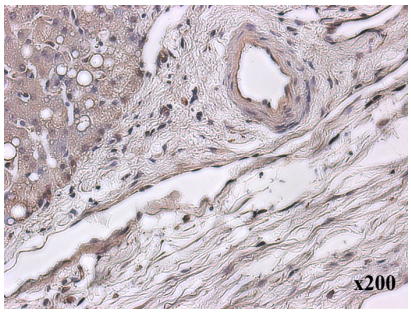

D

Notch1 expression was studied in rat liver using mouse embryo tissue as positive control material using the original purchased antibodies (Santa Cruz Biotechnology, USA). Inconclusive and variable results were obtained, with apparent Notch1 staining of venules and stroma surrounding bile ducts.

Embryo

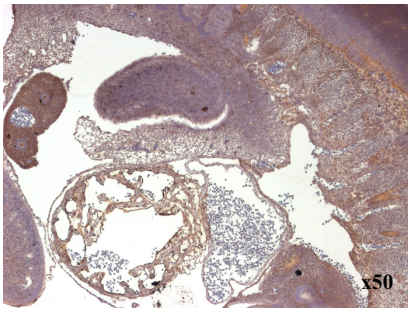

Embryo

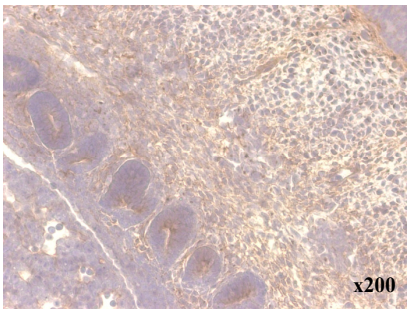

Portal Triad

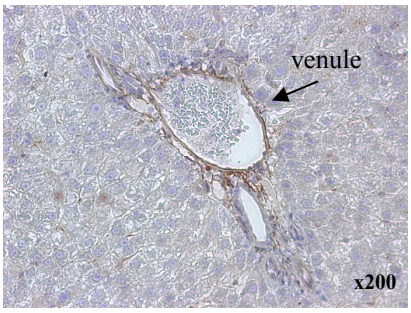

Ductular expansion

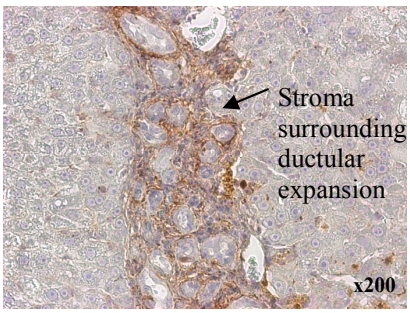

Tumour

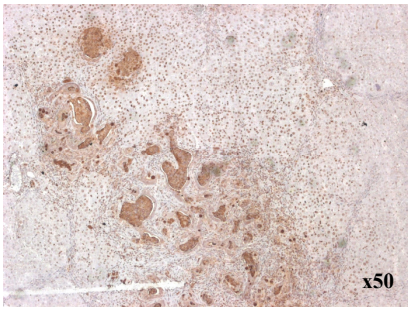

Tumour

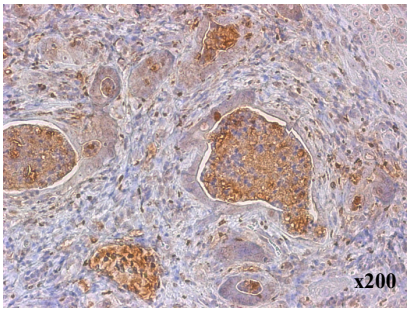

Negative control

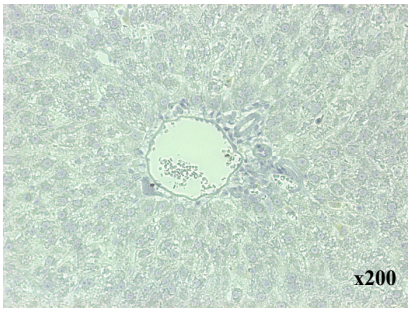

Negative control

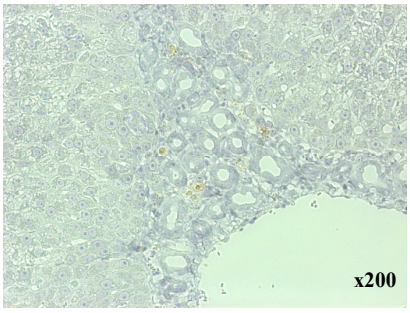

E

Similarly, Notch2 expression was studied using mouse embryo tissue as positive control material. Again, inconclusive and variable results were obtained, with apparent Notch2 staining of venules, stroma surrounding proliferating bile ducts, larger vessels and also malignant bile ducts in tumours.

Embryo

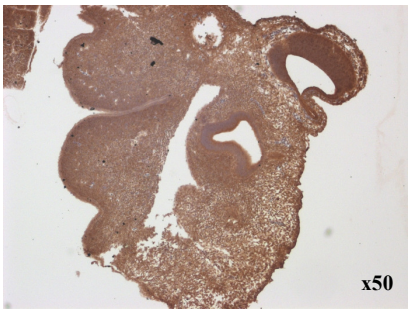

Embryo

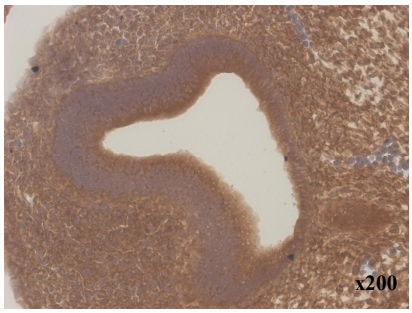

Portal Triad

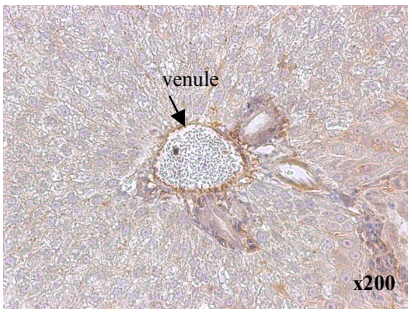

Ductular expansion

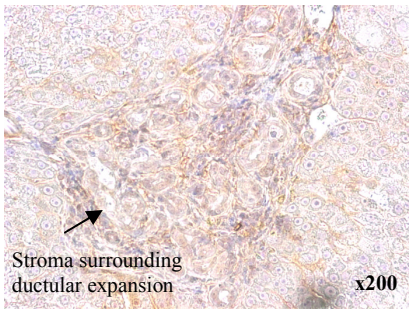

Tumour

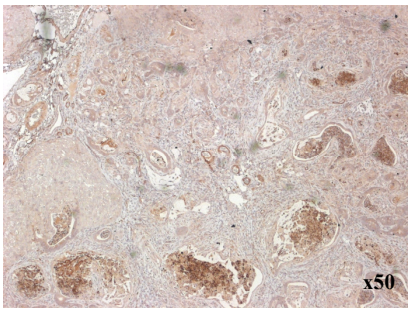

Tumour

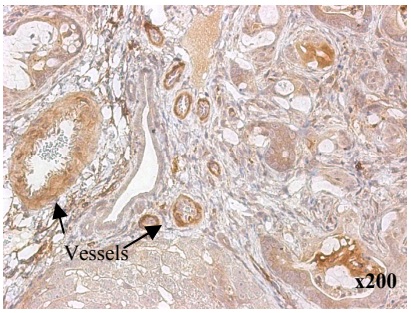

Negative control

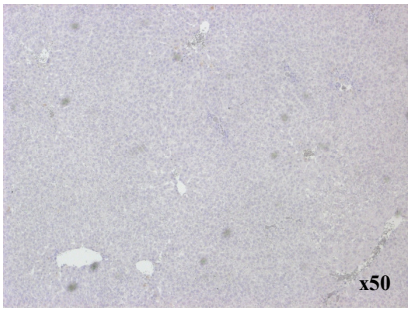

Tumour

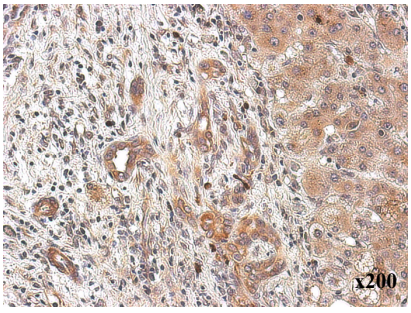

F

Jagged2 expression was studied using mouse embryo tissue as positive control material. It did not prove possible to reliably stain embryonic or adult tissue with this antibody and no positive staining was identified.

Embryo

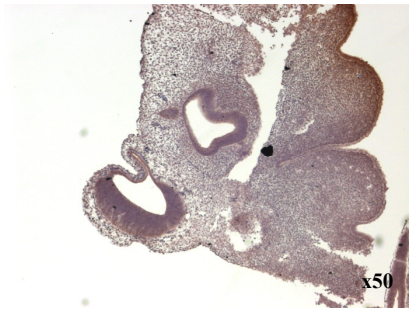

Embryo

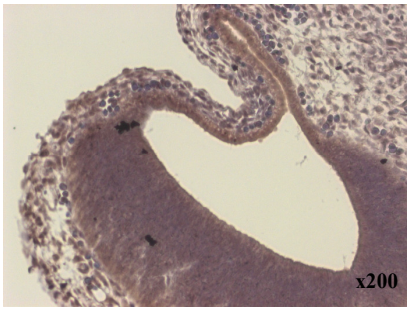

Portal Triad

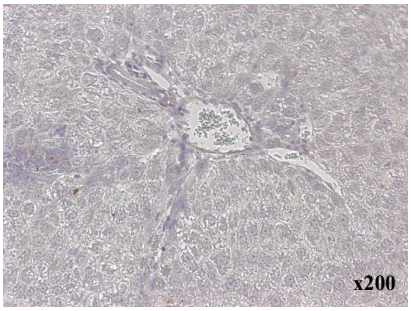

Ductular expansion

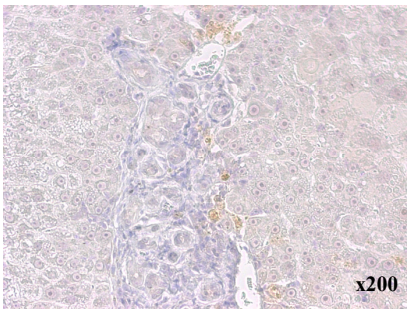

Tumour

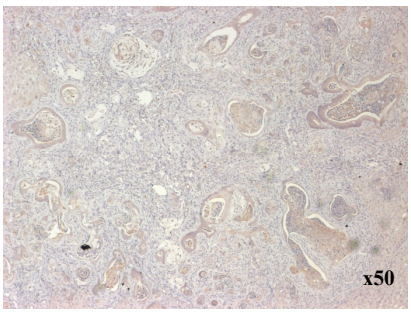

Tumour

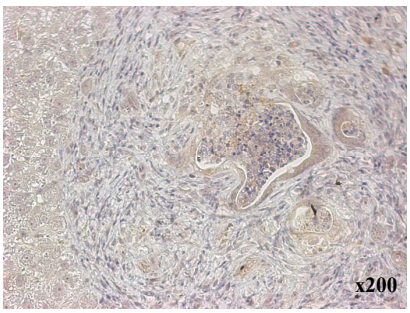

Negative control

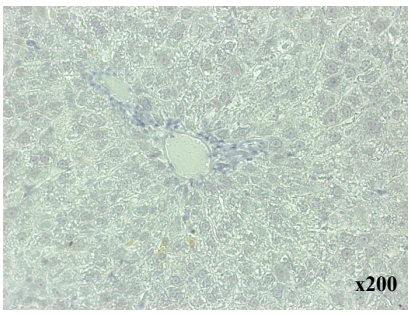

Tumour

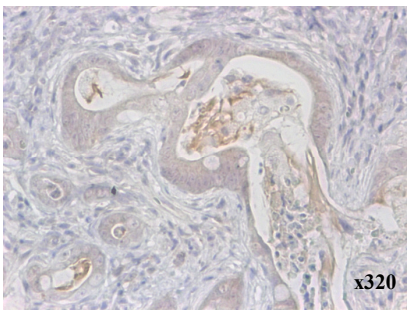

The Notch pathway in CCA is functionally active *in vitro* and inhibition of the pathway inhibits CCA cell line growth

The biological activity of the canonical Notch signalling pathway was measured in CCA cell lines using a luciferase reporter assay kindly provided by Dr Sally Lowell. Briefly, the technique comprises a 12CSL reporter complex that is transiently transfected into cells of interest. This comprises 12 copies of the CSL-binding site for NICD as a synthetic promotor upstream from a firefly luciferase sequence. Upon Notch pathway activation, binding of NICD to CSL target sites in the nucleus promotes expression of firefly luciferase which then acts on exogenously administered luciferin substrate to generate a quantifiable fluorescent output. Co-transfection of a constitutively-expressing SV40-renilla luciferase reporter construct enables normalisation relative to cell population by calculating firefly:renilla luciferase expression ratios. As a control for transfection efficiency, transfection with a constitutively expressing GFP construct is undertaken whereby GFP may be visualised under a fluorescent microscope. Positive control of 12CSL responsivity to Notch signalling is tested by co-transfection of NICD construct which over-expresses NICD intracellularly, thus driving 12CSL reporter and upregulating luciferase expression.

In order to generate sufficient reporter construct material for experiments, the plasmid constructs were first expanded in bacteria (DH5α-competent cells, Invitrogen Inc) and repurified. The putative NICD construct was then sequenced to confirm correlation with the known NICD sequence in the literature. Optimisation of transfection was undertaken and this was found to be efficient with lipofectamine. Activity of the 12CSL luciferase reporter was then assayed in response to co-transfection with NICD contstruct, confirming 12CSL responsivity to Notch signalling in CCA cell lines. See the methods chapter for details on how this was undertaken.

The role of Notch signalling and subsequent pathway inhibition on the behaviour of CCA was tested *in vitro*. Cell lines were transiently transfected with 12CSL notch

pathway reporter and SV40-renilla constructs. CCA cell lines were treated for 48 hours *in vitro* with the γ-secretase inhibitor, N-[N-(3,5-Difluorophenacetryl)-L-alanyl]-S-phenylglycine t-butyl ester (DAPT). This inhibits the Notch signalling pathway by preventing cleavage of the Notch intracellular domain (NICD) and thus preventing downstream signalling of the pathway following receptor-ligand binding. As a result of DAPT administration, the Notch pathway was downregulated in CCA cell lines together with a concomitant dose-dependent decrease in cell proliferation as measured by MTT assay. (**Figure 6.4**). Maximal inhibition of the Notch pathway appeared to be reached by 5μM DAPT whereas maximal inhibition of proliferation (MTT) was achieved with higher doses of DAPT. This augmented effect above 5μM was presumably due to *in vitro* cell toxicity rather than Notch pathway inhibition *per se*.

Figure 6.4: Notch signalling pathway is responsive to inhibition *in vitro*

A

DAPT downregulates the Notch signalling pathway in CCA cell lines (S1079 and S1196) after 48 hours of treatment (12CSL luciferase assay). ($P<0.05$ for 5μM and 50 μM DAPT compared to vehicle control, ANOVA).

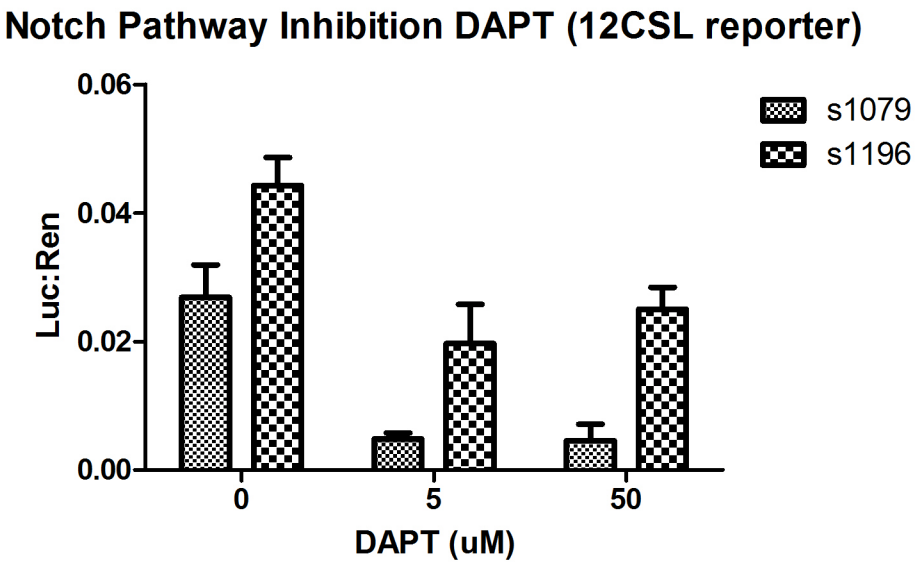

B

Proliferation of CCA cell lines (S1079 and S1196) is inhibited after 48 hours of treatment with DAPT compared to vehicle control (MTT assay). Data are described relative to CCA cell lines (S1079 and S1196) cultured with vehicle.

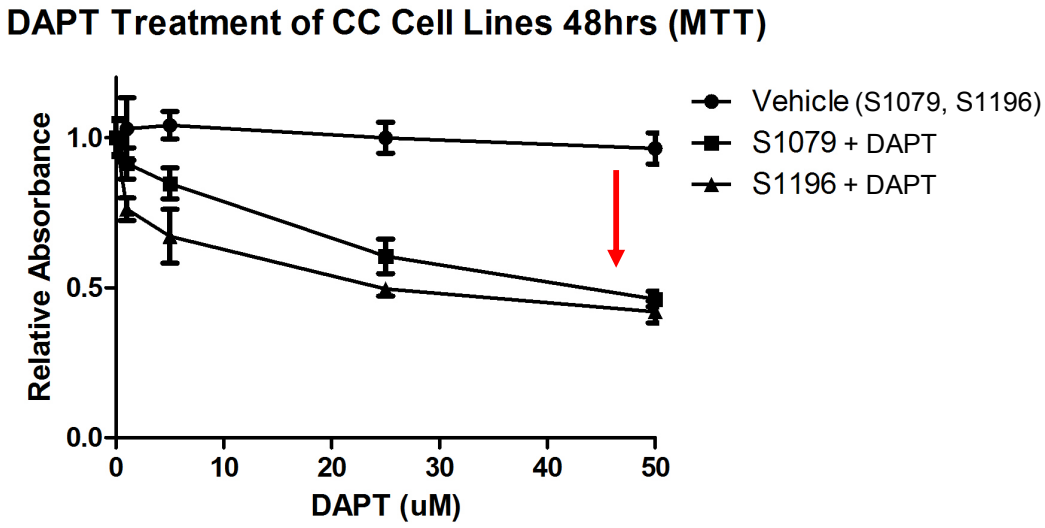

Inhibition of the Notch pathway appears to augment chemosensitivity *in vitro*

Cisplatin and 5-FU were chosen as chemotherapeutic drugs because of the BILCAP and ABC-02 trials. 5-FU was chosen as the BILCAP trial, currently recruiting in the UK, is a randomised clinical trial evaluating adjuvant capecitabine chemotherapy (oral 5-FU) compared to expectant treatment alone following surgery for biliary tract cancer. Cisplatin was selected because the ABC-02 trial of cisplatin with gemcitabine was shown to provide a survival advantage of 3.6 months over gemcitabine alone for patients with locally advanced or metastatic biliary tract cancer (11.7 v 8.1 months) [132].

CCA cell lines were treated with 5-FU, cisplatin and the γ-secretase inhibitor DAPT as individual therapeutic drugs and in combination for up to 48hours. Combining low dose DAPT with low dose chemotherapy significantly augmented CCA chemosensitivity (MTT assay) ($p<0.05$). (**Figure 6.5**). In light of the observed marked effect, it would have been preferable to include analysis of the effect of 5μM DAPT when not combined with chemotherapy in this experimental series. However, this was not included in the experimental design and would be of interest to undertake for future work.

Figure 6.5: Notch signalling pathway inhibition appears to augment chemotherapeutic effect on CCA cell line proliferation *in vitro*

S1196 (**A**) and S1079 (**B**) cell lines were studied. Combination of low dose DAPT (5μM) with low dose chemotherapeutic drugs (20μM 5-FU and 10μM cisplatin) inhibited cell proliferation by at least as much as high dose chemotherapy (320μM 5-FU and 80μM cisplatin) after 48 hours of treatment (MTT assay). (ANOVA with post-hoc Bonferroni).

A

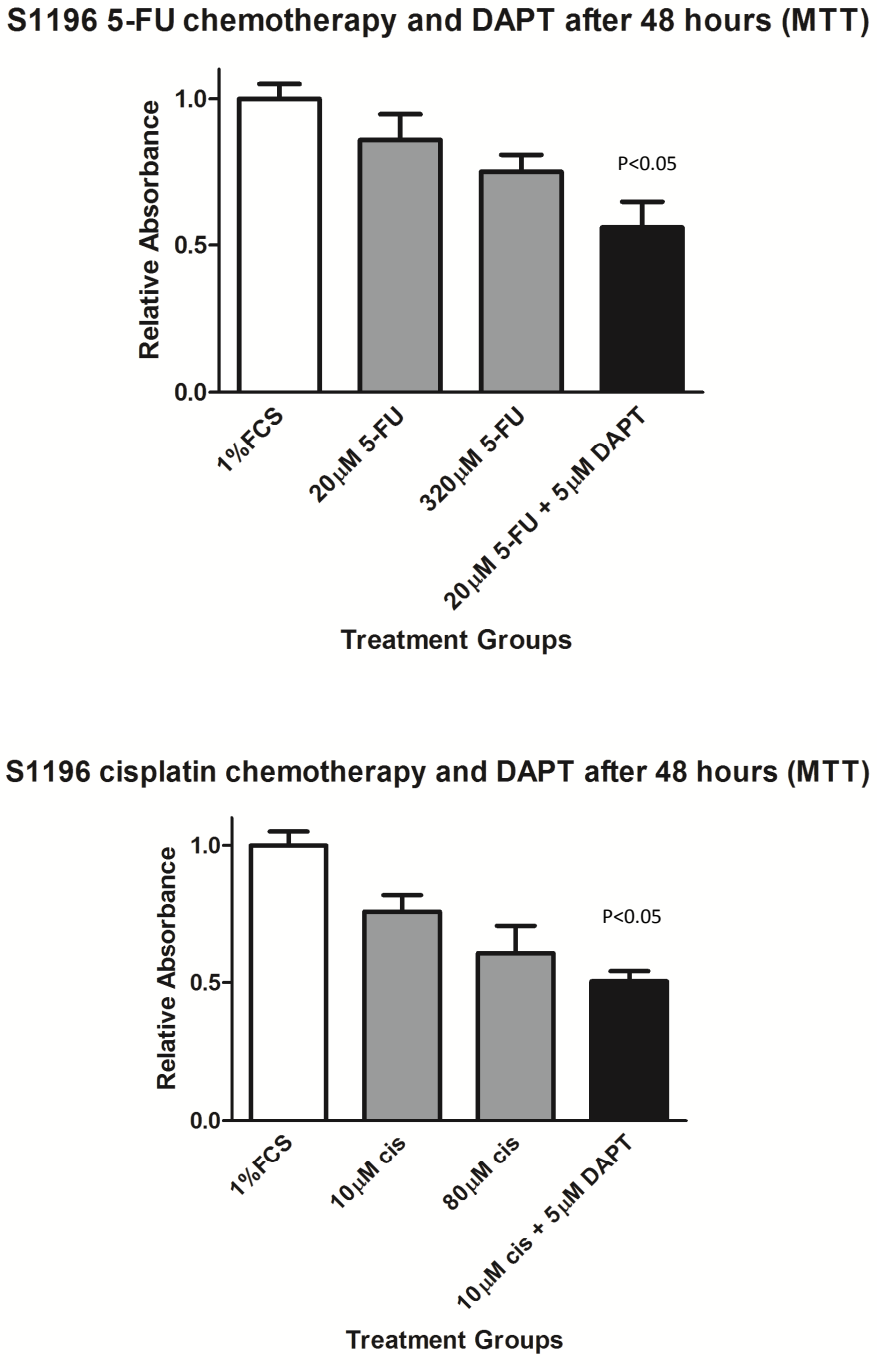

B

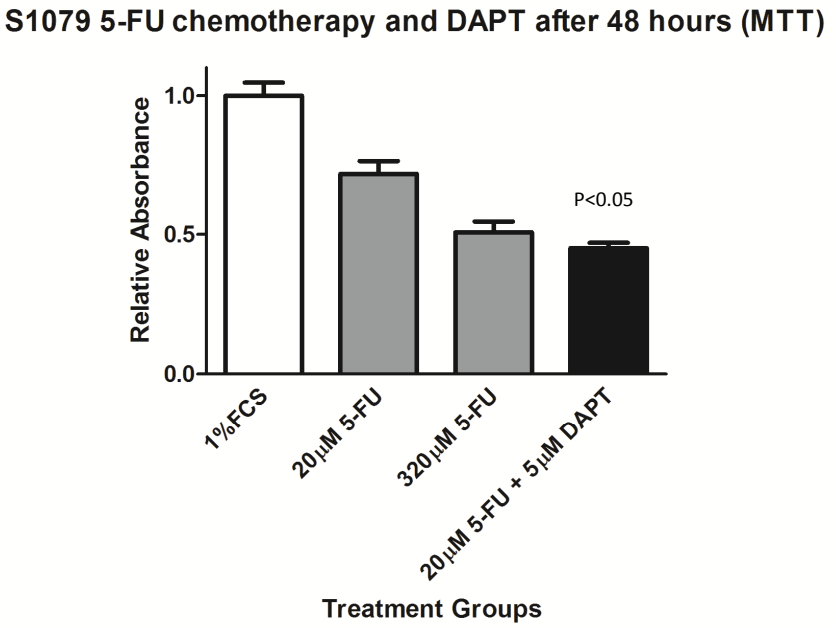
S1079 5-FU chemotherapy and DAPT after 48 hours (MTT)
Relative Absorbance
1.0
0.5
0.0
P<0.05
1%FCS
20μM 5-FU
320μM 5-FU
20μM 5-FU + 5μM DAPT
Treatment Groups

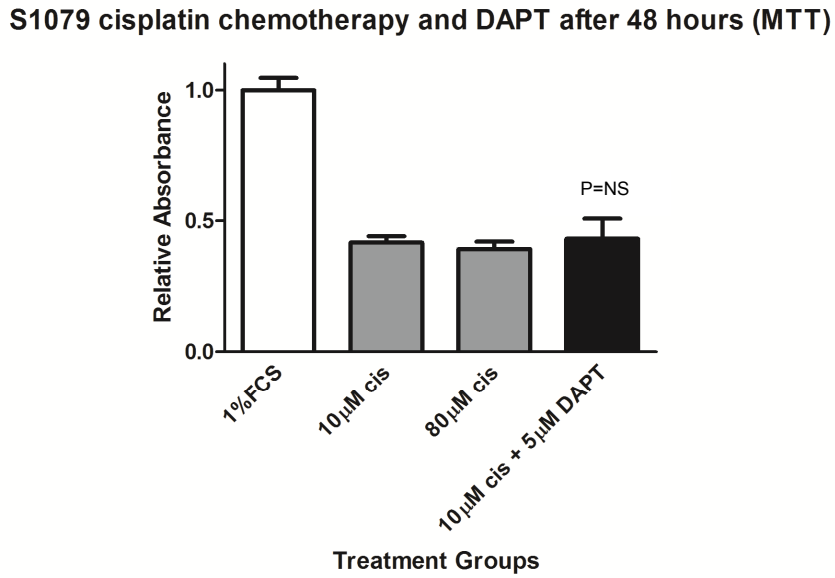
S1079 cisplatin chemotherapy and DAPT after 48 hours (MTT)
Relative Absorbance
1.0
0.5
0.0
P=NS
1%FCS
10μM cis
80μM cis
10μM cis + 5μM DAPT
Treatment Groups

Co-culture of myofibroblasts and CCA cell lines *in vitro* does not appear to alter Notch signalling in CCA cells

To investigate the role of Notch signalling between stromal cells and malignant biliary epithelial cells, CCA cell lines were transiently transfected with the 12CSL reporter construct and co-cultured with human myofibroblasts derived from a range of sources – LX2 activated stellate cell line, fresh cultured hepatic stellate cells and fresh cultured tumour associated myofibroblasts from human CCA lesions. ($4x10^4$ CCA cells with $5x10^3$ myofibroblast cells per well in a 24 well plate). Notch pathway activation was measured in CCA cell lines following 48 hours of co-culture. No significant differences were noted compared to monoculture of CCA cell lines alone (p=NS, ANOVA). (**Figure 6.6**).

The range of myofibroblasts was specifically chosen and cultured in order to address the role of non-tumour associated and tumour associated stromal cells, as there may be a difference noted between the cell populations. It is possible that the negative findings here may reflect the limitations of two dimensional co-culture as compared to three dimensional relationships *in vivo*, that reduces the actual cell:cell contact interface and hence measurable cell:cell signalling. Furthermore, rapid *in vitro* cell cycling or autostimulation of the CCA cell lines themselves may have masked fine changes in Notch pathway regulation *in vitro*.

Figure 6.6: **Notch signalling pathway does not appear to be upregulated by *in vitro* co-culture with myofibroblasts**

A: LP and s1196 CCA cell lines were transiently transfected with the 12CSL reporter and then co-cultured for 48 hours with LX2 hepatic stellate cell line, cultured fresh human hepatic stellate cells (hSC) and myofibroblasts cultured from two human CCA lesions (CCA-1 and CCA-2). No significant differences in Notch pathway activation expression were identified compared to mono-culture of the CCA cell lines (ANOVA).
B: Representative photomicrograph of s1196 cell line in co-culture with myofibroblasts.

A

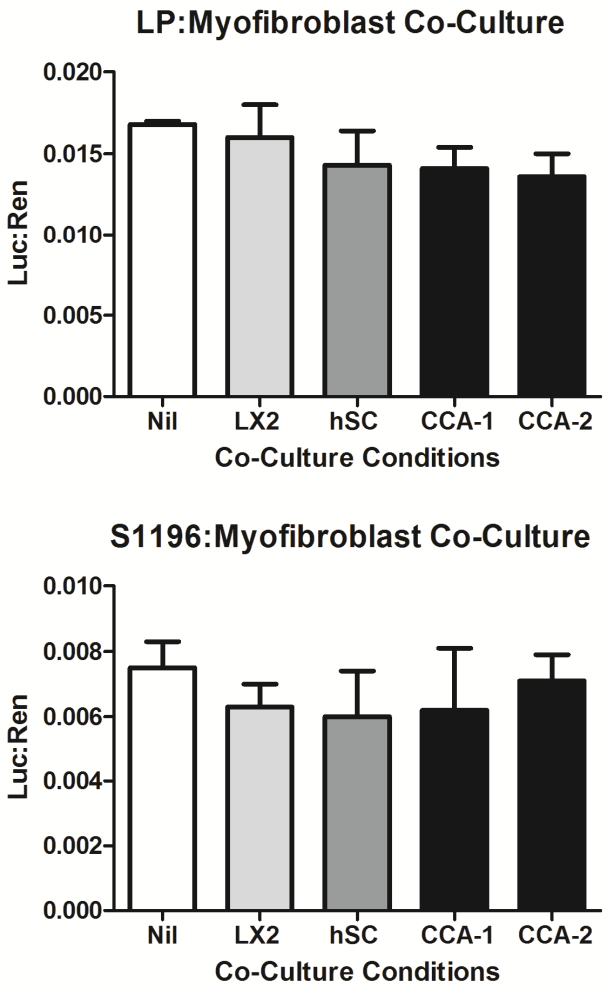

B

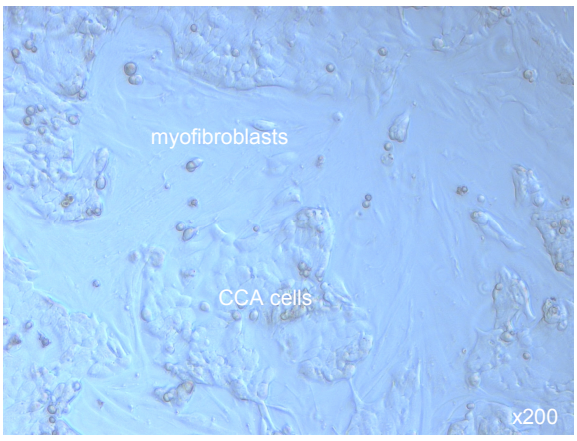

Co-culture of M1 and M2 polarised macrophages with CCA cell lines in vitro does not appear to have an effect

In a similar fashion, CCA cell lines transiently transfected with the 12CSL Notch reporter were co-cultured with either M1 or M2 polarised human macrophages for 48 hours. Polarisation was performed using GM-CSF and M-CSF. LP and s1196 cell lines were co-cultured with macrophages derived from two donors ($4x10^4$ CCA cells with $4x10^5$ macrophage cells per well in a 24 well plate). Statistical analysis was undertaken using one way ANOVA with post-hoc Bonferroni testing. (**Figure 6.7**).

In the case of both cell lines, ANOVA identified significant differences between treatment groups ($p<0.05$ in both cases). However, post-hoc testing demonstrated that this was explained by significant differences between mono-culture and M1 MΦa in the case of LP co-culture ($p<0.05$, 95% CI 0.012-0.096) and between mono-culture and M2 MΦa in the case of S1196 co-culture ($p<0.05$, 95% CI 0.006-0.053). These findings did not appear to have clinical significance and did not reproduce across the two cell lines in co-culture with macrophages and were therefore disregarded for interpretation of data. Specifically, there were no statistical differences in Notch pathway activation in the cell lines as a result of the M1 or M2 co-culture conditions.

In this case, I was unable to identify an effect of co-culture on Notch pathway signalling in tumour cells.

Figure 6.7: Notch signalling pathway does not appear to be differentially upregulated in vitro co-culture with M1 or M2 macrophages (MΦ)

LP (**A**) and s1196 (**B**) CCA cell lines were transiently transfected with the 12CSL reporter and co-cultured for 48 hours with either M1 or M2 polarised macrophages from two different donors (MΦa and MΦb). No significant differences in Notch pathway activation expression were identified between M1 and M2 polarising culture conditions (ANOVA with post-hoc Bonferroni testing).

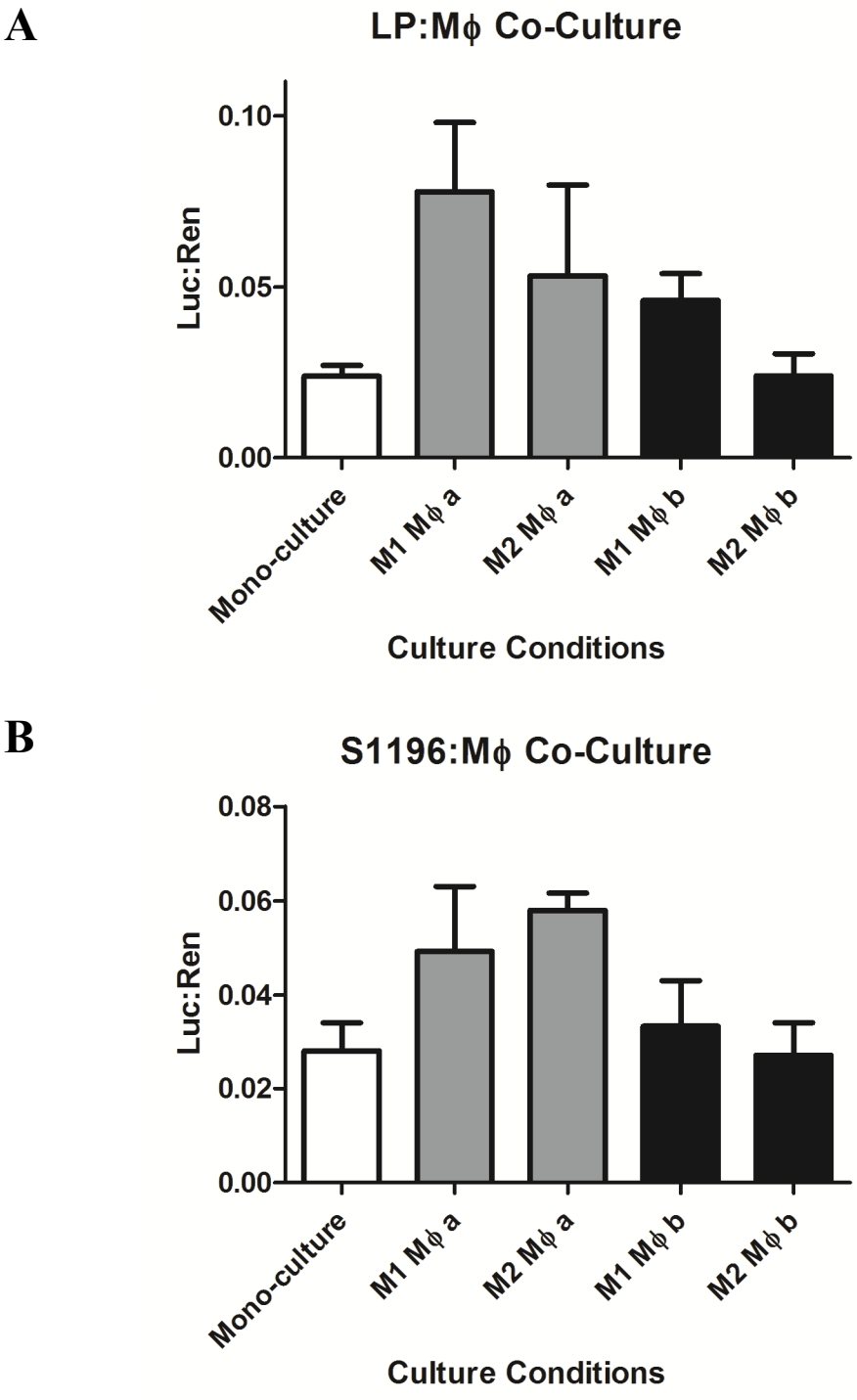

Discussion

Evidence presented here demonstrates that the Notch signalling pathway is upregulated in human CCA, specifically Notch2 and Notch3 receptors, Jagged1 and Jagged2 ligands together with downstream elements. This upregulation occurs during cholangiocarcinogenesis as identified in the rat TAA model. Whereas other groups [79, 532] have identified upregulation of Notch1 in tissue arrays of intrahepatic and extrahepatic CCA, we found that Notch3 exhibited the most striking dysregulation in our experimental series.

When considering the compartmental distribution of the Notch signalling pathway in this study, although immunohistochemical studies proved challenging, Notch receptors localised to biliary epithelia (and vasculature) whereas Jagged1 ligand localised to the tumour associated stroma, specifically appearing to be expressed by tumour associated myofibroblasts. During pre-neoplastic biliary proliferation in the rat model, Notch3 and Jagged1 was upregulated, together with downstream effector genes heyL. The significance of this is unclear and putative Notch signalling within the tumour niche is likely to be complex, with bidirectional relationships across the compartments. For example, it is possible that the progressive expression of Jagged1 ligand during cholangiocarcinogenesis reflects an accumulation of stromal cells in concert with an expansion of Notch3-expressing progenitors and dysplastic biliary cells. Jagged1 expression may then sustain Notch signalling and tumour progression. Assessment of this would be possible by immunohistochemical analysis of the pattern of receptor/ligand expression in the rat TAA model, which was not completed in this thesis. Currently, this study has not demonstrated expression of Notch3 in biliary cells or the stroma of tumours as the antibody stains were not optimised for analysis. Although the current model proposed in this study comprises of ligand-expressing stromal cells interacting with receptor-expressing epithelial cells, it is conceivable that Notch receptors could be also expressed by stromal cells in the tumours. If this were the case, then the Notch signalling pathway may play a role in controlling proliferation and maintenance of the tumour-associated stroma itself. Examples of this from other systems include observations that stromal cells control

dendritic cell fate and proliferation in bone marrow through Notch pathway signalling [440]. Similarly, macrophage polarisation appears to be in part mediated by Notch signalling: Notch pathway activation drives cells to an M1 phenotype and downregulation is associated with an M2 phenotype [441]. Additionally, M1 activated macrophages express upregulated levels of Notch1 and Jagged1 [442] and the ligand delta-like 4 [443]. Furthermore, Notch3 mediated signalling increases macrophages' proinflammatory function [443]. Alternatively, a non-canonical relationship may exist between tumour stroma and malignant epithelial cells, such as characterised by the pleiotropic cytokine, IL-6. IL-6 is known to promote CCA growth and, in breast cancer, it has been shown that IL-6 producing cancer-associated fibroblasts promote tumour invasiveness in a Notch3 and Jagged-1 dependent manner [533].

CCA is highly resistant to chemotherapy, the mechanisms of which are likely to be multifactorial. When considering the rationale for chemotherapy and cell signalling manipulation, the Notch pathway is an attractive target as it is responsible for biliary fate specification and proliferation specifically within the biliary tree. Furthermore, combining inhibition of the Notch pathway with chemotherapy has a rationale insofar as conventional chemotherapy appears to upregulate the Notch pathway in certain cancers. For example, oxaliplatin upregulates the Notch pathway in colorectal cancer cell lines whilst γ-secretase inhibition sensitises cells to chemotherapy [534]. Activated Notch signalling in cancer subsets results in downregulation of cell cycle regulating genes such as PTEN [535] and p53 [536]; this effect is abrogated by Notch pathway inhibition and chemosensitivity is enhanced. In this study, CCA cell lines are sensitive to Notch pathway inhibition *in vitro* with a dose dependent inhibition of proliferation. Notch pathway inhibition results in reduced cell proliferation and, within the caveats described in Figure 6.5, appears to augment the chemotherapeutic effect of 5-FU and cisplatin *in vitro*. These findings would clearly need further assessment and validation *in vivo*.

Notch signalling appears to play oncogenic or tumour suppressor roles in different solid organ tumours, as described in Chapter One - Introduction: The Notch Signalling Pathway. The tumour promoting role of the Notch pathway in CCA

identified in this study is in contrast to hepatocellular carcinoma (HCC) where the Notch pathway appears to act as a tumour suppressor [537]. These observations are in line with the role of the Notch pathway in directing biliary rather than hepatic cell fate in the regenerative liver niche. As such, Notch pathway inhibition may represent a future therapeutic target in the treatment of CCA.

A current limitation of inhibiting the Notch pathway in the clinical context is that Notch1 (and Notch2 to a lesser extent) signalling plays a central homeostatic role within adult gastrointestinal stem cell compartments [538]. Clinical trials of γ-secretase inhibitors have been hindered by the considerable gastrointestinal problems experienced by participants [539]. Despite the range of γ-secretase inhibitors developed by pharmaceutical companies, failure to progress beyond Phase I trials in the treatment of solid tumours is a hallmark of current outcomes although attempts have been made to combine treatment with glucocorticoids to counteract gastrointestinal toxicity in haematological malignancies. In light of this, specific inactivation of Notch3 represents a potential focused target for enhancing chemotherapy in CCA. Furthermore, the intent to limit drug toxicity may provide a rationale for low dose multimodality treatment approaches to chemotherapy.

CHAPTER SEVEN

CONCLUSIONS AND FUTURE PERSPECTIVES

Intrahepatic CCA is increasing in incidence and yet survival remains dismally poor[35]. It is hoped that improved understanding of the underlying tumour biology of the disease will contribute to studies and efforts to improve outcomes by delivering patient-specific, targeted therapies using multi-modality approaches. This would combine chemotherapeutic protocols that minimise toxicity with appropriate surgical strategies.

Solid organ tumours comprise a complex three-dimensional network of malignant epithelial cells in intimate relationship with inflammatory cells (myofibroblasts, macrophages, neutrophils, immune cells), neovasculature and ECM components. It is increasingly apparent that the microenvironment of solid organ cancers plays a crucial role in tumour behaviour. Intrahepatic CCA represents an excellent example of a solid organ tumour and I have studied CCA within this context in this thesis. I have undertaken to identify the origin of the cellular components of the tumour microenvironment, to assess whether epithelial cells may be derived from extra-hepatic sources and to begin to characterise stromal:epithelial cell relationships, with a focus on the Notch signalling pathway as a possible cell signalling mediator.

To that end, I have optimised and accelerated the TAA rat model of intrahepatic CCA following a review of available *in vitro* and *in vivo* model systems for CCA. I have demonstrated that although TAA administration induces hepatic fibrosis in C57bl6 mice, it does not generate frank CCA lesions in these animals. However, I have demonstrated that TAA administration reliably induces CCA formation in a rat model. Furthermore, the lesions produced show excellent histological congruence with human intrahepatic CCA in terms of the anatomical distribution and relationships between malignant biliary cells (CK19+/panCK), myofibroblasts (αSMA), macrophages (ED1/CD68, ED2/CD163), and extracellular matrix components such as laminin. I have identified that, during cholangiocarcinogenesis, progressive changes occur in the liver, in terms of accumulation of inflammatory cells and fibrosis, in concert with progressive proliferation of bipotential progenitors (oval cells). These changes precede the development of frank CCA lesions. I have investigated the utility of small animal imaging in the CCA model and demonstrated

the limitations of ultrasound and fluorescence based tools together with the prohibitive cost:benefit ratio of MRI studies in SD rats.

I then went on to characterise the roles of the stromal components (ECM, myofibroblasts and macrophages) in CCA together with an assessment of the *in vitro* evidence for the existence of cancer stem cells in CCA. I identified that, *in vitro*, the cellular component of CCA contains stem cell compartments consisting specifically of SP cells. These cells generate both SP and non-SP cells and express markers (CK19 and AFP) consistent with maintenance of non-differentiated state, unlike non-SP cells that express only CK19. Cholangiocarcinoma lesions comprise a complex three-dimensional structure of malignant biliary epithelial cells couched in a dense inflammatory cellular and ECM network. Considering the tumour niche in terms of the cellular and ECM contributors, I aimed to recapitulate these components *in vitro*. I identified that ECM components induce characteristic cell proliferation patterns with enhancement of growth of cancer cells on collagen I and IV, but a reduced effect with laminin (the ECM component that ensheathes CCA cells *in vivo*). CCA lesions are known to be very chemoresistant and in this study, no *in vitro* evidence of variable cell sensitivity to chemotherapy was identified as a result of different ECM components. There was no protective effect of different ECM components on chemosensitivity *in vitro*.

When stromal:CCA cell interactions were studied, I found *in vitro* evidence for bidirectional interaction between CCA cells and hepatic stellate cells (mediated by soluble factors), together with autocrine stimulation of CCA growth. In order to study direct cell:cell signalling between tumour and stromal cells, I developed a direct co-culture system of stained CCA and differentially-polarised human macrophages to enable tracking of cell proliferation and phagocytosis. Using this system, I identified that macrophage polarisation appears to play a role in CCA tumour progression with M2 polarised macrophages appearing to both enhance cell proliferation and be associated with an *in vitro* environment in which cell phagocytosis is reduced. An optimised form of macrophage:CCA co-culture system was developed and validated which shows experimental promise.

To study the origins of the stromal cells and epithelial cells in CCA lesions, I established syngeneic BM transplantation in SD rats with subsequent TAA administration. Using independent techniques, I confirmed that persistent reconstitution of both the haematopoietic and mesenchymal stem cell compartments occurred. I generated three separate groups of transplant chimeras – male *wt* to female *wt*, male EGFP to male *wt* and female EGFP to male *wt* SD rats. Silencing of EGFP did not appear to occur upon adoptive transfer, neither was there evidence for cell fusion in the chimeric CCA lesions. I identified the optimum timepoint at which to start administration of TAA (following maximal BM reconstitution) and generated chimeric CCA lesions. The timecourse of development of these lesions was studied, with accumulation of inflammatory cells prior to development of CCA. These lesions demonstrated that haematopoietic but not mesenchymal cells were recruited from the BM. Specifically, macrophages and neutrophils but not myofibroblasts were BM derived. Furthermore, there was no evidence for BM derivation of malignant epithelial cells. These findings were confirmed in a number of spontaneously arising breast, skin and colon lesions in chimeric SD rats.

There are clearly a number of other cell types within the tumour stroma that are of interest. Particular examples include subtypes of CAFs (FSP+/FAP+) and vascular stromal pericytes and fibrovascular structures (NG2+) [328]. Whilst the study of these additional cell types was beyond the scope of this thesis, further analysis of the origin of these cells would be relatively straightforward to undertake from the tissue generated by this study. Furthermore, it would be of interest to undertake a functional analysis of cell behaviour based on their compartmental origins. For example, the significance of distantly-derived as opposed to locally-derived stromal cells include the possibility of therapeutically modulating the chemoattractant axes that drive cell chemotaxis and migration of cells towards inflamed or malignant tissues. An illustration of this includes the CXCR4/SDF-1 axis [540] [327]. The receptor CXCR4 is expressed on multiple cell types including lymphocytes, hematopoietic stem cells, endothelial and epithelial cells, and cancer cells; the pathway is recognised to play roles in tumour progression, angiogenesis and metastasis [541].

Notch signalling represents a potential mechanism by which cells may communicate whilst in direct contact. This pathway is dysregulated in CCA. Using a qPCR array, I identified that in human CCA lesions Notch pathway components, specifically Notch2, Notch3, Jagged1 and Jagged2, are upregulated compared to control liver tissue. The greatest increase was observed for Notch3. The upregulation of Notch pathway components appears to occur sequentially during cholangiocarcinogenesis in the TAA rat model. I identified that in CCA the Notch pathway was functionally active *in vitro* and manipulation of the pathway inhibited cell growth. Furthermore, inhibition of Notch signalling appeared to augment CCA chemosensitivity *in vitro*. However, I did not identify *in vitro* evidence for endogenous macrophage or myofibroblast stromal:CCA cell Notch pathway interaction by means of 12CSL reporter transient transfection.

Inevitably, there are clearly a number of limitations to this work, in light of which conclusions should be cautiously drawn. An advantage of the TAA rat model is that it results in an inflammatory milieu in the hepatobiliary axis that recapitulates the premalignant environment found in many of the known aetiological causes that contribute to the formation of CCA. One specific reason for pursuing rat studies was the absence of mouse models with CCA on a pure genetic background that would enable adoptive transfer without encountering immunological hurdles. Unfortunately, limitations of the rat TAA model include the relatively long duration of tumourigenesis, rendering it difficult to study CCA in a short timeframe and also limiting manipulation of the model in terms of cell depletion or treatment strategies due to the timecourses involved. Furthermore, the rat is a less well studied model system than the mouse, with fewer experimental reagents available and fewer well characterised cell markers. Due to the considerably larger size of the rat, systemic treatments such as stromal cell depletion strategies (macrophage, myofibroblast) and signalling pathway manipulation (for example Notch pathway) become considerably more expensive, and in some cases prohibitively so.

This thesis has made considerable use of *in vitro* technology. *In vitro* studies must be interpreted with caution unless corroborated by *in vivo* data. For example, the existence of SP cells in CCA was studied *in vitro* and would now benefit from being extended into *in vivo* analysis. Furthermore, the *in vitro* study of cancer cell biology relies on representative cell lines, which do not perfectly reflect the behaviour of tumours *in vivo*. However, *in vitro* studies have validity insofar as that they enable controllable investigations and rapid testing of hypotheses on human cells. Indeed, the field of cancer biology relies on *in vitro* experiments to form the basis of the overwhelming majority of studies.

Methodologically, there are various ways of undertaking *in vitro* studies of cancer biology and assessments of chemotherapeutic effectiveness. In addition to the strategies used in this thesis, further ways to extend the analysis include *in vitro* half maximal inhibitory concentration (IC_{50}) studies, which are a measure of the quantity of a drug required to inhibit a biological process, such as proliferation, by half. It may be argued that my use of a range of different cell lines in different elements of the thesis is problematic. This occurred in part because lines were cultured at different times of the study and also in part because some cell lines were experimentally more tractable than others (e.g. s1079 was not transfectable so I used LP line instead). I would suggest the converse in that the use of different lines enables broader applicability of the *in vitro* results and is actually an advantage.

In this thesis, *in vitro* analysis of macrophage and myofibroblast stromal relationships with CCA cell lines was confined to controlled *in vitro* observations without *in vivo* confirmation. Preliminary results were identified with apparent promotion of CCA progression whilst cultured with M2 macrophages compared to M1 macrophages. However, there was no evidence of differences in Notch mediated signalling between macrophage polarity types. Three dimensional (rather than two dimensional) culture conditions may have recapitulated the *in vivo* environment more coherently, enabling more informative results for *in vitro* stroma:CCA studies.

With regard to the studies on Notch signalling in CCA, much of the information is preliminary and raises further questions. Going forward, it would be of interest to confirm the qPCR array results with qPCR for individual pathway components. The initial immunohistochemical findings studies of Notch signalling should now be continued by undertaking a more complete panel of immunohistochemical studies. The initial observation that Notch3, in particular, is upregulated in human CCA offers a novel dysregulated component of the Notch pathway that would be very interesting to characterise further and test definitively to evaluate potential clinical relevance. Taking this study forward, the finding in this thesis that inhibition of Notch signalling augments chemotherapy *in vitro* would benefit from being tested *in vivo* by assessing the effect of inhibition of Notch signalling (both by commercially available γ-secretase inhibitors and by Notch3-specific inhibition) and chemotherapy.

The results of this thesis raise further avenues for study and questions to answer. Development of a mouse model of CCA that form histologically realistic lesions within a short timeframe would be of considerable interest. One potential option would be to employ mouse genetic knockout models with administration of hepatotoxicants to drive cholangiocarcinogenesis. Inevitably with a rare cancer, this thesis made use of a limited number of human CCA specimens. Acquisition of more lesions to generate a tissue bank, either through serial acquisition in our institution or through collaboration, would be of immense value for future studies to provide more generalisable experimental information.

With regard to stromal:CCA interactions and Notch signalling, the focus of this thesis was exclusively on tumour cell behaviour. It is tempting to question the possibility of a signalling effect of malignant cells on stromal cells themselves. Of note, there is evidence in the literature that stromal cell profiles within tumours are affected by Notch signalling [533, 542] and it may well be that dysregulated signalling alters the phenotype of stromal cells within lesions. Studying this particular question in CCA would require a considerable investment of time and, although beyond the remit of this thesis, would be of considerable interest.

In conclusion, intrahepatic CCA acts as an exemplar of solid organ tumour biology, demonstrating that the dynamic tumour:stroma complex draws on both distant and locally recruited cells. The tumour stroma may play a role in promoting tumour survival in CCA and this merits further study. It is anticipated that understanding this dynamic tumour:stroma relationship will contribute in due course to improving survival outcomes for patients with this increasingly prevalent disease.

REFERENCES

1. Blechacz B, Gores GJ. Cholangiocarcinoma: advances in pathogenesis, diagnosis, and treatment. Hepatology 2008;48:308-21.
2. Altaee MY, Johnson PJ, Farrant JM, Williams R. Etiologic and clinical characteristics of peripheral and hilar cholangiocarcinoma. Cancer 1991;68:2051-5.
3. Ferlay J, Shin HR, Bray F, Forman D, Mathers C, Parkin DM. Estimates of worldwide burden of cancer in 2008: GLOBOCAN 2008. Int J Cancer 2010;127:2893-917.
4. Klatskin G. Adenocarcinoma of the Hepatic Duct at Its Bifurcation within the Porta Hepatis. An Unusual Tumor with Distinctive Clinical and Pathological Features. Am J Med 1965;38:241-56.
5. Nakanuma Y. Intrahepatic cholangiocarcinoma. International Agency for Research on Cancer [IARC], 2010.
6. Edge SB, Byrd DR, Compton CC, Fritz AG, Greene FL, A. T. AJCC Cancer Staging Manual. American Joint Committee on Cancer. 7th ed. New York, NY: Springer, 2010:201-205; 219-230.
7. Blechacz B, Komuta M, Roskams T, Gores GJ. Clinical diagnosis and staging of cholangiocarcinoma. Nat Rev Gastroenterol Hepatol 2011;8:512-22.
8. Bismuth H, Nakache R, Diamond T. Management strategies in resection for hilar cholangiocarcinoma. Ann Surg 1992;215:31-8.
9. Japan LCSGo. The general rules for the clinical and pathological study of primary liver cancer. Kanehara, 2000.
10. Lim JH, Park CK. Pathology of cholangiocarcinoma. Abdom Imaging 2004;29:540-7.
11. Farges O, Fuks D, Le Treut YP, Azoulay D, Laurent A, Bachellier P, Nuzzo G, Belghiti J, Pruvot FR, Regimbeau JM. AJCC 7th edition of TNM staging accurately discriminates outcomes of patients with resectable intrahepatic cholangiocarcinoma: By the AFC-IHCC-2009 study group. Cancer 2011;117:2170-7.
12. Ishak KG, Anthony PP, Sobin LH. Histological typing of tumours of the liver (WHO. World Health Organization. International Histological Classification Of Tumours). Springer-Verlag, 1994.
13. Hamilton SR and Aaltonen LA. World Health Organization Classification of Tumours. Pathology and Genetics of Tumours of the Digestive System. Lyon: IARC Press, 2000.
14. Broome U, Olsson R, Loof L, Bodemar G, Hultcrantz R, Danielsson A, Prytz H, Sandberg-Gertzen H, Wallerstedt S, Lindberg G. Natural history and prognostic factors in 305 Swedish patients with primary sclerosing cholangitis. Gut 1996;38:610-5.
15. Bergquist A, Broome U. Hepatobiliary and extra-hepatic malignancies in primary sclerosing cholangitis. Best Pract Res Clin Gastroenterol 2001;15:643-56.
16. Malhi H, Gores GJ. Cholangiocarcinoma: modern advances in understanding a deadly old disease. J Hepatol 2006;45:856-67.
17. Burak K, Angulo P, Pasha TM, Egan K, Petz J, Lindor KD. Incidence and risk factors for cholangiocarcinoma in primary sclerosing cholangitis. Am J Gastroenterol 2004;99:523-6.

18. Chalasani N, Baluyut A, Ismail A, Zaman A, Sood G, Ghalib R, McCashland TM, Reddy KR, Zervos X, Anbari MA, Hoen H. Cholangiocarcinoma in patients with primary sclerosing cholangitis: a multicenter case-control study. Hepatology 2000;31:7-11.
19. Welzel TM, Graubard BI, El-Serag HB, Shaib YH, Hsing AW, Davila JA, McGlynn KA. Risk factors for intrahepatic and extrahepatic cholangiocarcinoma in the United States: a population-based case-control study. Clin Gastroenterol Hepatol 2007;5:1221-8.
20. Haswell-Elkins MR, Mairiang E, Mairiang P, Chaiyakum J, Chamadol N, Loapaiboon V, Sithithaworn P, Elkins DB. Cross-sectional study of Opisthorchis viverrini infection and cholangiocarcinoma in communities within a high-risk area in northeast Thailand. Int J Cancer 1994;59:505-9.
21. Yamao K, Mizutani S, Nakazawa S, Inui K, Kanemaki N, Miyoshi H, Segawa K, Zenda H, Kato T. Prospective study of the detection of anomalous connections of pancreatobiliary ducts during routine medical examinations. Hepatogastroenterology 1996;43:1238-45.
22. Patel T. Cholangiocarcinoma. Nat Clin Pract Gastroenterol Hepatol 2006;3:33-42.
23. Kubo S, Kinoshita H, Hirohashi K, Hamba H. Hepatolithiasis associated with cholangiocarcinoma. World J Surg 1995;19:637-41.
24. Shaib Y, El-Serag HB. The epidemiology of cholangiocarcinoma. Semin Liver Dis 2004;24:115-25.
25. Welzel TM, Mellemkjaer L, Gloria G, Sakoda LC, Hsing AW, El Ghormli L, Olsen JH, McGlynn KA. Risk factors for intrahepatic cholangiocarcinoma in a low-risk population: a nationwide case-control study. Int J Cancer 2007;120:638-41.
26. Khan SA, Toledano MB, Taylor-Robinson SD. Epidemiology, risk factors, and pathogenesis of cholangiocarcinoma. HPB (Oxford) 2008;10:77-82.
27. Sorensen HT, Friis S, Olsen JH, Thulstrup AM, Mellemkjaer L, Linet M, Trichopoulos D, Vilstrup H, Olsen J. Risk of liver and other types of cancer in patients with cirrhosis: a nationwide cohort study in Denmark. Hepatology 1998;28:921-5.
28. Shaib YH, El-Serag HB, Davila JA, Morgan R, McGlynn KA. Risk factors of intrahepatic cholangiocarcinoma in the United States: a case-control study. Gastroenterology 2005;128:620-6.
29. Palmer WC, Patel T. Are common factors involved in the pathogenesis of primary liver cancers? A meta-analysis of risk factors for intrahepatic cholangiocarcinoma. J Hepatol 2012.
30. Thorium. Human Health Fact Sheet. Chicago: Argonne National Laboratory, EVS, 2005.
31. Ishikawa Y, Wada I, Fukumoto M. Alpha-particle carcinogenesis in Thorotrast patients: epidemiology, dosimetry, pathology, and molecular analysis. J Environ Pathol Toxicol Oncol 2001;20:311-5.
32. Bond GG, McLaren EA, Sabel FL, Bodner KM, Lipps TE, Cook RR. Liver and biliary tract cancer among chemical workers. Am J Ind Med 1990;18:19-24.
33. Hardell L, Bengtsson NO, Jonsson U, Eriksson S, Larsson LG. Aetiological aspects on primary liver cancer with special regard to alcohol, organic

solvents and acute intermittent porphyria--an epidemiological investigation. Br J Cancer 1984;50:389-97.
34. Toledano MB. Spatial epidemiology of biliary tract tumours, In British Association for Study of the Liver (BASL), Imperial College, London, 2007.
35. Khan SA, Thomas HC, Davidson BR, Taylor-Robinson SD. Cholangiocarcinoma. Lancet 2005;366:1303-14.
36. Khan SA, Taylor-Robinson SD, Toledano MB, Beck A, Elliott P, Thomas HC. Changing international trends in mortality rates for liver, biliary and pancreatic tumours. J Hepatol 2002;37:806-13.
37. Patel T. Worldwide trends in mortality from biliary tract malignancies. BMC Cancer 2002;2:10.
38. Shaib YH, Davila JA, McGlynn K, El-Serag HB. Rising incidence of intrahepatic cholangiocarcinoma in the United States: a true increase? J Hepatol 2004;40:472-7.
39. Taylor-Robinson SD, Toledano MB, Arora S, Keegan TJ, Hargreaves S, Beck A, Khan SA, Elliott P, Thomas HC. Increase in mortality rates from intrahepatic cholangiocarcinoma in England and Wales 1968-1998. Gut 2001;48:816-20.
40. Patel T. Increasing incidence and mortality of primary intrahepatic cholangiocarcinoma in the United States. Hepatology 2001;33:1353-7.
41. Wood R, Brewster DH, Fraser LA, Brown H, Hayes PC, Garden OJ. Do increases in mortality from intrahepatic cholangiocarcinoma reflect a genuine increase in risk? Insights from cancer registry data in Scotland. Eur J Cancer 2003;39:2087-92.
42. Khan SA, Emadossadaty S, Ladep NG, Thomas HC, Elliott P, Taylor-Robinson SD, Toledano MB. Rising trends in cholangiocarcinoma: is the ICD classification system misleading us? J Hepatol 2012;56:848-54.
43. Welzel TM, McGlynn KA, Hsing AW, O'Brien TR, Pfeiffer RM. Impact of classification of hilar cholangiocarcinomas (Klatskin tumors) on the incidence of intra- and extrahepatic cholangiocarcinoma in the United States. J Natl Cancer Inst 2006;98:873-5.
44. El-Serag HB, Rudolph KL. Hepatocellular carcinoma: epidemiology and molecular carcinogenesis. Gastroenterology 2007;132:2557-76.
45. Fava G, Lorenzini I. Molecular pathogenesis of cholangiocarcinoma. Int J Hepatol 2012;2012:630543.
46. Nomoto K, Tsuneyama K, Cheng C, Takahashi H, Hori R, Murai Y, Takano Y. Intrahepatic cholangiocarcinoma arising in cirrhotic liver frequently expressed p63-positive basal/stem-cell phenotype. Pathol Res Pract 2006;202:71-6.
47. Roskams T. Liver stem cells and their implication in hepatocellular and cholangiocarcinoma. Oncogene 2006;25:3818-22.
48. Jaiswal M, LaRusso NF, Gores GJ. Nitric oxide in gastrointestinal epithelial cell carcinogenesis: linking inflammation to oncogenesis. Am J Physiol Gastrointest Liver Physiol 2001;281:G626-34.
49. Sia D, Tovar V, Moeini A, Llovet JM. Intrahepatic cholangiocarcinoma: pathogenesis and rationale for molecular therapies. Oncogene 2013.
50. Andersen JB, Spee B, Blechacz BR, Avital I, Komuta M, Barbour A, Conner EA, Gillen MC, Roskams T, Roberts LR, Factor VM, Thorgeirsson SS.

Genomic and genetic characterization of cholangiocarcinoma identifies therapeutic targets for tyrosine kinase inhibitors. Gastroenterology 2012;142:1021-1031 e15.
51. Berthiaume EP, Wands J. The molecular pathogenesis of cholangiocarcinoma. Semin Liver Dis 2004;24:127-37.
52. Sirica AE, Campbell DJ, Dumur CI. Cancer-associated fibroblasts in intrahepatic cholangiocarcinoma. Curr Opin Gastroenterol 2011;27:276-84.
53. Wadsworth CA, Dixon PH, Wong JH, Chapman MH, McKay SC, Sharif A, Spalding DR, Pereira SP, Thomas HC, Taylor-Robinson SD, Whittaker J, Williamson C, Khan SA. Genetic factors in the pathogenesis of cholangiocarcinoma. Dig Dis 2011;29:93-7.
54. Prawan A, Kukongviriyapan V, Tassaneeyakul W, Pairojkul C, Bhudhisawasdi V. Association between genetic polymorphisms of CYP1A2, arylamine N-acetyltransferase 1 and 2 and susceptibility to cholangiocarcinoma. Eur J Cancer Prev 2005;14:245-50.
55. Dergham ST, Dugan MC, Kucway R, Du W, Kamarauskiene DS, Vaitkevicius VK, Crissman JD, Sarkar FH. Prevalence and clinical significance of combined K-ras mutation and p53 aberration in pancreatic adenocarcinoma. Int J Pancreatol 1997;21:127-43.
56. Farazi PA, Zeisberg M, Glickman J, Zhang Y, Kalluri R, DePinho RA. Chronic bile duct injury associated with fibrotic matrix microenvironment provokes cholangiocarcinoma in p53-deficient mice. Cancer Res 2006;66:6622-7.
57. O'Dell MR, Huang JL, Whitney-Miller CL, Deshpande V, Rothberg P, Grose V, Rossi RM, Zhu AX, Land H, Bardeesy N, Hezel AF. Kras(G12D) and p53 mutation cause primary intrahepatic cholangiocarcinoma. Cancer Res 2012;72:1557-67.
58. Sia D, Hoshida Y, Villanueva A, Roayaie S, Ferrer J, Tabak B, Peix J, Sole M, Tovar V, Alsinet C, Cornella H, Klotzle B, Fan JB, Cotsoglou C, Thung SN, Fuster J, Waxman S, Garcia-Valdecasas JC, Bruix J, Schwartz ME, Beroukhim R, Mazzaferro V, Llovet JM. Integrative Molecular Analysis of Intrahepatic Cholangiocarcinoma Reveals 2 Classes That Have Different Outcomes. Gastroenterology 2013.
59. Chen L, Yan HX, Yang W, Hu L, Yu LX, Liu Q, Li L, Huang DD, Ding J, Shen F, Zhou WP, Wu MC, Wang HY. The role of microRNA expression pattern in human intrahepatic cholangiocarcinoma. J Hepatol 2009;50:358-69.
60. Li B, Han Q, Zhu Y, Yu Y, Wang J, Jiang X. Down-regulation of miR-214 contributes to intrahepatic cholangiocarcinoma metastasis by targeting Twist. FEBS J 2012;279:2393-8.
61. Meng F, Henson R, Lang M, Wehbe H, Maheshwari S, Mendell JT, Jiang J, Schmittgen TD, Patel T. Involvement of human micro-RNA in growth and response to chemotherapy in human cholangiocarcinoma cell lines. Gastroenterology 2006;130:2113-29.
62. Oishi N, Kumar MR, Roessler S, Ji J, Forgues M, Budhu A, Zhao X, Andersen JB, Ye QH, Jia HL, Qin LX, Yamashita T, Woo HG, Kim YJ, Kaneko S, Tang ZY, Thorgeirsson SS, Wang XW. Transcriptomic profiling reveals hepatic stem-like gene signatures and interplay of miR-200c and

epithelial-mesenchymal transition in intrahepatic cholangiocarcinoma. Hepatology 2012;56:1792-803.
63. Varjosalo M, Taipale J. Hedgehog: functions and mechanisms. Genes Dev 2008;22:2454-72.
64. Scales SJ, de Sauvage FJ. Mechanisms of Hedgehog pathway activation in cancer and implications for therapy. Trends Pharmacol Sci 2009;30:303-12.
65. Tang L, Tan YX, Jiang BG, Pan YF, Li SX, Yang GZ, Wang M, Wang Q, Zhang J, Zhou WP, Dong LW, Wang HY. The prognostic significance and therapeutic potential of hedgehog signaling in intrahepatic cholangiocellular carcinoma. Clin Cancer Res 2013;19:2014-24.
66. Kim Y, Kim MO, Shin JS, Park SH, Kim SB, Kim J, Park SC, Han CJ, Ryu JK, Yoon YB, Kim YT. Hedgehog signaling between cancer cells and hepatic stellate cells in promoting cholangiocarcinoma. Ann Surg Oncol 2014;21:2684-98.
67. Park J, Tadlock L, Gores GJ, Patel T. Inhibition of interleukin 6-mediated mitogen-activated protein kinase activation attenuates growth of a cholangiocarcinoma cell line. Hepatology 1999;30:1128-33.
68. Kobayashi S, Werneburg NW, Bronk SF, Kaufmann SH, Gores GJ. Interleukin-6 contributes to Mcl-1 up-regulation and TRAIL resistance via an Akt-signaling pathway in cholangiocarcinoma cells. Gastroenterology 2005;128:2054-65.
69. Hodge DR, Hurt EM, Farrar WL. The role of IL-6 and STAT3 in inflammation and cancer. Eur J Cancer 2005;41:2502-12.
70. Isomoto H, Mott JL, Kobayashi S, Werneburg NW, Bronk SF, Haan S, Gores GJ. Sustained IL-6/STAT-3 signaling in cholangiocarcinoma cells due to SOCS-3 epigenetic silencing. Gastroenterology 2007;132:384-96.
71. Yamagiwa Y, Meng F, Patel T. Interleukin-6 decreases senescence and increases telomerase activity in malignant human cholangiocytes. Life Sci 2006;78:2494-502.
72. Yoshikawa D, Ojima H, Iwasaki M, Hiraoka N, Kosuge T, Kasai S, Hirohashi S, Shibata T. Clinicopathological and prognostic significance of EGFR, VEGF, and HER2 expression in cholangiocarcinoma. Br J Cancer 2008;98:418-25.
73. Yoon JH, Gwak GY, Lee HS, Bronk SF, Werneburg NW, Gores GJ. Enhanced epidermal growth factor receptor activation in human cholangiocarcinoma cells. J Hepatol 2004;41:808-14.
74. Miyamoto M, Ojima H, Iwasaki M, Shimizu H, Kokubu A, Hiraoka N, Kosuge T, Yoshikawa D, Kono T, Furukawa H, Shibata T. Prognostic significance of overexpression of c-Met oncoprotein in cholangiocarcinoma. Br J Cancer 2011;105:131-8.
75. Lai GH, Radaeva S, Nakamura T, Sirica AE. Unique epithelial cell production of hepatocyte growth factor/scatter factor by putative precancerous intestinal metaplasias and associated "intestinal-type" biliary cancer chemically induced in rat liver. Hepatology 2000;31:1257-65.
76. Leelawat K, Leelawat S, Tepaksorn P, Rattanasinganchan P, Leungchaweng A, Tohtong R, Sobhon P. Involvement of c-Met/hepatocyte growth factor pathway in cholangiocarcinoma cell invasion and its therapeutic inhibition with small interfering RNA specific for c-Met. J Surg Res 2006;136:78-84.

77. Comoglio PM, Giordano S, Trusolino L. Drug development of MET inhibitors: targeting oncogene addiction and expedience. Nat Rev Drug Discov 2008;7:504-16.
78. Gao SP, Mark KG, Leslie K, Pao W, Motoi N, Gerald WL, Travis WD, Bornmann W, Veach D, Clarkson B, Bromberg JF. Mutations in the EGFR kinase domain mediate STAT3 activation via IL-6 production in human lung adenocarcinomas. J Clin Invest 2007;117:3846-56.
79. Ishimura N, Bronk SF, Gores GJ. Inducible nitric oxide synthase up-regulates Notch-1 in mouse cholangiocytes: implications for carcinogenesis. Gastroenterology 2005;128:1354-68.
80. Sansone P, Storci G, Tavolari S, Guarnieri T, Giovannini C, Taffurelli M, Ceccarelli C, Santini D, Paterini P, Marcu KB, Chieco P, Bonafe M. IL-6 triggers malignant features in mammospheres from human ductal breast carcinoma and normal mammary gland. J Clin Invest 2007;117:3988-4002.
81. Rebay I, Fleming RJ, Fehon RG, Cherbas L, Cherbas P, Artavanis-Tsakonas S. Specific EGF repeats of Notch mediate interactions with Delta and Serrate: implications for Notch as a multifunctional receptor. Cell 1991;67:687-99.
82. Li T, Wen H, Brayton C, Das P, Smithson LA, Fauq A, Fan X, Crain BJ, Price DL, Golde TE, Eberhart CG, Wong PC. Epidermal growth factor receptor and notch pathways participate in the tumor suppressor function of gamma-secretase. J Biol Chem 2007;282:32264-73.
83. Purow BW, Sundaresan TK, Burdick MJ, Kefas BA, Comeau LD, Hawkinson MP, Su Q, Kotliarov Y, Lee J, Zhang W, Fine HA. Notch-1 regulates transcription of the epidermal growth factor receptor through p53. Carcinogenesis 2008;29:918-25.
84. de Groen PC, Gores GJ, LaRusso NF, Gunderson LL, Nagorney DM. Biliary tract cancers. N Engl J Med 1999;341:1368-78.
85. Khan SA, Davidson BR, Goldin RD, Heaton N, Karani J, Pereira SP, Rosenberg WM, Tait P, Taylor-Robinson SD, Thillainayagam AV, Thomas HC, Wasan H. Guidelines for the diagnosis and treatment of cholangiocarcinoma: an update. Gut 2012;61:1657-69.
86. Guidelines for Management of Cholangiocarcinoma & Gallbladder cancer Glasgow: Scottish Hepato-Pancreato-Biliary Managed Cancer Network, 2010.
87. Patel AH, Harnois DM, Klee GG, LaRusso NF, Gores GJ. The utility of CA 19-9 in the diagnoses of cholangiocarcinoma in patients without primary sclerosing cholangitis. Am J Gastroenterol 2000;95:204-7.
88. Tao LY, Cai L, He XD, Liu W, Qu Q. Comparison of serum tumor markers for intrahepatic cholangiocarcinoma and hepatocellular carcinoma. Am Surg 2010;76:1210-3.
89. Uenishi T, Kubo S, Hirohashi K, Tanaka H, Shuto T, Yamamoto T, Nishiguchi S. Cytokeratin-19 fragments in serum (CYFRA 21-1) as a marker in primary liver cancer. Br J Cancer 2003;88:1894-9.
90. Uenishi T, Yamazaki O, Tanaka H, Takemura S, Yamamoto T, Tanaka S, Nishiguchi S, Kubo S. Serum cytokeratin 19 fragment (CYFRA21-1) as a prognostic factor in intrahepatic cholangiocarcinoma. Ann Surg Oncol 2008;15:583-9.

91. Loyer EM, Chin H, DuBrow RA, David CL, Eftekhari F, Charnsangavej C. Hepatocellular carcinoma and intrahepatic peripheral cholangiocarcinoma: enhancement patterns with quadruple phase helical CT--a comparative study. Radiology 1999;212:866-75.
92. Manfredi R, Barbaro B, Masselli G, Vecchioli A, Marano P. Magnetic resonance imaging of cholangiocarcinoma. Semin Liver Dis 2004;24:155-64.
93. Breitenstein S, Apestegui C, Clavien PA. Positron emission tomography (PET) for cholangiocarcinoma. HPB (Oxford) 2008;10:120-1.
94. Petrowsky H, Wildbrett P, Husarik DB, Hany TF, Tam S, Jochum W, Clavien PA. Impact of integrated positron emission tomography and computed tomography on staging and management of gallbladder cancer and cholangiocarcinoma. J Hepatol 2006;45:43-50.
95. Heimbach JK, Sanchez W, Rosen CB, Gores GJ. Trans-peritoneal fine needle aspiration biopsy of hilar cholangiocarcinoma is associated with disease dissemination. HPB (Oxford) 2011;13:356-60.
96. Goere D, Wagholikar GD, Pessaux P, Carrere N, Sibert A, Vilgrain V, Sauvanet A, Belghiti J. Utility of staging laparoscopy in subsets of biliary cancers : laparoscopy is a powerful diagnostic tool in patients with intrahepatic and gallbladder carcinoma. Surg Endosc 2006;20:721-5.
97. Mansfield JC, Griffin SM, Wadehra V, Matthewson K. A prospective evaluation of cytology from biliary strictures. Gut 1997;40:671-7.
98. Kipp BR, Stadheim LM, Halling SA, Pochron NL, Harmsen S, Nagorney DM, Sebo TJ, Therneau TM, Gores GJ, de Groen PC, Baron TH, Levy MJ, Halling KC, Roberts LR. A comparison of routine cytology and fluorescence in situ hybridization for the detection of malignant bile duct strictures. Am J Gastroenterol 2004;99:1675-81.
99. Abu-Hamda EM, Baron TH. Endoscopic management of cholangiocarcinoma. Semin Liver Dis 2004;24:165-75.
100. Draganov PV, Chauhan S, Wagh MS, Gupte AR, Lin T, Hou W, Forsmark CE. Diagnostic accuracy of conventional and cholangioscopy-guided sampling of indeterminate biliary lesions at the time of ERCP: a prospective, long-term follow-up study. Gastrointest Endosc 2012;75:347-53.
101. Ramchandani M, Reddy DN, Gupta R, Lakhtakia S, Tandan M, Darisetty S, Sekaran A, Rao GV. Role of single-operator peroral cholangioscopy in the diagnosis of indeterminate biliary lesions: a single-center, prospective study. Gastrointest Endosc 2011;74:511-9.
102. Parodi A, Fisher D, Giovannini M, Baron T, Conio M. Endoscopic management of hilar cholangiocarcinoma. Nat Rev Gastroenterol Hepatol 2012;9:105-12.
103. Backman V, Roy HK. Light-scattering technologies for field carcinogenesis detection: a modality for endoscopic prescreening. Gastroenterology 2011;140:35-41.
104. Yamasaki S. Intrahepatic cholangiocarcinoma: macroscopic type and stage classification. J Hepatobiliary Pancreat Surg 2003;10:288-91.
105. Okabayashi T, Yamamoto J, Kosuge T, Shimada K, Yamasaki S, Takayama T, Makuuchi M. A new staging system for mass-forming intrahepatic cholangiocarcinoma: analysis of preoperative and postoperative variables. Cancer 2001;92:2374-83.

106. Nathan H, Aloia TA, Vauthey JN, Abdalla EK, Zhu AX, Schulick RD, Choti MA, Pawlik TM. A proposed staging system for intrahepatic cholangiocarcinoma. Ann Surg Oncol 2009;16:14-22.
107. Zervos EE, Osborne D, Goldin SB, Villadolid DV, Thometz DP, Durkin A, Carey LC, Rosemurgy AS. Stage does not predict survival after resection of hilar cholangiocarcinomas promoting an aggressive operative approach. Am J Surg 2005;190:810-5.
108. Blechacz BR, Sanchez W, Gores GJ. A conceptual proposal for staging ductal cholangiocarcinoma. Curr Opin Gastroenterol 2009;25:238-9.
109. Deoliveira ML, Schulick RD, Nimura Y, Rosen C, Gores G, Neuhaus P, Clavien PA. New staging system and a registry for perihilar cholangiocarcinoma. Hepatology 2011;53:1363-71.
110. Igami T, Ebata T, Yokoyama Y, Sugawara G, Takahashi Y, Nagino M. Staging of peripheral-type intrahepatic cholangiocarcinoma: appraisal of the new TNM classification and its modifications. World J Surg 2011;35:2501-9.
111. Bile Duct (Cholangiocarcinoma) Cancer. Learn about Cancer. Atlanta, GA: American Cancer Society, 2011.
112. Shaib YH, Davila JA, Henderson L, McGlynn KA, El-Serag HB. Endoscopic and surgical therapy for intrahepatic cholangiocarcinoma in the united states: a population-based study. J Clin Gastroenterol 2007;41:911-7.
113. Jarnagin WR, Shoup M. Surgical management of cholangiocarcinoma. Semin Liver Dis 2004;24:189-99.
114. Young AL, Prasad KR, Toogood GJ, Lodge JP. Surgical treatment of hilar cholangiocarcinoma in a new era: comparison among leading Eastern and Western centers, Leeds. J Hepatobiliary Pancreat Sci 2010;17:497-504.
115. de Jong MC, Nathan H, Sotiropoulos GC, Paul A, Alexandrescu S, Marques H, Pulitano C, Barroso E, Clary BM, Aldrighetti L, Ferrone CR, Zhu AX, Bauer TW, Walters DM, Gamblin TC, Nguyen KT, Turley R, Popescu I, Hubert C, Meyer S, Schulick RD, Choti MA, Gigot JF, Mentha G, Pawlik TM. Intrahepatic cholangiocarcinoma: an international multi-institutional analysis of prognostic factors and lymph node assessment. J Clin Oncol;29:3140-5.
116. Meyer CG, Penn I, James L. Liver transplantation for cholangiocarcinoma: results in 207 patients. Transplantation 2000;69:1633-7.
117. Rosen CB, Heimbach JK, Gores GJ. Liver transplantation for cholangiocarcinoma. Transpl Int 2010;23:692-7.
118. Cash WJC, A.; Egan, B.; McDermott, E.; Leen, R.; Baker, Z.; Judge, E.; McCormick, A.; Hegarty, J.; Traynor, O.; Geoghan, J.; Maguire, D. . Mayo Protocol for Unresectable Cholangiocarcinoma - Experience of the Irish Transplant Unit. . Journal of Hepatology 2009;50::S64.
119. Darwish Murad S, Kim WR, Harnois DM, Douglas DD, Burton J, Kulik LM, Botha JF, Mezrich JD, Chapman WC, Schwartz JJ, Hong JC, Emond JC, Jeon H, Rosen CB, Gores GJ, Heimbach JK. Efficacy of neoadjuvant chemoradiation, followed by liver transplantation, for perihilar cholangiocarcinoma at 12 US centers. Gastroenterology 2012;143:88-98 e3; quiz e14.

120. Igami T, Nishio H, Ebata T, Yokoyama Y, Sugawara G, Nimura Y, Nagino M. Surgical treatment of hilar cholangiocarcinoma in the "new era": the Nagoya University experience. J Hepatobiliary Pancreat Sci 2010;17:449-54.
121. Grandadam S, Compagnon P, Arnaud A, Olivie D, Malledant Y, Meunier B, Launois B, Boudjema K. Role of preoperative optimization of the liver for resection in patients with hilar cholangiocarcinoma type III. Ann Surg Oncol 2010;17:3155-61.
122. Young AL, Igami T, Senda Y, Adair R, Farid S, Toogood GJ, Prasad KR, Lodge JP. Evolution of the surgical management of perihilar cholangiocarcinoma in a Western centre demonstrates improved survival with endoscopic biliary drainage and reduced use of blood transfusion. HPB (Oxford) 2011;13:483-93.
123. Figueras J, Llado L, Valls C, Serrano T, Ramos E, Fabregat J, Rafecas A, Torras J, Jaurrieta E. Changing strategies in diagnosis and management of hilar cholangiocarcinoma. Liver Transpl 2000;6:786-94.
124. van der Gaag NA, Rauws EA, van Eijck CH, Bruno MJ, van der Harst E, Kubben FJ, Gerritsen JJ, Greve JW, Gerhards MF, de Hingh IH, Klinkenbijl JH, Nio CY, de Castro SM, Busch OR, van Gulik TM, Bossuyt PM, Gouma DJ. Preoperative biliary drainage for cancer of the head of the pancreas. N Engl J Med 2010;362:129-37.
125. Anderson CD, Pinson CW, Berlin J, Chari RS. Diagnosis and treatment of cholangiocarcinoma. Oncologist 2004;9:43-57.
126. Stern N, Sturgess R. Endoscopic therapy in the management of malignant biliary obstruction. Eur J Surg Oncol 2008;34:313-7.
127. Kaassis M, Boyer J, Dumas R, Ponchon T, Coumaros D, Delcenserie R, Canard JM, Fritsch J, Rey JF, Burtin P. Plastic or metal stents for malignant stricture of the common bile duct? Results of a randomized prospective study. Gastrointest Endosc 2003;57:178-82.
128. Saleem A, Leggett CL, Murad MH, Baron TH. Meta-analysis of randomized trials comparing the patency of covered and uncovered self-expandable metal stents for palliation of distal malignant bile duct obstruction. Gastrointest Endosc 2011;74:321-327 e1-3.
129. Ortner ME, Caca K, Berr F, Liebetruth J, Mansmann U, Huster D, Voderholzer W, Schachschal G, Mossner J, Lochs H. Successful photodynamic therapy for nonresectable cholangiocarcinoma: a randomized prospective study. Gastroenterology 2003;125:1355-63.
130. Zoepf T, Jakobs R, Arnold JC, Apel D, Riemann JF. Palliation of nonresectable bile duct cancer: improved survival after photodynamic therapy. Am J Gastroenterol 2005;100:2426-30.
131. Pereira S, Hughes S, Roughton M, O'Donoghue P, Wasan H, Valle J, Bridgewater J. Photostent-02; Porfirmer Sodium photodynamic therapy plus stenting versus stenting alone in patients with advanced or metastatic cholangiocarcinomas and other biliary tract tumours: a multicentre, randomised phase III trial. ESMO 2010 (Abstract 8020). . Ann Oncol 2010;21:viii250-viii263.
132. Valle J, Wasan H, Palmer DH, Cunningham D, Anthoney A, Maraveyas A, Madhusudan S, Iveson T, Hughes S, Pereira SP, Roughton M, Bridgewater J.

Cisplatin plus gemcitabine versus gemcitabine for biliary tract cancer. N Engl J Med 2010;362:1273-81.
133. Roth JA, Carlson JJ. Cost-effectiveness of gemcitabine + cisplatin vs. gemcitabine monotherapy in advanced biliary tract cancer. J Gastrointest Cancer 2012;43:215-23.
134. Saito H, Takada T, Miyazaki M, Miyakawa S, Tsukada K, Nagino M, Kondo S, Furuse J, Tsuyuguchi T, Kimura F, Yoshitomi H, Nozawa S, Yoshida M, Wada K, Amano H, Miura F. Radiation therapy and photodynamic therapy for biliary tract and ampullary carcinomas. J Hepatobiliary Pancreat Surg 2008;15:63-8.
135. Pitt HA, Nakeeb A, Abrams RA, Coleman J, Piantadosi S, Yeo CJ, Lillemore KD, Cameron JL. Perihilar cholangiocarcinoma. Postoperative radiotherapy does not improve survival. Ann Surg 1995;221:788-97; discussion 797-8.
136. Skipworth JR, Olde Damink SW, Imber C, Bridgewater J, Pereira SP, Malago M. Review article: surgical, neo-adjuvant and adjuvant management strategies in biliary tract cancer. Aliment Pharmacol Ther 2011;34:1063-78.
137. Shinohara ET, Mitra N, Guo M, Metz JM. Radiation therapy is associated with improved survival in the adjuvant and definitive treatment of intrahepatic cholangiocarcinoma. Int J Radiat Oncol Biol Phys 2008;72:1495-501.
138. Shinohara ET, Mitra N, Guo M, Metz JM. Radiotherapy is associated with improved survival in adjuvant and palliative treatment of extrahepatic cholangiocarcinomas. Int J Radiat Oncol Biol Phys 2009;74:1191-8.
139. Park SY, Kim JH, Yoon HJ, Lee IS, Yoon HK, Kim KP. Transarterial chemoembolization versus supportive therapy in the palliative treatment of unresectable intrahepatic cholangiocarcinoma. Clin Radiol 2011;66:322-8.
140. Wu ZF, Zhang HB, Yang N, Zhao WC, Fu Y, Yang GS. Postoperative adjuvant transcatheter arterial chemoembolisation improves survival of intrahepatic cholangiocarcinoma patients with poor prognostic factors: results of a large monocentric series. Eur J Surg Oncol 2012;38:602-10.
141. Xu HX, Wang Y, Lu MD, Liu LN. Percutaneous ultrasound-guided thermal ablation for intrahepatic cholangiocarcinoma. Br J Radiol 2012;85:1078-84.
142. Hoffmann RT, Paprottka PM, Schon A, Bamberg F, Haug A, Durr EM, Rauch B, Trumm CT, Jakobs TF, Helmberger TK, Reiser MF, Kolligs FT. Transarterial hepatic yttrium-90 radioembolization in patients with unresectable intrahepatic cholangiocarcinoma: factors associated with prolonged survival. Cardiovasc Intervent Radiol 2012;35:105-16.
143. Valle J. Cediranib versus placebo plus cisplatin/gemcitabine chemotherapy for patients with advanced biliary tract cancers (ABC-03) NTC00939848: ClinicalTrials.gov, 2011.
144. Dvorak HF. Tumors: wounds that do not heal. Similarities between tumor stroma generation and wound healing. N Engl J Med 1986;315:1650-9.
145. De Wever O, Mareel M. Role of tissue stroma in cancer cell invasion. J Pathol 2003;200:429-47.
146. Egeblad M, Nakasone ES, Werb Z. Tumors as organs: complex tissues that interface with the entire organism. Dev Cell 2010;18:884-901.

147. Nakanuma Y, Harada K, Ishikawa A, Zen Y, Sasaki M. Anatomic and molecular pathology of intrahepatic cholangiocarcinoma. J Hepatobiliary Pancreat Surg 2003;10:265-81.
148. Lu P, Weaver VM, Werb Z. The extracellular matrix: a dynamic niche in cancer progression. J Cell Biol 2012;196:395-406.
149. Guerrero I, Chiang C. A conserved mechanism of Hedgehog gradient formation by lipid modifications. Trends Cell Biol 2007;17:1-5.
150. Hynes RO. The extracellular matrix: not just pretty fibrils. Science 2009;326:1216-9.
151. Shi Y, Massague J. Mechanisms of TGF-beta signaling from cell membrane to the nucleus. Cell 2003;113:685-700.
152. Mohammadi M, Olsen SK, Goetz R. A protein canyon in the FGF-FGF receptor dimer selects from an a la carte menu of heparan sulfate motifs. Curr Opin Struct Biol 2005;15:506-16.
153. Schultz GS, Wysocki A. Interactions between extracellular matrix and growth factors in wound healing. Wound Repair Regen 2009;17:153-62.
154. Lu P, Takai K, Weaver VM, Werb Z. Extracellular matrix degradation and remodeling in development and disease. Cold Spring Harb Perspect Biol 2011;3.
155. Paszek MJ, Zahir N, Johnson KR, Lakins JN, Rozenberg GI, Gefen A, Reinhart-King CA, Margulies SS, Dembo M, Boettiger D, Hammer DA, Weaver VM. Tensional homeostasis and the malignant phenotype. Cancer Cell 2005;8:241-54.
156. Clarijs R, Ruiter DJ, De Waal RM. Pathophysiological implications of stroma pattern formation in uveal melanoma. J Cell Physiol 2003;194:267-71.
157. Liang Y, Diehn M, Bollen AW, Israel MA, Gupta N. Type I collagen is overexpressed in medulloblastoma as a component of tumor microenvironment. J Neurooncol 2008;86:133-41.
158. Tancred TM, Belch AR, Reiman T, Pilarski LM, Kirshner J. Altered expression of fibronectin and collagens I and IV in multiple myeloma and monoclonal gammopathy of undetermined significance. J Histochem Cytochem 2009;57:239-47.
159. Weinberg RA. The Biology of Cancer. Garland Science, 2007.
160. Levental KR, Yu H, Kass L, Lakins JN, Egeblad M, Erler JT, Fong SF, Csiszar K, Giaccia A, Weninger W, Yamauchi M, Gasser DL, Weaver VM. Matrix crosslinking forces tumor progression by enhancing integrin signaling. Cell 2009;139:891-906.
161. Egeblad M, Rasch MG, Weaver VM. Dynamic interplay between the collagen scaffold and tumor evolution. Curr Opin Cell Biol 2010;22:697-706.
162. Curino AC, Engelholm LH, Yamada SS, Holmbeck K, Lund LR, Molinolo AA, Behrendt N, Nielsen BS, Bugge TH. Intracellular collagen degradation mediated by uPARAP/Endo180 is a major pathway of extracellular matrix turnover during malignancy. J Cell Biol 2005;169:977-85.
163. Sabeh F, Ota I, Holmbeck K, Birkedal-Hansen H, Soloway P, Balbin M, Lopez-Otin C, Shapiro S, Inada M, Krane S, Allen E, Chung D, Weiss SJ. Tumor cell traffic through the extracellular matrix is controlled by the membrane-anchored collagenase MT1-MMP. J Cell Biol 2004;167:769-81.

164. Fridman R, Giaccone G, Kanemoto T, Martin GR, Gazdar AF, Mulshine JL. Reconstituted basement membrane (matrigel) and laminin can enhance the tumorigenicity and the drug resistance of small cell lung cancer cell lines. Proc Natl Acad Sci U S A 1990;87:6698-702.
165. Sethi T, Rintoul RC, Moore SM, MacKinnon AC, Salter D, Choo C, Chilvers ER, Dransfield I, Donnelly SC, Strieter R, Haslett C. Extracellular matrix proteins protect small cell lung cancer cells against apoptosis: a mechanism for small cell lung cancer growth and drug resistance in vivo. Nat Med 1999;5:662-8.
166. Armstrong T, Packham G, Murphy LB, Bateman AC, Conti JA, Fine DR, Johnson CD, Benyon RC, Iredale JP. Type I collagen promotes the malignant phenotype of pancreatic ductal adenocarcinoma. Clin Cancer Res 2004;10:7427-37.
167. Tanentzapf G, Devenport D, Godt D, Brown NH. Integrin-dependent anchoring of a stem-cell niche. Nat Cell Biol 2007;9:1413-8.
168. Garcion E, Halilagic A, Faissner A, ffrench-Constant C. Generation of an environmental niche for neural stem cell development by the extracellular matrix molecule tenascin C. Development 2004;131:3423-32.
169. Engler AJ, Sen S, Sweeney HL, Discher DE. Matrix elasticity directs stem cell lineage specification. Cell 2006;126:677-89.
170. Giraudo E, Inoue M, Hanahan D. An amino-bisphosphonate targets MMP-9-expressing macrophages and angiogenesis to impair cervical carcinogenesis. J Clin Invest 2004;114:623-33.
171. Bignon M, Pichol-Thievend C, Hardouin J, Malbouyres M, Brechot N, Nasciutti L, Barret A, Teillon J, Guillon E, Etienne E, Caron M, Joubert-Caron R, Monnot C, Ruggiero F, Muller L, Germain S. Lysyl oxidase-like protein-2 regulates sprouting angiogenesis and type IV collagen assembly in the endothelial basement membrane. Blood 2011;118:3979-89.
172. Adair-Kirk TL, Senior RM. Fragments of extracellular matrix as mediators of inflammation. Int J Biochem Cell Biol 2008;40:1101-10.
173. Adler B, Ashkar S, Cantor H, Weber GF. Costimulation by extracellular matrix proteins determines the response to TCR ligation. Cell Immunol 2001;210:30-40.
174. Kaplan G. In vitro differentiation of human monocytes. Monocytes cultured on glass are cytotoxic to tumor cells but monocytes cultured on collagen are not. J Exp Med 1983;157:2061-72.
175. Meyaard L. The inhibitory collagen receptor LAIR-1 (CD305). J Leukoc Biol 2008;83:799-803.
176. Tarin D, Croft CB. Ultrastructural features of wound healing in mouse skin. J Anat 1969;105:189-90.
177. Chang HY, Chi JT, Dudoit S, Bondre C, van de Rijn M, Botstein D, Brown PO. Diversity, topographic differentiation, and positional memory in human fibroblasts. Proc Natl Acad Sci U S A 2002;99:12877-82.
178. Morgan MR, Humphries MJ, Bass MD. Synergistic control of cell adhesion by integrins and syndecans. Nat Rev Mol Cell Biol 2007;8:957-69.
179. Kalluri R, Zeisberg M. Fibroblasts in cancer. Nat Rev Cancer 2006;6:392-401.

180. Tomasek JJ, Gabbiani G, Hinz B, Chaponnier C, Brown RA. Myofibroblasts and mechano-regulation of connective tissue remodelling. Nat Rev Mol Cell Biol 2002;3:349-63.
181. McAnulty RJ. Fibroblasts and myofibroblasts: their source, function and role in disease. Int J Biochem Cell Biol 2007;39:666-71.
182. Reed RK, Berg A, Gjerde EA, Rubin K. Control of interstitial fluid pressure: role of beta1-integrins. Semin Nephrol 2001;21:222-30.
183. Heldin CH, Rubin K, Pietras K, Ostman A. High interstitial fluid pressure - an obstacle in cancer therapy. Nat Rev Cancer 2004;4:806-13.
184. Costea DE, Loro LL, Dimba EA, Vintermyr OK, Johannessen AC. Crucial effects of fibroblasts and keratinocyte growth factor on morphogenesis of reconstituted human oral epithelium. J Invest Dermatol 2003;121:1479-86.
185. Kuperwasser C, Chavarria T, Wu M, Magrane G, Gray JW, Carey L, Richardson A, Weinberg RA. Reconstruction of functionally normal and malignant human breast tissues in mice. Proc Natl Acad Sci U S A 2004;101:4966-71.
186. Ina K, Kitamura H, Tatsukawa S, Fujikura Y. Significance of alpha-SMA in myofibroblasts emerging in renal tubulointerstitial fibrosis. Histol Histopathol 2011;26:855-66.
187. Leask A, Abraham DJ. TGF-beta signaling and the fibrotic response. FASEB J 2004;18:816-27.
188. Werner S, Grose R. Regulation of wound healing by growth factors and cytokines. Physiol Rev 2003;83:835-70.
189. Powell DW, Mifflin RC, Valentich JD, Crowe SE, Saada JI, West AB. Myofibroblasts. I. Paracrine cells important in health and disease. Am J Physiol 1999;277:C1-9.
190. Gold LI. The role for transforming growth factor-beta (TGF-beta) in human cancer. Crit Rev Oncog 1999;10:303-60.
191. Tettamanti G, Grimaldi A, Rinaldi L, Arnaboldi F, Congiu T, Valvassori R, de Eguileor M. The multifunctional role of fibroblasts during wound healing in Hirudo medicinalis (Annelida, Hirudinea). Biol Cell 2004;96:443-55.
192. Montesano R, Orci L. Transforming growth factor beta stimulates collagen-matrix contraction by fibroblasts: implications for wound healing. Proc Natl Acad Sci U S A 1988;85:4894-7.
193. Werner S, Krieg T, Smola H. Keratinocyte-fibroblast interactions in wound healing. J Invest Dermatol 2007;127:998-1008.
194. Iredale JP, Benyon RC, Pickering J, McCullen M, Northrop M, Pawley S, Hovell C, Arthur MJ. Mechanisms of spontaneous resolution of rat liver fibrosis. Hepatic stellate cell apoptosis and reduced hepatic expression of metalloproteinase inhibitors. J Clin Invest 1998;102:538-49.
195. Kisseleva T, Cong M, Paik Y, Scholten D, Jiang C, Benner C, Iwaisako K, Moore-Morris T, Scott B, Tsukamoto H, Evans SM, Dillmann W, Glass CK, Brenner DA. Myofibroblasts revert to an inactive phenotype during regression of liver fibrosis. Proc Natl Acad Sci U S A;109:9448-53.
196. Krizhanovsky V, Yon M, Dickins RA, Hearn S, Simon J, Miething C, Yee H, Zender L, Lowe SW. Senescence of activated stellate cells limits liver fibrosis. Cell 2008;134:657-67.

197. Wang J, Dodd C, Shankowsky HA, Scott PG, Tredget EE. Deep dermal fibroblasts contribute to hypertrophic scarring. Lab Invest 2008;88:1278-90.
198. Zhou Y, Huang X, Hecker L, Kurundkar D, Kurundkar A, Liu H, Jin TH, Desai L, Bernard K, Thannickal VJ. Inhibition of mechanosensitive signaling in myofibroblasts ameliorates experimental pulmonary fibrosis. J Clin Invest 2013;123:1096-108.
199. Sappino AP, Skalli O, Jackson B, Schurch W, Gabbiani G. Smooth-muscle differentiation in stromal cells of malignant and non-malignant breast tissues. Int J Cancer 1988;41:707-12.
200. Allinen M, Beroukhim R, Cai L, Brennan C, Lahti-Domenici J, Huang H, Porter D, Hu M, Chin L, Richardson A, Schnitt S, Sellers WR, Polyak K. Molecular characterization of the tumor microenvironment in breast cancer. Cancer Cell 2004;6:17-32.
201. Maffini MV, Soto AM, Calabro JM, Ucci AA, Sonnenschein C. The stroma as a crucial target in rat mammary gland carcinogenesis. J Cell Sci 2004;117:1495-502.
202. Micke P, Ostman A. Tumour-stroma interaction: cancer-associated fibroblasts as novel targets in anti-cancer therapy? Lung Cancer 2004;45 Suppl 2:S163-75.
203. Tlsty TD, Hein PW. Know thy neighbor: stromal cells can contribute oncogenic signals. Curr Opin Genet Dev 2001;11:54-9.
204. Sirica AE. The role of cancer-associated myofibroblasts in intrahepatic cholangiocarcinoma. Nat Rev Gastroenterol Hepatol 2011;9:44-54.
205. Camps JL, Chang SM, Hsu TC, Freeman MR, Hong SJ, Zhau HE, von Eschenbach AC, Chung LW. Fibroblast-mediated acceleration of human epithelial tumor growth in vivo. Proc Natl Acad Sci U S A 1990;87:75-9.
206. Picard O, Rolland Y, Poupon MF. Fibroblast-dependent tumorigenicity of cells in nude mice: implication for implantation of metastases. Cancer Res 1986;46:3290-4.
207. Olumi AF, Grossfeld GD, Hayward SW, Carroll PR, Tlsty TD, Cunha GR. Carcinoma-associated fibroblasts direct tumor progression of initiated human prostatic epithelium. Cancer Res 1999;59:5002-11.
208. Orimo A, Gupta PB, Sgroi DC, Arenzana-Seisdedos F, Delaunay T, Naeem R, Carey VJ, Richardson AL, Weinberg RA. Stromal fibroblasts present in invasive human breast carcinomas promote tumor growth and angiogenesis through elevated SDF-1/CXCL12 secretion. Cell 2005;121:335-48.
209. Tanaka S, Sugimachi K, Kameyama T, Maehara S, Shirabe K, Shimada M, Wands JR, Maehara Y. Human WISP1v, a member of the CCN family, is associated with invasive cholangiocarcinoma. Hepatology 2003;37:1122-9.
210. Faouzi S, Le Bail B, Neaud V, Boussarie L, Saric J, Bioulac-Sage P, Balabaud C, Rosenbaum J. Myofibroblasts are responsible for collagen synthesis in the stroma of human hepatocellular carcinoma: an in vivo and in vitro study. J Hepatol 1999;30:275-84.
211. Boire A, Covic L, Agarwal A, Jacques S, Sherifi S, Kuliopulos A. PAR1 is a matrix metalloprotease-1 receptor that promotes invasion and tumorigenesis of breast cancer cells. Cell 2005;120:303-13.
212. Lochter A, Galosy S, Muschler J, Freedman N, Werb Z, Bissell MJ. Matrix metalloproteinase stromelysin-1 triggers a cascade of molecular alterations

that leads to stable epithelial-to-mesenchymal conversion and a premalignant phenotype in mammary epithelial cells. J Cell Biol 1997;139:1861-72.
213. Cohen SJ, Alpaugh RK, Palazzo I, Meropol NJ, Rogatko A, Xu Z, Hoffman JP, Weiner LM, Cheng JD. Fibroblast activation protein and its relationship to clinical outcome in pancreatic adenocarcinoma. Pancreas 2008;37:154-8.
214. Rasanen K, Vaheri A. Activation of fibroblasts in cancer stroma. Exp Cell Res 2010;316:2713-22.
215. Liao D, Luo Y, Markowitz D, Xiang R, Reisfeld RA. Cancer associated fibroblasts promote tumor growth and metastasis by modulating the tumor immune microenvironment in a 4T1 murine breast cancer model. PLoS One 2009;4:e7965.
216. Grum-Schwensen B, Klingelhofer J, Berg CH, El-Naaman C, Grigorian M, Lukanidin E, Ambartsumian N. Suppression of tumor development and metastasis formation in mice lacking the S100A4(mts1) gene. Cancer Res 2005;65:3772-80.
217. Kraman M, Bambrough PJ, Arnold JN, Roberts EW, Magiera L, Jones JO, Gopinathan A, Tuveson DA, Fearon DT. Suppression of antitumor immunity by stromal cells expressing fibroblast activation protein-alpha. Science 2010;330:827-30.
218. De Monte L, Reni M, Tassi E, Clavenna D, Papa I, Recalde H, Braga M, Di Carlo V, Doglioni C, Protti MP. Intratumor T helper type 2 cell infiltrate correlates with cancer-associated fibroblast thymic stromal lymphopoietin production and reduced survival in pancreatic cancer. J Exp Med 2011;208:469-78.
219. Valtieri M, Sorrentino A. The mesenchymal stromal cell contribution to homeostasis. J Cell Physiol 2008;217:296-300.
220. Keating A. Mesenchymal stromal cells: new directions. Cell Stem Cell 2012;10:709-16.
221. Crisan M, Yap S, Casteilla L, Chen CW, Corselli M, Park TS, Andriolo G, Sun B, Zheng B, Zhang L, Norotte C, Teng PN, Traas J, Schugar R, Deasy BM, Badylak S, Buhring HJ, Giacobino JP, Lazzari L, Huard J, Peault B. A perivascular origin for mesenchymal stem cells in multiple human organs. Cell Stem Cell 2008;3:301-13.
222. Lee CC, Christensen JE, Yoder MC, Tarantal AF. Clonal analysis and hierarchy of human bone marrow mesenchymal stem and progenitor cells. Exp Hematol 2010;38:46-54.
223. Bergfeld SA, DeClerck YA. Bone marrow-derived mesenchymal stem cells and the tumor microenvironment. Cancer Metastasis Rev 2010;29:249-61.
224. Pittenger MF, Mackay AM, Beck SC, Jaiswal RK, Douglas R, Mosca JD, Moorman MA, Simonetti DW, Craig S, Marshak DR. Multilineage potential of adult human mesenchymal stem cells. Science 1999;284:143-7.
225. Roche S, Delorme B, Oostendorp RA, Barbet R, Caton D, Noel D, Boumediene K, Papadaki HA, Cousin B, Crozet C, Milhavet O, Casteilla L, Hatzfeld J, Jorgensen C, Charbord P, Lehmann S. Comparative proteomic analysis of human mesenchymal and embryonic stem cells: towards the definition of a mesenchymal stem cell proteomic signature. Proteomics 2009;9:223-32.

226. Direkze NC, Forbes SJ, Brittan M, Hunt T, Jeffery R, Preston SL, Poulsom R, Hodivala-Dilke K, Alison MR, Wright NA. Multiple organ engraftment by bone-marrow-derived myofibroblasts and fibroblasts in bone-marrow-transplanted mice. Stem Cells 2003;21:514-20.
227. Ishii G, Sangai T, Ito T, Hasebe T, Endoh Y, Sasaki H, Harigaya K, Ochiai A. In vivo and in vitro characterization of human fibroblasts recruited selectively into human cancer stroma. Int J Cancer 2005;117:212-20.
228. Direkze NC, Hodivala-Dilke K, Jeffery R, Hunt T, Poulsom R, Oukrif D, Alison MR, Wright NA. Bone marrow contribution to tumor-associated myofibroblasts and fibroblasts. Cancer Res 2004;64:8492-5.
229. Thiery JP. Epithelial-mesenchymal transitions in tumour progression. Nat Rev Cancer 2002;2:442-54.
230. Sun S, Ning X, Zhang Y, Lu Y, Nie Y, Han S, Liu L, Du R, Xia L, He L, Fan D. Hypoxia-inducible factor-1alpha induces Twist expression in tubular epithelial cells subjected to hypoxia, leading to epithelial-to-mesenchymal transition. Kidney Int 2009;75:1278-87.
231. Siegel PM, Massague J. Cytostatic and apoptotic actions of TGF-beta in homeostasis and cancer. Nat Rev Cancer 2003;3:807-21.
232. Kurose K, Gilley K, Matsumoto S, Watson PH, Zhou XP, Eng C. Frequent somatic mutations in PTEN and TP53 are mutually exclusive in the stroma of breast carcinomas. Nat Genet 2002;32:355-7.
233. Petersen OW, Nielsen HL, Gudjonsson T, Villadsen R, Rank F, Niebuhr E, Bissell MJ, Ronnov-Jessen L. Epithelial to mesenchymal transition in human breast cancer can provide a nonmalignant stroma. Am J Pathol 2003;162:391-402.
234. Gordon S, Martinez FO. Alternative activation of macrophages: mechanism and functions. Immunity 2010;32:593-604.
235. Murray PJ, Wynn TA. Protective and pathogenic functions of macrophage subsets. Nat Rev Immunol 2011;11:723-37.
236. Ruffell B, Affara NI, Coussens LM. Differential macrophage programming in the tumor microenvironment. Trends Immunol 2012;33:119-26.
237. Martinez FO, Gordon S, Locati M, Mantovani A. Transcriptional profiling of the human monocyte-to-macrophage differentiation and polarization: new molecules and patterns of gene expression. J Immunol 2006;177:7303-11.
238. Nathan CF, Murray HW, Wiebe ME, Rubin BY. Identification of interferon-gamma as the lymphokine that activates human macrophage oxidative metabolism and antimicrobial activity. J Exp Med 1983;158:670-89.
239. Adams DO. Molecular interactions in macrophage activation. Immunol Today 1989;10:33-5.
240. Englaro W, Bahadoran P, Bertolotto C, Busca R, Derijard B, Livolsi A, Peyron JF, Ortonne JP, Ballotti R. Tumor necrosis factor alpha-mediated inhibition of melanogenesis is dependent on nuclear factor kappa B activation. Oncogene 1999;18:1553-9.
241. Shi Y, Liu CH, Roberts AI, Das J, Xu G, Ren G, Zhang Y, Zhang L, Yuan ZR, Tan HS, Das G, Devadas S. Granulocyte-macrophage colony-stimulating factor (GM-CSF) and T-cell responses: what we do and don't know. Cell Res 2006;16:126-33.

242. Mantovani A, Sica A, Locati M. New vistas on macrophage differentiation and activation. Eur J Immunol 2007;37:14-6.
243. Lawrence T, Natoli G. Transcriptional regulation of macrophage polarization: enabling diversity with identity. Nat Rev Immunol 2011;11:750-61.
244. Verreck FA, de Boer T, Langenberg DM, Hoeve MA, Kramer M, Vaisberg E, Kastelein R, Kolk A, de Waal-Malefyt R, Ottenhoff TH. Human IL-23-producing type 1 macrophages promote but IL-10-producing type 2 macrophages subvert immunity to (myco)bacteria. Proc Natl Acad Sci U S A 2004;101:4560-5.
245. Sindrilaru A, Peters T, Wieschalka S, Baican C, Baican A, Peter H, Hainzl A, Schatz S, Qi Y, Schlecht A, Weiss JM, Wlaschek M, Sunderkotter C, Scharffetter-Kochanek K. An unrestrained proinflammatory M1 macrophage population induced by iron impairs wound healing in humans and mice. J Clin Invest 2011;121:985-97.
246. Szekanecz Z, Koch AE. Macrophages and their products in rheumatoid arthritis. Curr Opin Rheumatol 2007;19:289-95.
247. Mosser DM, Edwards JP. Exploring the full spectrum of macrophage activation. Nat Rev Immunol 2008;8:958-69.
248. Xiao W, Hong H, Kawakami Y, Lowell CA, Kawakami T. Regulation of myeloproliferation and M2 macrophage programming in mice by Lyn/Hck, SHIP, and Stat5. J Clin Invest 2008;118:924-34.
249. Arnold L, Henry A, Poron F, Baba-Amer Y, van Rooijen N, Plonquet A, Gherardi RK, Chazaud B. Inflammatory monocytes recruited after skeletal muscle injury switch into antiinflammatory macrophages to support myogenesis. J Exp Med 2007;204:1057-69.
250. Martinez FO, Helming L, Gordon S. Alternative activation of macrophages: an immunologic functional perspective. Annu Rev Immunol 2009;27:451-83.
251. Lacey DC, Achuthan A, Fleetwood AJ, Dinh H, Roiniotis J, Scholz GM, Chang MW, Beckman SK, Cook AD, Hamilton JA. Defining GM-CSF- and macrophage-CSF-dependent macrophage responses by in vitro models. J Immunol 2012;188:5752-65.
252. Fleetwood AJ, Lawrence T, Hamilton JA, Cook AD. Granulocyte-macrophage colony-stimulating factor (CSF) and macrophage CSF-dependent macrophage phenotypes display differences in cytokine profiles and transcription factor activities: implications for CSF blockade in inflammation. J Immunol 2007;178:5245-52.
253. Barron L, Wynn TA. Fibrosis is regulated by Th2 and Th17 responses and by dynamic interactions between fibroblasts and macrophages. Am J Physiol Gastrointest Liver Physiol 2011;300:G723-8.
254. Murray LA, Chen Q, Kramer MS, Hesson DP, Argentieri RL, Peng X, Gulati M, Homer RJ, Russell T, van Rooijen N, Elias JA, Hogaboam CM, Herzog EL. TGF-beta driven lung fibrosis is macrophage dependent and blocked by Serum amyloid P. Int J Biochem Cell Biol 2011;43:154-62.
255. Murray LA, Rosada R, Moreira AP, Joshi A, Kramer MS, Hesson DP, Argentieri RL, Mathai S, Gulati M, Herzog EL, Hogaboam CM. Serum amyloid P therapeutically attenuates murine bleomycin-induced pulmonary fibrosis via its effects on macrophages. PLoS One 2010;5:e9683.

256. Vidal B, Serrano AL, Tjwa M, Suelves M, Ardite E, De Mori R, Baeza-Raja B, Martinez de Lagran M, Lafuste P, Ruiz-Bonilla V, Jardi M, Gherardi R, Christov C, Dierssen M, Carmeliet P, Degen JL, Dewerchin M, Munoz-Canoves P. Fibrinogen drives dystrophic muscle fibrosis via a TGFbeta/alternative macrophage activation pathway. Genes Dev 2008;22:1747-52.
257. Kerr-Valentic MA, Samimi K, Rohlen BH, Agarwal JP, Rockwell WB. Marjolin's ulcer: modern analysis of an ancient problem. Plast Reconstr Surg 2009;123:184-91.
258. Hartnett L, Egan LJ. Inflammation, DNA methylation and colitis-associated cancer. Carcinogenesis 2012;33:723-31.
259. Kuper H, Adami HO, Trichopoulos D. Infections as a major preventable cause of human cancer. J Intern Med 2000;248:171-83.
260. Ernst PB, Gold BD. The disease spectrum of Helicobacter pylori: the immunopathogenesis of gastroduodenal ulcer and gastric cancer. Annu Rev Microbiol 2000;54:615-40.
261. Moghaddam SJ, Li H, Cho SN, Dishop MK, Wistuba, II, Ji L, Kurie JM, Dickey BF, Demayo FJ. Promotion of lung carcinogenesis by chronic obstructive pulmonary disease-like airway inflammation in a K-ras-induced mouse model. Am J Respir Cell Mol Biol 2009;40:443-53.
262. Pikarsky E, Porat RM, Stein I, Abramovitch R, Amit S, Kasem S, Gutkovich-Pyest E, Urieli-Shoval S, Galun E, Ben-Neriah Y. NF-kappaB functions as a tumour promoter in inflammation-associated cancer. Nature 2004;431:461-6.
263. Greten FR, Eckmann L, Greten TF, Park JM, Li ZW, Egan LJ, Kagnoff MF, Karin M. IKKbeta links inflammation and tumorigenesis in a mouse model of colitis-associated cancer. Cell 2004;118:285-96.
264. Qian BZ, Pollard JW. Macrophage diversity enhances tumor progression and metastasis. Cell 2010;141:39-51.
265. Fidler IJ, Schroit AJ. Recognition and destruction of neoplastic cells by activated macrophages: discrimination of altered self. Biochim Biophys Acta 1988;948:151-73.
266. Klimp AH, de Vries EG, Scherphof GL, Daemen T. A potential role of macrophage activation in the treatment of cancer. Crit Rev Oncol Hematol 2002;44:143-61.
267. Romieu-Mourez R, Solis M, Nardin A, Goubau D, Baron-Bodo V, Lin R, Massie B, Salcedo M, Hiscott J. Distinct roles for IFN regulatory factor (IRF)-3 and IRF-7 in the activation of antitumor properties of human macrophages. Cancer Res 2006;66:10576-85.
268. Pang B, Zhou X, Yu H, Dong M, Taghizadeh K, Wishnok JS, Tannenbaum SR, Dedon PC. Lipid peroxidation dominates the chemistry of DNA adduct formation in a mouse model of inflammation. Carcinogenesis 2007;28:1807-13.
269. Meira LB, Bugni JM, Green SL, Lee CW, Pang B, Borenshtein D, Rickman BH, Rogers AB, Moroski-Erkul CA, McFaline JL, Schauer DB, Dedon PC, Fox JG, Samson LD. DNA damage induced by chronic inflammation contributes to colon carcinogenesis in mice. J Clin Invest 2008;118:2516-25.
270. Deng L, Zhou JF, Sellers RS, Li JF, Nguyen AV, Wang Y, Orlofsky A, Liu Q, Hume DA, Pollard JW, Augenlicht L, Lin EY. A novel mouse model of

inflammatory bowel disease links mammalian target of rapamycin-dependent hyperproliferation of colonic epithelium to inflammation-associated tumorigenesis. Am J Pathol 2010;176:952-67.
271. Naugler WE, Sakurai T, Kim S, Maeda S, Kim K, Elsharkawy AM, Karin M. Gender disparity in liver cancer due to sex differences in MyD88-dependent IL-6 production. Science 2007;317:121-4.
272. Mantovani A, Sozzani S, Locati M, Allavena P, Sica A. Macrophage polarization: tumor-associated macrophages as a paradigm for polarized M2 mononuclear phagocytes. Trends Immunol 2002;23:549-55.
273. Saccani A, Schioppa T, Porta C, Biswas SK, Nebuloni M, Vago L, Bottazzi B, Colombo MP, Mantovani A, Sica A. p50 nuclear factor-kappaB overexpression in tumor-associated macrophages inhibits M1 inflammatory responses and antitumor resistance. Cancer Res 2006;66:11432-40.
274. Doedens AL, Stockmann C, Rubinstein MP, Liao D, Zhang N, DeNardo DG, Coussens LM, Karin M, Goldrath AW, Johnson RS. Macrophage expression of hypoxia-inducible factor-1 alpha suppresses T-cell function and promotes tumor progression. Cancer Res 2010;70:7465-75.
275. Zeh HJ, 3rd, Lotze MT. Addicted to death: invasive cancer and the immune response to unscheduled cell death. J Immunother 2005;28:1-9.
276. Kuang DM, Wu Y, Chen N, Cheng J, Zhuang SM, Zheng L. Tumor-derived hyaluronan induces formation of immunosuppressive macrophages through transient early activation of monocytes. Blood 2007;110:587-95.
277. Lin EY, Li JF, Gnatovskiy L, Deng Y, Zhu L, Grzesik DA, Qian H, Xue XN, Pollard JW. Macrophages regulate the angiogenic switch in a mouse model of breast cancer. Cancer Res 2006;66:11238-46.
278. Zeisberger SM, Odermatt B, Marty C, Zehnder-Fjallman AH, Ballmer-Hofer K, Schwendener RA. Clodronate-liposome-mediated depletion of tumour-associated macrophages: a new and highly effective antiangiogenic therapy approach. Br J Cancer 2006;95:272-81.
279. Lin EY, Li JF, Bricard G, Wang W, Deng Y, Sellers R, Porcelli SA, Pollard JW. Vascular endothelial growth factor restores delayed tumor progression in tumors depleted of macrophages. Mol Oncol 2007;1:288-302.
280. Stockmann C, Doedens A, Weidemann A, Zhang N, Takeda N, Greenberg JI, Cheresh DA, Johnson RS. Deletion of vascular endothelial growth factor in myeloid cells accelerates tumorigenesis. Nature 2008;456:814-8.
281. Condeelis J, Pollard JW. Macrophages: obligate partners for tumor cell migration, invasion, and metastasis. Cell 2006;124:263-6.
282. Kubota Y, Takubo K, Shimizu T, Ohno H, Kishi K, Shibuya M, Saya H, Suda T. M-CSF inhibition selectively targets pathological angiogenesis and lymphangiogenesis. J Exp Med 2009;206:1089-102.
283. Aharinejad S, Paulus P, Sioud M, Hofmann M, Zins K, Schafer R, Stanley ER, Abraham D. Colony-stimulating factor-1 blockade by antisense oligonucleotides and small interfering RNAs suppresses growth of human mammary tumor xenografts in mice. Cancer Res 2004;64:5378-84.
284. Wyckoff J, Wang W, Lin EY, Wang Y, Pixley F, Stanley ER, Graf T, Pollard JW, Segall J, Condeelis J. A paracrine loop between tumor cells and macrophages is required for tumor cell migration in mammary tumors. Cancer Res 2004;64:7022-9.

285. DeNardo DG, Barreto JB, Andreu P, Vasquez L, Tawfik D, Kolhatkar N, Coussens LM. CD4(+) T cells regulate pulmonary metastasis of mammary carcinomas by enhancing protumor properties of macrophages. Cancer Cell 2009;16:91-102.
286. Hernandez L, Smirnova T, Kedrin D, Wyckoff J, Zhu L, Stanley ER, Cox D, Muller WJ, Pollard JW, Van Rooijen N, Segall JE. The EGF/CSF-1 paracrine invasion loop can be triggered by heregulin beta1 and CXCL12. Cancer Res 2009;69:3221-7.
287. Kessenbrock K, Plaks V, Werb Z. Matrix metalloproteinases: regulators of the tumor microenvironment. Cell 2010;141:52-67.
288. Mason SD, Joyce JA. Proteolytic networks in cancer. Trends Cell Biol 2011;21:228-37.
289. Sangaletti S, Di Carlo E, Gariboldi S, Miotti S, Cappetti B, Parenza M, Rumio C, Brekken RA, Chiodoni C, Colombo MP. Macrophage-derived SPARC bridges tumor cell-extracellular matrix interactions toward metastasis. Cancer Res 2008;68:9050-9.
290. Kaplan RN, Riba RD, Zacharoulis S, Bramley AH, Vincent L, Costa C, MacDonald DD, Jin DK, Shido K, Kerns SA, Zhu Z, Hicklin D, Wu Y, Port JL, Altorki N, Port ER, Ruggero D, Shmelkov SV, Jensen KK, Rafii S, Lyden D. VEGFR1-positive haematopoietic bone marrow progenitors initiate the pre-metastatic niche. Nature 2005;438:820-7.
291. Hiratsuka S, Watanabe A, Aburatani H, Maru Y. Tumour-mediated upregulation of chemoattractants and recruitment of myeloid cells predetermines lung metastasis. Nat Cell Biol 2006;8:1369-75.
292. Hiratsuka S, Nakamura K, Iwai S, Murakami M, Itoh T, Kijima H, Shipley JM, Senior RM, Shibuya M. MMP9 induction by vascular endothelial growth factor receptor-1 is involved in lung-specific metastasis. Cancer Cell 2002;2:289-300.
293. Qian B, Deng Y, Im JH, Muschel RJ, Zou Y, Li J, Lang RA, Pollard JW. A distinct macrophage population mediates metastatic breast cancer cell extravasation, establishment and growth. PLoS One 2009;4:e6562.
294. Kuang DM, Zhao Q, Peng C, Xu J, Zhang JP, Wu C, Zheng L. Activated monocytes in peritumoral stroma of hepatocellular carcinoma foster immune privilege and disease progression through PD-L1. J Exp Med 2009;206:1327-37.
295. Kryczek I, Zou L, Rodriguez P, Zhu G, Wei S, Mottram P, Brumlik M, Cheng P, Curiel T, Myers L, Lackner A, Alvarez X, Ochoa A, Chen L, Zou W. B7-H4 expression identifies a novel suppressive macrophage population in human ovarian carcinoma. J Exp Med 2006;203:871-81.
296. Curiel TJ, Coukos G, Zou L, Alvarez X, Cheng P, Mottram P, Evdemon-Hogan M, Conejo-Garcia JR, Zhang L, Burow M, Zhu Y, Wei S, Kryczek I, Daniel B, Gordon A, Myers L, Lackner A, Disis ML, Knutson KL, Chen L, Zou W. Specific recruitment of regulatory T cells in ovarian carcinoma fosters immune privilege and predicts reduced survival. Nat Med 2004;10:942-9.
297. Hagemann T, Lawrence T, McNeish I, Charles KA, Kulbe H, Thompson RG, Robinson SC, Balkwill FR. "Re-educating" tumor-associated macrophages by targeting NF-kappaB. J Exp Med 2008;205:1261-8.

298. Biswas SK, Gangi L, Paul S, Schioppa T, Saccani A, Sironi M, Bottazzi B, Doni A, Vincenzo B, Pasqualini F, Vago L, Nebuloni M, Mantovani A, Sica A. A distinct and unique transcriptional program expressed by tumor-associated macrophages (defective NF-kappaB and enhanced IRF-3/STAT1 activation). Blood 2006;107:2112-22.
299. Movahedi K, Laoui D, Gysemans C, Baeten M, Stange G, Van den Bossche J, Mack M, Pipeleers D, In't Veld P, De Baetselier P, Van Ginderachter JA. Different tumor microenvironments contain functionally distinct subsets of macrophages derived from Ly6C(high) monocytes. Cancer Res 2010;70:5728-39.
300. Lewis JS, Landers RJ, Underwood JC, Harris AL, Lewis CE. Expression of vascular endothelial growth factor by macrophages is up-regulated in poorly vascularized areas of breast carcinomas. J Pathol 2000;192:150-8.
301. Imtiyaz HZ, Williams EP, Hickey MM, Patel SA, Durham AC, Yuan LJ, Hammond R, Gimotty PA, Keith B, Simon MC. Hypoxia-inducible factor 2alpha regulates macrophage function in mouse models of acute and tumor inflammation. J Clin Invest 2010;120:2699-714.
302. Imtiyaz HZ, Simon MC. Hypoxia-inducible factors as essential regulators of inflammation. Curr Top Microbiol Immunol 2010;345:105-20.
303. Paez-Ribes M, Allen E, Hudock J, Takeda T, Okuyama H, Vinals F, Inoue M, Bergers G, Hanahan D, Casanovas O. Antiangiogenic therapy elicits malignant progression of tumors to increased local invasion and distant metastasis. Cancer Cell 2009;15:220-31.
304. Hanahan D, Weinberg RA. The hallmarks of cancer. Cell 2000;100:57-70.
305. Hanahan D, Weinberg RA. Hallmarks of cancer: the next generation. Cell 2011;144:646-74.
306. Okabe H, Beppu T, Hayashi H, Horino K, Masuda T, Komori H, Ishikawa S, Watanabe M, Takamori H, Iyama K, Baba H. Hepatic stellate cells may relate to progression of intrahepatic cholangiocarcinoma. Ann Surg Oncol 2009;16:2555-64.
307. Hasita H, Komohara Y, Okabe H, Masuda T, Ohnishi K, Lei XF, Beppu T, Baba H, Takeya M. Significance of alternatively activated macrophages in patients with intrahepatic cholangiocarcinoma. Cancer Sci 2010;101:1913-9.
308. Olive KP, Jacobetz MA, Davidson CJ, Gopinathan A, McIntyre D, Honess D, Madhu B, Goldgraben MA, Caldwell ME, Allard D, Frese KK, Denicola G, Feig C, Combs C, Winter SP, Ireland-Zecchini H, Reichelt S, Howat WJ, Chang A, Dhara M, Wang L, Ruckert F, Grutzmann R, Pilarsky C, Izeradjene K, Hingorani SR, Huang P, Davies SE, Plunkett W, Egorin M, Hruban RH, Whitebread N, McGovern K, Adams J, Iacobuzio-Donahue C, Griffiths J, Tuveson DA. Inhibition of Hedgehog signaling enhances delivery of chemotherapy in a mouse model of pancreatic cancer. Science 2009;324:1457-61.
309. Loeffler M, Kruger JA, Niethammer AG, Reisfeld RA. Targeting tumor-associated fibroblasts improves cancer chemotherapy by increasing intratumoral drug uptake. J Clin Invest 2006;116:1955-62.
310. Santos AM, Jung J, Aziz N, Kissil JL, Pure E. Targeting fibroblast activation protein inhibits tumor stromagenesis and growth in mice. J Clin Invest 2009;119:3613-25.

311. Tortora G, Ciardiello F, Gasparini G. Combined targeting of EGFR-dependent and VEGF-dependent pathways: rationale, preclinical studies and clinical applications. Nat Clin Pract Oncol 2008;5:521-30.
312. Kerbel RS. Tumor angiogenesis. N Engl J Med 2008;358:2039-49.
313. Ahn GO, Tseng D, Liao CH, Dorie MJ, Czechowicz A, Brown JM. Inhibition of Mac-1 (CD11b/CD18) enhances tumor response to radiation by reducing myeloid cell recruitment. Proc Natl Acad Sci U S A 2010;107:8363-8.
314. Beatty GL, Chiorean EG, Fishman MP, Saboury B, Teitelbaum UR, Sun W, Huhn RD, Song W, Li D, Sharp LL, Torigian DA, O'Dwyer PJ, Vonderheide RH. CD40 agonists alter tumor stroma and show efficacy against pancreatic carcinoma in mice and humans. Science 2011;331:1612-6.
315. Russo FP, Alison MR, Bigger BW, Amofah E, Florou A, Amin F, Bou-Gharios G, Jeffery R, Iredale JP, Forbes SJ. The bone marrow functionally contributes to liver fibrosis. Gastroenterology 2006;130:1807-21.
316. Duffield JS, Forbes SJ, Constandinou CM, Clay S, Partolina M, Vuthoori S, Wu S, Lang R, Iredale JP. Selective depletion of macrophages reveals distinct, opposing roles during liver injury and repair. J Clin Invest 2005;115:56-65.
317. Kidd S, Spaeth E, Dembinski JL, Dietrich M, Watson K, Klopp A, Battula VL, Weil M, Andreeff M, Marini FC. Direct evidence of mesenchymal stem cell tropism for tumor and wounding microenvironments using in vivo bioluminescent imaging. Stem Cells 2009;27:2614-23.
318. Goldstein RH, Reagan MR, Anderson K, Kaplan DL, Rosenblatt M. Human bone marrow-derived MSCs can home to orthotopic breast cancer tumors and promote bone metastasis. Cancer Res 2010;70:10044-50.
319. Direkze NC, Jeffery R, Hodivala-Dilke K, Hunt T, Playford RJ, Elia G, Poulsom R, Wright NA, Alison MR. Bone marrow-derived stromal cells express lineage-related messenger RNA species. Cancer Res 2006;66:1265-9.
320. Sangai T, Ishii G, Kodama K, Miyamoto S, Aoyagi Y, Ito T, Magae J, Sasaki H, Nagashima T, Miyazaki M, Ochiai A. Effect of differences in cancer cells and tumor growth sites on recruiting bone marrow-derived endothelial cells and myofibroblasts in cancer-induced stroma. Int J Cancer 2005;115:885-92.
321. Spaeth EL, Dembinski JL, Sasser AK, Watson K, Klopp A, Hall B, Andreeff M, Marini F. Mesenchymal stem cell transition to tumor-associated fibroblasts contributes to fibrovascular network expansion and tumor progression. PLoS One 2009;4:e4992.
322. Marx J. Cancer biology. All in the stroma: cancer's Cosa Nostra. Science 2008;320:38-41.
323. Khakoo AY, Pati S, Anderson SA, Reid W, Elshal MF, Rovira, II, Nguyen AT, Malide D, Combs CA, Hall G, Zhang J, Raffeld M, Rogers TB, Stetler-Stevenson W, Frank JA, Reitz M, Finkel T. Human mesenchymal stem cells exert potent antitumorigenic effects in a model of Kaposi's sarcoma. J Exp Med 2006;203:1235-47.
324. Dawson MR, Chae SS, Jain RK, Duda DG. Direct evidence for lineage-dependent effects of bone marrow stromal cells on tumor progression. Am J Cancer Res 2011;1:144-54.
325. Bierie B, Moses HL. Tumour microenvironment: TGFbeta: the molecular Jekyll and Hyde of cancer. Nat Rev Cancer 2006;6:506-20.

326. Suzuki K, Sun R, Origuchi M, Kanehira M, Takahata T, Itoh J, Umezawa A, Kijima H, Fukuda S, Saijo Y. Mesenchymal stromal cells promote tumor growth through the enhancement of neovascularization. Mol Med 2011;17:579-87.
327. Quante M, Tu SP, Tomita H, Gonda T, Wang SS, Takashi S, Baik GH, Shibata W, Diprete B, Betz KS, Friedman R, Varro A, Tycko B, Wang TC. Bone marrow-derived myofibroblasts contribute to the mesenchymal stem cell niche and promote tumor growth. Cancer Cell 2011;19:257-72.
328. Kidd S, Spaeth E, Watson K, Burks J, Lu H, Klopp A, Andreeff M, Marini FC. Origins of the tumor microenvironment: quantitative assessment of adipose-derived and bone marrow-derived stroma. PLoS One 2012;7:e30563.
329. Rafii S, Lyden D, Benezra R, Hattori K, Heissig B. Vascular and haematopoietic stem cells: novel targets for anti-angiogenesis therapy? Nat Rev Cancer 2002;2:826-35.
330. Nolan DJ, Ciarrocchi A, Mellick AS, Jaggi JS, Bambino K, Gupta S, Heikamp E, McDevitt MR, Scheinberg DA, Benezra R, Mittal V. Bone marrow-derived endothelial progenitor cells are a major determinant of nascent tumor neovascularization. Genes Dev 2007;21:1546-58.
331. Peters BA, Diaz LA, Polyak K, Meszler L, Romans K, Guinan EC, Antin JH, Myerson D, Hamilton SR, Vogelstein B, Kinzler KW, Lengauer C. Contribution of bone marrow-derived endothelial cells to human tumor vasculature. Nat Med 2005;11:261-2.
332. Pina Y, Boutrid H, Murray TG, Jager MJ, Cebulla CM, Schefler A, Ly LV, Alegret A, Celdran M, Feuer W, Jockovich ME. Impact of tumor-associated macrophages in LH(BETA)T(AG) mice on retinal tumor progression: relation to macrophage subtype. Invest Ophthalmol Vis Sci 2010;51:2671-7.
333. Houghton J, Stoicov C, Nomura S, Rogers AB, Carlson J, Li H, Cai X, Fox JG, Goldenring JR, Wang TC. Gastric cancer originating from bone marrow-derived cells. Science 2004;306:1568-71.
334. Li H, Fan X, Kovi RC, Jo Y, Moquin B, Konz R, Stoicov C, Kurt-Jones E, Grossman SR, Lyle S, Rogers AB, Montrose M, Houghton J. Spontaneous expression of embryonic factors and p53 point mutations in aged mesenchymal stem cells: a model of age-related tumorigenesis in mice. Cancer Res 2007;67:10889-98.
335. Bussolati B, Bruno S, Grange C, Ferrando U, Camussi G. Identification of a tumor-initiating stem cell population in human renal carcinomas. FASEB J 2008;22:3696-705.
336. Kubota K, Soeda J, Misawa R, Mihara M, Miwa S, Ise H, Takahashi M, Miyagawa S. Bone marrow-derived cells fuse with hepatic oval cells but are not involved in hepatic tumorigenesis in the choline-deficient ethionine-supplemented diet rat model. Carcinogenesis 2008;29:448-54.
337. Avital I, Moreira AL, Klimstra DS, Leversha M, Papadopoulos EB, Brennan M, Downey RJ. Donor-derived human bone marrow cells contribute to solid organ cancers developing after bone marrow transplantation. Stem Cells 2007;25:2903-9.
338. Janin A, Murata H, Leboeuf C, Cayuela JM, Gluckman E, Legres L, Desveaux A, Varna M, Ratajczak P, Soulier J, de The H, Bertheau P, Socie

G. Donor-derived oral squamous cell carcinoma after allogeneic bone marrow transplantation. Blood 2009;113:1834-40.
339. Ando S, Abe R, Sasaki M, Murata J, Inokuma D, Shimizu H. Bone marrow-derived cells are not the origin of the cancer stem cells in ultraviolet-induced skin cancer. Am J Pathol 2009;174:595-601.
340. Cogle CR, Theise ND, Fu D, Ucar D, Lee S, Guthrie SM, Lonergan J, Rybka W, Krause DS, Scott EW. Bone marrow contributes to epithelial cancers in mice and humans as developmental mimicry. Stem Cells 2007;25:1881-7.
341. Petersen BE, Bowen WC, Patrene KD, Mars WM, Sullivan AK, Murase N, Boggs SS, Greenberger JS, Goff JP. Bone marrow as a potential source of hepatic oval cells. Science 1999;284:1168-70.
342. Ishikawa H, Nakao K, Matsumoto K, Nishimura D, Ichikawa T, Hamasaki K, Eguchi K. Bone marrow engraftment in a rodent model of chemical carcinogenesis but no role in the histogenesis of hepatocellular carcinoma. Gut 2004;53:884-9.
343. Lorenzini S, Bird TG, Boulter L, Bellamy C, Samuel K, Aucott R, Clayton E, Andreone P, Bernardi M, Golding M, Alison MR, Iredale JP, Forbes SJ. Characterisation of a stereotypical cellular and extracellular adult liver progenitor cell niche in rodents and diseased human liver. Gut 2010;59:645-54.
344. Vig P, Russo FP, Edwards RJ, Tadrous PJ, Wright NA, Thomas HC, Alison MR, Forbes SJ. The sources of parenchymal regeneration after chronic hepatocellular liver injury in mice. Hepatology 2006;43:316-24.
345. Roskams T, Desmet V. Embryology of extra- and intrahepatic bile ducts, the ductal plate. Anat Rec (Hoboken) 2008;291:628-35.
346. Roskams TA, Theise ND, Balabaud C, Bhagat G, Bhathal PS, Bioulac-Sage P, Brunt EM, Crawford JM, Crosby HA, Desmet V, Finegold MJ, Geller SA, Gouw AS, Hytiroglou P, Knisely AS, Kojiro M, Lefkowitch JH, Nakanuma Y, Olynyk JK, Park YN, Portmann B, Saxena R, Scheuer PJ, Strain AJ, Thung SN, Wanless IR, West AB. Nomenclature of the finer branches of the biliary tree: canals, ductules, and ductular reactions in human livers. Hepatology 2004;39:1739-45.
347. Boulter L, Govaere O, Bird TG, Radulescu S, Ramachandran P, Pellicoro A, Ridgway RA, Seo SS, Spee B, Van Rooijen N, Sansom OJ, Iredale JP, Lowell S, Roskams T, Forbes SJ. Macrophage-derived Wnt opposes Notch signaling to specify hepatic progenitor cell fate in chronic liver disease. Nat Med 2012;18:572-9.
348. Lemmer ER, Vessey CJ, Gelderblom WC, Shephard EG, Van Schalkwyk DJ, Van Wijk RA, Marasas WF, Kirsch RE, Hall Pde L. Fumonisin B1-induced hepatocellular and cholangiocellular tumors in male Fischer 344 rats: potentiating effects of 2-acetylaminofluorene on oval cell proliferation and neoplastic development in a discontinued feeding study. Carcinogenesis 2004;25:1257-64.
349. Alison MR, Lovell MJ. Liver cancer: the role of stem cells. Cell Prolif 2005;38:407-21.
350. Durnez A, Verslype C, Nevens F, Fevery J, Aerts R, Pirenne J, Lesaffre E, Libbrecht L, Desmet V, Roskams T. The clinicopathological and prognostic

relevance of cytokeratin 7 and 19 expression in hepatocellular carcinoma. A possible progenitor cell origin. Histopathology 2006;49:138-51.
351. Ramalho FS, Ramalho LN, Della Porta L, Zucoloto S. Comparative immunohistochemical expression of p63 in human cholangiocarcinoma and hepatocellular carcinoma. J Gastroenterol Hepatol 2006;21:1276-80.
352. Houghton J, Morozov A, Smirnova I, Wang TC. Stem cells and cancer. Semin Cancer Biol 2007;17:191-203.
353. Hamburger A, Salmon SE. Primary bioassay of human myeloma stem cells. J Clin Invest 1977;60:846-54.
354. Hamburger AW, Salmon SE. Primary bioassay of human tumor stem cells. Science 1977;197:461-3.
355. Clarke MF, Dick JE, Dirks PB, Eaves CJ, Jamieson CH, Jones DL, Visvader J, Weissman IL, Wahl GM. Cancer stem cells--perspectives on current status and future directions: AACR Workshop on cancer stem cells. Cancer Res 2006;66:9339-44.
356. Frank NY, Schatton T, Frank MH. The therapeutic promise of the cancer stem cell concept. J Clin Invest 2010;120:41-50.
357. Takebe N, Harris PJ, Warren RQ, Ivy SP. Targeting cancer stem cells by inhibiting Wnt, Notch, and Hedgehog pathways. Nat Rev Clin Oncol 2011;8:97-106.
358. Hermann PC, Huber SL, Herrler T, Aicher A, Ellwart JW, Guba M, Bruns CJ, Heeschen C. Distinct populations of cancer stem cells determine tumor growth and metastatic activity in human pancreatic cancer. Cell Stem Cell 2007;1:313-23.
359. O'Brien CA, Pollett A, Gallinger S, Dick JE. A human colon cancer cell capable of initiating tumour growth in immunodeficient mice. Nature 2007;445:106-10.
360. Singh SK, Hawkins C, Clarke ID, Squire JA, Bayani J, Hide T, Henkelman RM, Cusimano MD, Dirks PB. Identification of human brain tumour initiating cells. Nature 2004;432:396-401.
361. Al-Hajj M, Wicha MS, Benito-Hernandez A, Morrison SJ, Clarke MF. Prospective identification of tumorigenic breast cancer cells. Proc Natl Acad Sci U S A 2003;100:3983-8.
362. Dalerba P, Dylla SJ, Park IK, Liu R, Wang X, Cho RW, Hoey T, Gurney A, Huang EH, Simeone DM, Shelton AA, Parmiani G, Castelli C, Clarke MF. Phenotypic characterization of human colorectal cancer stem cells. Proc Natl Acad Sci U S A 2007;104:10158-63.
363. Li C, Heidt DG, Dalerba P, Burant CF, Zhang L, Adsay V, Wicha M, Clarke MF, Simeone DM. Identification of pancreatic cancer stem cells. Cancer Res 2007;67:1030-7.
364. Goodell MA, Rosenzweig M, Kim H, Marks DF, DeMaria M, Paradis G, Grupp SA, Sieff CA, Mulligan RC, Johnson RP. Dye efflux studies suggest that hematopoietic stem cells expressing low or undetectable levels of CD34 antigen exist in multiple species. Nat Med 1997;3:1337-45.
365. Hirschmann-Jax C, Foster AE, Wulf GG, Nuchtern JG, Jax TW, Gobel U, Goodell MA, Brenner MK. A distinct "side population" of cells with high drug efflux capacity in human tumor cells. Proc Natl Acad Sci U S A 2004;101:14228-33.

366. Zhou S, Schuetz JD, Bunting KD, Colapietro AM, Sampath J, Morris JJ, Lagutina I, Grosveld GC, Osawa M, Nakauchi H, Sorrentino BP. The ABC transporter Bcrp1/ABCG2 is expressed in a wide variety of stem cells and is a molecular determinant of the side-population phenotype. Nat Med 2001;7:1028-34.
367. Chiba T, Kita K, Zheng YW, Yokosuka O, Saisho H, Iwama A, Nakauchi H, Taniguchi H. Side population purified from hepatocellular carcinoma cells harbors cancer stem cell-like properties. Hepatology 2006;44:240-51.
368. Ho MM, Ng AV, Lam S, Hung JY. Side population in human lung cancer cell lines and tumors is enriched with stem-like cancer cells. Cancer Res 2007;67:4827-33.
369. Wang J, Guo LP, Chen LZ, Zeng YX, Lu SH. Identification of cancer stem cell-like side population cells in human nasopharyngeal carcinoma cell line. Cancer Res 2007;67:3716-24.
370. Kondo T, Setoguchi T, Taga T. Persistence of a small subpopulation of cancer stem-like cells in the C6 glioma cell line. Proc Natl Acad Sci U S A 2004;101:781-6.
371. Schatton T, Murphy GF, Frank NY, Yamaura K, Waaga-Gasser AM, Gasser M, Zhan Q, Jordan S, Duncan LM, Weishaupt C, Fuhlbrigge RC, Kupper TS, Sayegh MH, Frank MH. Identification of cells initiating human melanomas. Nature 2008;451:345-9.
372. van Rhenen A, Feller N, Kelder A, Westra AH, Rombouts E, Zweegman S, van der Pol MA, Waisfisz Q, Ossenkoppele GJ, Schuurhuis GJ. High stem cell frequency in acute myeloid leukemia at diagnosis predicts high minimal residual disease and poor survival. Clin Cancer Res 2005;11:6520-7.
373. Zhou BB, Zhang H, Damelin M, Geles KG, Grindley JC, Dirks PB. Tumour-initiating cells: challenges and opportunities for anticancer drug discovery. Nat Rev Drug Discov 2009;8:806-23.
374. Li X, Lewis MT, Huang J, Gutierrez C, Osborne CK, Wu MF, Hilsenbeck SG, Pavlick A, Zhang X, Chamness GC, Wong H, Rosen J, Chang JC. Intrinsic resistance of tumorigenic breast cancer cells to chemotherapy. J Natl Cancer Inst 2008;100:672-9.
375. Yang ZF, Ho DW, Ng MN, Lau CK, Yu WC, Ngai P, Chu PW, Lam CT, Poon RT, Fan ST. Significance of CD90+ cancer stem cells in human liver cancer. Cancer Cell 2008;13:153-66.
376. Bao S, Wu Q, Li Z, Sathornsumetee S, Wang H, McLendon RE, Hjelmeland AB, Rich JN. Targeting cancer stem cells through L1CAM suppresses glioma growth. Cancer Res 2008;68:6043-8.
377. Chan KS, Espinosa I, Chao M, Wong D, Ailles L, Diehn M, Gill H, Presti J, Jr., Chang HY, van de Rijn M, Shortliffe L, Weissman IL. Identification, molecular characterization, clinical prognosis, and therapeutic targeting of human bladder tumor-initiating cells. Proc Natl Acad Sci U S A 2009;106:14016-21.
378. Lepourcelet M, Chen YN, France DS, Wang H, Crews P, Petersen F, Bruseo C, Wood AW, Shivdasani RA. Small-molecule antagonists of the oncogenic Tcf/beta-catenin protein complex. Cancer Cell 2004;5:91-102.
379. You L, He B, Xu Z, Uematsu K, Mazieres J, Fujii N, Mikami I, Reguart N, McIntosh JK, Kashani-Sabet M, McCormick F, Jablons DM. An anti-Wnt-2

monoclonal antibody induces apoptosis in malignant melanoma cells and inhibits tumor growth. Cancer Res 2004;64:5385-9.
380. Zhao C, Chen A, Jamieson CH, Fereshteh M, Abrahamsson A, Blum J, Kwon HY, Kim J, Chute JP, Rizzieri D, Munchhof M, VanArsdale T, Beachy PA, Reya T. Hedgehog signalling is essential for maintenance of cancer stem cells in myeloid leukaemia. Nature 2009;458:776-9.
381. van Es JH, van Gijn ME, Riccio O, van den Born M, Vooijs M, Begthel H, Cozijnsen M, Robine S, Winton DJ, Radtke F, Clevers H. Notch/gamma-secretase inhibition turns proliferative cells in intestinal crypts and adenomas into goblet cells. Nature 2005;435:959-63.
382. Bolos V, Grego-Bessa J, de la Pompa JL. Notch signaling in development and cancer. Endocr Rev 2007;28:339-63.
383. Mohr OL. Character Changes Caused by Mutation of an Entire Region of a Chromosome in Drosophila. Genetics 1919;4:275-82.
384. Koch U, Lehal R, Radtke F. Stem cells living with a Notch. Development 2013;140:689-704.
385. Lu J, Ye X, Fan F, Xia L, Bhattacharya R, Bellister S, Tozzi F, Sceusi E, Zhou Y, Tachibana I, Maru DM, Hawke DH, Rak J, Mani SA, Zweidler-McKay P, Ellis LM. Endothelial cells promote the colorectal cancer stem cell phenotype through a soluble form of Jagged-1. Cancer Cell 2013;23:171-85.
386. De Joussineau C, Soule J, Martin M, Anguille C, Montcourrier P, Alexandre D. Delta-promoted filopodia mediate long-range lateral inhibition in Drosophila. Nature 2003;426:555-9.
387. Yin L, Velazquez OC, Liu ZJ. Notch signaling: emerging molecular targets for cancer therapy. Biochem Pharmacol 2010;80:690-701.
388. D'Souza B, Miyamoto A, Weinmaster G. The many facets of Notch ligands. Oncogene 2008;27:5148-67.
389. Capaccione KM, Pine SR. The Notch signaling pathway as a mediator of tumor survival. Carcinogenesis 2013;34:1420-30.
390. Bray SJ. Notch signalling: a simple pathway becomes complex. Nat Rev Mol Cell Biol 2006;7:678-89.
391. Pece S, Confalonieri S, P RR, Di Fiore PP. NUMB-ing down cancer by more than just a NOTCH. Biochim Biophys Acta 2011;1815:26-43.
392. Brou C, Logeat F, Gupta N, Bessia C, LeBail O, Doedens JR, Cumano A, Roux P, Black RA, Israel A. A novel proteolytic cleavage involved in Notch signaling: the role of the disintegrin-metalloprotease TACE. Mol Cell 2000;5:207-16.
393. De Strooper B. Aph-1, Pen-2, and Nicastrin with Presenilin generate an active gamma-Secretase complex. Neuron 2003;38:9-12.
394. Oswald F, Winkler M, Cao Y, Astrahantseff K, Bourteele S, Knochel W, Borggrefe T. RBP-Jkappa/SHARP recruits CtIP/CtBP corepressors to silence Notch target genes. Mol Cell Biol 2005;25:10379-90.
395. High FA, Epstein JA. The multifaceted role of Notch in cardiac development and disease. Nat Rev Genet 2008;9:49-61.
396. Jarriault S, Le Bail O, Hirsinger E, Pourquie O, Logeat F, Strong CF, Brou C, Seidah NG, Isra l A. Delta-1 activation of notch-1 signaling results in HES-1 transactivation. Mol Cell Biol 1998;18:7423-31.

397. Bailey AM, Posakony JW. Suppressor of hairless directly activates transcription of enhancer of split complex genes in response to Notch receptor activity. Genes Dev 1995;9:2609-22.
398. Fisher AL, Ohsako S, Caudy M. The WRPW motif of the hairy-related basic helix-loop-helix repressor proteins acts as a 4-amino-acid transcription repression and protein-protein interaction domain. Mol Cell Biol 1996;16:2670-7.
399. Bjornson CR, Cheung TH, Liu L, Tripathi PV, Steeper KM, Rando TA. Notch signaling is necessary to maintain quiescence in adult muscle stem cells. Stem Cells 2012;30:232-42.
400. Nickoloff BJ, Qin JZ, Chaturvedi V, Denning MF, Bonish B, Miele L. Jagged-1 mediated activation of notch signaling induces complete maturation of human keratinocytes through NF-kappaB and PPARgamma. Cell Death Differ 2002;9:842-55.
401. Weijzen S, Velders MP, Elmishad AG, Bacon PE, Panella JR, Nickoloff BJ, Miele L, Kast WM. The Notch ligand Jagged-1 is able to induce maturation of monocyte-derived human dendritic cells. J Immunol 2002;169:4273-8.
402. Heitzler P. Biodiversity and noncanonical Notch signaling. Curr Top Dev Biol 2010;92:457-81.
403. Sade H, Krishna S, Sarin A. The anti-apoptotic effect of Notch-1 requires p56lck-dependent, Akt/PKB-mediated signaling in T cells. J Biol Chem 2004;279:2937-44.
404. Shawber C, Nofziger D, Hsieh JJ, Lindsell C, Bogler O, Hayward D, Weinmaster G. Notch signaling inhibits muscle cell differentiation through a CBF1-independent pathway. Development 1996;122:3765-73.
405. Talora C, Campese AF, Bellavia D, Felli MP, Vacca A, Gulino A, Screpanti I. Notch signaling and diseases: an evolutionary journey from a simple beginning to complex outcomes. Biochim Biophys Acta 2008;1782:489-97.
406. Wang J, Shelly L, Miele L, Boykins R, Norcross MA, Guan E. Human Notch-1 inhibits NF-kappa B activity in the nucleus through a direct interaction involving a novel domain. J Immunol 2001;167:289-95.
407. Espinosa L, Ingles-Esteve J, Robert-Moreno A, Bigas A. IkappaBalpha and p65 regulate the cytoplasmic shuttling of nuclear corepressors: cross-talk between Notch and NFkappaB pathways. Mol Biol Cell 2003;14:491-502.
408. Vacca A, Felli MP, Palermo R, Di Mario G, Calce A, Di Giovine M, Frati L, Gulino A, Screpanti I. Notch3 and pre-TCR interaction unveils distinct NF-kappaB pathways in T-cell development and leukemia. EMBO J 2006;25:1000-8.
409. Felli MP, Vacca A, Calce A, Bellavia D, Campese AF, Grillo R, Di Giovine M, Checquolo S, Talora C, Palermo R, Di Mario G, Frati L, Gulino A, Screpanti I. PKC theta mediates pre-TCR signaling and contributes to Notch3-induced T-cell leukemia. Oncogene 2005;24:992-1000.
410. Andersson ER, Sandberg R, Lendahl U. Notch signaling: simplicity in design, versatility in function. Development 2011;138:3593-612.
411. Yuan ZR, Kobayashi N, Kohsaka T. Human Jagged 1 mutants cause liver defect in Alagille syndrome by overexpression of hepatocyte growth factor. J Mol Biol 2006;356:559-68.

412. McDaniell R, Warthen DM, Sanchez-Lara PA, Pai A, Krantz ID, Piccoli DA, Spinner NB. NOTCH2 mutations cause Alagille syndrome, a heterogeneous disorder of the notch signaling pathway. Am J Hum Genet 2006;79:169-73.
413. Kodama Y, Hijikata M, Kageyama R, Shimotohno K, Chiba T. The role of notch signaling in the development of intrahepatic bile ducts. Gastroenterology 2004;127:1775-86.
414. Tanimizu N, Miyajima A. Notch signaling controls hepatoblast differentiation by altering the expression of liver-enriched transcription factors. J Cell Sci 2004;117:3165-74.
415. Nishikawa Y, Doi Y, Watanabe H, Tokairin T, Omori Y, Su M, Yoshioka T, Enomoto K. Transdifferentiation of mature rat hepatocytes into bile duct-like cells in vitro. Am J Pathol 2005;166:1077-88.
416. Leong KG, Karsan A. Recent insights into the role of Notch signaling in tumorigenesis. Blood 2006;107:2223-33.
417. Leong KG, Gao WQ. The Notch pathway in prostate development and cancer. Differentiation 2008;76:699-716.
418. Jensen CH, Jauho EI, Santoni-Rugiu E, Holmskov U, Teisner B, Tygstrup N, Bisgaard HC. Transit-amplifying ductular (oval) cells and their hepatocytic progeny are characterized by a novel and distinctive expression of delta-like protein/preadipocyte factor 1/fetal antigen 1. Am J Pathol 2004;164:1347-59.
419. Kohler C, Bell AW, Bowen WC, Monga SP, Fleig W, Michalopoulos GK. Expression of Notch-1 and its ligand Jagged-1 in rat liver during liver regeneration. Hepatology 2004;39:1056-65.
420. Weng AP, Ferrando AA, Lee W, Morris JPt, Silverman LB, Sanchez-Irizarry C, Blacklow SC, Look AT, Aster JC. Activating mutations of NOTCH1 in human T cell acute lymphoblastic leukemia. Science 2004;306:269-71.
421. Ranganathan P, Weaver KL, Capobianco AJ. Notch signalling in solid tumours: a little bit of everything but not all the time. Nat Rev Cancer 2011;11:338-51.
422. Pece S, Serresi M, Santolini E, Capra M, Hulleman E, Galimberti V, Zurrida S, Maisonneuve P, Viale G, Di Fiore PP. Loss of negative regulation by Numb over Notch is relevant to human breast carcinogenesis. J Cell Biol 2004;167:215-21.
423. Weijzen S, Rizzo P, Braid M, Vaishnav R, Jonkheer SM, Zlobin A, Osborne BA, Gottipati S, Aster JC, Hahn WC, Rudolf M, Siziopikou K, Kast WM, Miele L. Activation of Notch-1 signaling maintains the neoplastic phenotype in human Ras-transformed cells. Nat Med 2002;8:979-86.
424. Stylianou S, Clarke RB, Brennan K. Aberrant activation of notch signaling in human breast cancer. Cancer Res 2006;66:1517-25.
425. Gallahan D, Callahan R. The mouse mammary tumor associated gene INT3 is a unique member of the NOTCH gene family (NOTCH4). Oncogene 1997;14:1883-90.
426. Westhoff B, Colaluca IN, D'Ario G, Donzelli M, Tosoni D, Volorio S, Pelosi G, Spaggiari L, Mazzarol G, Viale G, Pece S, Di Fiore PP. Alterations of the Notch pathway in lung cancer. Proc Natl Acad Sci U S A 2009;106:22293-8.
427. Allen TD, Rodriguez EM, Jones KD, Bishop JM. Activated Notch1 induces lung adenomas in mice and cooperates with Myc in the generation of lung adenocarcinoma. Cancer Res 2011;71:6010-8.

428. Dang TP, Gazdar AF, Virmani AK, Sepetavec T, Hande KR, Minna JD, Roberts JR, Carbone DP. Chromosome 19 translocation, overexpression of Notch3, and human lung cancer. J Natl Cancer Inst 2000;92:1355-7.
429. Mazur PK, Einwachter H, Lee M, Sipos B, Nakhai H, Rad R, Zimber-Strobl U, Strobl LJ, Radtke F, Kloppel G, Schmid RM, Siveke JT. Notch2 is required for progression of pancreatic intraepithelial neoplasia and development of pancreatic ductal adenocarcinoma. Proc Natl Acad Sci U S A 2010;107:13438-43.
430. Pierfelice TJ, Schreck KC, Dang L, Asnaghi L, Gaiano N, Eberhart CG. Notch3 activation promotes invasive glioma formation in a tissue site-specific manner. Cancer Res 2011;71:1115-25.
431. Konishi J, Kawaguchi KS, Vo H, Haruki N, Gonzalez A, Carbone DP, Dang TP. Gamma-secretase inhibitor prevents Notch3 activation and reduces proliferation in human lung cancers. Cancer Res 2007;67:8051-7.
432. Nicolas M, Wolfer A, Raj K, Kummer JA, Mill P, van Noort M, Hui CC, Clevers H, Dotto GP, Radtke F. Notch1 functions as a tumor suppressor in mouse skin. Nat Genet 2003;33:416-21.
433. Graziani I, Eliasz S, De Marco MA, Chen Y, Pass HI, De May RM, Strack PR, Miele L, Bocchetta M. Opposite effects of Notch-1 and Notch-2 on mesothelioma cell survival under hypoxia are exerted through the Akt pathway. Cancer Res 2008;68:9678-85.
434. Bolos V, Blanco M, Medina V, Aparicio G, Diaz-Prado S, Grande E. Notch signalling in cancer stem cells. Clin Transl Oncol 2009;11:11-9.
435. Simmons MJ, Serra R, Hermance N, Kelliher MA. NOTCH1 inhibition in vivo results in mammary tumor regression and reduced mammary tumorsphere-forming activity in vitro. Breast Cancer Res 2012;14:R126.
436. Harrison H, Farnie G, Howell SJ, Rock RE, Stylianou S, Brennan KR, Bundred NJ, Clarke RB. Regulation of breast cancer stem cell activity by signaling through the Notch4 receptor. Cancer Res 2010;70:709-18.
437. Xie M, Zhang L, He CS, Xu F, Liu JL, Hu ZH, Zhao LP, Tian Y. Activation of Notch-1 enhances epithelial-mesenchymal transition in gefitinib-acquired resistant lung cancer cells. J Cell Biochem 2012;113:1501-13.
438. McAuliffe SM, Morgan SL, Wyant GA, Tran LT, Muto KW, Chen YS, Chin KT, Partridge JC, Poole BB, Cheng KH, Daggett J, Jr., Cullen K, Kantoff E, Hasselbatt K, Berkowitz J, Muto MG, Berkowitz RS, Aster JC, Matulonis UA, Dinulescu DM. Targeting Notch, a key pathway for ovarian cancer stem cells, sensitizes tumors to platinum therapy. Proc Natl Acad Sci U S A 2012;109:E2939-48.
439. Wang J, Wakeman TP, Lathia JD, Hjelmeland AB, Wang XF, White RR, Rich JN, Sullenger BA. Notch promotes radioresistance of glioma stem cells. Stem Cells 2010;28:17-28.
440. Cheng P, Nefedova Y, Corzo CA, Gabrilovich DI. Regulation of dendritic-cell differentiation by bone marrow stroma via different Notch ligands. Blood 2007;109:507-15.
441. Wang YC, He F, Feng F, Liu XW, Dong GY, Qin HY, Hu XB, Zheng MH, Liang L, Feng L, Liang YM, Han H. Notch signaling determines the M1 versus M2 polarization of macrophages in antitumor immune responses. Cancer Res 2010;70:4840-9.

442. Monsalve E, Perez MA, Rubio A, Ruiz-Hidalgo MJ, Baladron V, Garcia-Ramirez JJ, Gomez JC, Laborda J, Diaz-Guerra MJ. Notch-1 up-regulation and signaling following macrophage activation modulates gene expression patterns known to affect antigen-presenting capacity and cytotoxic activity. J Immunol 2006;176:5362-73.
443. Fung E, Tang SM, Canner JP, Morishige K, Arboleda-Velasquez JF, Cardoso AA, Carlesso N, Aster JC, Aikawa M. Delta-like 4 induces notch signaling in macrophages: implications for inflammation. Circulation 2007;115:2948-56.
444. Han YJ, Kwon YG, Chung HT, Lee SK, Simmons RL, Billiar TR, Kim YM. Antioxidant enzymes suppress nitric oxide production through the inhibition of NF-kappa B activation: role of H(2)O(2) and nitric oxide in inducible nitric oxide synthase expression in macrophages. Nitric Oxide 2001;5:504-13.
445. Choi JH, Park JT, Davidson B, Morin PJ, Shih Ie M, Wang TL. Jagged-1 and Notch3 juxtacrine loop regulates ovarian tumor growth and adhesion. Cancer Res 2008;68:5716-23.
446. Ince N, de la Monte SM, Wands JR. Overexpression of human aspartyl (asparaginyl) beta-hydroxylase is associated with malignant transformation. Cancer Res 2000;60:1261-6.
447. Cantarini MC, de la Monte SM, Pang M, Tong M, D'Errico A, Trevisani F, Wands JR. Aspartyl-asparagyl beta hydroxylase over-expression in human hepatoma is linked to activation of insulin-like growth factor and notch signaling mechanisms. Hepatology 2006;44:446-57.
448. Novosyadlyy R, Tron K, Dudas J, Ramadori G, Scharf JG. Expression and regulation of the insulin-like growth factor axis components in rat liver myofibroblasts. J Cell Physiol 2004;199:388-98.
449. Lavaissiere L, Jia S, Nishiyama M, de la Monte S, Stern AM, Wands JR, Friedman PA. Overexpression of human aspartyl(asparaginyl)beta-hydroxylase in hepatocellular carcinoma and cholangiocarcinoma. J Clin Invest 1996;98:1313-23.
450. Maeda T, Sepe P, Lahousse S, Tamaki S, Enjoji M, Wands JR, de la Monte SM. Antisense oligodeoxynucleotides directed against aspartyl (asparaginyl) beta-hydroxylase suppress migration of cholangiocarcinoma cells. J Hepatol 2003;38:615-22.
451. Jarnagin WR, Zager JS, Hezel M, Stanziale SF, Adusumilli PS, Gonen M, Ebright MI, Culliford A, Gusani NJ, Fong Y. Treatment of cholangiocarcinoma with oncolytic herpes simplex virus combined with external beam radiation therapy. Cancer Gene Ther 2006;13:326-34.
452. Tepsiri N, Chaturat L, Sripa B, Namwat W, Wongkham S, Bhudhisawasdi V, Tassaneeyakul W. Drug sensitivity and drug resistance profiles of human intrahepatic cholangiocarcinoma cell lines. World J Gastroenterol 2005;11:2748-53.
453. Juntavee A, Sripa B, Pugkhem A, Khuntikeo N, Wongkham S. Expression of sialyl Lewis(a) relates to poor prognosis in cholangiocarcinoma. World J Gastroenterol 2005;11:249-54.
454. Tang WH, Yuan ST, Wang BS, Lu LJ, Ding J, Yuan ZR. Establishment of a subcutaneous model of the human extrahepatic bile duct carcinoma in nude

mice via transplantation of histologically intact tumor tissue. J Exp Clin Cancer Res 2004;23:661-7.
455. Ku JL, Yoon KA, Kim IJ, Kim WH, Jang JY, Suh KS, Kim SW, Park YH, Hwang JH, Yoon YB, Park JG. Establishment and characterisation of six human biliary tract cancer cell lines. Br J Cancer 2002;87:187-93.
456. Steffen M, Zuehlke I, Scherdin U. Motility factors identified in supernatants of human cholangiocarcinoma cell lines. Int J Oncol 2001;18:1107-12.
457. Kim DG, Park SY, You KR, Lee GB, Kim H, Moon WS, Chun YH, Park SH. Establishment and characterization of chromosomal aberrations in human cholangiocarcinoma cell lines by cross-species color banding. Genes Chromosomes Cancer 2001;30:48-56.
458. Jiao W, Yakushiji H, Kitajima Y, Ogawa A, Miyazaki K. Establishment and characterization of human hilar bile duct carcinoma cell line and cell strain. J Hepatobiliary Pancreat Surg 2000;7:417-25.
459. Takiyama I, Terashima M, Ikeda K, Kawamura H, Kashiwaba M, Tamura G, Suto T, Nakashima F, Sasaki R, Saito K. Establishment and characterization of a new human extrahepatic bile duct carcinoma cell line (ICBD-1). Oncol Rep 1998;5:463-7.
460. Yamada N, Chung Y, Ohtani H, Ikeda T, Onoda N, Sawada T, Nishiguchi Y, Hasuma T, Sowa M. Establishment and characterization of a new human gallbladder carcinoma cell line (OCUG-1) producing TA-4. Int J Oncol 1997;10:1251-5.
461. Saijyo S, Kudo T, Suzuki M, Katayose Y, Shinoda M, Muto T, Fukuhara K, Suzuki T, Matsuno S. Establishment of a new extrahepatic bile duct carcinoma cell line, TFK-1. Tohoku J Exp Med 1995;177:61-71.
462. Yamada N, Chung YS, Arimoto Y, Sawada T, Seki S, Sowa M. Establishment of a new human extrahepatic bile duct carcinoma cell line (OCUCh-LM1) and experimental liver metastatic model. Br J Cancer 1995;71:543-8.
463. Purdum PP, 3rd, Ulissi A, Hylemon PB, Shiffman ML, Moore EW. Cultured human gallbladder epithelia. Methods and partial characterization of a carcinoma-derived model. Lab Invest 1993;68:345-53.
464. Iemura A, Maruiwa M, Yano H, Kojiro M. A new human cholangiocellular carcinoma cell line (KMC-1). J Hepatol 1992;15:288-98.
465. Shimizu Y, Demetris AJ, Gollin SM, Storto PD, Bedford HM, Altarac S, Iwatsuki S, Herberman RB, Whiteside TL. Two new human cholangiocarcinoma cell lines and their cytogenetics and responses to growth factors, hormones, cytokines or immunologic effector cells. Int J Cancer 1992;52:252-60.
466. Yano H, Maruiwa M, Iemura A, Mizoguchi A, Kojiro M. Establishment and characterization of a new human extrahepatic bile duct carcinoma cell line (KMBC). Cancer 1992;69:1664-73.
467. Storto PD, Saidman SL, Demetris AJ, Letessier E, Whiteside TL, Gollin SM. Chromosomal breakpoints in cholangiocarcinoma cell lines. Genes Chromosomes Cancer 1990;2:300-10.
468. Miyagiwa M, Ichida T, Tokiwa T, Sato J, Sasaki H. A new human cholangiocellular carcinoma cell line (HuCC-T1) producing carbohydrate antigen 19/9 in serum-free medium. In Vitro Cell Dev Biol 1989;25:503-10.

469. Kusaka Y, Tokiwa T, Sato J. Establishment and characterization of a cell line from a human cholangiocellular carcinoma. Res Exp Med (Berl) 1988;188:367-75.
470. Murakami T, Yano H, Maruiwa M, Sugihara S, Kojiro M. Establishment and characterization of a human combined hepatocholangiocarcinoma cell line and its heterologous transplantation in nude mice. Hepatology 1987;7:551-6.
471. Scherdin G, Garbrecht M, Klouche M. In vitro interaction of á-difluoromethylornithine (DFMO) and human recombinant interferon-α (rIFN-α) on human cancer cell lines. Immunobiology 1987;175:1-143.
472. Knuth A, Gabbert H, Dippold W, Klein O, Sachsse W, Bitter-Suermann D, Prellwitz W, Meyer zum Buschenfelde KH. Biliary adenocarcinoma. Characterisation of three new human tumor cell lines. J Hepatol 1985;1:579-96.
473. Flavell DJ, Lucas SB. Promotion of N-nitrosodimethylamine-initiated bile duct carcinogenesis in the hamster by the human liver fluke, Opisthorchis viverrini. Carcinogenesis 1983;4:927-30.
474. Elmore LW, Sirica AE. "Intestinal-type" of adenocarcinoma preferentially induced in right/caudate liver lobes of rats treated with furan. Cancer Res 1993;53:254-9.
475. Xu X, Kobayashi S, Qiao W, Li C, Xiao C, Radaeva S, Stiles B, Wang RH, Ohara N, Yoshino T, LeRoith D, Torbenson MS, Gores GJ, Wu H, Gao B, Deng CX. Induction of intrahepatic cholangiocellular carcinoma by liver-specific disruption of Smad4 and Pten in mice. J Clin Invest 2006;116:1843-52.
476. Marsh V, Winton DJ, Williams GT, Dubois N, Trumpp A, Sansom OJ, Clarke AR. Epithelial Pten is dispensable for intestinal homeostasis but suppresses adenoma development and progression after Apc mutation. Nat Genet 2008;40:1436-44.
477. Sirica AE, Zhang Z, Lai GH, Asano T, Shen XN, Ward DJ, Mahatme A, Dewitt JL. A novel "patient-like" model of cholangiocarcinoma progression based on bile duct inoculation of tumorigenic rat cholangiocyte cell lines. Hepatology 2008;47:1178-90.
478. Fitzhugh OG, Nelson AA. Liver Tumors in Rats Fed Thiourea or Thioacetamide. Science 1948;108:626-8.
479. Gupta DN. Production of cancer of the bile ducts with thioacetamide. Nature 1955;175:257.
480. Yeh CN, Maitra A, Lee KF, Jan YY, Chen MF. Thioacetamide-induced intestinal-type cholangiocarcinoma in rat: an animal model recapitulating the multi-stage progression of human cholangiocarcinoma. Carcinogenesis 2004;25:631-6.
481. Liu EH, Chen MF, Yeh TS, Ho YP, Wu RC, Chen TC, Jan YY, Pan TL. A useful model to audit liver resolution from cirrhosis in rats using functional proteomics. J Surg Res 2007;138:214-23.
482. Laverman P, Blokx WA, Te Morsche RH, Frielink C, Boerman OC, Oyen WJ, Drenth JP. [(18)F]FDG accumulation in an experimental model of multistage progression of cholangiocarcinoma. Hepatol Res 2007;37:127-32.

483. Al-Bader A, Mathew TC, Abul H, Al-Sayer H, Singal PK, Dashti HM. Cholangiocarcinoma and liver cirrhosis in relation to changes due to thioacetamide. Mol Cell Biochem 2000;208:1-10.
484. Laleman W, Vander Elst I, Zeegers M, Servaes R, Libbrecht L, Roskams T, Fevery J, Nevens F. A stable model of cirrhotic portal hypertension in the rat: thioacetamide revisited. Eur J Clin Invest 2006;36:242-9.
485. Fava G, Alpini G, Rychlicki C, Saccomanno S, DeMorrow S, Trozzi L, Candelaresi C, Venter J, Di Sario A, Marzioni M, Bearzi I, Glaser S, Alvaro D, Marucci L, Francis H, Svegliati-Baroni G, Benedetti A. Leptin enhances cholangiocarcinoma cell growth. Cancer Res 2008;68:6752-61.
486. Okabe M, Ikawa M, Kominami K, Nakanishi T, Nishimune Y. 'Green mice' as a source of ubiquitous green cells. FEBS Lett 1997;407:313-9.
487. Ito T, Suzuki A, Imai E, Okabe M, Hori M. Bone marrow is a reservoir of repopulating mesangial cells during glomerular remodeling. J Am Soc Nephrol 2001;12:2625-35.
488. Van Rooijen N, Sanders A. Liposome mediated depletion of macrophages: mechanism of action, preparation of liposomes and applications. J Immunol Methods 1994;174:83-93.
489. Turner ME, Martin C, Martins AS, Dunmire J, Farkas J, Ely DL, Milsted A. Genomic and expression analysis of multiple Sry loci from a single Rattus norvegicus Y chromosome. BMC Genet 2007;8:11.
490. User Bulletin #2 ABI PRISM 7700 Sequence Detection System. 2001:36.
491. Gronthos S, Graves SE, Ohta S, Simmons PJ. The STRO-1+ fraction of adult human bone marrow contains the osteogenic precursors. Blood 1994;84:4164-73.
492. Sonoyama W, Liu Y, Fang D, Yamaza T, Seo BM, Zhang C, Liu H, Gronthos S, Wang CY, Wang S, Shi S. Mesenchymal stem cell-mediated functional tooth regeneration in swine. PLoS One 2006;1:e79.
493. Yang X, Zhang W, van den Dolder J, Walboomers XF, Bian Z, Fan M, Jansen JA. Multilineage potential of STRO-1+ rat dental pulp cells in vitro. J Tissue Eng Regen Med 2007;1:128-35.
494. Jarriault S, Brou C, Logeat F, Schroeter EH, Kopan R, Israel A. Signalling downstream of activated mammalian Notch. Nature 1995;377:355-8.
495. Mosmann T. Rapid colorimetric assay for cellular growth and survival: application to proliferation and cytotoxicity assays. J Immunol Methods 1983;65:55-63.
496. Tsuji M, Kashihara T, Terada N, Mori H. An immunohistochemical study of hepatic atypical adenomatous hyperplasia, hepatocellular carcinoma, and cholangiocarcinoma with alpha-fetoprotein, carcinoembryonic antigen, CA19-9, epithelial membrane antigen, and cytokeratins 18 and 19. Pathol Int 1999;49:310-7.
497. Dijkstra CD, Dopp EA, Joling P, Kraal G. The heterogeneity of mononuclear phagocytes in lymphoid organs: distinct macrophage subpopulations in the rat recognized by monoclonal antibodies ED1, ED2 and ED3. Immunology 1985;54:589-99.
498. Ricciardelli C, Rodgers RJ. Extracellular matrix of ovarian tumors. Semin Reprod Med 2006;24:270-82.

499. Ikeda K, Iyama K, Ishikawa N, Egami H, Nakao M, Sado Y, Ninomiya Y, Baba H. Loss of expression of type IV collagen alpha5 and alpha6 chains in colorectal cancer associated with the hypermethylation of their promoter region. Am J Pathol 2006;168:856-65.
500. Tanjore H, Kalluri R. The role of type IV collagen and basement membranes in cancer progression and metastasis. Am J Pathol 2006;168:715-7.
501. Okamura N, Yoshida M, Shibuya A, Sugiura H, Okayasu I, Ohbu M. Cellular and stromal characteristics in the scirrhous hepatocellular carcinoma: comparison with hepatocellular carcinomas and intrahepatic cholangiocarcinomas. Pathol Int 2005;55:724-31.
502. Xu L, Hui AY, Albanis E, Arthur MJ, O'Byrne SM, Blaner WS, Mukherjee P, Friedman SL, Eng FJ. Human hepatic stellate cell lines, LX-1 and LX-2: new tools for analysis of hepatic fibrosis. Gut 2005;54:142-51.
503. Vander Griend DJ, Karthaus WL, Dalrymple S, Meeker A, DeMarzo AM, Isaacs JT. The role of CD133 in normal human prostate stem cells and malignant cancer-initiating cells. Cancer Res 2008;68:9703-11.
504. Maeshima A, Sakurai H, Nigam SK. Adult kidney tubular cell population showing phenotypic plasticity, tubulogenic capacity, and integration capability into developing kidney. J Am Soc Nephrol 2006;17:188-98.
505. van Rooijen N, van Nieuwmegen R. Elimination of phagocytic cells in the spleen after intravenous injection of liposome-encapsulated dichloromethylene diphosphonate. An enzyme-histochemical study. Cell Tissue Res 1984;238:355-8.
506. Wright MC, Issa R, Smart DE, Trim N, Murray GI, Primrose JN, Arthur MJ, Iredale JP, Mann DA. Gliotoxin stimulates the apoptosis of human and rat hepatic stellate cells and enhances the resolution of liver fibrosis in rats. Gastroenterology 2001;121:685-98.
507. Hagens WI, Beljaars L, Mann DA, Wright MC, Julien B, Lotersztajn S, Reker-Smit C, Poelstra K. Cellular targeting of the apoptosis-inducing compound gliotoxin to fibrotic rat livers. J Pharmacol Exp Ther 2008;324:902-10.
508. MacDonald KP, Palmer JS, Cronau S, Seppanen E, Olver S, Raffelt NC, Kuns R, Pettit AR, Clouston A, Wainwright B, Branstetter D, Smith J, Paxton RJ, Cerretti DP, Bonham L, Hill GR, Hume DA. An antibody against the colony-stimulating factor 1 receptor depletes the resident subset of monocytes and tissue- and tumor-associated macrophages but does not inhibit inflammation. Blood 2010;116:3955-63.
509. Knox C, Law V, Jewison T, Liu P, Ly S, Frolkis A, Pon A, Banco K, Mak C, Neveu V, Djoumbou Y, Eisner R, Guo AC, Wishart DS. DrugBank 3.0: a comprehensive resource for 'omics' research on drugs. Nucleic Acids Res 2011;39:D1035-41.
510. Longley DB, Harkin DP, Johnston PG. 5-fluorouracil: mechanisms of action and clinical strategies. Nat Rev Cancer 2003;3:330-8.
511. Magrassi L, Grimaldi P, Ibatici A, Corselli M, Ciardelli L, Castello S, Podesta M, Frassoni F, Rossi F. Induction and survival of binucleated Purkinje neurons by selective damage and aging. J Neurosci 2007;27:9885-92.

512. Spees JL, Pociask DA, Sullivan DE, Whitney MJ, Lasky JA, Prockop DJ, Brody AR. Engraftment of bone marrow progenitor cells in a rat model of asbestos-induced pulmonary fibrosis. Am J Respir Crit Care Med 2007;176:385-94.
513. Toth ZE, Shahar T, Leker R, Szalayova I, Bratincsak A, Key S, Lonyai A, Nemeth K, Mezey E. Sensitive detection of GFP utilizing tyramide signal amplification to overcome gene silencing. Exp Cell Res 2007;313:1943-50.
514. Gordon-Keylock S. Haematopoeitic differentiation of mouse embryonic stem cells. Volume PhD Thesis. Edinburgh: University of Edinburgh, 2009:1-234.
515. McCurley AT, Callard GV. Characterization of housekeeping genes in zebrafish: male-female differences and effects of tissue type, developmental stage and chemical treatment. BMC Mol Biol 2008;9:102.
516. Hayakawa J, Migita M, Ueda T, Shimada T, Fukunaga Y. Generation of a chimeric mouse reconstituted with green fluorescent protein-positive bone marrow cells: a useful model for studying the behavior of bone marrow cells in regeneration in vivo. Int J Hematol 2003;77:456-62.
517. Themeli M, Waterhouse M, Finke J, Spyridonidis A. DNA chimerism and its consequences after allogeneic hematopoietic cell transplantation. Chimerism 2011;2:25-28.
518. Mussano F, Lee KJ, Zuk P, Tran L, Cacalano NA, Jewett A, Carossa S, Nishimura I. Differential effect of ionizing radiation exposure on multipotent and differentiation-restricted bone marrow mesenchymal stem cells. J Cell Biochem 2010;111:322-32.
519. Dickhut A, Schwerdtfeger R, Kuklick L, Ritter M, Thiede C, Neubauer A, Brendel C. Mesenchymal stem cells obtained after bone marrow transplantation or peripheral blood stem cell transplantation originate from host tissue. Ann Hematol 2005;84:722-7.
520. Rieger K, Marinets O, Fietz T, Korper S, Sommer D, Mucke C, Reufi B, Blau WI, Thiel E, Knauf WU. Mesenchymal stem cells remain of host origin even a long time after allogeneic peripheral blood stem cell or bone marrow transplantation. Exp Hematol 2005;33:605-11.
521. Suire C, Brouard N, Hirschi K, Simmons PJ. Isolation of the stromal-vascular fraction of mouse bone marrow markedly enhances the yield of clonogenic stromal progenitors. Blood 2012;119:e86-95.
522. Dominici M, Le Blanc K, Mueller I, Slaper-Cortenbach I, Marini F, Krause D, Deans R, Keating A, Prockop D, Horwitz E. Minimal criteria for defining multipotent mesenchymal stromal cells. The International Society for Cellular Therapy position statement. Cytotherapy 2006;8:315-7.
523. Yang X, van der Kraan PM, van den Dolder J, Walboomers XF, Bian Z, Fan M, Jansen JA. STRO-1 selected rat dental pulp stem cells transfected with adenoviral-mediated human bone morphogenetic protein 2 gene show enhanced odontogenic differentiation. Tissue Eng 2007;13:2803-12.
524. Yang X, van den Dolder J, Walboomers XF, Zhang W, Bian Z, Fan M, Jansen JA. The odontogenic potential of STRO-1 sorted rat dental pulp stem cells in vitro. J Tissue Eng Regen Med 2007;1:66-73.
525. Shellabarger CJ, Cronkite EP, Bond VP, Lippincott SW. The occurrence of mammary tumors in the rat after sublethal whole-body irradiation. Radiat Res 1957;6:501-12.

526. Wagers AJ, Sherwood RI, Christensen JL, Weissman IL. Little evidence for developmental plasticity of adult hematopoietic stem cells. Science 2002;297:2256-9.
527. Theise ND, Henegariu O, Grove J, Jagirdar J, Kao PN, Crawford JM, Badve S, Saxena R, Krause DS. Radiation pneumonitis in mice: a severe injury model for pneumocyte engraftment from bone marrow. Exp Hematol 2002;30:1333-8.
528. Macdonald RA. "Lifespan" of liver cells. Autoradio-graphic study using tritiated thymidine in normal, cirrhotic, and partially hepatectomized rats. Arch Intern Med 1961;107:335-43.
529. Magami Y, Azuma T, Inokuchi H, Kokuno S, Moriyasu F, Kawai K, Hattori T. Cell proliferation and renewal of normal hepatocytes and bile duct cells in adult mouse liver. Liver 2002;22:419-25.
530. Meng F, Han Y, Staloch D, Francis T, Stokes A, Francis H. The H4 histamine receptor agonist, clobenpropit, suppresses human cholangiocarcinoma progression by disruption of epithelial mesenchymal transition and tumor metastasis. Hepatology 2011;54:1718-28.
531. da Silva Meirelles L, Chagastelles PC, Nardi NB. Mesenchymal stem cells reside in virtually all post-natal organs and tissues. J Cell Sci 2006;119:2204-13.
532. Mazur PK, Riener MO, Jochum W, Kristiansen G, Weber A, Schmid RM, Siveke JT. Expression and Clinicopathological Significance of Notch Signaling and Cell-Fate Genes in Biliary Tract Cancer. Am J Gastroenterol 2011.
533. Studebaker AW, Storci G, Werbeck JL, Sansone P, Sasser AK, Tavolari S, Huang T, Chan MW, Marini FC, Rosol TJ, Bonafe M, Hall BM. Fibroblasts isolated from common sites of breast cancer metastasis enhance cancer cell growth rates and invasiveness in an interleukin-6-dependent manner. Cancer Res 2008;68:9087-95.
534. Meng RD, Shelton CC, Li YM, Qin LX, Notterman D, Paty PB, Schwartz GK. gamma-Secretase inhibitors abrogate oxaliplatin-induced activation of the Notch-1 signaling pathway in colon cancer cells resulting in enhanced chemosensitivity. Cancer Res 2009;69:573-82.
535. Ristorcelli E, Beraud E, Mathieu S, Lombardo D, Verine A. Essential role of Notch signaling in apoptosis of human pancreatic tumoral cells mediated by exosomal nanoparticles. Int J Cancer 2009;125:1016-26.
536. Wang Z, Li Y, Banerjee S, Kong D, Ahmad A, Nogueira V, Hay N, Sarkar FH. Down-regulation of Notch-1 and Jagged-1 inhibits prostate cancer cell growth, migration and invasion, and induces apoptosis via inactivation of Akt, mTOR, and NF-kappaB signaling pathways. J Cell Biochem 2010;109:726-36.
537. Viatour P, Ehmer U, Saddic LA, Dorrell C, Andersen JB, Lin C, Zmoos AF, Mazur PK, Schaffer BE, Ostermeier A, Vogel H, Sylvester KG, Thorgeirsson SS, Grompe M, Sage J. Notch signaling inhibits hepatocellular carcinoma following inactivation of the RB pathway. J Exp Med 2011;208:1963-76.
538. Fre S, Hannezo E, Sale S, Huyghe M, Lafkas D, Kissel H, Louvi A, Greve J, Louvard D, Artavanis-Tsakonas S. Notch lineages and activity in intestinal

stem cells determined by a new set of knock-in mice. PLoS One 2011;6:e25785.
539. Grosveld GC. Gamma-secretase inhibitors: Notch so bad. Nat Med 2009;15:20-1.
540. Mavier P, Martin N, Couchie D, Preaux AM, Laperche Y, Zafrani ES. Expression of stromal cell-derived factor-1 and of its receptor CXCR4 in liver regeneration from oval cells in rat. Am J Pathol 2004;165:1969-77.
541. Teicher BA, Fricker SP. CXCL12 (SDF-1)/CXCR4 pathway in cancer. Clin Cancer Res 2010;16:2927-31.
542. Sethi N, Dai X, Winter CG, Kang Y. Tumor-derived JAGGED1 promotes osteolytic bone metastasis of breast cancer by engaging notch signaling in bone cells. Cancer Cell 2011;19:192-205.